Advances in Alkali-Metal-Mediated Manganation and Comparisons with Magnesiation

By

Victoria L. Blair

February 2010

Acknowledgements

First and foremost I would like to thank my supervisor, Professor Robert E. Mulvey for giving me the opportunity to work on such an interesting and challenging research project. His never ending supply of new ideas, enthusiasm, friendship and constant support to me over the past few years are all very much appreciated. I must also congratulate him on putting up with my many 'blonde moments' and total lack of geography knowledge!

I must also thank those who have contributed directly to this research project; the X-ray crystallographers, Dr. Alan Kennedy, Professor William Clegg, Dr Luca Russo and Dr. Stuart Robertson for solving my crystal structures when no NMR data were available, Professor Eva Rentschler and Luca Carella for their magnetism studies on my compounds, Denise Gilmour for all my microanalysis results and Dr. David Armstrong for carrying out theoretical calculations. I would also like to thank Dr Jan Klett, without his great supervision and teaching in the lab my project would have got nowhere.

Particular thanks must go to my mum, dad, brother and sister for pretending to understand what I was doing ☺, (I really do make crystals!) and my close friends Kate, Mel, Rosie, Lyndsey and Joanne for all the good times and encouragement over the years. In particular I would like to thank Steven, for and all his support over the last three and a half years and for putting up with me during the writing of this thesis (sorry!). A special thank you must go to Dr Eva Hevia and Dr Allison Drummond who over the years have become good friends. Their help, support, and friendship is very much appreciated.

It remains for me to thank Dr Charlie O'Hara and my fellow lab workers in R526 in particular Ben, Pablo, Matt, Liam, Ross, and Gemma for all the comradery in the lab.

I also wish to thank the EPSRC for the funding required to carry out this research project.

Abstract

The primary aim of this research project was to develop the new concept of Alkali-Metal-Mediated Manganation (AMM*Mn*). Work focused on the reaction of the new Na/Mn alkyl-amido base [(TMEDA)Na(TMP)(CH_2SiMe_3)Mn(TMP)] (**16**) with a series of organic substrates.

Firstly we investigated the reaction of the polymeric dialkyl manganese(II) compound $[Mn(CH_2SiMe_3)_2]_\infty$ (**1**) with a range of Lewis base donors, amines and ketones. The new complexes produced various structural forms ranging from simple monomeric complexes such as [(TMEDA)$Mn(CH_2SiMe_3)_2$] (**2**) to more complicated polymeric species such as the dioxane bridged $[\{(dioxane)[Mn(CH_2SiMe_3)_2]_2\}_\infty]$ (**4**). Dialkyl manganese reagent **1** can also function as a deprotonation reagent in its reaction with the primary amine $DippNH_2$ to afford the trimeric compound $[(DippNH)_6Mn_3]$ (**11**), while its reaction with benzophenone furnishes the 1,2-addition product $[(Me_3SiCH_2)_2Mn_3\{\mu\text{-}OC(CH_2SiMe_3)Ph_2\}_4]$ (**13**)**.**

AMM*Mn* reactions of the synergic base [(TMEDA)Na(TMP)(CH_2SiMe_3)Mn(TMP)] (**16**) with a variety of functionalised and non-functionalised arene substrates resulted in nine examples of the first reported direct manganations. Highlights include the *meta* manganation of N, N-dimethylaniline [(TMEDA)Na(TMP)(*m*-C_6H_4-NMe_2)Mn(TMP)] (**21**), the *para* manganation of N, N-diisopropylaniline [(TMEDA)Na(TMP)(*p*-$C_6H_4N^iPr_2$)Mn(TMP)] (**22**) and the novel 6-position mangantion of N, N-dimethyl-1-naphthylamine [(TMEDA)Na(TMP){6-(1-Me_2N-$C_{10}H_6$)}Mn(TMP)] (**27**).

Extending the methodology to Mn(II) based inverse crown complexes proved successful with three new anionic guest molecules, namely a hydride, benzenediide and *n*-butoxide, successfully being encapsulated within host rings to give three new Mn(II) inverse crown complexes $[Na_2Mn_2(\mu\text{-}H)_2\{N(iPr)_2\}_4]\cdot(toluene)_2$ (**31**), $[(TMEDA)_2Na_2(TMP)_2(1,4\text{-}C_6H_4)Mn_2(TMP)_2]$ (**38**) and $[\{(TMEDA)Na(CH_2SiMe_3)(OBu)(o\text{-}C_6H_4OMe)Mn\}_2]$ (**36**) respectively.

Remarkably the reaction of the synergic base **16** with the cyclic ether THF results in a new type of cleavage reaction where the C_4 backbone of the THF is cleaved and four-fold deprotonated to furnish a 1, 4-manganated butadiene complex [[(TMEDA)Na(TMP)}$_2${1, 4-[Mn(TMP)]$_2$-C_4H_4}] (**42**) while the THF O atom is synergically trapped in a separate oxo-inverse crown [$Na_2Mn_2(TMP)_4O$] (**44**).

The magnetic fingerprints of some of the new Mn(II) compounds are discussed in Chapter 7.

Publications Arising from Research carried out in this Project

1. *Programming the Basicity of Synergic Bimetallic Reagents: Switching the Regioselectivity of the Direct Dimetalation of Toluene from 2, 5- to 3, 5-Positions,* V. L. Blair, L. M. Carrella, W. Clegg, B. Conway, R. W. Harrington, L. M. Hogg, J. Klett, R. E. Mulvey, E. Rentschler, L. Russo, *Angew. Chem. Int. Ed.* **2008**, *47*, 6208.

2. *Alkali-Metal-Mediated Manganation(II) of Functionalized Arenes and Applications of ortho-Manganated Products in Pd-Catalyzed Cross-Coupling Reactions with Iodobenzene,* V. L. Blair, W. Clegg, B. Conway, E. Hevia, A. R. Kennedy, J. Klett, R. E. Mulvey, L. Russo, *Chem. Eur. J.* **2008**, *14*, 65.

3. *Structural Complexity of the Magnesiation of Furan: an octadecanuclear product with a subporphyrin-like Mg_3(2, 5-fur-di-yl)$_3$ substructure,* V. L. Blair, A. R. Kennedy, J. Klett, R. E. Mulvey, *Chem. Comm.* **2008**, *42*, 5426.

4. *Structural and Magnetic Insights into the Trinuclear Ferrocenophane and Unexpected Hydrido Inverse Crown Products of Alkali-Metal-Mediated Mangantion(II) of Ferrocene,* V. L. Blair, M. Carrella, W. Clegg, J. Klett, R. E. Mulvey, E. Rentschler, L. Russo, Chem. Eur. J. **2009**, *15*, 856.

5. *Bis[(trimethylsilyl)methyl]manganese: Structural Variations of Its Solvent-Free and TMEDA-, Pyridine, and Dioxane-Complexed Forms,* A. Alberola, V. L. Blair, L. M. Carella, W. Clegg, A. R. Kennedy, J. Klett, R. E. Mulvey, S. Newton, E. Rentschler, L. Russo, Organometallics, **2009**, *28*, 2112.

6. *Alkali-Metal-Mediated Manganation(II) of Naphthalenes: Constructing Metalla-Anthracene and Metalla-Phenanthrene Structures,* V. L. Blair, W. Clegg, R. E. Mulvey, L. Russo, Inorganic Chemistry, **2009**, *48*, 8863.

Conference Presentations

1. *Main Group Dominance of Transition Metal Chemistry Alkali-Metal-Mediated Manganation*, Oral presentation, Main Group Chemistry Dalton Division Meeting, July 2007, Bristol.

2. *Alkali-Metal-Mediated Manganation(II) of Functionalised Arenes* Poster Presentation, Awarded Best Poster Prize, USIC, September 2007, Edinburgh.

3. *Magic Manganation*, Oral presentation, WestCHEM Research Day, May 2008, Glasgow.

4. *Synergic Encapsulation of 'Hot' Anions by Mixed-Metal Ate Reagents*, Oral Presentation, 236th ACS National Meeting and Exposition, July 2008, Philadelphia, USA.

5. *'Development of Alkali-Metal-Mediated Manganation(II)'*, Oral Presentation, USIC, September 2008, Glasgow.

6. *Alkali-Metal-Mediated Manganation(II) of Naphthalenes: Constructing Metalla-Anthracene and Metalla-Phenanthrene Structures*, Poster Presentation, 42nd IUPAC Congress Chemistry Solutions, August 2009, Glasgow.

Abbreviations

AMM*M*	Alkali Metal-Mediated Metallation
AMM*Mn*	Alkali Metal-Mediated Manganation
AMM*Mg*	Alkali Metal-Mediated Magnesiation
AMM*Zn*	Alkali Metal-Mediated Zincation
Bu	Butyl
*n*Bu	*n*-butyl
*n*BuLi	*n*-butyllithium
*n*BuNa	*n*-butylsodium
*t*Bu	*tert*-butyl
CCDB	Cambridge Crystallographic Database
COSY	Correlation Spectroscopy
Cp	Cyclopentadienyl
DA	Diisopropylamide
DA(H)	Diisopropylamine
DFT	Density Functional Theory
Dipp	2,6-diisopropylphenyl
D*o*M	Directed *ortho* Metallation
DME	1,2-dimethoxyethane
Et_2O	Diethylether
HMDS	1,1,1,3,3,3-hexamethyldisilazide
LDA	Lithium diisopropylamide
LIC-KOR	Alkyllithium/potassium alkoxide superbase
LiTMP	Lithium 2,2,6,6-tetramethylpiperidide
Me	Methyl
NaTMP	Sodium 2,2,6,6-tetramethylpiperidide
NMR	Nuclear Magnetic Resonance
Ph	Phenyl
PMDETA	N,N,N',N'',N''-pentamethyldiethylenetriamine
*i*Pr	*iso*-propyl
THF	Tetrahydrofuran
THP	Tetrahydropyran

THT	Tetrahydrothiophene
TMEDA	N,N,N’,N’,-tetramethylethylenediamine
TMP(H)	2,2,6,6-tetramethylpiperidine
XRD	X-ray Diffraction

Table of Contents

Chapter 1. Development of Mixed-Metal Chemistry

This chapter aims to provide a brief introduction to the major developments in mixed-metal chemistry both within and out with the Mulvey research group, with particular attention to the special cooperative chemistry that is observed when an alkali-metal is paired with a divalent metal, usually magnesium or zinc, in the same organoelement compound. The development of this unique synergic chemistry is the core basis of this PhD research programme and thus will be discussed in great detail.

1.1. General Background of s-Block Organometallics

Today deprotonative metallation is one of the most common techniques used in synthetic laboratories across the world, not only in academia but also in industry.[1] Conventionally metal amides, mainly organolithium reagents such as *n*-butyllithium (*n*BuLi) and the more sterically demanding lithium diisopropylamide (LDA), lithium HMDS (HMDS =1,1,1,3,3,3-hexamethyldisilazide) and LiTMP (TMP =2,2,6,6-tetramethylpiperidide) (Figure 1) play an integral part in the deprotonation of countless organic substrates due to the high reactivity of the predominately ionic $Li^{\delta+}$-$N^{\delta-}$ and $C^{\delta-}$ bonds.[2] However, without exception all organolithium and lithium amide reagents have limitations in metallation chemistry. Prominent among these are attacks on sensitive functional groups, competitive nucleophilic addition, low kinetic stability of metallated intermediates and the general requirement for low temperature reaction conditions. These limitations have prompted synthetic chemists to seek out new and improved alternative metallating reagents which can offer clean and effective regioselective abstraction of a hydrogen atom from an organic substrate without unwanted side reactions.

Recently significant progress towards this goal has been made through the use of diverse multimetallic complexes such as ate complexes which can effectively deprotonate aromatic substrates under milder reaction conditions and with a greater tolerance to many functional groups. The first ate compound was discovered over 150 years ago by Wanklyn.[3] Moving to the 1950s Wittig and Bickelhaupt[4] amongst others,

made further developments in ate chemistry investigating complexes of the type RLi.RM (M = a heavier alkali metal), but it was not until 30 years later in 1988 that

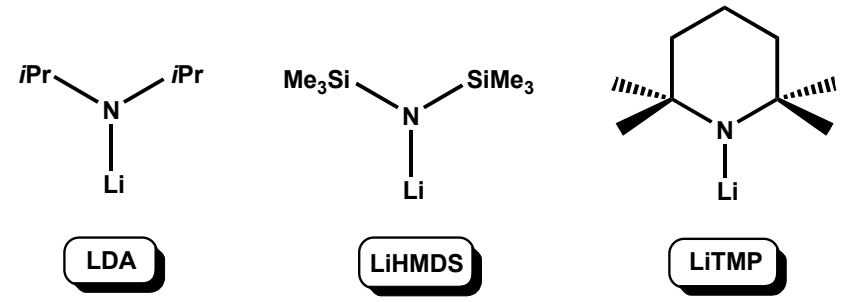

Figure 1: Chem Draw representations of the popular lithium amides.

Weiss confirmed the formation of an ate complex, the mixed lithium-sodium arylide, $[Na(TMEDA)]_3[LiPh_4]$[5] by X-ray crystallographic studies. However, it is only now, in the 21th century, that the true synthetic potential of such mixed-metal reagents have begun to come to light. Several groups around the world have established alternative metallating reagents which have become more complex than their simple monoanionic-monocatonic predecessors such as BuLi or LDA. Figure 2 shows a selection of the best known composite metallating reagents which can be classed into four separate categories; ates, mixed-metal superbases, uni-metal superbases and turbo-Grignard reagents which all possess composite compositions made up of two or more distinct families of compounds.

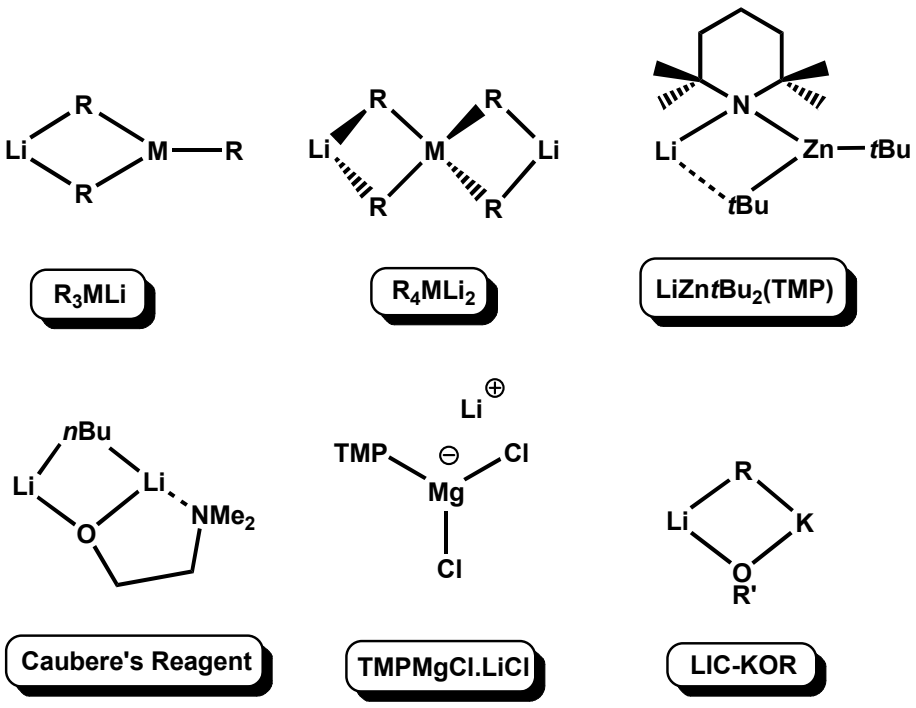

Figure 2: Chem Draw representations of a selection of composite metallating reagents.

Ate complexes commonly have the general formula 'R_3MLi' or 'R_4MLi_2' with their composition being best thought of as a mixture of an organolithium compound 'LiR' with an organometallic compound 'MR_2', where M is a divalent metal (for example Mg or Zn), in either a 1:1 or 2:1 mixture respectively. As aforementioned, Wittig was a pioneer in this area of chemistry who realised the special reactivity of these multimetallic complexes in deprotonation reactions[6, 7] in contrast to that of their single metallic components. Recently Mongin has been using mixed lithium arylmagnesiates for the deprotonation of fluoro aromatics,[8] thiophenes,[9] chloropyridines[10] and furans[11] with the arylmagnesiates being trapped with electrophiles or involved in palladium-catalysed cross-couplings. For example, the use of the highly coordinated dilithium tetrabutylmagnesiate Bu_4MgLi_2 proved to be a highly efficient base in the deprotonation of furan allowing after iodolysis 1-iodofuran to be isolated in an almost quantitative yield[11] (Scheme 1).

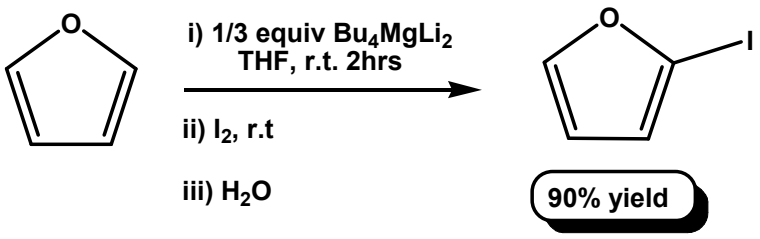

Scheme 1: Deprotonation of furan with Bu_4MgLi_2 and subsequent quenching with iodine.

In the latter part of the 20th century synthetic chemists began to realise an increase in basicity of an alkyl lithium compound when it is combined with a metal alkoxide.[12-14] This increase in basicity is accompanied by a dramatic increase in the reactivity of the system hence the appellation 'superbase' was coined.[15] In their simplest forms, superbases can be considered as organolithiums solvated by very electron-donating ligands. The most widely used of these superbases is the Lochmann-Schlosser reagent LIC-KOR[16] which is obtained by combining equivalent amounts of BuLi and K*t*BuO. For classical metallating reagents such as butyl lithium most deprotonation reactions require a relatively high CH acidity in order for a hydrogen/metal exchange to take place. However, the use of a superbase reagent allows deprotonation to occur smoothly even when the hydrocarbon substrate is in the low acidity range.[17] A wide range of organic substrates have been extensively studied using the LIC-KOR reagent through *in situ* electrophilic quenching studies.[14, 18] For example deprotonation of benzene, which

is not particularly acidic having a pK_a of 43, proceeds rapidly with LIC-KOR which is in contrast to its deprotonation with BuLi which proceeds slower and requires the presence of an activating electron donating agent such as TMEDA. However, the exact nature and structural composition of the heavily utilised LIC-KOR reagent, whether it be an organolithium, organopotassium or a mixture of the two, is still unknown. As an example of the unique reactivity of LIC-KOR, Scheme 2 highlights the differences in metallation sites of 2-fluoroanisole using LIC-KOR and conventional BuLi.[19, 20]

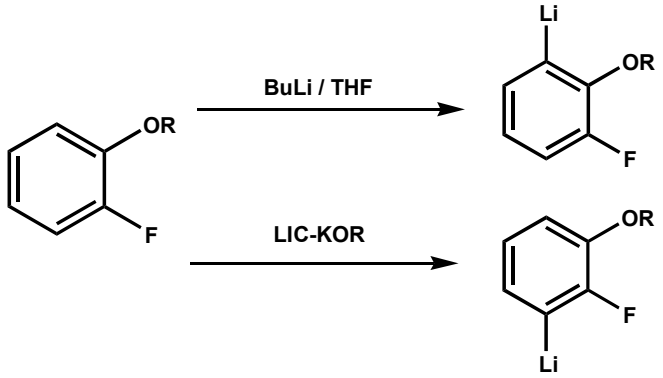

Scheme 2: Site-selective metallation of 2-fluoroanisole between i) BuLi and ii) LIC-KOR.

The powerful reactivity of the super basic LIC-KOR reagent does however come with some drawbacks. As examples relevant to deprotonations carried out in this work, its use in the di-metallation of benzene does not proceed smoothly and a mixture of monosubstituted and *meta*- and *para*-disubstituted products are obtained,[21] whilst its reaction with the larger polycyclic aromatic substrate naphthalene results in a complicated mixture of all ten disubstituted isomers.[21] Sometimes LIC-KOR is too aggressive towards organic substrates, and complicated mixtures of products and decomposition materials are obtained.

Complementing the mixed metal LIC-KOR superbase is a series of hono-metallic superbases. Best known is the *n*BuLi/lithium aminoalkoxide complex *n*BuLi–$Me_2N(CH_2)_2OLi$ popularly referred to as Cauberes reagent,[22] which has proven to be a synthetically useful lithiating reagent. The complex nature of the unimetal superbase has meant little progress in understanding the structural mechanics of superbasicity has been achieved. Recently, Gross and Fort[23] have extensively studied the use of Caubere's reagent in the direct metallation of pyridine and its derivatives. Their findings highlight the uni-metal superbases excellent compatibility with a wide range of sensitive

functional groups such as amines, ethers and phosphines as well as offering routes to unprecedented chemo- and regio-selective products in the pyridine series (Scheme 3).

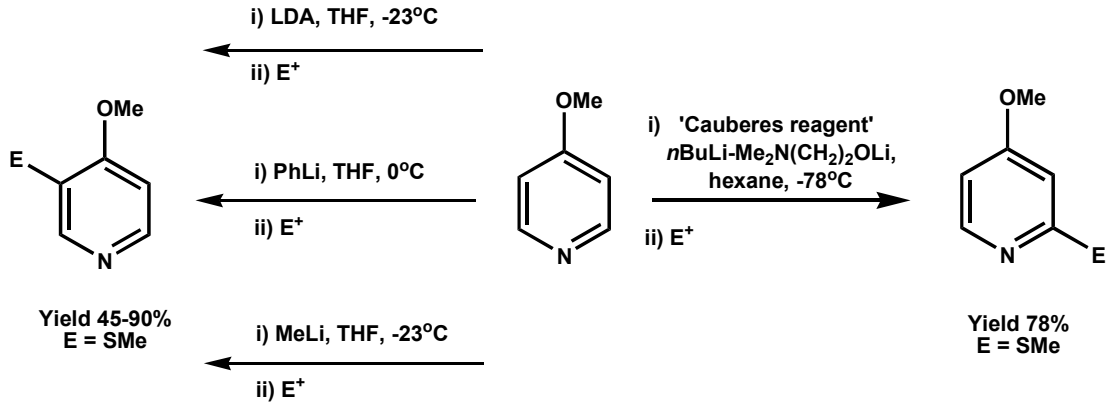

Scheme 3: Lithiation of 4-methoxypyridine with conventional lithiating reagents or with Caubere's reagent.

Another category of compound that can be considered to be superbasic is the aptly named 'turbo Grignard'.[24] Developed by Knochel it can be best described as a mixed lithium/magnesium alkyl/halogen co-complex which displays enhanced reactivity in comparison to that of conventional Grignard reagents (RMgX). Whilst investigating the reactivity and synthesis of organomagnesium compounds it was revealed that addition of the salt LiCl to the Grignard reagent *i*PrMgCl produced a highly reactive reagent of the formula *i*PrMgCl.LiCl[24-26] a turbo-Grignard reagent, (Figure 3) that allowed halogen-metal exchange reactions to be performed at an increased rate compared to those of the reagents RMgX and R_2Mg in the absence of any LiCl salt.[27]

Figure 3: Chem draw representation of the 'turbo Grignard' reagent *i*PrMgCl.LiCl.

Recently, Knochel developed this chemistry further by synthesising a corresponding mixed lithium/magnesium amide base of empirical formula $R_2NMgCl.LiCl$ (where R = *i*Pr or R_2N = TMP) which is highly reactive and soluble in THF. These resulting mixed magnesium/lithium bases have improved kinetic basicity and regioselectivity for the magnesiation of a wide range of functionalised aromatics and heteroaromatic substrates.

For example isoquinoline can be selectively magnesiated at the 2-position at room temperature after 2 hours employing the 'turbo Grignard' reagent TMPMgCl.LiCl that after iodolysis gives an almost quantitative yield of 92% of the desired iodinated product (Scheme 4). The enhanced reactivity has been postulated[27] to involve LiCl which acts to break up oligomeric aggregates of magnesium amides allowing mixed-metal reagents such as TMPMgCl.LiCl to form and enhancing solubility properties. Thus this system allows access to new magnesium species not readily available via halogen/metal exchange processes or from previously reported metallation attempts.

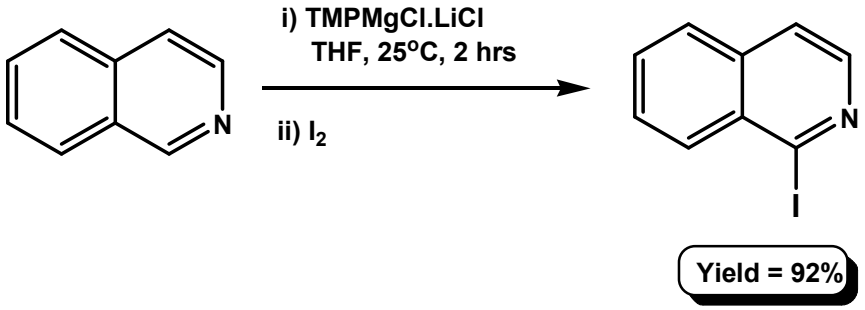

Scheme 4: Magnesiation of isoquinoline with TMPMgCl.LiCl.

However, despite the success of the 'turbo Grignard' system all the chemistry is employed as an *in situ* reagent with no solid composition or structural information available about the actual active species performing the metallation or halogen/metal exchange. Recently in 2008, the Mulvey group managed to shed light on the possible structures of these mixed-metal complexes by crystallographically characterising the first 'turbo Grignard' reagent[28] $[(THF)_2Li(Cl)_2Mg(THF)TMP]$ (Figure 4).

Revealing the structure of the turbo Grignard reagent allows a number of conclusions to be drawn regarding its regioselective magnesiating ability, for example, i) it is a molecular halide, rather than a salt; ii) the active basic TMP ligand binds to magnesium, not lithium; iii) the Mg-(TMP) linkage is terminal, and thus only one bond needs to be broken to release the active base; iv) the magnesium centre is four coordinate and coordinatively saturated, but has a (potentially) labile THF ligand next to the TMP, which if lost could allow the coordination of a functionalised aromatic substrate prior to its magnesiation, and v) the bimetallic ate ("$Li^+MgR_3^-$") formulation, augmented by the presence of strongly electronegative ligands could be a key factor in its enhanced magnesiating ability.[28] With this structural insight there now appears to be structural

justification for the special magnesiating ability exhibited by the whole 'turbo Grignard' reagent family.

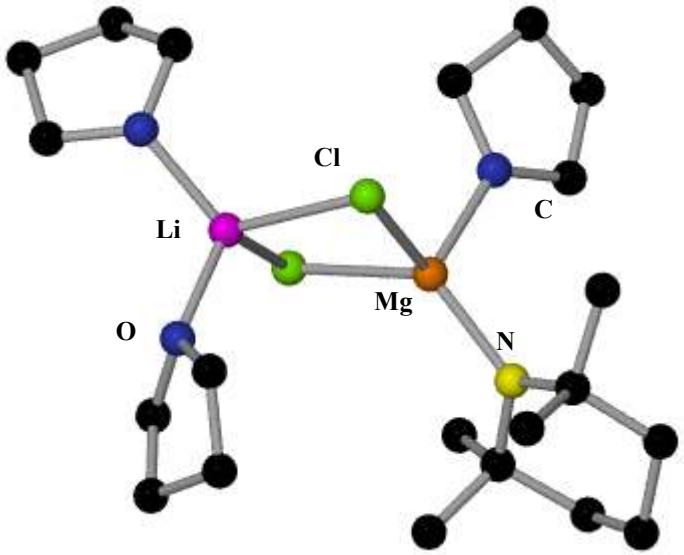

Figure 4: Molecular structure of the 'turbo Grignard' $[(THF)_2Li(Cl)_2Mg(THF)TMP]$.

Mixed-metal work developed by Kondo and Uchiyama, closely related to the studies outlined in this thesis, involved the development of ate complexes, zincates in particular which displayed a unique reactivity which was not reproducible by their monometallic components. Initially they investigated the use of lithium trialkylzincates, such as lithium tri-*tert*-butylzincate,[29] for the chemoselective metal-halogen exchange reaction of aryl halides containing electrophilic functional groups.[29-32] However, in the late 1990's their investigations turned to the use of these mixed-metal ate bases as direct metallators. Utilizing the newly composed monoamido-dialkyl zincate $[Li(TMP)Zn{t}Bu_2]$ in Direct *ortho*-Metallation (D*o*M) methodology (see page 17) they demonstrated the high selectivity and reactivity of the zincate reagent in these type of reactions.[33] The base was found to be highly chemoselective achieving the direct zincation of a wide variety of functionalised aromatic and heteroaromatic substrates including for example those with ester, cyano, halogen and amine functions as well as various substituted thiophene, pyridine and isoquinoline heteroaromatics (Scheme 5). It must be stressed that no structural details of the zincate reagent or of any of the metallated intermediates were reported in these early studies.

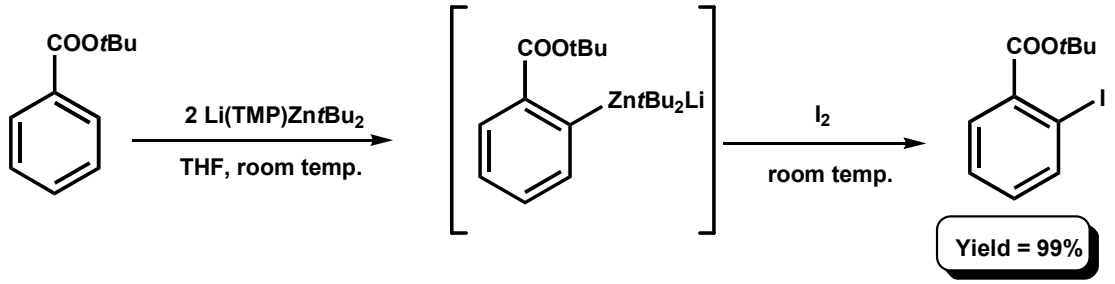

Scheme 5: Deprotonation of *tert*-butyl benzoate with LiTMPZn*t*Bu$_2$ and subsequent iodine trapping.

All the metallating reagents so far have been synthesised *in situ* by mixing together two or more distinct components to combine different cations with different anions in various formulations. Most of these new mixed-metal reagents have been discovered experimentally through trial and error approaches with little or no knowledge of the structure of the actual reagent carrying out the deprotonation. Nevertheless complex metallators are generating worldwide interest from both organic and inorganic chemists and are fast becoming an essential tool in the chemist's toolbox.

1.2. Alkali-Metal-Mediated *Metallation*: The Synergic Effect

Our group's development of inverse crown ether complexes brought about a new development in mixed metal chemistry that appeared to run counter to the established rules of reactivity of metal reagents. This unique synergic reactivity exhibited by certain heterobimetallic or mixed metal (ate) compounds happens when an alkali metal (Li, Na or K) is paired with magnesium or zinc and has become the prime focus of research in this group and a few other research groups across the world. These new species of synergic compounds allow selective deprotonations and polydeprotonations to be carried out on a wide variety of organic substrates including arene, metallocene and aromatic heterocyclic substrates. The core focus of the Mulvey group has been to rationally design and study these mixed-metal compounds, both the starting bases and metallic intermediates, directly by isolating the compounds for structural analysis. This section will summarise the main achievements made during the development of the synergic effect.

It was during the attempted preparation of a novel mixed lithium-magnesium utility amide in 1998 that the first inverse crown ether $[Li_2Mg_2(HMDS)_4(O)_x(O_2)_y]$ was serendipitously synthesised.[34] The composition of a typical inverse crown consists of an eight-membered cationic ring made up of amide-N bridged metal cations. The centre of the ring is filled by an anionic guest, usually a single oxide or peroxide ion. The mechanism of insertion of these oxy-anion is as yet still unknown for these magnesium systems but has been initially attributed to the presences of adventitious moisture or oxygen.

Compared to conventional crown ether complexes the Lewis basic (anionic) and Lewis acidic (cationic) sites have been interchanged (Figure 5). Since this is an inversion of the common crown-ether complex system, this led to the coining of the term "inverse crown ether complexes" for this new family of mixed-metal compounds.

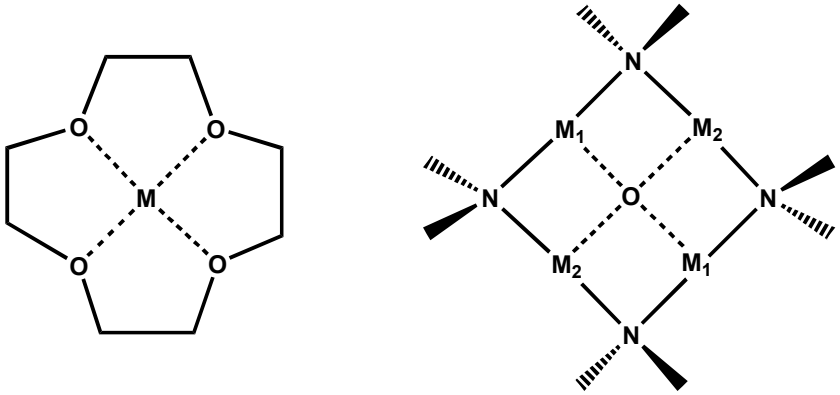

Figure 5: Comparison of the motifs of a typical crown ether (LHS) and inverse crown ether (RHS).

The host-guest system within these inverse crown complexes can be varied extensively with the successful synthesis of lithium, sodium and potassium derivatives[34-39] paired with either magnesium or zinc with various anionic guests, including alkoxides. The use of different amido bridges has also been investigated with incorporation of the sterically demanding amides TMP and HMDS while the use of β-hydride containing DAH (DAH = diisopropylamide) led to a new type of inverse crown structure containing 'hydride' guest anions.[40, 41]

The next variable within inverse crown chemistry that was investigated was the importance of the bulk solvent. Previously inverse crown ether complexes had been

synthesised in bulk hydrocarbon media but reactions carried out in the presence of arene solvents allowed the incorporation of a new 'guest' molecule. One notable example which illustrates this is when benzene or toluene is used as a co-solvent with the monoalkyl-bisamido base "NaMg(*n*Bu)$(TMP)_2$" Scheme 6.

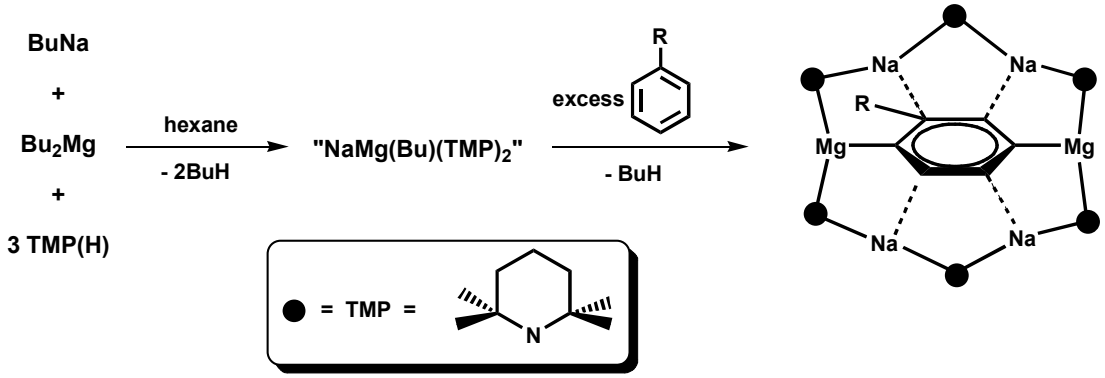

Scheme 6: Synthesis of arenediide-encapsulated inverse crowns with R = H or Me.

In both cases two-fold deprotonation of the aromatic ring is observed selectively at the 1, 4-positions in benzene and 2, 5-positions in toluene.[42] The latter example is particularly significant as the thermodynamically most acidic hydrogen of toluene (in pK_a terms) belongs to the methyl group, and it is here that conventional organometallic reagents would normally attack to produce the resonance stabilised benzyl anion $PhCH_2^-$.[43] Here the methyl group remains intact and the metallation occurs selectively on the aryl ring. The removal of more than one proton from these aromatic compounds has been previously achieved by the activated alkyl lithium system BuLi/TMEDA however regioselectivity is poor and complicated mixtures of products are often obtained.[44, 45] Another key aspect of the reactions is that the positions previously occupied by hydrogen atoms are now occupied by magnesium centres; however, neither Bu_2Mg or $Mg(TMP)_2$ can deprotonate benzene or toluene (even once) on their own and consequently it can be deduced that the presence of the alkali metal is essential for these regioselective deprotonations to occur. Thus these reactions can be more accurately described as Alkali-Metal-Mediated Magnesiations (AMM*Mg*).

With the aim of establishing the identity of the active base carrying out these selective deprotonations the reaction mixture of $BuNa/Bu_2Mg/TMP(H)$ in a 1:1:3 stoichiometric ratio was repeated in the presence of the popular chelating diamine TMEDA in

hydrocarbon solvent. Instead of the expected trisamide complex, the new bis-amido monoalkyl magnesiate [(TMEDA)Na(*n*Bu)(TMP)Mg(TMP)] was obtained (Scheme 7). This product can be considered as a co-complex of BuNa and $Mg(TMP)_2$ and was particularly interesting as it contained both alkyl and amido functionalities, both well-established bases in monometallic compounds.

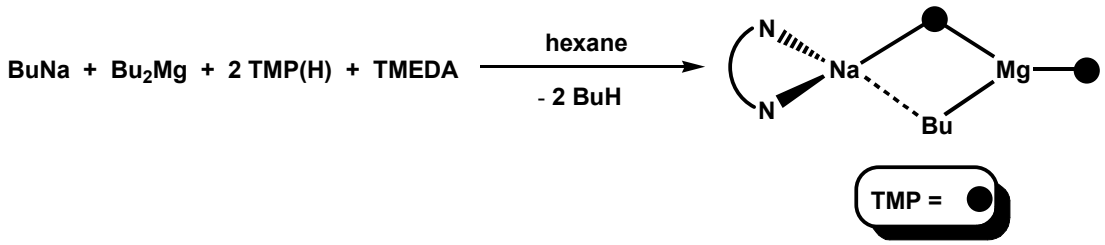

Scheme 7: Synergic synthesis of the bis-amido monoalkyl magnesiate [(TMEDA)Na(*n*Bu)(TMP)Mg(TMP)].

Subsequently, the new magnesiate base was reacted with a series of organic substrates to investigate its deprotonative ability. Upon reaction with benzene, the bridging butyl group is eliminated and replaced by a Ph ring to produce the aryl derivative [(TMEDA)Na(C_6H_5)(TMP)Mg(TMP)].[46] More remarkably, its reaction with toluene also involves the loss of the butyl bridge, but this time, it is replaced by an aryl anion deprotonated at the *meta* position, with the more acidic methyl group still with its full complement of hydrogen atoms.[43] Overall the magnesiate base in Scheme 8 behaves as an alkyl base in effecting this *meta* selectivity. This special regioselectivity toward toluene has never been observed before to any synthetically significant extent by any homometallic base. The *meta* substitution pattern of toluene was quantified through electrophilic quenching studies with trimethylsilyl triflate where after aqueous work up almost quantitative conversion to trimethyl(*m*-tolyl)silane was achieved.

These two deprotonation reactions represented the first examples of AMM*Mg*. In both these cases sodium prefers to interact with the π system of the aromatic ring via an electrostatic interaction while the magnesium form a stronger σ-type bond with the deprotonated substrate. This σ/π notation has become a prominent feature throughout AMM*M*.

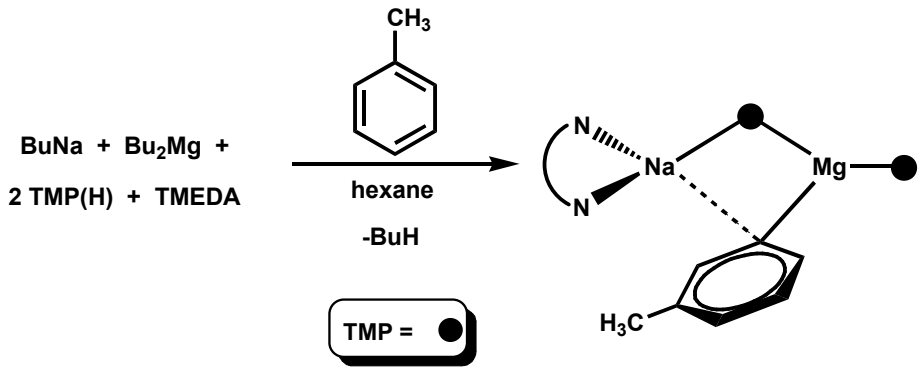

Scheme 8: *Meta*-magnesiation of toluene manifested by the sodium-magnesium base [(TMEDA)Na(*n*Bu)(TMP)Mg(TMP)].

Multiple deprotonations can be accomplished when AMM*M* is applied to metallocene deprotonative chemistry. Until recently, this was the most powerful result and important breakthrough in the development of synergic chemistry, showing that classical molecules in organometallic chemistry, such as ferrocene could be regioselectively fourfold-deprotonated allowing access to new ring substituted derivatives. The use of alkyl lithium reagents, in the presence of a donor solvent such as TMEDA, is the most common route used to deprotonate a metallocene. Both mono- and di-lithiation is possible[47, 48] but controlled higher lithiation had not been achieved to any synthetically useful extent. However, research within our group has shown that using the mixed-metal synergic species 'NaMg(DA)$_3$' (DA = diisopropylamide) has provided a synthetic route to the fourfold-metallation of ferrocene (Scheme 9).[49] This unprecedented regioselective metallation pattern was also successfully extended to the other Group 8 metallocenes ruthenocene and osmocene.[50]

The products of these metallations are 16-atom inverse crown rings of general formula [$Na_4Mg_4(DA)_8$], with metallocene cores regioselectively fourfold-deprotonated at the 1,1',3,3' positions. Since magnesium atoms replace the hydrogen atoms these novel metallocenetetraide complexes can be classified as magnesiations (that is, magnesium-hydrogen exchange reactions). The importance of the alkali metal, sodium in this case, is again highlighted, by the fact that magnesium bis(diisopropylamide) is inert towards ferrocene. Similarly, conventional organomagnesium reagents, such as alkyls or Grignards, cannot directly magnesiate these metallocenes showing that the alkali metal boosts the Brønsted basicity of the magnesium reagent allowing metallation to occur.

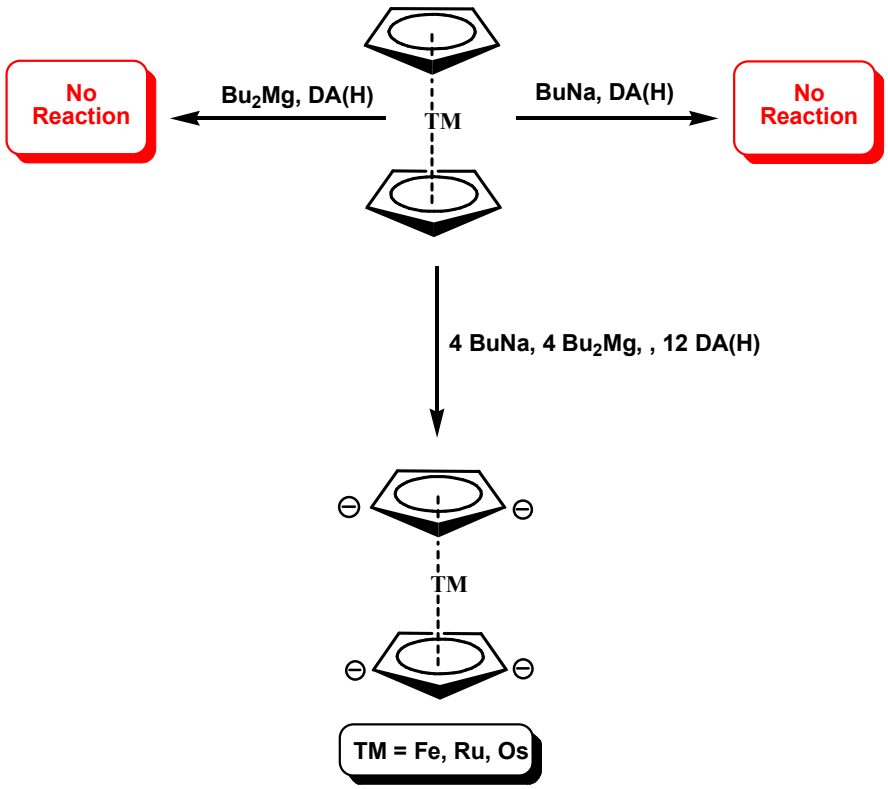

Scheme 9: Synergic synthesis of fourfold-metallated metallocenes, omitting inverse crown host ring.

The success of these AMM*Mg* reactions opened up a new area of study within the Mulvey research group. The most important aspect to address was whether the synergic effect could be applied, or even improved upon by using different metal partners in place of magnesium?

In this regard both zinc and aluminium proved to offer similar synergic reactivities in the form of new alkali metal-zinc and alkali metal-aluminium bases. Thus in particular the zinc reagent [(TMEDA)Na(TMP)(*t*Bu)Zn(*t*Bu)][51] made from the co-complexation of NaTMP, tBu$_2$Zn, and TMEDA showed a large degree selectivity in deprotonation reactions of a wide range of aromatic substrates. This zincate base agrees closely to the structural template for the aforementioned magnesiate base [(TMEDA)Na(*n*Bu)(TMP)Mg(TMP)] but with the distinction of a bisalkyl-monoamido composition rather than a monoalkyl-bisamido one. Benzene is easily zincated by this sodium/zinc base to afford heterotrileptic [(TMEDA)Na(TMP)(C$_6$H$_5$)Zn(*t*Bu)][51] showing overall alkyl basicity through the loss of the expelled bridging *t*Bu group in the form of *iso*-butane. This regioselective metallation can be extended further to polycyclic

aromatic compounds using the same sodium-TMP zincate reagent. Thus naphthalene can be transformed into zincated derivatives that are not directly accessible via mainstream organozinc reagents. These AMM*Zn* reactions with naphthalene show a high degree of stoichiometric control as mixtures in a 1:1 ratio afford the mono-zincated complex [(TMEDA)Na(TMP)(2-$C_{10}H_7$)Zn(*t*Bu)], while in contrast 1:2 ratios produce predominately the dizincated modification [$(TMEDA)_2Na_2$(2,6-$C_{10}H_6$)$Zn_2(TMP)_2$(*t*Bu)$_2$] (Scheme 10). These selective metallations are a considerable improvement on conventional metallation reactions of naphthalene performed by BuLi[52] and LIC-KOR[53] reagents in which nonselective mixtures of the 1- and 2-monosubstituted isomers are generated along with all ten possible disubstituted isomers.

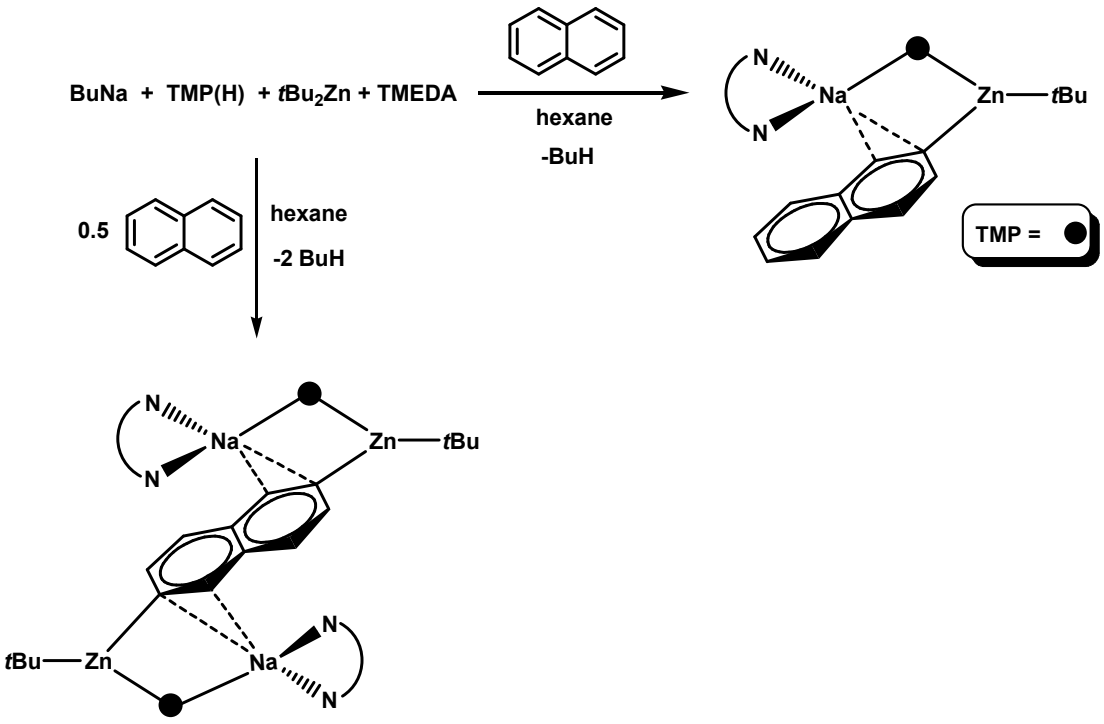

Scheme 10: Regioselective mono- and di-zincation of naphthalene.

Turning to the Group 13 aluminium, the TMP-aluminate reagent [(TMEDA)Li(TMP)(*i*Bu)Al(*i*Bu)$_2$] also exhibited synergic reactivity when reacted with N, N-diisopropylbenzamide. Acting as a dual alkyl/amido base it surprisingly produced the novel heterobimetallic-heteroanionic complex [{PhC(=O)N(*i*Pr)$_2$}.Li{2-[1-C(=O)N(*i*Pr)$_2$]C_6H_4}{$Me_2NCH_2CH_2N(Me)CH_2$)}Al(*i*Bu)$_2$][54] which in addition to having an *ortho*-deprotonated benzamide ligand, also contains a methyl-deprotonated TMEDA ligand. The structure is completed by a neutral benzamide ligand which is

coordinated to the lithium through its carbonyl function (Scheme 11). Deprotonation/alumination of TMEDA was particularly unexpected as NC(*H*) bonds of amines are normally difficult to cleave.

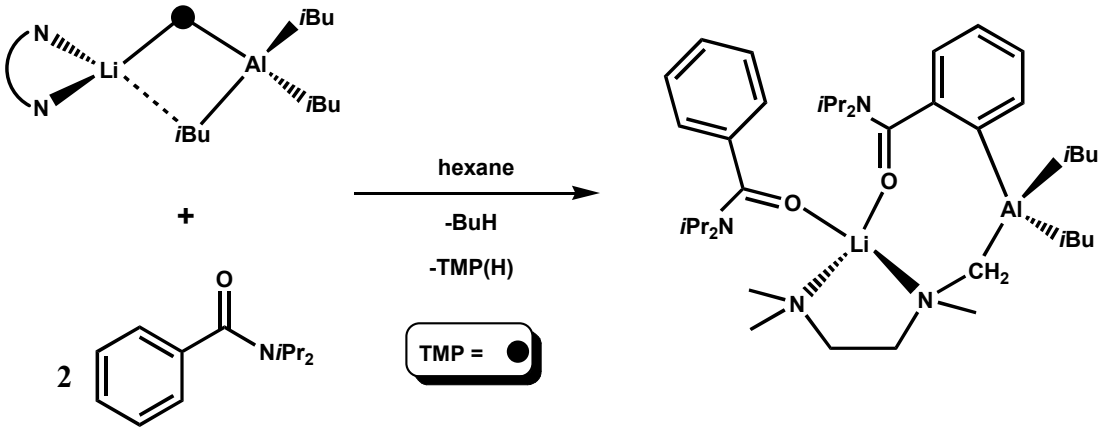

Scheme 11: Synthesis of a novel heterobimetallic-heteroanionic lithium aluminate complex.

With the Groups success at incorporating zinc and aluminium into our synergic mixed-metal chemistry the next question to be addressed was 'could this synergic chemistry be broadened even more by having a transition metal take the place of magnesium?'

In 2006, our Group were successful in combining an alkali and transition metal within the one synergic molecule. The transition metal alkyl trimethylsilylmethylmanganese $[(Me_3SiCH_2)_2Mn]$ was chosen as the transition metal source due to its thermal stability, strong basicity and lack of β-hydrogen atoms. This manganese(II) reagent was successfully combined with both lithium and sodium amide species to form several new mixed-metal synergic bases. The two most reactive manganese bases to date are the lithium- and sodium-TMP manganates $[(TMEDA)Li(TMP)(Me_3SiCH_2)Mn(CH_2SiMe_3)]$[55] and $[(TMEDA)Na(TMP)(Me_3SiCH_2)Mn(TMP)]$[56] respectively (Figure 6). Both bases have slightly different formulations with the Li/Mn reagent having a monoamido-dialkyl composition while in contrast the Na/Mn reagent has a diamido-monoalkyl one. Both these structures bear a close resemblance to those of Mg- and Zn-TMP metallating reagents, in particular the aforementioned [(TMEDA)Na(TMP)(*n*Bu)Mg(TMP)] and [(TMEDA)Na(TMP)(*t*Bu)Zn(*t*Bu)], thus arguing well for their potential to execute alkali-metal-mediated manganation (AMM*Mn*).

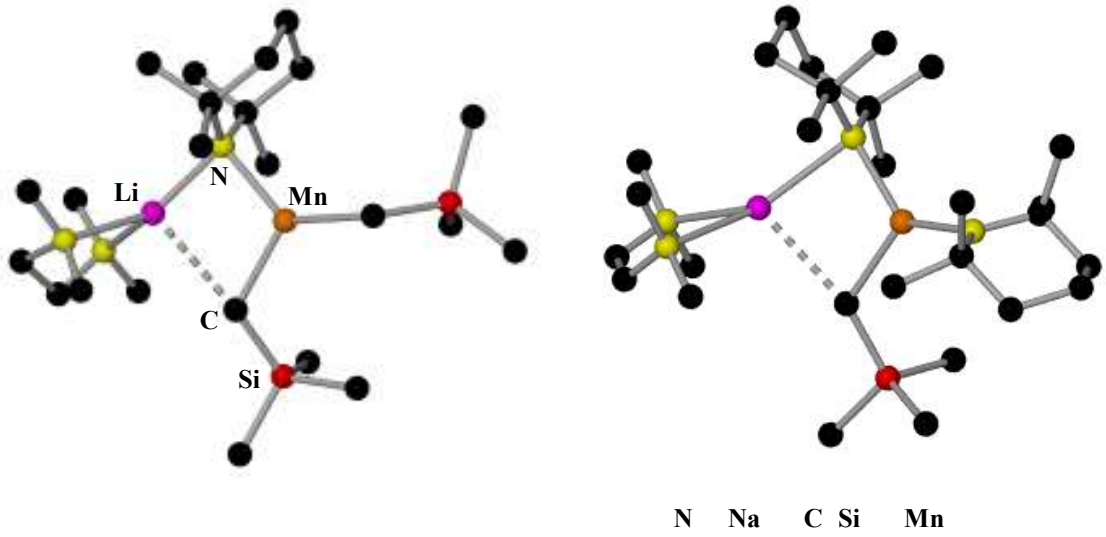

Figure 6: Molecular structures of the Li/Mn (LHS) and Na/Mn (RHS) synergic bases.

Ferrocene was the first substrate chosen for testing the manganating ability of the new Li/Mn reagent [(TMEDA)Li(TMP)(Me_3SiCH_2)Mn(CH_2SiMe_3)], and the reaction afforded the trinuclear ferrocenophane [(TMEDA)$_2$Li$_2$Mn$_2${Fe(C_5H_4)$_2$}$_3$][55] (Figure 7). In this product ferrocene has been selectively two-fold deprotonated in the 1, 1'-positions by Mn(II) and thus it was proof of the concept AMM*Mn*. Previous to this work no reactions or crystal structures had been reported where direct manganation of an aromatic molecule has been accomplished.

Investigations into the reactivity of these new Mn(II) alkali-metal bases continued when benzene was reacted with the sodium/manganese base [(TMEDA)Na(TMP)(Me_3SiCH_2)Mn(TMP)].[56] This reaction produced the new aryl manganate [(TMEDA)Na(TMP)(C_6H_5)Mn(TMP)][56] (Scheme 12), in which benzene has been mono-deprotonated. Extending this chemistry to synthesize a transition metal host inverse crown proved fruitful. Changing the reaction stoichiometry to a 4:6:2:1 mixture of BuNa, TMP(H), Mn(CH_2SiMe_3)$_2$ and benzene respectively, without TMEDA, gave the unique manganese-based inverse crown complex [Na_4Mn_2(TMP)$_6$(C_6H_4)][56] (Scheme 12). This complex comprises a 12-atom 'host' ring, in which a 'guest' dianion of benzene has been selectively manganated in the sterically optimal 1- and 4-positions and trapped in the core. These initial results of AMM*Mn* show that the application of transition metals in synergic chemistry is realistic.

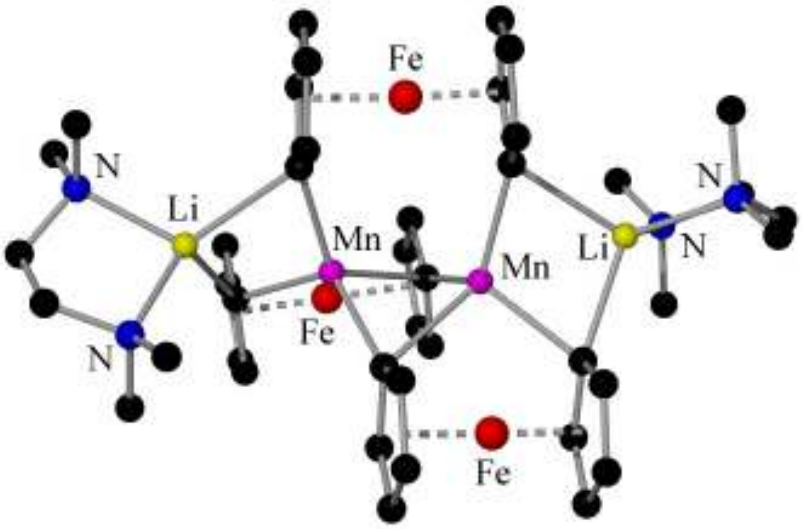

Figure 7: Molecular structure of $[(TMEDA)_2Li_2Mn_2\{Fe(C_5H_4)_2\}_3]$.

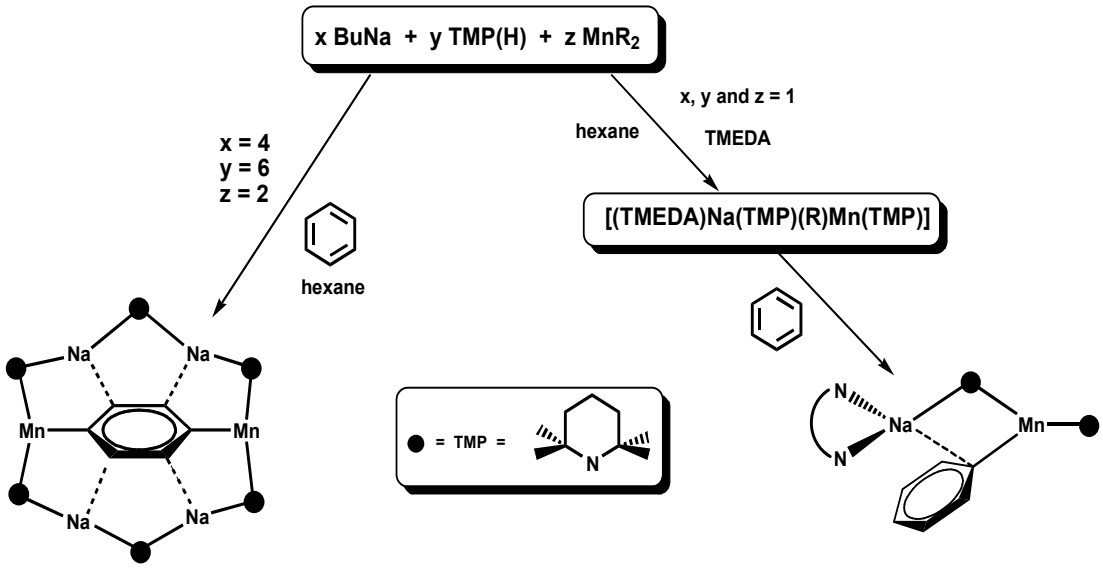

Scheme 12: Products of the AMM*Mn* of benzene with (RHS) and without (LHS) the participation of TMEDA.

1.3. Directed *Ortho*-Metallation

As the main aim of this Ph.D. research programme was to develop the AMM*Mn* of aromatic molecules, it is germane to present some background on the long established concept of *ortho*lithiation. Directed *ortho*-Metallation ('D*o*M') is one of the most important synthetic tools available to the modern synthetic chemist that allows the functionalization of a rich, diverse variety of aromatic substrates. D*o*M has arguably

surpassed electrophilic aromatic substitution in terms of its versatility and scope. Pioneered by Wittig[57] and Gilman[52] and first applied to the metallation of anisole it can be defined as the metallation, usually lithiation of a proton of a C-H bond on an aromatic ring adjacent to a heteroatom containing functional group.[2] Over the years this area of chemistry has substantially increased and there are now many directing groups available for exploitation on various aromatic substrates.[58, 59] The process of *ortho*lithiation is most commonly carried out by butyllithium or lithium diisopropylamide with the deprotonation process having two main contributing factors that are depicted in Scheme 13.

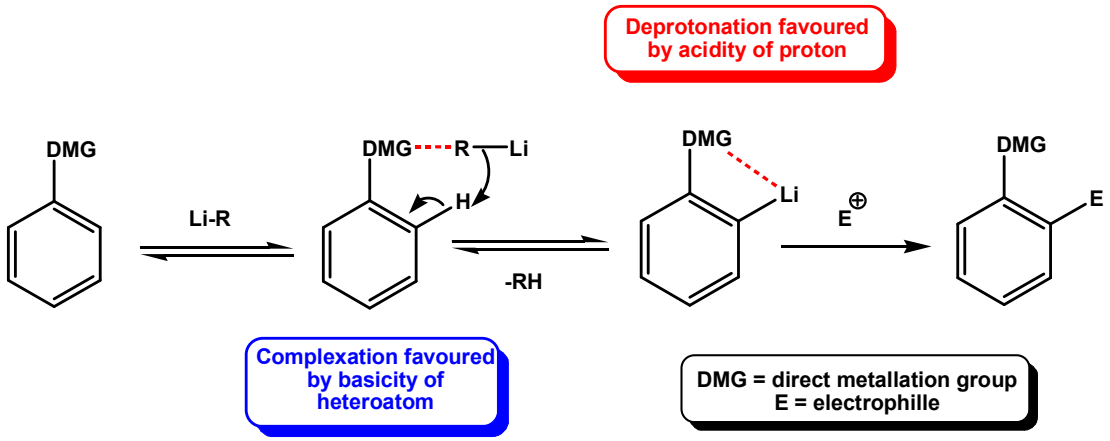

Scheme 13: A simple description of the DoM process.

D*o*M depends critically on the substituent, the heteroatom in particular, providing the alkyl lithium (or another base) with a point of coordination, thus enhancing the reactivity close to the coordination site and hence directing the regioselectivity to a specific site (the *ortho* position). However the ability of the directing group to acidify the nearby protons via an inductive effect is also a crucially important aspect of D*o*M. When coordination to the heteroatom is geometrically or electronically prohibited, it is the inductive effect that directs the lithiation. The most effective directing groups for deprotonation therefore have a balance of strong coordination to the organometallic reagent and excellent electron withdrawing properties.

Directing groups can be classed into two different main categories namely strong D*o*M or weak D*o*M groups. Strong D*o*M groups comprise of carboxylic acid and carbonyl derived functions containing both oxygen and nitrogen (Scheme 14). These functional groups have a highly basic heteroatom as well as many of them being strongly electron

withdrawing which acidifies adjacent hydrogen atoms of the aromatic ring. However they do have a drawback, in that they all contain an electrophilic carbonyl group which itself can suffer attack by the lithiating reagent, so the metallation reaction usually has to be done at sub-ambient temperatures (−78 to −50°C).

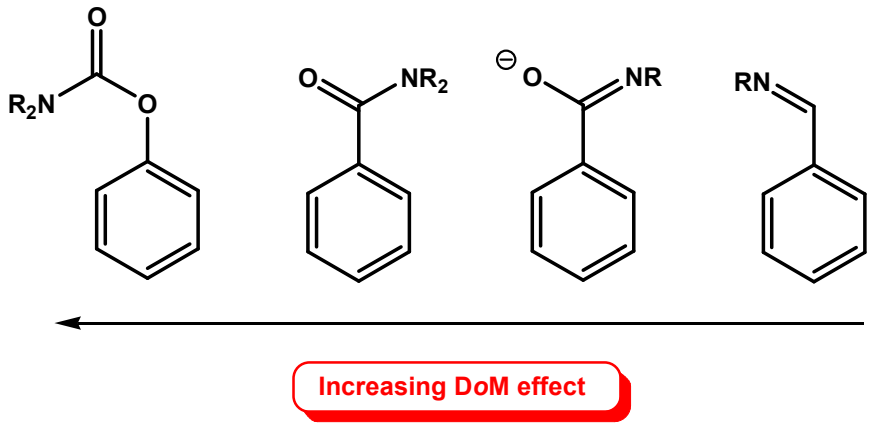

Scheme 14: A selection of strong D*o*M groups.

Weak D*o*M groups can be oxygen only based such as ethers, acetals, and carboxylates or nitrogen-only based functional groups such as amines, anilines or nitriles (Scheme 15). They are less powerful in terms of their directing ability, due to them being less basic and less acidifying in character. They typically undergo direct metallation at a slower rate and often higher temperatures have to be used. Nonetheless, their main advantage is that they do not undergo attack from the lithiation reagent. Finally, halogens can also be classed in this category as they rely solely on an inductive, acidifying effect, however, they are often seen as a less important class of director.

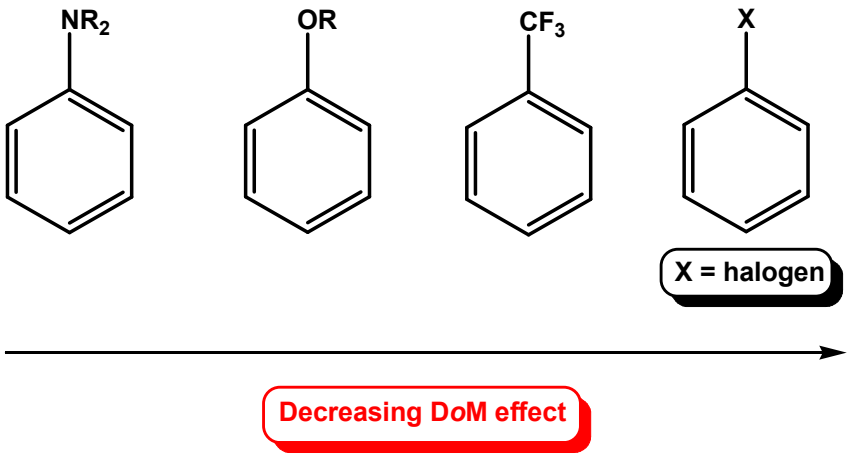

Scheme 15: A selection of weak DoM groups.

The D*o*M process is so widely applicable today that almost every substrate featured in this thesis has at some point been previously subjected to D*o*M with conventional monometallic reagents such as alkyllithiums. With recent developments in D*o*M chemistry it has now been successfully established that through AMM*Zn* and AMM*Mg* many of the substrates have also been directly zincated or magnesiated, the majority of which are inert towards metallation with the parent homometallic Zn/Mg reagents. However, the bulk of these substrates have never been manganated (or directly manganated) especially under such mild reaction conditions as will be discussed in detail in the results and discussion part of this thesis.

The success of these preliminary results on alkali-metal mediated manganation opened up a new area of study within the research group. This brief outline brings the research within the Mulvey group to its current point, and consequently the starting point for the experimental programme followed in this Ph.D. study.

Chapter 2. Introduction to Organomanganese(II) Chemistry

The synthetic and structural organometallic chemistry of Mn in the +2 oxidation state is atypical of organotransition metal chemistry in general due to the observation of the essentially ionic manganese(II)-carbon bond, a property more commonly observed in s-block organometallic compounds. Compared to other main group and transition metals like palladium, nickel, rhodium and ruthenium manganese offers other attractions especially important in the context of modern industrial chemistry such as its relative cheapness, toxilogical benignity and high relative natural abundance which is in plentiful supply globally in the form of high grade ores.[60] Therefore it might seem somewhat surprising that it is only in the past 30 years that its synthetic potential in a range of novel applications in both organic and organometallic synthesis and polymerisation catalysis have been developed. In stark contrast to this, organomanganese(I) chemistry is much better developed. For example the (direct) cyclomanganation of substituted, donor activated arenes by Mn(I) reagents such as R'$Mn(CO)_5$ (R' = Me, CH_2Ph, etc) is a well documented methodology[61] that finds extensive employment in organic synthesis. Recently a comprehensive review by Layfield[62] on manganese(II) organometallics was published highlighting its many useful synthetic applications and diverse structural chemistry. However, for brevity this chapter will only summarise some key developments in manganese(II) chemistry particularly focusing on alkyl and mixed-metal systems relevant to the work carried out during this project.

2.1. Organomanganese(II) History

Scheme 16: Synthesis of manganocene.

As long ago as 1937 Gilman[63, 64] reported the first organometallic complexes of manganese(II), Ph_2Mn and PhMnI made from the reaction of phenyllithium and the salt manganese iodide in etheral solutions however neither was isolated nor structurally characterised. In 1954 Wilkinson reacted $MnCl_2$ with NaCp (Cp = C_5H_5) forming the

first well-defined organomanganese complex $Mn(Cp)_2$ (manganocene) (Scheme 16)[65, 66] that was found to adopt a very unusual structural composition compared to that of the related metallocenes $M(Cp)_2$ M= V, Cr, Fe, Co, and Ni which all share the usual 'sandwich' metallocene structure. Manganocene in contrast adopts a polymeric zig-zag structure (Figure 8) which more closely resembles that of main group metal cyclopentadienyl structures.[67] Its enhanced reactivity, in comparison to the other 3d metallocenes, can be attributed to its highly polar Mn(II)-C bonds making it a useful reagent for the synthesis of Mn(II) containing complexes with many reported structural and magnetic studies on simple substituted derivatives reported in the literature.[68, 69]

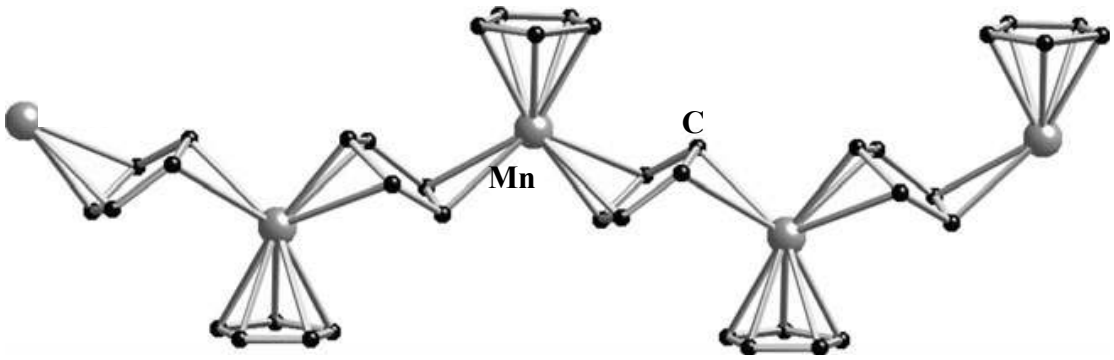

Figure 8: A segment of the polymeric structure of $Mn(Cp)_2$.

Manganocene has been widely studied by Wright and Layfield for the synthesis of Mn(II)/amido cage complexes that exhibit interesting deprotonative and magnetic properties.[70] In one study $Mn(Cp)_2$ twofold deprotonates the pyrimidine substituted primary amine [2-NH_2(4,6-Me_2(N_2C_4H)] to give the high nuclearity Mn(II)-nitrogen cage complex [(η^5-Cp)Mn{2NH(4,6-Me_2pm)}.Mn{N(4,6-Me_2pm)}]$_4$[71] (pm = pyrimidine) (Scheme 17) which represents a novel example of a manganese(II) imide compound.

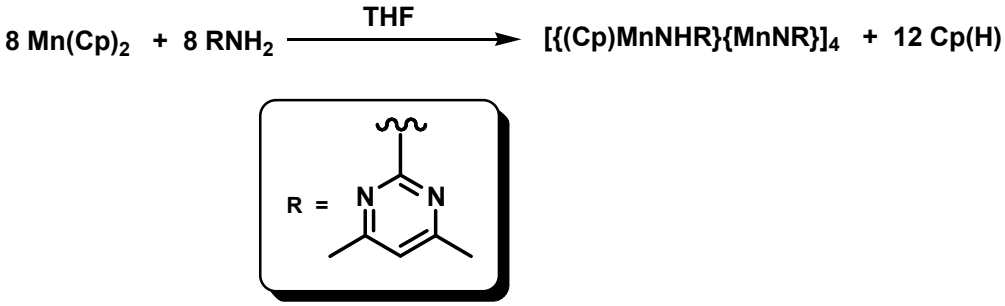

Scheme 17: Double deprotonation of an amido-pyrimidine with $Mn(Cp)_2$.

Following the pioneering work on manganocene by Wilkinson, organomanganese(II) chemistry evolved at a relatively slow rate with only sporadic reports in the literature on the reactivity and preparation of new complexes. In 1976 Cahiez and Normant prepared three new types of organomanganese reagent, namely organomanganese halides (RMnX), dialkylmanganeses (MnR_2) and tri- and tetra-organomanganates (R_3MnM or R_4MnM_2; M= Li or Mg) all prepared via transmetallation approaches (Scheme 18). A wide variety of alkyl, alkenyl, alkynyl, allyl, benzyl, aryl or heteroarylmanganese compounds can be prepared by these methods with the only limitation being in the preparation of the starting organolithium or organomagnesium reagent.[72, 73] The successful synthesis of these organomanganese reagents opened up the possibility of them being potentially useful in organic/inorganic synthesis. Note that these reagents are generally utilised in ethereal-type solvents (commonly ether or THF). Each of these complex types will now be discussed briefly in turn.

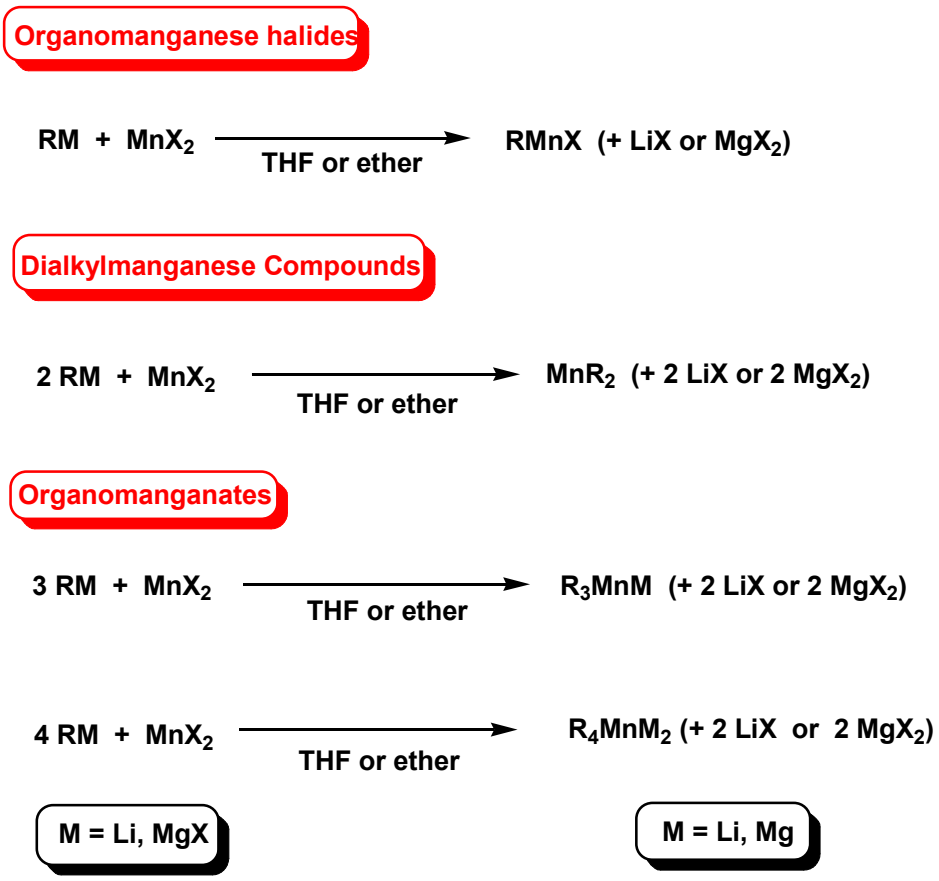

Scheme 18: Preparation of different types of organomanganese complex.

2.2. Organomanganese Halides, RMnX

Organomanganese halides, RMnX, conform to the same general formula as their parent Mg analogues, Grignard reagents, which are one of the most widely used synthetic reagents in the world. However, in contrast, their organomanganese analogues are not as widespread in organic chemistry receiving until recently very little synthetic use or attention. Lately, Cahiez has utilised organomanganese halides in a variety of organic applications. For example, his group reported the successful cross-coupling of a variety of organomanganese halides with functionalised aryl halides or triflates under Pd catalysis to produce functionalised unsymmetrical biaryl products in moderate to high yields (Scheme 19). They have also shown that transition metal catalysed (Cu or Fe) coupling reactions of organomanganese reagents with alkyl and vinyl halides are extremely efficient and of synthetic interest in preparative organic chemistry due to their high yielding nature, selectivity, and employment of relatively mild experimental conditions.[74-76] Organomanganese halide reagents have also been utilised in nucleophilic addition reactions with ketones, aldehydes, carbon dioxide, and isocyanates[77, 78] with some reaction conditions achieving high levels of chemo- and regioselectivity.[72, 79, 80]

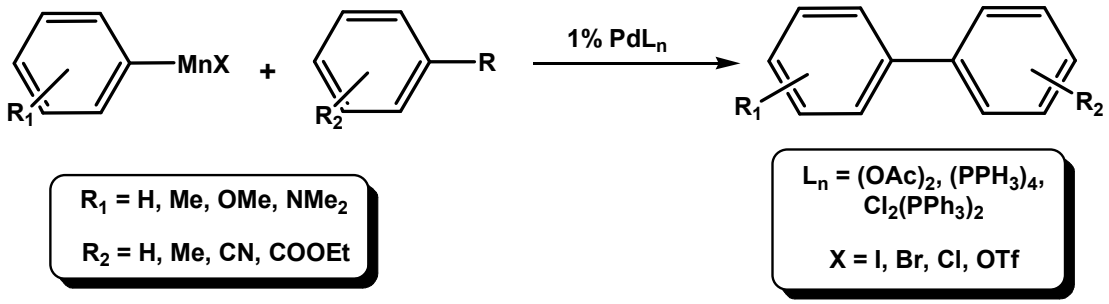

Scheme 19: Typical Pd catalysed cross-coupling reactions involving organomanganese halides.

However this chemistry has its disadvantages and limitations. To elaborate, the synthesis of the organomanganese halide is limited to the range of Grignard reagents available, which have functional group tolerance problems associated with them (esters, ketones, nitriles etc. are not generally compatible with Grignard reagents and readily lead to undesired decomposition products). Also the formation of an ionic salt co-product is not always advantageous and can lead to solubility problems in common

organic solvents. More expensive, polar solvents must be used as an alternative, which greatly increases the costs involved, especially in large scale applications.

2.3. Dialkylmanganese Complexes, MnR_2

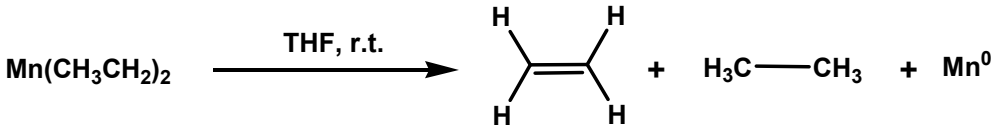

Scheme 20: Typical decomposition of a dialkylmanganese(II) complex.

Known for several decades dialkylmanganese(II) reagents are commonly prepared through the *in situ* reaction of $MnCl_2$ and a Grignard reagent. Studied in the 1970s mainly by Kochi[81] they tend to decompose through β-hydrogen elimination reactions commonly seen in alkyl transition metal derivatives to give a mixture of alkane and alkene (Scheme 20) making them the least stable of the Mn(II) reagents depicted in Scheme 18. For this reason, and their extremely air-sensitive nature, few dialkylmanganese(II) complexes have been isolated from solution and fully structurally characterised.

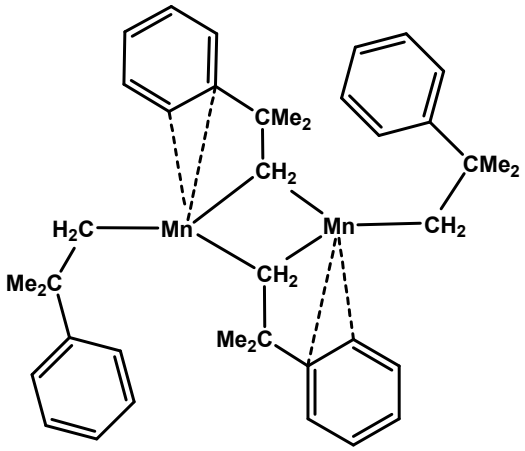

Figure 9: Structure of dineophylmanganese(II).

However, when the alkyl group contains no β–hydrogen atoms the dialkylmanganese(II) compound has an enhanced stability which has allowed several dialkylmanganese(II) complexes to be structurally characterised over the years. For example, these include the bulky monomeric $[Mn\{C(SiMe_3)_3\}_2]$,[82] the dimeric neophyl complex $[Mn(CH_2CMe_2Ph)_2]_2$ (Figure 9),[83] the trimeric $[Mn(2,4,6\text{-}C_6H_2Mes_3)_2]_3$[84] and the

tetrameric $[Mn(CH_2CMe_3)_2]_4$[83] complex. Several Lewis base adducts of these and other dialkylmanganese(II) complexes have also been reported[83, 85-89] There is also an example of a polymeric dialkyl species namely bis(trimethylsilylmethyl)manganese(II) $[Mn(CH_2SiMe_3)_2]_\infty$,[83] first prepared in 1976, which plays an important role in the new synergic chemistry carried out in this Ph.D. research project and which therefore will be discussed in full detail in the results and discussion section of Chapter 3.

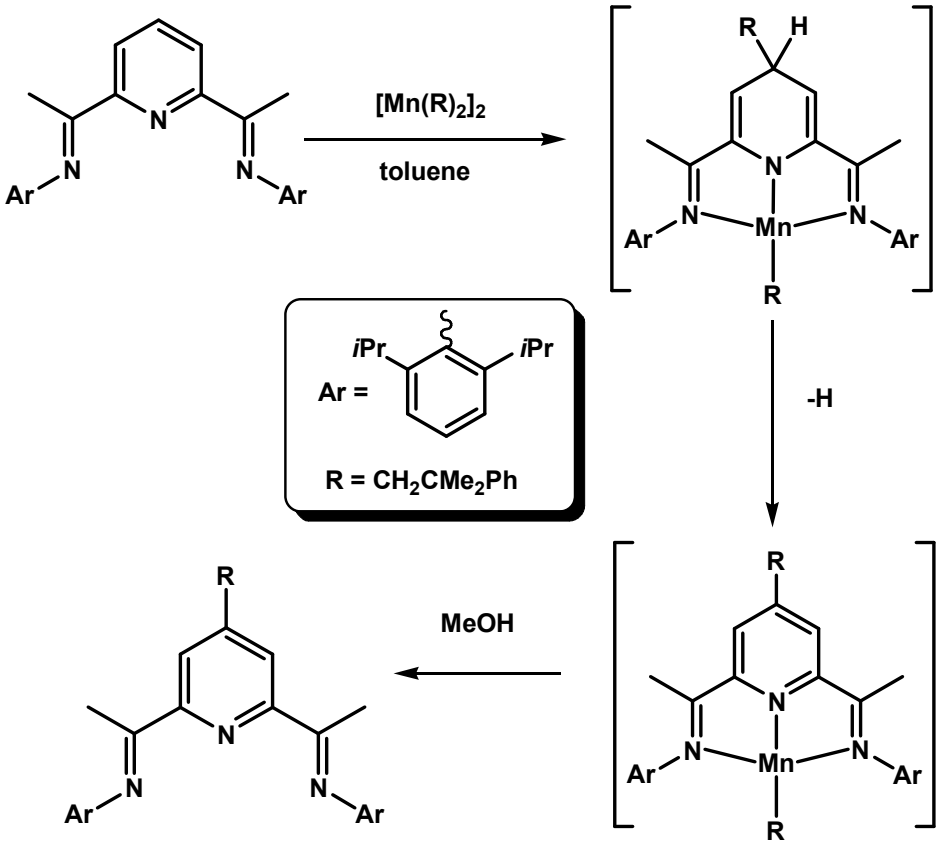

Scheme 21: Reaction of a 2,6-diiminopyridine derivative with a dialkylmanganese(II) reagent.

From a synthetic standpoint dialkyl manganese(II) complexes are gaining in popularity in a wide range of organic reaction applications. For example, while diiminopyridines ligands are known with a wide variety of substituents on the terminal imine nitrogen atoms, substitution of the pyridine ring itself is a synthetically much more challenging task. These ligands are used extensively in iron and cobalt complexes due to their high reactivity in olefin polymerisation catalysis.[90-92] Recently the dialkylmanganese reagent $[Mn(CH_2CMe_2Ph)_2]_2$ has been used for the direct alkylation of the pyridine ring in these 2,6-diiminopyridine ligand systems (Scheme 21).[93] The versatility of this reaction has been demonstrated by the use of a variety of dialkylmanganese(II)

complexes allowing various alkyl groups (e.g. CH_2CMe_2Ph, CH_2Ph and CH_2CHCH_2) to be substituted on the pyridine ring. These new 4-alkylated iminopyridine ligands, not available through conventional metallation, are being currently investigated as new ligand systems for olefin polymerisation.[93] Note, however, there have been no structural characterisation of the manganese intermediates involved in these reactions.

Recently dialkylmanganese(II) complexes have also been used to probe how organometallic compounds attach to solid supports, such as silica. To elaborate the dialkylmanganese(II) complex $[Mn(CH_2tBu)_2(TMEDA)]$[83] reacts with silica, partially dehydroxylated at 200, 300, 500 and 700°C, via deprotonation of the hydroxyl groups to produce various Mn(II) grafted complexes.[94] It is reported that at higher silica dehydroxylation temperatures less Mn(II) is grafted onto the silica surface. During the reaction it was possible to isolate and structurally characterise two separate complexes namely the mono-siloxy complex $[(\equiv SiO)Mn(CH_2tBu)(TMEDA)]$ and the cyclic bis(siloxy) complex $[(\equiv SiO)_2Mn(TMEDA)]$[94] (where ≡SiO = four-coordinate surface silicon) which were found in different proportions dependent on the silica dehydroxylation temperature (Scheme 22).

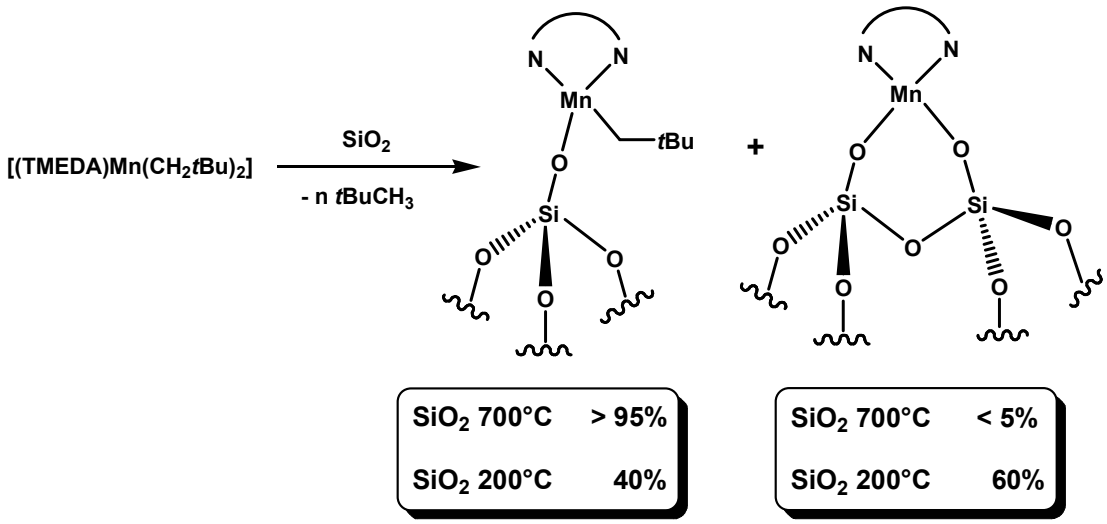

Scheme 22: Surface complexes from reaction of $[(TMEDA)Mn(CH_2tBu)_2]$ with pre-treated silica at different temperatures.

2.4. Organomanganates

Tri- and tetra-alkylmanganates ($MMnR_3$ or M_2MnR_4 respectively; M= Li or Mg) are amongst the most stable organomanganese complexes represented in Scheme 18 making them easier to isolate, study, and characterise. Wilkinson synthesised the first examples of tetra-alkylmanganates in 1976 which were isolated as Et_2O, THF, or TMEDA solvates of formula $[Li_2MnMe_4.0.5(Et_2O)]$, $[Li_2MnMe_4.2(THF)]$, or $[Li_2MnMe_4.2(TMEDA)]$.[83] However, although there is discussion about isolating crystals in the paper only microanalysis and melting point data are actually reported. A decade on in 1988 Power reported the first structurally characterised trialkyl manganates in $[\{Li(Et_2O)_2\}_2Mn_2Ph_6]$, $[Li(THF)_4]_2[Mn_2Ph_6]$ and $[Li(THF)_4][MnMes_3]$[95] (Mes = 2,4,6-$Me_3C_6H_2$) which were all synthesised from the reaction of three molar equivalents of their parent aryllithium reagents with manganese bromide or iodide (Scheme 23). Since these initial studies there have been a few other contributions to the area by various different research groups allowing the isolation and structural characterisation of several new organomanganate complexes such as $[Li(TMEDA)]_2[MnMe_4]$,[96] $[Li(TMEDA)]_2[MnEt_4]$,[97] and $[Li(TMEDA)]_2[Mn(CH_2CH_2tBu)_4]$.[97] In all of these structures the Mn(II) atoms adopt a four-coordinate, tetrahedral geometry.

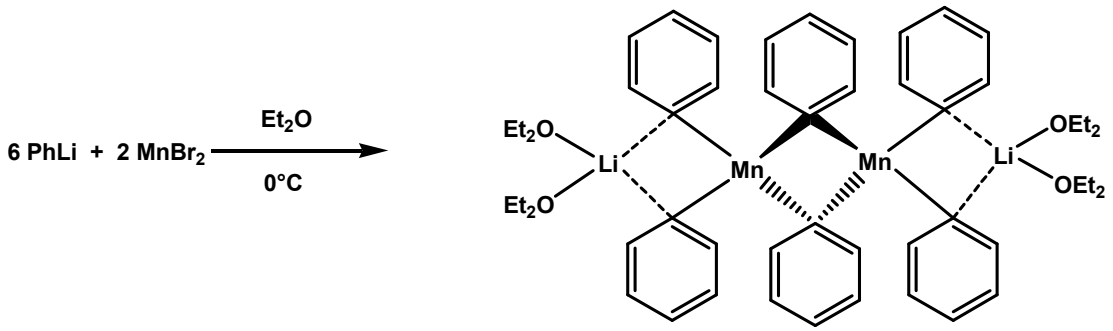

Scheme 23: Synthesis of the hexaorganomanganate $[\{Li(Et_2O)_2\}_2Mn_2Ph_6]$.

As a developing class of ate reagent, organomanganates offer versatility in various organic synthetic applications. Oshima[98] reports in an excellent review their wide-ranging employment in alkylation, addition, and radical cyclization reactions some of which can even be done catalytically. For example, the treatment of *gem*-dibromocyclopropanes with a trialkylmanganate gives dialkylated cyclopropanes after treatment with an electrophile (Scheme 24). This reaction involves a manganese-

halogen exchange step followed by an alkyl migration under Br^- elimination finished by an electrophilic quench to give the final product.

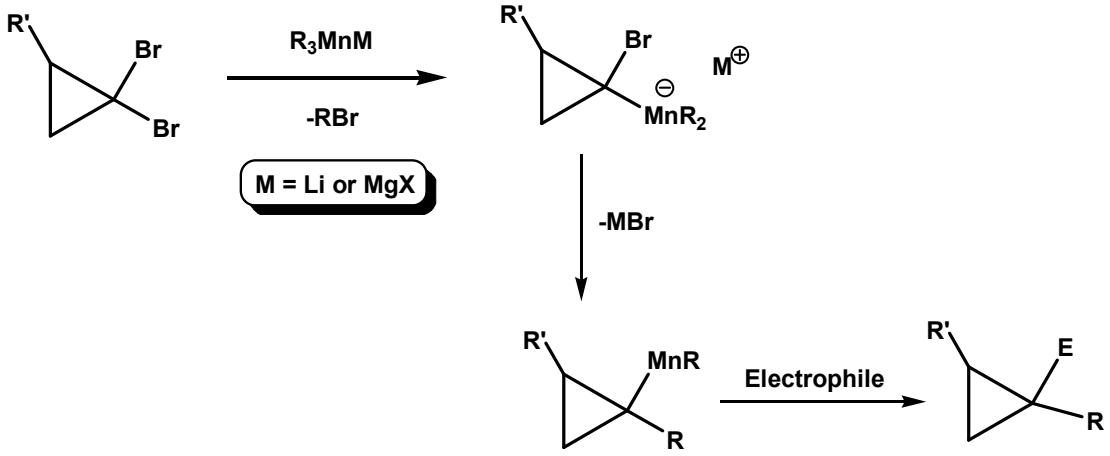

Scheme 24: Reaction of a *gem*-dibromocyclopropane with a trialkylmanganate.

In another synthetic application Hosomi[99] showed through manganese-hydrogen exchange reactions that treatment of allylic or prop-2-ynylic bromides with the tetrabutyl-manganate Bu_4MnLi_2 leads to the formation of a new allylated or prop-2-ynylated product in high yield (Scheme 25). They propose the reaction proceeds through an intermediate allylic manganese species; however, it should be noted that no structural characterisation of the intermediate was achieved with only the air-stable products of electrophilic quenches being isolated and characterised.

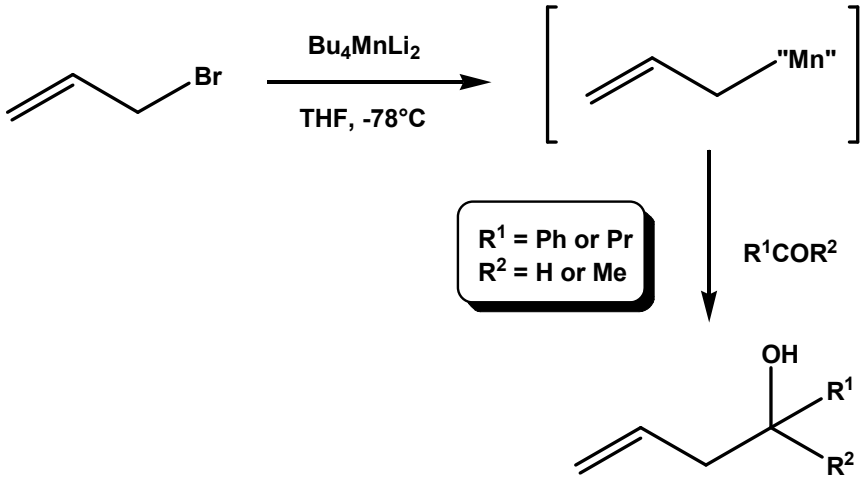

Scheme 25: Typical halogen-manganese exchange reaction.

An important observation to make about these reactions by Oshima and Hosomi in the context of this present research project, is that no direct metallations are observed. Instead the reactions consist of a mixture of nucleophilic addition, halogen-metal exchange or elimination processes.

2.5. Mixed-Metal Manganese(II) Complexes

Structurally characterised heterobimetallic compounds containing Mn in the +2 oxidation state paired with an alkali metal are relatively scarce. Apart from the aforementioned lithium/manganese(II) organomanganates in the previous section most of the previously documented complexes involve the use of the Cp ligand. However, of the complexes that have been structurally characterised some are particularly interesting from a bonding perspective. For example, Layfield has recently reported the mixed manganese(II)/lithium tris(allyl) complex $[Mn\{\eta^3\text{-}C_3H_3(SiMe_3)_2\}\{\eta^3\text{-}C_3H_3(SiMe_3)_2\}_2]^-[Li(THF)_4]^+$[100] which contains both σ and π bound $[(Me_3Si)_2C_3H_3]^-$ allyl ligands in a solvent-separated ion pair arrangement(Figure 10).

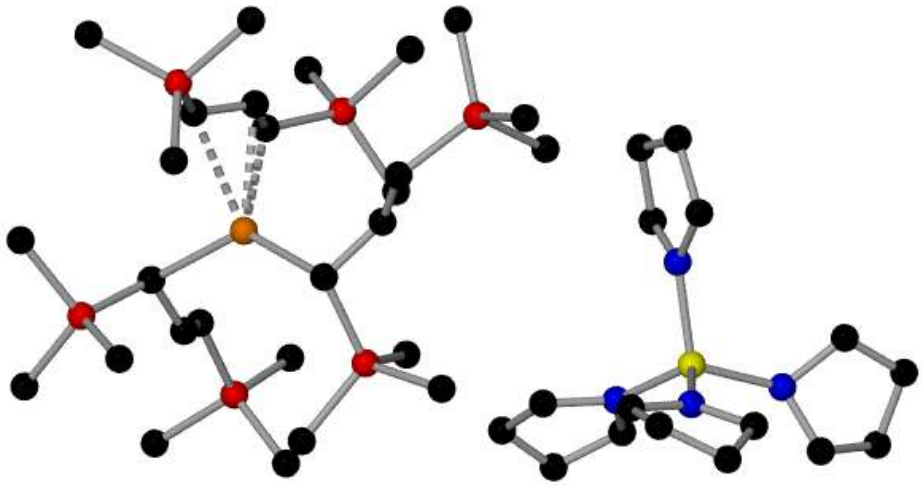

Figure 10: Solvent separated structure of tris(allyl)manganate $[Mn\{\eta^3\text{-}C_3H_3(SiMe_3)_2\}\{\eta^3\text{-}C_3H_3(SiMe_3)_2\}_2]^-[Li(THF)_4]^+$ dashed line indicates π-bonding.

Continuing with the mixed-metal theme, Knochel has recently reported the successful manganation of functionalised arenes and heterocycles using the trimetallic base mixture $(TMP)_2Mn.2MgCl.4LiCl$.[101] This composite manganese base shows a unique

chemoselective reactivity enabling the efficient formation of C-C and C-N bonds. Made by combining two molar equivalents of the commercially available Turbo-Hauser reagent TMPMgCl**.**LiCl (discussed in Chapter 1) with one molar equivalent of $MnCl_2$**.**2LiCl,[102] the manganese amide-halide complex $(TMP)_2$Mn**.**2MgCl**.**4LiCl can be conveniently stored at room temperature in THF solution for over 8 weeks without any signs of decomposition. It displays a distinct reactivity to that of the parent magnesium base TMPMgCl.LiCl. This distinction is depicted in Scheme 26 where the manganese base allows the metallation of 2-phenyl-1,3,4-oxadiazole whereas in contrast the magnesium base produces only ring fragmentation products. [101] This manganation procedure can be extended to a wide range of functionalised aromatic and heterocyclic substrates with the resulting diaryl manganese(II) intermediates reacted subsequently with various electrophiles or alternatively being employed in Pd-catalysed arylations. It should be noted that no structural data on the manganate intermediates of these reactions were reported, meaning the composition of the actual active species performing the deprotonations is unknown as only quenched or cross-coupled products were isolated and identified.

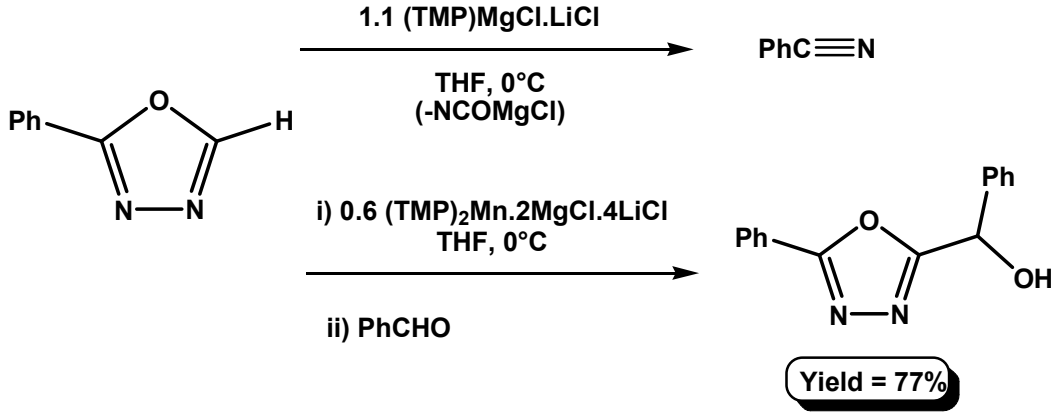

Scheme 26: Contrasting reactivity of magnesium base TMPMgCl**.**LiCl and manganese base TMP_2Mn**.**2MgCl**.**4LiCl towards 2-phenyl-1,3,4-oxadiazole.

Manganese(II) was chosen by our group as a suitable transition metal candidate to replace and mimic magnesium in our mixed-metal synergic base systems due to their similar ionic radii and stable + 2 oxidation states. Within the literature a variety of Mn(II) structures exist that have analogous Mg complexes strengthening our choice of transition metal chosen to substitute magnesium. To illustrate this point, the mixed lithium-manganate trisamide $[Mn\{N(SiMe_3)_2\}_3Li(THF)]$ synthesised by Power[103] in

1984 was the first monomeric homoleptic three-coordinate manganese amide to be structurally characterised and reported in the literature. The isostructural magnesium analogue $[Mg\{N(SiMe_3)_2\}_3Li(THF)]$[104] was synthesised almost 20 years later by our own research group and is known to be the precursor to the oxo-inverse crown complex $[Li_2Mg_2\{N(SiMe_3)_2\}_4(O)]$.[34] Both THF solvates are contact ion pairs with divalent Mg/Mn both having trigonal planar, three-coordinate geometries (Figure 11). This relatively small coordination number is enforced by the large steric bulk of the three HMDS ligands.

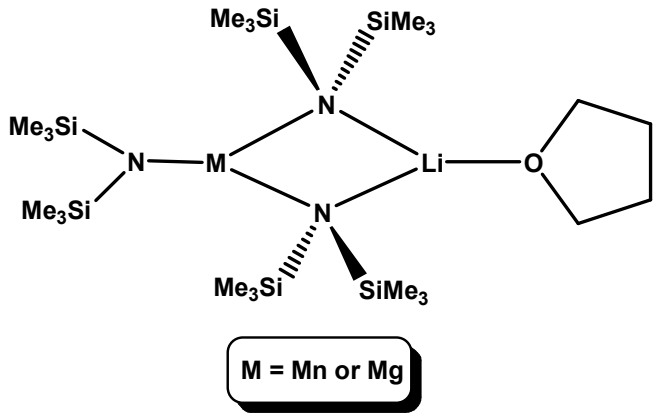

Figure 11: Isostructural molecules of $[M\{N(SiMe_3)_2\}_3Li(THF)]$ where M = Mn or Mg.

The diverse chemistry surrounding organomanganese(II) reagents is unique within organotransition metal chemistry offering not only a wide array of synthetic applications but a fascinating range of structural compositions. Unlike the main group metal Mg and the pseudo main group metal Zn, Mn(II) would potentially open up a 'treasure chest' of new chemistry given the much greater breadth of properties such as redox, magnetic, and catalytic available to an open shell *d*-block element (note Zn has in contrast a full d^{10} shell, which rules out participation of its *d* orbitals in bonding/reactions). By incorporating manganese(II) into our mixed-metal synergic systems we hope to develop the direct manganation (that is manganese-hydrogen exchange reactions) of a wide variety of substrates and at the same time uncover new and exciting compositions and structures.

Chapter 3. Precursors to Mixed-Metal Compounds

This chapter focuses on the structure of the dialkyl manganese(II) compound $[Mn(CH_2SiMe_3)_2]_\infty$, a key precursor to the mixed-metal compounds synthesised in this project, and its reactivity towards a variety of Lewis base donors, amines and ketones. The resulting complexes adopt various structural forms ranging from simple monomeric species to more complex polymers and addition products.

3.1. Bis[(trimethylsilyl)methyl]manganese

The manganese(II) dialkyl compound $[Mn(CH_2SiMe_3)_2]_\infty$ (**1**) was originally synthesised by Wilkinson in 1976[105] but at the time no detailed crystallographic information was reported. In this original paper it states through a personal communication that 'in the crystal the compound is polymeric with alkyl bridges, each Mn(II) atom being four coordinate', but no further details are given. Being a key starting material in our present studies we decided to try and synthesise suitable crystals of $[Mn(CH_2SiMe_3)_2]_\infty$ in order to obtain full crystallographic data of the compound.

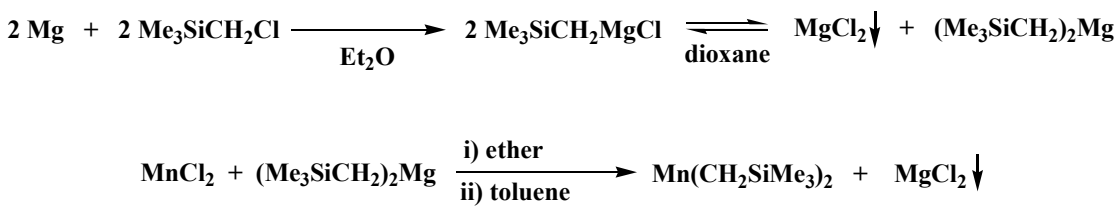

Scheme 27: Synthesis of bis[(trimethylsilyl)methyl]manganese.

Following the original literature,[105] we synthesised **1** by the salt metathesis reaction between the magnesium congener $[Mg(CH_2SiMe_3)_2]_\infty$, which was freshly prepared from the Grignard reagent $(Me_3SiCH_2)MgCl$ by manipulation of the Schlenk equilibrium via the dioxane precipitation method, and $MnCl_2$ in ether solution (Scheme 27). After letting the reaction stir for 3-5 days and replacing the ether solvent with toluene allowed the formation of small bright orange needle crystals of **1** which were initially too small for X-ray crystallographic study. However, by taking a small amount of crystalline **1**

and subliming it at 150ºC under vacuum larger orange prism crystals could be grown which were suitable for X-ray crystallographic analysis. Figure 12 shows a trinuclear section of **1** with relevant bond lengths and bond angles listed in the legend while Figure 13 reveals a longer section of **1** to give an appreciation of its extended polymeric chain structure.

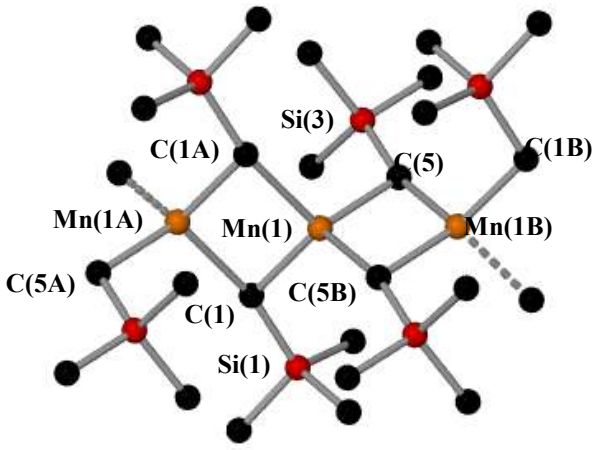

Figure 12: A trinuclear section of $[Mn(CH_2SiMe_3)_2]_\infty$ **1** with selected atom labelling. Hydrogen atoms are omitted for clarity. Selected bond lengths [Å] and bond angles [º]: Mn(1)-C(1), 2.2023(17); Mn(1)-C(1A), 2.4358(17); Mn(1)-C(5), 2.2039(17); Mn(1)-C(5B), 2.4203(17); Mn(1A)-C(1), 2.4358(17); Mn(1B)-C(5), 2.4203(17); Mn(1)···Mn(1A), 2.8874(5); Mn(1)···Mn(1B), 2.8897(5); Mn(1A)···Mn(1)···Mn(1B), 161.39(2); C(5)-Mn(1)-C(5B), 102.81(5); C(5)-Mn(1)-C(1), 120.31(7); C(5)-Mn(1)-C(1A), 114.83(6); C(5B)-Mn(1)-C(1), 114.33(6); C(5B)-Mn(1)-C(1A), 99.84(6); C(1)-Mn(1)-C(1A), 103.18(5); Mn(1)-C(1)-Mn(1A), 76.82(5); Mn(1)-C(5)-Mn(1B), 77.19(5).

The polynuclear molecular structure of **1** shows one unique spiro manganese atom, Mn(1), with its nearest neighbour Mn(1A) and Mn(1B) generated by symmetry. Metal···metal separations [Mn(1)···Mn(1A), 2.8874(5) Å; Mn(1)···Mn(1B), 2.8897(5) Å] in **1** are distinct but essentially equivalent in size. The Mn(1A)···Mn(1)···Mn(1B) linkages are connected via bridging alkyl μ_2-C ligands in a non-linear [161.39(2) Å] arrangement. Each Mn atom makes four discrete Mn-C bonds that can be placed into two categories: short [Mn(1)-C(1), 2.2023(17) Å; Mn(1)-C(5), 2.2039(17) Å] and long [Mn(1)-C(1A), 2.4358(17) Å; Mn(1)-C(5B), 2.4203(17) Å]. The widest bond angle at the metal centre is C(1)-Mn(1)-C(5) [120.31º(7)], and the narrowest is C(1A)-Mn(1)-C(5B) [99.84º(6)], with the overall mean (109.21º) being indicative of a highly distorted

tetrahedral coordination. The α–C(H_2) atoms of the ligand form acute bridges to the metal (mean Mn-C-Mn bond angle 77.00º) to propagate the chain.

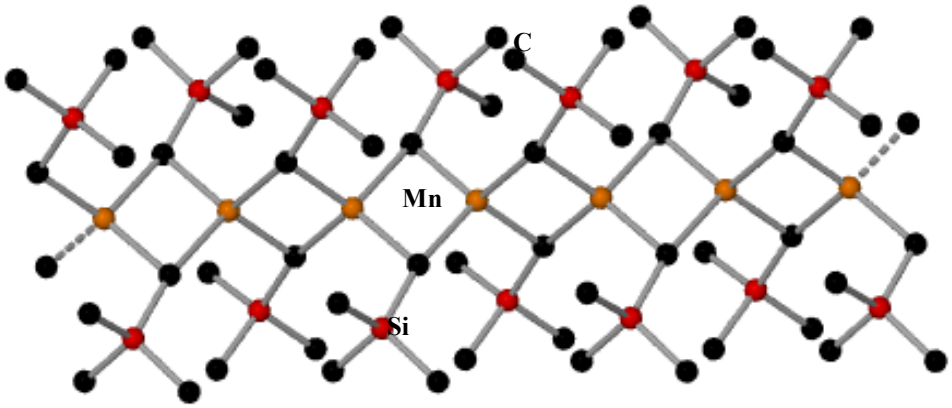

Figure 13: Polymeric chain arrangement of **1** with selected atom labelling. Hydrogen atoms are omitted for clarity.

To the best of our knowledge **1** represents the first structurally characterised example of a polymeric manganese(II) dialkyl complex or indeed of any polymer that propagates through Mn-C-Mn sp^3 σ–bonded linkages. On searching the literature there are two reported Mn(II) polymeric compounds namely the π–bound ionic manganocene [Mn(η^5-Cp)$_2$], which exhibits a Mn-Cp-Mn zig-zag chain arrangement[106] and the recently characterised diphenylmanganese $(MnPh_2)_\infty$ (Ph = C_6H_5) which displays a linear chain like structure.[107] To date the next highest oligomeric manganese(II) diorganyl to be crystallographically characterised is the linear trimer [{Mn(Mes)$_2$}$_3$] (Mes = 2,4,6-$C_6H_2Me_3$), reported by Floriani.[84][108]

With limited previously crystallographically characterised manganese(II) dialkyl polymers available, we can look to its s-block relative Mg(II) for a comparison to **1** given the close similarities between the two metals as discussed in the introduction. The solvent free mixed alkyl-bromide complex $[(Np_3Mg_2Br)_\infty]$ (Np = tBuCH$_2$)[109] provides a relevant example but the best analogy is provided by the isostructural magnesium bis[(trimethylsilyl)methyl] complex $[Mg(CH_2SiMe_3)_2]_\infty$.[110] The polymeric chain structure of $[(Np_3Mg_2Br)_\infty]$ is composed of a mixture of Mg_2Np_2 and Mg_2Br_2 spiro rings in a 3:1 ratio, with Mg-C bonds ranging from 2.20(2) to 2.42(2) Å and thus of a length similar to that of the Mn-C bonds in **1**. In the isostructural $[Mg(CH_2SiMe_3)_2]_\infty$, the bridging alkyl μ_2-C ligands adopt a similar non-linear [164.84(2)º] arrangement to **1** with the Mg-C bond lengths ranging from short [2.2146(9), 2.2159(9) Å] to long

[2.3654(10), 2.3790(9) Å] comparing favourably with those in isostructural **1**. If the bridging ligand is reduced in steric bulk and size to the more planar phenyl group in $(MnPh_2)_\infty$[107] then an overall shorter Mn-C distance is seen [2.245(4) Å; mean 2.316 Å in **1**] as well as a perfect Mn···Mn···Mn linear (180.0º) arrangement. Intranuclear Mn···Mn separations in **1** [2.8874(5) Å] are significantly longer than those in $(MnPh_2)_\infty$ [2.8134(3) Å] and closer to those in the aforementioned trimer $[\{Mn(Mes)_2\}_3]$ (average 2.8515 Å).

3.2. Reactions of $[Mn(CH_2SiMe_3)_2]_\infty$ 1 with TMEDA and Pyridine

Following on from the original communication in 1976 we wanted to obtain structural information on the products obtained from reactions of **1** with some common Lewis bases. We initially reacted **1** with the diamine TMEDA and heterocyclic pyridine. Both Lewis acid Lewis base reactions were previously reported by Wilkinson but with lack of any structural information with only microanalysis and melting point values reported for each compound. Addition of TMEDA or pyridine to a hexane suspension of **1** gives instantaneous bright yellow/orange solutions (Scheme 28). After a few hours stirring at room temperature and reduction of the solvent volume under vacuum bright orange plate crystals were deposited from both reaction solutions. The products of the reactions were $[(TMEDA)Mn(CH_2SiMe_3)_2]$ **2** and $[(pyridine)_2Mn(CH_2SiMe_3)_2]$ **3** in crystalline yields of 32 and 62% respectively. X-ray crystallographic studies established the molecular structures of **2** and **3**.

$$\mathbf{[Mn(CH_2SiMe_3)_2]_\infty + TMEDA \xrightarrow[hexane]{} [(TMEDA)Mn(CH_2SiMe_3)_2]}$$

$$\mathbf{[Mn(CH_2SiMe_3)_2]_\infty + Pyridine \xrightarrow[hexane]{} [(pyridine)_2Mn(CH_2SiMe_3)_2]}$$

Scheme 28: Reactions of $[Mn(CH_2SiMe_3)_2]_\infty$ with TMEDA and pyridine.

The molecular structure of **2** (Figure 14) possesses crystallographic C_2 symmetry with the rotation axis passing through Mn(1) and bisecting TMEDA. Mn(1) occupies a distorted tetrahedral C_2N_2 environment (mean bond angle at Mn(1), 106.77º) forming

short bonds to the anionic C atoms [Mn(1)-C(1), 2.1379(15) Å] and longer dative bonds to the TMEDA N atoms [Mn(1)-N(1), 2.3284(12) Å]. Distortion from perfect tetrahedral geometry is most pronounced at C(1)-Mn(1)-C(1A) [140.50(9)º] which can be attributed to the minimisation of steric clashing between the sterically demanding alkyl ligands. This is offset by an acute N(1)-Mn(1)-N(1A) bond angle [79.92(6)º] imposed by the restrictive bidentate bite of the chelating TMEDA molecule.

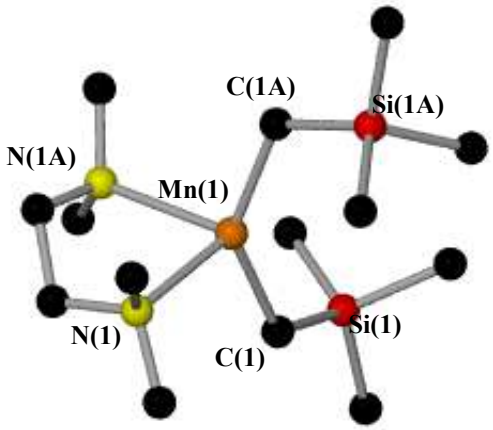

Figure 14: Molecular structure of [(TMEDA)Mn(CH_2SiMe_3)$_2$] **2** with selected atom labelling. Hydrogen atoms are omitted for clarity. Selected bond lengths [Å] and bond angles [º]: Mn(1)-N(1), 2.3284(12); Mn(1)-C(1), 2.1379(15); N(1)-Mn(1)-N(1A), 79.92(6); N(1)-Mn(1)-C(1), 117.68(6); N(1)-Mn(1)-C(1A), 109.26(6); N(1A)-Mn(1)-C(1), 102.92(6); N(1A)-Mn(1)-C(1A), 106.89(6); C(1)-Mn(1)-C(1A), 132.84(7).

The crystal structure of the pyridine complex **3** has two crystallographically independent molecules in its unit cell. As both molecules are nearly identical only one is shown in Figure 15. Both molecules show a distorted tetrahedral C_2N_2 environment for their Mn atoms. Again similar to **2** the σ-bonds between manganese and the carbon atoms [Mn(1)-C(1), 2.144(4) Å; Mn1-C(5), 2.143(4) Å; Mn(2)-C(19), 2.1504(4) Å; Mn(2)-C(23), 2.145(4) Å] are shorter than the manganese-nitrogen bonds of the coordinating pyridines [Mn(1)-N(1), 2.263(3) Å; Mn(1)-N(2), 2.260(3) Å; Mn(2)-N(3), 2.251(3) Å; Mn(2)-N(4), 2.244(3) Å]. The large C(1)-Mn(1)-C(5) [C(19)-Mn(2)-C(23)] bond angle of 138.69(18)º [138.46(17)º] expresses the high steric demand of the two (trimethylsilyl)methyl ligands, whereas the two pyridine molecules with their less bulky

and planar character allow narrower N(1)-Mn(1)-N(2) [N(3)-Mn(2)-N(4)] bond angles of 90.74(12)º [90.87(12)º].

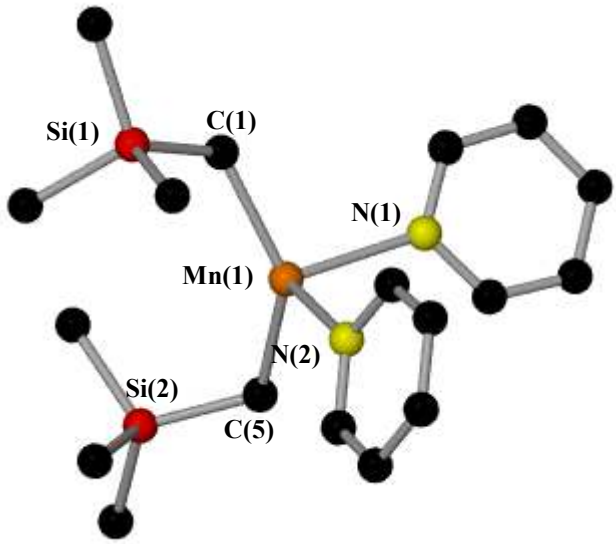

Figure 15: Molecular structure of (pyridine)$_2$Mn(CH$_2$SiMe$_3$)$_2$ **3**. Only one of two independent molecules is shown. Hydrogen atoms have been omitted for clarity. Selected bond lengths [Å] and bond angles [º]: Mn(1)-C(1), 2.144(4); Mn(1)-C(5), 2.143(4); Mn(1)-N(1), 2.263(3); Mn(1)-N(2), 2.260(3); C(1)-Mn(1)-N(1), 104.42(14); C(1)-Mn(1)-N(2), 101.35(14); C(1)-Mn(1)-C(5), 138.69(18); N(1)-Mn(1)-N(2), 90.74(12); N(1)-Mn(1)-C(5), 107.42(16); C(5)-Mn(1)-N(2), 103.83(15).

To the best of our knowledge **2** and **3** are the second and third monomeric bis[trimethyl(silyl)methyl]manganese(II) complexes to be crystallographically characterised after the chiral diamine analogue [((-)-sparteine)Mn(CH$_2$SiMe$_3$)$_2$].[111] Unlike **2** and **3** which were prepared by the direct addition of their Lewis acidic and Lewis basic components, [((-)-sparteine)Mn(CH$_2$SiMe$_3$)$_2$] was prepared by first making the ((-)-sparteine)manganese(II) dibromide complex and then treating it with two molar equivalents of [(trimethylsilyl)methyl]lithium[112] in a metathesis reaction. Searching the CCDB for existing structural examples of TMEDA and pyridine coordinated Mn complexes results in over 80 hits. For comparison to **2** the Mn-N(TMEDA) distances found in polymeric [(TMEDA)MnCl$_2$]$_\infty$ [113] (average 2.361 Å) lie in a similar range to **2** [2.3284(12) Å] while shorter Mn-N distances are observed in the monomeric [(TMEDA)Mn(SSiPh$_3$)$_2$][114] complex (average, 2.258 Å). Turning to the pyridine

complex **3**, similar Mn-N(pyridine) bonds are observed in the HMDS complex $[Mn(HMDS)_2(pyridine)_2]$[115] (average 2.269 Å, cf. 2.255 Å in **3**) while shorter Mn-N bond lengths are observed in the dimeric $[Mn_2(3,5\text{-}t\text{Bu}_2C_6H_2O_2)_2(pyridine)_6]$[116] (average 2.385 Å).

3.3. Reactions of $[Mn(CH_2SiMe_3)_2]_\infty$ 1 with Dioxane

Next we investigated the reaction of **1** with the weaker cyclic donor dioxane. The addition of one equivalent of dioxane to a hexane suspension of **1** afforded an instant light brown solution. After a few hours stirring at room temperature and concentrating the solution under vacuum light pink needle crystals were deposited that were subsequently identified by X-ray crystallography to be the hemi-dioxane complex $[\{(dioxane)[Mn(CH_2SiMe_3)_2]_2\}_\infty]$ **4**. However, if the solution is left to stand for several days at room temperature or alternatively placed in the freezer (at -27ºC) then colourless block crystals are obtained that were structurally identified to be the different, full dioxane complex $[\{(dioxane)[Mn(CH_2SiMe_3)_2]\}_\infty]$ **5** (Scheme 29).

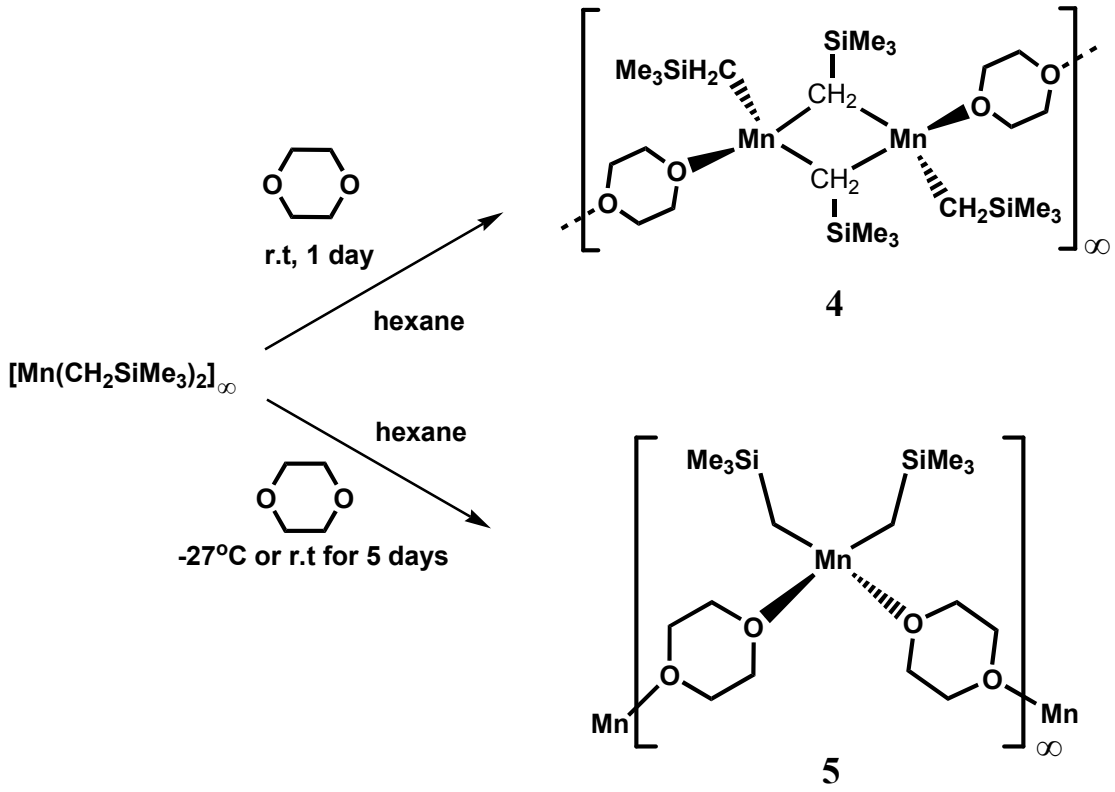

Scheme 29: Synthesis of the hemi- and full dioxane complexes **4** and **5**.

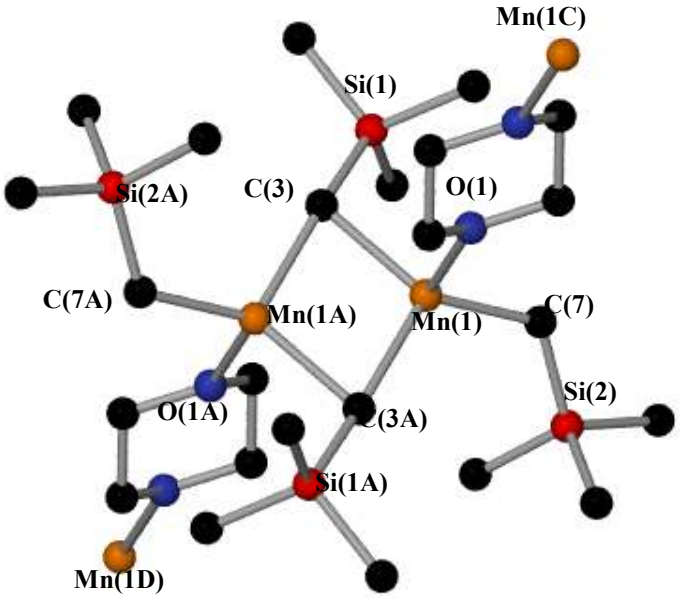

Figure 16: Dimeric section of $[\{(dioxane)[Mn(CH_2SiMe_3)_2]_2\}_\infty]$ **4**. Only one of two crystallographically independent molecules is shown. Hydrogen atoms have been omitted for clarity. Selected bond lengths [Å] and bond angles [º]: Mn(1)-C(3), 2.202(3); Mn(1)-C(3A), 2.365(3); Mn(1)-C(7), 2.120(3); Mn(1)-O(1), 2.2515(15); Mn(1)-Mn(1A), 2.7715(8); O(1)-Mn(1)-C(7), 109.72(9); O(1)-Mn(1)-C(3A), 93.53(8); O(1)-Mn(1)-C(3), 98.18(8); C(7)-Mn(1)-C(3A), 116.26(10); C(7)-Mn(1)-C(3), 127.13(10); C(3A)-Mn(1)-C(3), 105.37(8).

The pink hemi-dioxane **4** (Figure 16 and Figure 17) adopts a polymeric structure, made up of dimeric $[Mn(CH_2SiMe_3)_2]_2$ linked together by dioxane $O(CH_2\text{-}CH_2)_2O$ chairs via dative Mn-O bonds (mean lengths 2.2467 Å). Each Mn centre of the dimeric subunits carries one bridging and one terminal alkyl ligand making it part of a planar $(MnC)_2$ ring. There are two crystallographically distinct polymeric chains, though the distinction is limited to small differences in dimensions; both extend along the crystallographic *a* axis. Terminal Mn-C bonds (mean lengths 2.123 Å) are shorter compared to their bridging counterparts (mean 2.282 Å), consistent with the lower coordination of the terminal ligands. A distorted tetrahedral environment is seen around the manganese atom in **4** with bond angles covering the range 93.53(8) [O(1)-Mn(1)-C(3A)] to 129.38(14) [C(13)-Mn(1A)-C(17B)]. This propagating Mn-dioxane-Mn coordination of the polymer has not been observed before with any other Mn(II) alkyl complex, or indeed with any other manganese compound of any type. However dioxane linkages of this type are well known for various other metal systems.[117-121] For example the mixed-metal lanthanide/magnesium complexes $[Ln(\eta^3\text{-}C_3H_5)_3(C_4H_8O).Mg(\eta^1\text{-}$

$C_3H_5)_2(C_4H_8O_2)_{1.5}]_\infty$[120] (Ln= La or Y) which exhibit a similar dioxane-bridged coordination polymeric arrangement as that seen in **4** and **5**

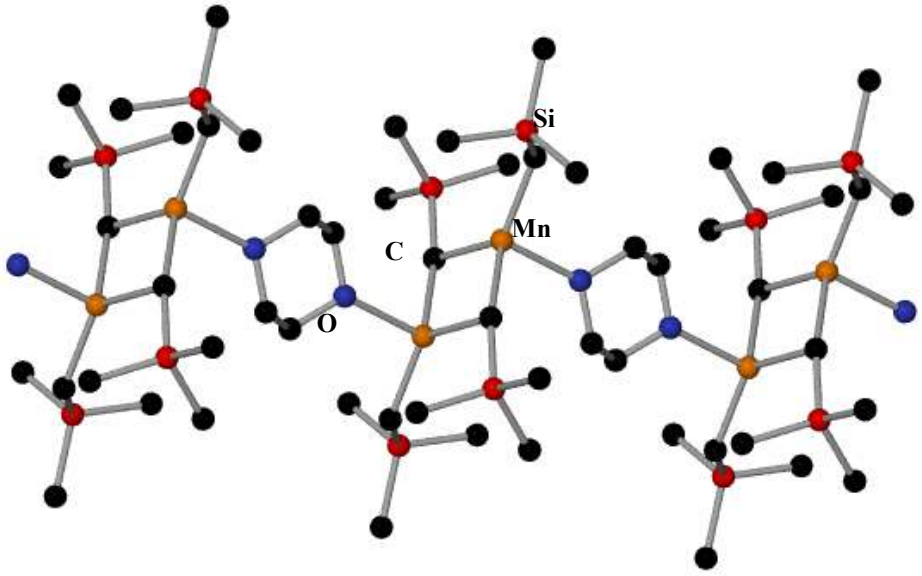

Figure 17: A longer section of polymeric **4**.

The molecular structure of **5** (Figure 18 and Figure 19) exhibits a 1:1 dioxane:Mn ratio. The polymeric complex contains monomeric $Mn(CH_2SiMe_3)_2$ units linked together by bridging dioxane molecules, forming a zig-zag chain along the crystallographic *c* axis. Lying on the corners of the chain, the manganese atoms show a distorted tetrahedral C_2O_2 environment (average bond angle, 107.08°). The Mn-C bonds to the two C_2-symmetrically equivalent alkyl groups [Mn(1)-C(1)/C(1A), 2.1386(12) Å] are separated by a C(1)-Mn(1)-C(1A) bond angle of 145.46(7)º which is wider than the angle between the manganese oxygen bonds [Mn(1)-O(1)/O(1A), 2.2611(9) Å] of 87.27º to the chain propagating dioxane molecules. This expresses the high steric bulk of the (trimethylsilyl)methyl groups on the Mn(II) centre.

Despite the different structural arrangements within each polymer chain, the dimensions involving the ligating dioxane molecules show very little change with the Mn-O bond lengths, 2.251(15) and 2.2611(9) Å in **4** and **5** respectively being essentially equivalent. Similarly the C-O-C bond angle in the dioxane shows very little change [average 109.71° in **4** and 110.35° in **5**].

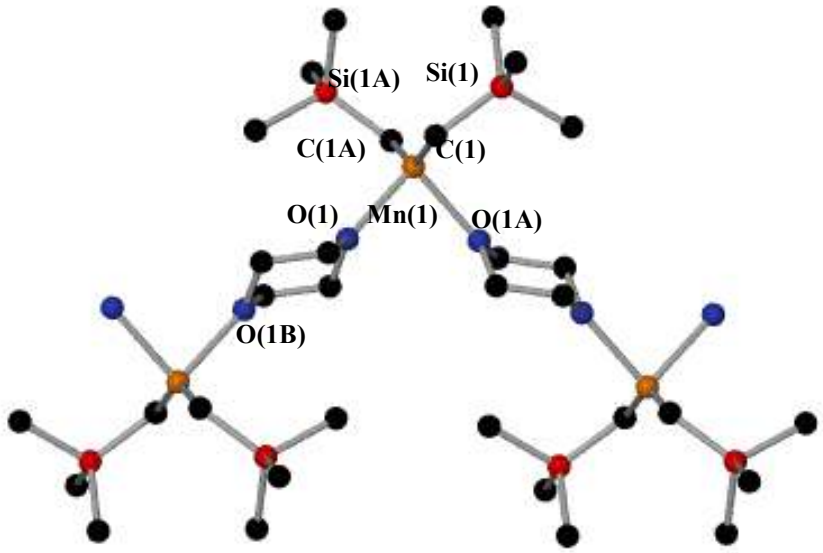

Figure 18: A trimeric section of [{(dioxane)[Mn(CH_2SiMe_3)$_2$]}$_\infty$] **5**. Hydrogen atoms have been omitted for clarity. Selected bond lengths [Å] and bond angles [º]: Mn(1)-C(1), 2.1385(12); Mn(1)-C(1A), 2.1386(12); Mn(1)-O(1), 2.2611(9); Mn(1)-O(1A), 2.2611(9); C(1)-Mn(1)-O(1A), 106.54(4); C(1)-Mn(1)-O(1), 98.34(4); C(1)-Mn(1)-C(1A), 145.46(7); O(1A)-Mn(1)-O(1), 87.27(5); O(1A)-Mn(1)-C(1A), 98.34(4); O(1)-Mn(1)-C(1A), 106.54(5).

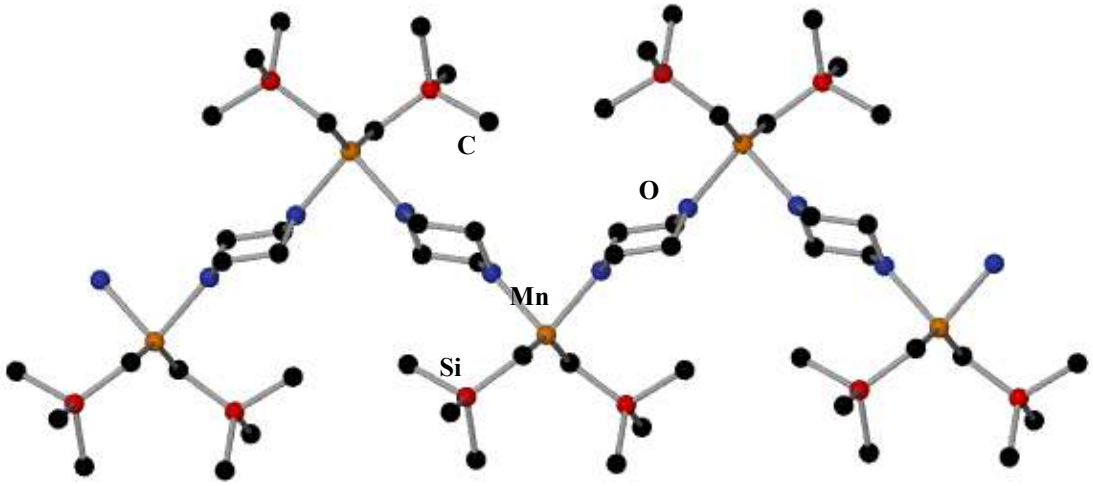

Figure 19: Extended zig-zag polymeric chain arrangement of **5**.

3.4. Reaction of [Mn(CH_2SiMe_3)$_2$]$_\infty$ 1 with Triphenylphosphine

To this point we have reacted the polymeric alkyl manganese(II) complex **1** with various oxygen and nitrogen donor ligands to furnish monomeric and new polymeric

complexes. However, several phosphine ligands such as PMe_3 and $PMePh_2$ are reported in the literature to give dimeric complexes of formula $[Mn(CH_2SiMe_3)_2PMe_3]_2$[122] and $[Mn(CH_2SiMe_3)_2PMePh_2]_2$[85] respectively when reacted with **1**. We therefore reacted **1** with the triphenylphosphine PPh_3 with the aim of preparing a representative phosphine complex that could be crystallographically characterised. The addition of one molar equivalent of PPh_3 to a hexane suspension of **1** gave a bright red/pink solution upon gently heating. As the solution cooled to room temperature large cubic pink crystals were deposited in an isolated crystalline yield of 39% established by X-ray crystallography to be the dimeric complex $[Mn(CH_2SiMe_3)_2PPh_3]_2$ (**6)** (Scheme 30).

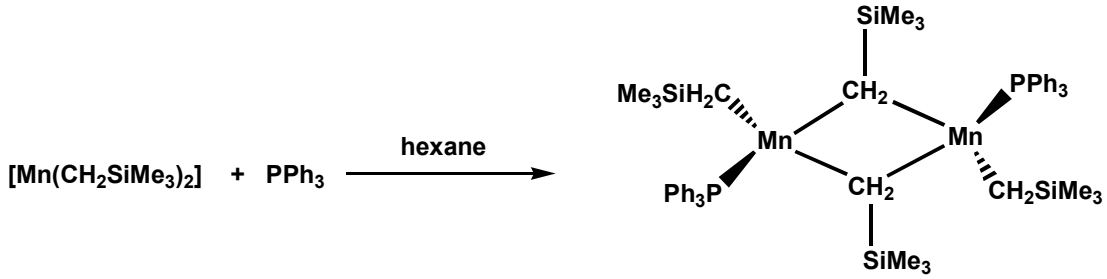

Scheme 30: Synthesis of the phosphine complex $[Mn(CH_2SiMe_3)_2PPh_3]_2$ **6**.

The centrosymmetric dimeric structure of **6** (Figure 20) has a fourfold coordinated Mn atom bound to a terminal PPh_3 group [Mn(1)-P(1), 2.7271(4) Å], a terminal CH_2SiMe_3 group [Mn(1)-C(5), 2.1400(16) Å] and two additional bridging CH_2SiMe_3 groups. The CH_2SiMe_3 bridge is noticeably asymmetric with a Mn(1)-C(1) distance of 2.1985(16) Å and a Mn(1)-C(1A) distance of 2.3592(16) Å, a difference of 0.1607 Å. Mn(1) occupies a distorted tetrahedral C_3P environment with bond angles ranging from 102.54(5)º to 123.49(6)º with an overall mean value of 108.9º. As expected increasing the steric bulk of the phosphine ligand from PMe_3[122] to PPh_2Me[85] to PPh_3 the Mn···Mn separation distance in each dimer gradually increases [2.771(2) Å, 2.828(1) Å and 2.8542(1) Å respectively] as does the retrospective Mn-P distance [2.650(1) Å, 2.684(1) Å and 2.727(4) Å respectively]. All three compounds show the same asymmetry in the carbon bridges with the Mn-C bridging distances being longer than the Mn-C terminal distances.

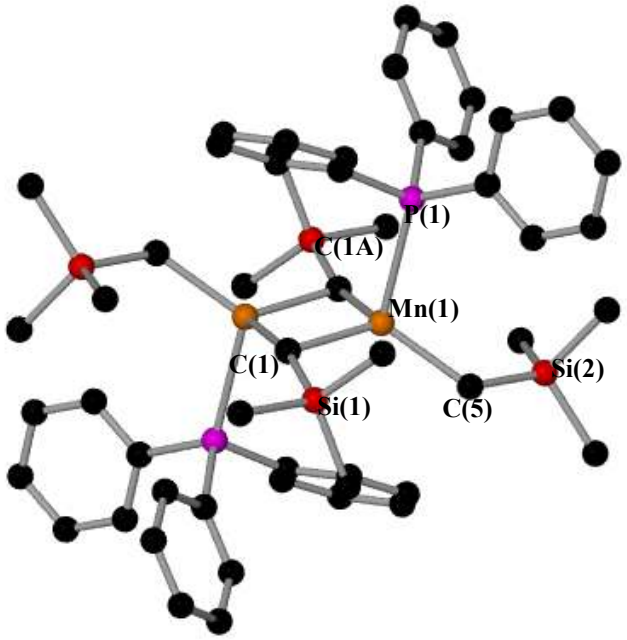

Figure 20: Molecular structure of $[Mn(CH_2SiMe_3)_2PPh_3]_2$ **6**. Hydrogen atoms have been omitted for clarity. Selected bond lengths [Å] and bond angles [º]: Mn(1)-C(1), 2.1985(16); Mn(1)-C(1A), 2.3592(16); Mn(1)-C(5), 2.1400(16); Mn(1)-P(1), 2.7271(4); Mn(1)-Mn(1A), 2.8542(5); C(5)-Mn(1)-C(1), 123.49(6); C(5)-Mn(1)-C(1A), 114.53(6); C(5)-Mn(1)-P(1), 110.93(5); C(1)-Mn(1)-C(1A), 102.54(5); C(1)-Mn(1)-P(1), 101.86(5); C(1A)-Mn(1)-P(1), 100.46(4).

Table 1. Comparative data (in Å and degrees°) from crystallographically characterised manganese(II) bis[(trimethylsilyl)methyl] compounds.

Compound	Mn···Mn	Mn-C	C-Mn-C	Mn-C-Mn
$[Mn(CH_2SiMe_3)_2]_\infty$ (**1**)	2.8885^{m}	2.200^{m} 2.428^{m}	109.2^{m}	77.0^{m}
[TMEDA.$Mn(CH_2SiMe_3)_2$] (**2**)		2.1379	140.50	
$[(pyridine)_2Mn(CH_2SiMe_3)_2]$ (**3**)		2.146^{m}	138.69 138.46	
[((-)sparteine)$Mn(CH_2SiMe_3)_2$] (**7**)		2.162^{m}	132.84	
$[\{(dioxane)[Mn(CH_2SiMe_3)_2]_2\}_\infty]$ (**4**)	2.7731	$2.123^{m,t}$ $2.282^{m,b}$	$105.3^{m,e}$	$74.7^{m,e}$
$[\{(dioxane)[Mn(CH_2SiMe_3)_2]\}_\infty]$ (**5**)		2.1385	145.46	
$[Mn(CH_2SiMe_3)_2PPh_3]_2$ (**6**)	2.8542	$2.278^{m,b}$ 2.140^{t}	102.54	77.46
$[Mn_2(CH_2SiMe_3)_4(PMePh_2)_2]$ (**8**)	2.828	$2.291^{m,b}$ 2.117^{t}	103.9	76.1
$[Mn_2(CH_2SiMe_3)_4(PMe_3)_2]$ **(9)**	2.772	$2.289^{m,b}$ 2.111^{t}	105.5	74.5
$[Mn_2(CH_2SiMe_3)_4(THF)_2]$ **(10)**	2.7878	$2.287^{m,b}$ 2.129^{t}	105.28	75.07

key: m, mean; b, bridging bond; t, terminal; e, endocyclic bond angle.

Table 1 lists selected metrical data for a range of organomanganese(II) crystal structures containing the $Me_3SiCH_2^-$ ligand, including the six new structures obtained in this work. The selection contains one unique alkyl-propagated chain polymer, two dioxane propagated chain polymers with either dimeric or monomeric manganese dialkyl subsections, four discrete dimers and three discrete monomers. Previously mentioned (-) sparteine complex **7** is the most sterically crowded monomer with the narrowest inter alkyl ligand separation of 132.84°. However there is a lessening of the alkyl-alkyl repulsion in the TMEDA (**2**) and pyridine (**3**) monomers with C-Mn-C bond angles of 140.5° and 138.69°/139.46°.[111] Steric crowding at the Mn atom is relaxed further when the ligating solvent molecule is changed to THF (in **10**)[123] or a phosphine (in **6**, **8**[85] and **9**[122]) since dimerisation can now proceed. Dioxane solvate **4** also comes into this category, though its second O donor atom allows its dimeric units to join together to form a polymeric chain. However if two molecules of dioxane (per Mn) sufficient amounts of donor are present then dioxane is are present, then the dimeric unit in **4** can be broken down to the monomeric unit in **5**. Unlike **2** and **3**, this monomeric unit is not discrete but propagates into a polymer via Mn-dioxane-Mn bridges. All four dimers show a planar CMnCMn ring with remarkably similar obtuse C-Mn-C and acute Mn-C-Mn endocyclic bond angles. The Mn-C terminal bonds are shorter that their bridging counterparts in all four dimers. An interesting feature not apparent from Table 1 is the marked asymmetry in the bridging Mn-C bond lengths within each individual dimer: in **6**, 2.1985(16)/2.3592(16) Å (difference 0.1607 Å); in **8**, 2.193(5)/2.389(5) Å (difference 0.196 Å); in **9**, 2.208(3)/2.369(5) Å (difference 0.161 Å); in **10**, 2.214(3)/2.360(3) Å (difference 0.146 Å); in **4**, 2.202(2)/2.365(3) (difference 0.163 Å) and 2.218(3)/2.346(2) Å (difference 0.128 Å). These bond lengths reflect the unsymmetrical coordination around the Mn atoms which all have three alkyl ligands (two bridging, one terminal) and one non alkyl ligand attached.

3.5. Reaction of $[Mn(CH_2SiMe_3)_2]_\infty$ 1 with the amines $DippNH_2$ and TMP(H)

Our next area of study was to probe the reactivity of the dialkyl manganese compound **1** towards various primary and secondary amines. Such Mn(II)-amido complexes could be potentially usefully in synthesising future mixed-metal manganate complexes. We

chose the primary amine $DippNH_2$ (Dipp = 2, 6 $^{i}Pr_2C_6H_3$) and the secondary amine TMP(H) (2,2,6,6- tetramethylpiperidine) as suitable candidates to evaluate the proton abstracting ability of **1** (Figure 21).

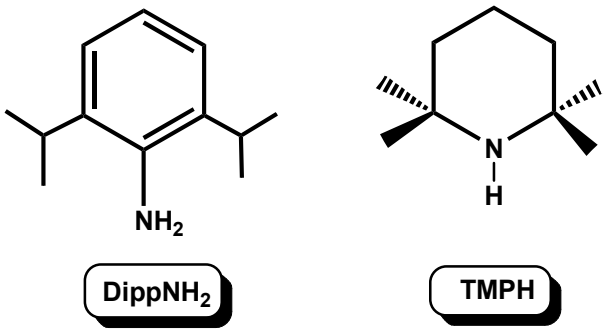

Figure 21: Primary and secondary amines $DippNH_2$ and TMPH.

3.6. Reaction of $[Mn(CH_2SiMe_3)_2]_\infty$ 1 with $DippNH_2$

To effect a deprotonation of the primary amine, an equimolar amount of it was added to a hexane suspension of **1**. After stirring at room temperature overnight an off-white precipitate was observed in the solution. Gentle heating gave a clear light yellow/green solution that upon cooling to room temperature deposited a crop of green plate crystals (Scheme 31). Analysis by X-ray crystallography revealed the complex produced to be the trimer $[(DippNH)_6Mn_3]$ **11**. Note that the ratio of Mn:DippN(H) in **11** is 1:2 which conflicts with the 1:1 stoichiometry used in the reaction. Also, the primary NH_2 units have only been monodeprotonated to NH, not dideprotonated. A maximum yield of **11** can therefore only be 50% (actual yield = 21%). However, repeating the reaction with the correct stoichiometry increases the crystalline yield to 55%.

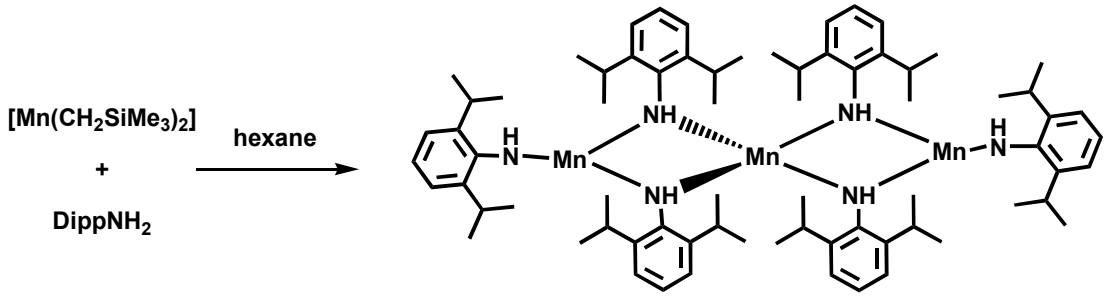

Scheme 31: Synthesis of $[(DippNH)_6Mn_3]$ **11**.

The resulting centrosymmetric molecular structure of **11** (Figure 22 and Figure 23) contains three Mn(II) atoms, two terminal DippNH ligands and four bridging DippNH ligands in an almost linear [175.95(2)°] trimeric arrangement. The two outer-positioned Mn atoms, Mn(2) and Mn(2A) are tricoordinate bonding to one terminal and two bridging DippNH ligands. In contrast, the central Mn(1), adopts a highly distorted tetrahedral geometry with bond angles ranging from 89.62(7)° to 130.33(7)° (mean 105.73°). The monoanionic DippNH ligand shows both a bridging and terminal mode which along with the differing coordination number of the manganese affects the Mn-N bond distances. Thus the shortest Mn-N bond distance is found for Mn(2)-N(3) [1.9530(19) Å] which involves a deprotonated terminal DippNH ligand. Following coordination number arguments, the shortest bridging Mn-N bond [Mn(2)-N(1), 2.0945(18) Å] belongs to the tricoordinate Mn(2) atom; while the longest bridging Mn-N bond [Mn(1)-N(2), 2.1648(17) Å] is present on the tetrahedral Mn(1) atom. The core of the complex contains two fused $(MnN)_2$ planar rings (sum of endocyclic angles 359.9°), connected by a central Mn(1) spiro atom.

On searching the literature few structurally characterised amido–manganese(II) compounds are known with the vast majority bearing the $N(SiMe_3)_2$ ligand.[103, 124-128] Examples containing a linear arrangement of three manganese(II) centres are particularly rare with two examples including the maroon coloured trimer $[Mn_3(Mesityl)_6]$,[84, 129] prepared by Floriani and the pentadienyl complex $[Mn_3(3\text{-}CH_3C_5H_6)_4]$.[130] However, the best comparison for **11** can be found in the trinuclear heteroleptic compound $[(Me_3Si)_2N]_2Mn_3[(DippNH)]_4.C_7H_8$[131] **12** which was synthesised from the equimolar reaction of $Mn[N(SiMe_3)_2]_2$ with $DippNH_2$ to furnish ruby-red crystals of **12** in a 76% yield. The Mn-N distances in **12** compare favourably to those found in **11** (terminal Mn-N, 1.980(3) Å; bridging 2.141 Å mean) along with having a comparable near-linear Mn···Mn···Mn [170.3(1)°] arrangement. The Mn···Mn separation distances are essentially equivalent at 3.0053(12) Å in **11** and 3.021(1) Å in **12**.

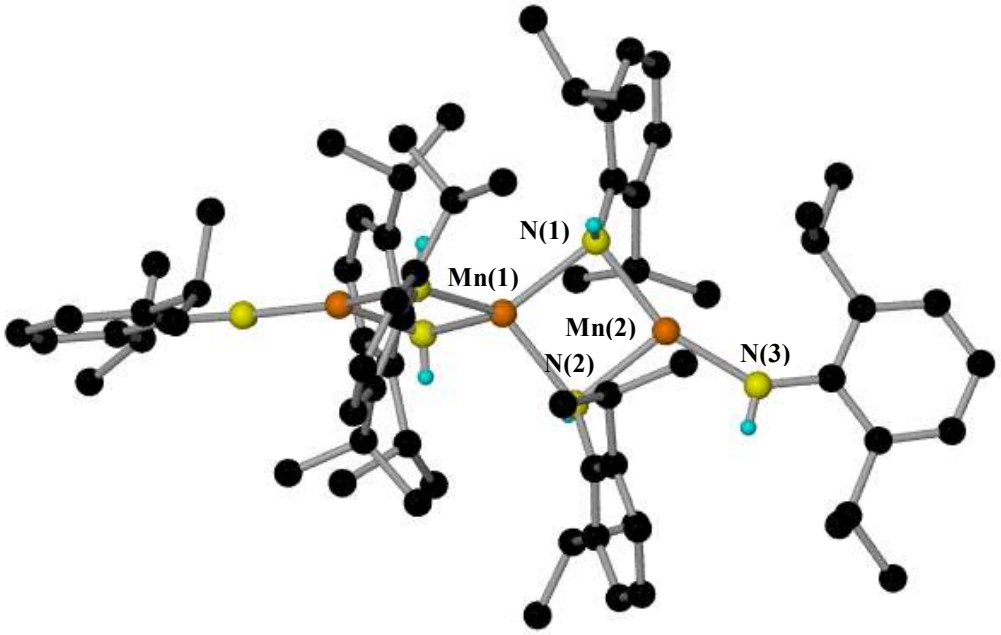

Figure 22: Molecular structure of $[(DippNH)_6Mn_3]$ **11**. Hydrogen atoms have been omitted for clarity (except amido N-H ones). Selected Bond lengths [Å] and angles[º]: Mn(1)-N(1), 2.1648(16); Mn(1)-N(2), 2.1242(18); Mn(2)-N(1), 2.0945(18); Mn(2)-N(2), 2.1426(18); Mn(2)-N(3), 1.9530(19); Mn(1)-Mn(2), 3.0053(12); Mn(2)-Mn(1)-Mn(1A), 175.95(2); N(1)-Mn(1)-N(2), 89.62(7); N(1)-Mn(1)-N(2A), 130.33(7); N(1)-Mn(1)-N(1A), 116.46(10); N(2)-Mn(1)-N(2A), 105.07(11); N(2)Mn(1)-N(1A), 103.32(7); N(2A)-Mn(1)-N(1A), 89.62(7); N(1)-Mn(2)-N(2), 91.02(7); N(1)-Mn(2)-N(3), 158.34(8); N(2)-Mn(2)-N(3), 110.42(8).

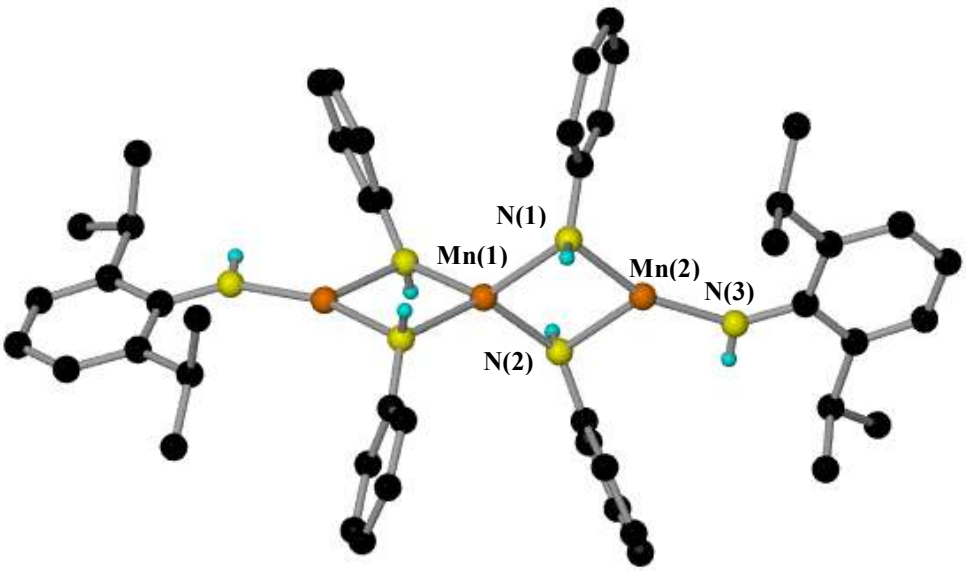

Figure 23: An alternative view of $[(DippNH)_6Mn_3]$ **11** with the 2- and 6-*i*Pr groups removed from the bridging DippNH ligands for clarity.

To the best of our knowledge **11** represents the first homoleptic trinuclear amido-manganese(II) complex with the only other crystallographically characterised homoleptic Mn(II) trimer being the aryl complex derived from mesitylene, $[Mn_3(Mesityl)_6]$,[84, 129] reported by Floriani *et al*.

3.7. Reaction of $[Mn(CH_2SiMe_3)_2]_\infty$ 1 with TMP(H)

Turning to the secondary amine TMP(H), a hexane suspension of **1** on addition of one molar equivalent of TMP(H) gave an immediate colour change to an intense deep purple. Reduction of the solvent volume and storage of the solution at room temperature, in a refrigerator (at 5°C) or freezer (at -27°C) did not induce crystallisation. The intense purple colour and solubilisation of the starting reagents indicate that a reaction has certainly occurred. Normally NMR spectroscopy would help identify the nature of the reactive products in solution, however, due to Mn(II) being high spin d^5 and paramagnetic, NMR studies cannot be conducted on this particular reaction mixture. Clearly a crystalline product is needed here to understand the outcome of this attempted amination.

3.8. Reaction of $[Mn(CH_2SiMe_3)_2]_\infty$ 1 with various ketones

In organic synthesis organomanganese compounds, particularly organomanganese halides allow reactions such as 1,2- and 1, 4-additions, acylations and alkylations etc. to be achieved.[132] Wanting to test the synthetic utility and versatility the organomanganese reagent **1**, we decided to test its reactivity towards several ketones with different steric and electronic properties namely benzophenone, 2, 4, 6-trimethylacetophenone and 2, 2, 2-trifluoroacetophenone (Figure 24).

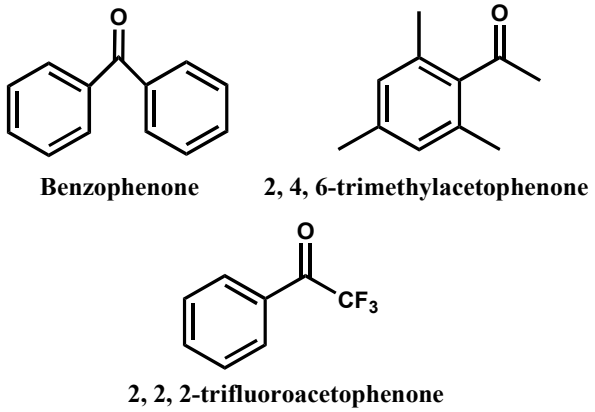

Figure 24: Structural formulae of ketones investigated with complex **1.**

3.9. Reaction of $[Mn(CH_2SiMe_3)_2]_\infty$ 1 with benzophenone

Our first reaction studied involved the sterically bulky diaryl ketone benzophenone. This ketone could react with the organomanganese complex in two ways; firstly in a coordinative way through the lone pair of the oxygen, which we have seen before in this chapter with various other donor ligands or secondly, through a 1, 2-addition reaction across the carbonyl functional group. In the reaction, one molar equivalent of benzophenone was introduced to a hexane suspension of the organomanganese reagent **1** to give a light pink solution after stirring for a few minutes at room temperature. Storage of the solution at room temperature allowed light pink cubic crystals to be deposited that were identified by X-ray crystallography to be the trimeric Mn(II) compound $[(Me_3SiCH_2)_2Mn_3\{\mu\text{-}OC(CH_2SiMe_3)Ph_2\}_4]$ **13** (Scheme 32).

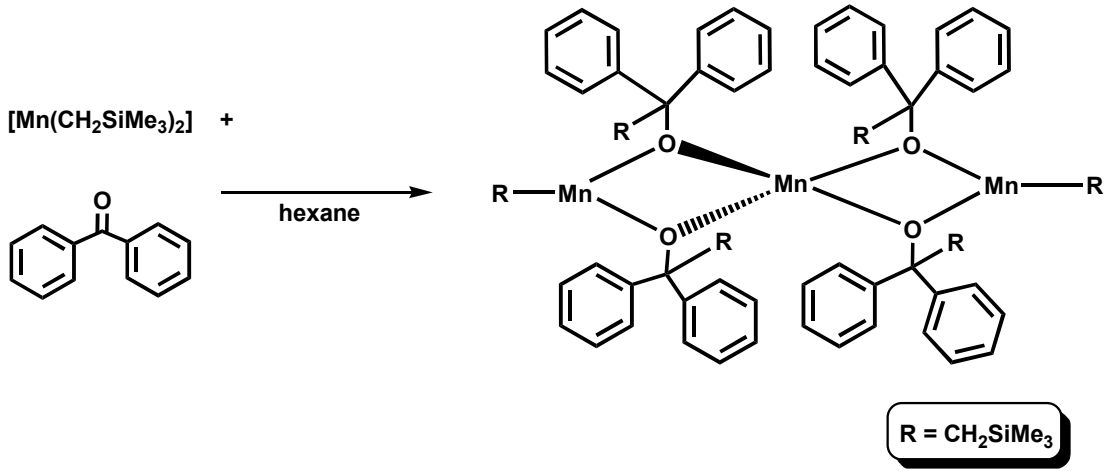

Scheme 32: Synthesis of trimeric $[(Me_3SiCH_2)_2Mn_3\{\mu\text{-}OC(CH_2SiMe_3)Ph_2\}_4]$ **13**.

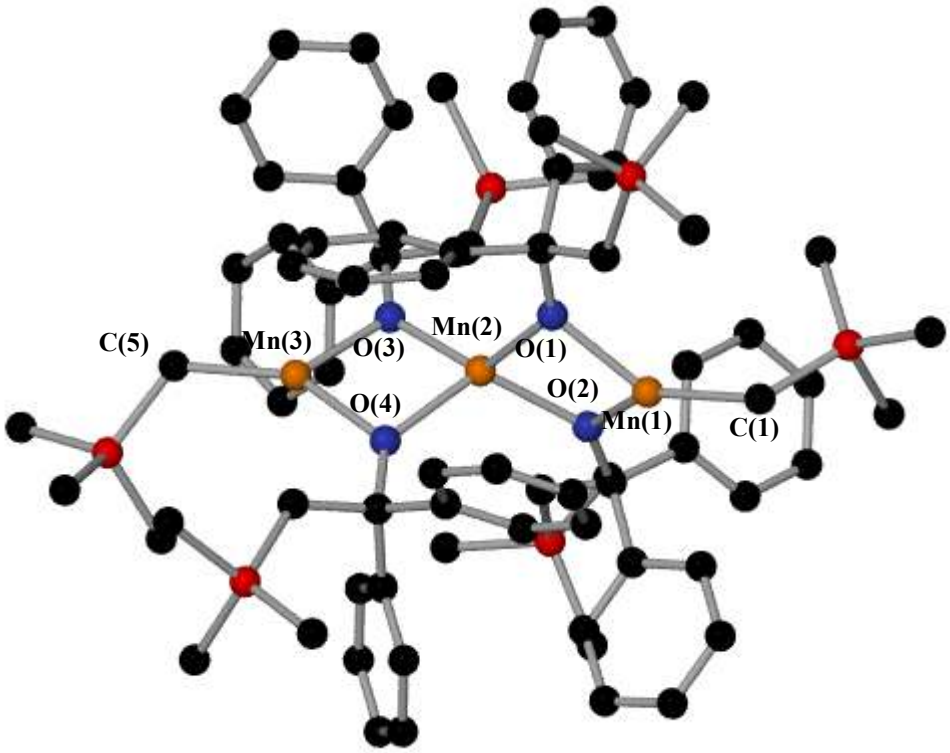

Figure 25: Molecular structure of $[(Me_3SiCH_2)_2Mn_3\{\mu\text{-}OC(Me_3SiCH_2)Ph_2\}_4]$ **13**. Hydrogen atoms are omitted for clarity. Selected bond lengths [Å] and angles [º]: Mn(1)-C(1), 2.109(2); Mn(1)-O(1), 2.0376(15); Mn(1)-O(2), 2.0442(15); Mn(2)-O(1), 2.0514(14); Mn(2)-O(2), 2.0662(15); Mn(2)-O(3), 2.0568(14); Mn(2)-O(4), 2.0624(15); Mn(3)-O(3), 2.0379(15); Mn(3)-O(4), 2.0287(15); Mn(3)-C(5), 2.117(3); Mn(1)-Mn(2), 3.0611(5); Mn(2)-Mn(3), 3.0823(5); Mn(1)-Mn(2)-Mn(3), 158.474(16); C(1)-Mn(1)-O(2), 142.89(9); C(1)-Mn(1)-O(1), 133.26(9); O(1)-Mn(1)-O(2), 82.05(6); O(1)-Mn(2)-O(2), 81.18(6); O(1)-Mn(2)-O(4), 119.49(6); O(1)-Mn(2)-O(3), 126.10(6); O(2)-Mn(2)-O(4), 118.85(6); O(2)-Mn(2)-O(3), 135.18(6); O(4)-Mn(2)-O(3), 80.98(6); C(5)-Mn(3)-O(3), 125.62(12); C(5)-Mn(3)-O(4), 149.16(11); O(3)-Mn(3)-O(4), 82.26(6).

The molecular structure of **13** (Figure 25 and Figure 26) consists of three Mn(II) atoms linked together by four alkoxy ligands in a bent conformation [158.474(16)°]. The four bridging alkoxy ligands $[OC(CH_2SiMe_3)Ph_2]$ have originated from the 1, 2- addition reaction of Me_3SiCH_2 to the electrophilic carbon centre of the benzophenone with the metal preferring the highly electronegative O atom. A further two unreacted CH_2SiMe_3 groups take up terminal positions on the outer-positioned Mn(1) and Mn(3) atoms. Unlike the previously synthesised homoleptic amido trimer **11**, **12** is not centrosymmetric. Surrounded by four O atoms, the central atom adopts a highly

distorted geometry, with O-Mn-O bond angles varying from 135.18(6) Å to 80.49(6) Å with a mean value of 110.36°. In contrast the outer positioned Mn(1) and Mn(3) are tri coordinate with two bridging alkoxy ligands and one terminal alkyl ligand. The terminal Mn-C bonds [Mn(1)-C(1), 2.109(2) Å, Mn(3)-C(5), 2.117(3) Å] fall into the range of terminal Mn-C bonds (C = CH_2SiMe_3) see previously in this report (compounds **8**, **9** and **10** mean 2.124 Å) while the Mn-O bridging bonds have an average length of 2.048 Å.

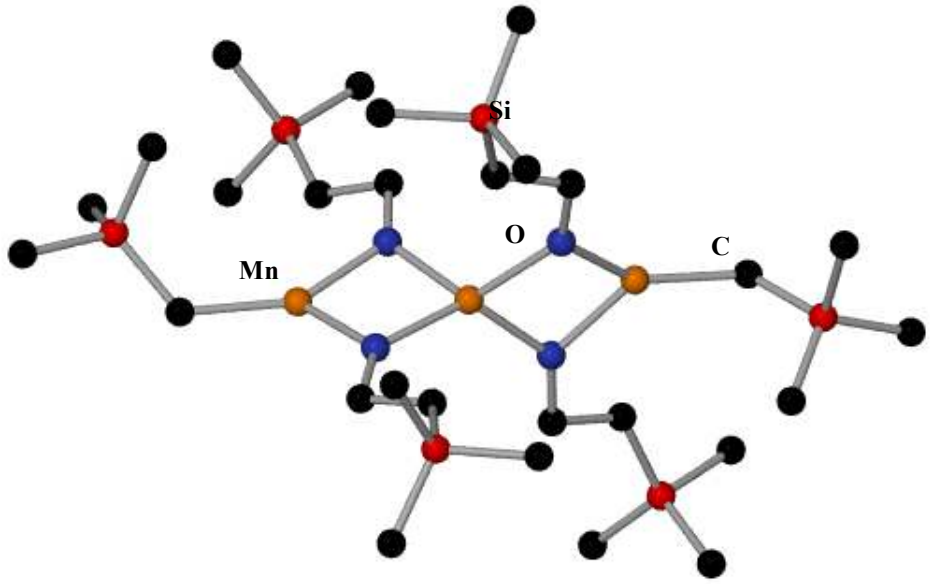

Figure 26: Molecular structure of **13** with the phenyl rings of the alkoxy ligand and all hydrogen atoms omitted for clarity.

Complex **13** is the first alkoxy bridged Mn(II) trimer to be synthesised via an addition reaction. However, other Mn(II) trimeric complexes with alkoxy bridges $[Mn_3(OCH\text{-}tBu_2)_6]$[133] **14** and $[O(Ph_2SiO)_2]_2Mn_3[N(SiMe_3)_2]_2(THF)_2.(THF)_{0.5}$[134] **15** are known. In contrast to **13**, **14** and **15** are synthesised from their parent alcohol ligands, making them products of deprotonation reactions unlike **13** which was made via a nucleophilic addition approach. The bent conformation of the three Mn(II) atoms in **13** is best compared to that in **14** [154.0(1)°] but far removed from the angular arrangement found in **15** [139.5°]. The Mn-O bonds in **13** can be compared favourably to those found in **14** [average of bridging alkoxy ligands 2.055 Å] and **15** [average bond length of bridging siloxane 2.092 Å].

Previously within our group we have observed addition reactions when utilising synergic organometallic reagents. An unusual example concerns the mixed sodium-zinc alkyl-amide base [(TMEDA)Na(TMP)(*t*Bu)Zn(*t*Bu)] as it reacts with benzophenone to give the mono-*tert*-butylated 1, 6 adduct [(TMEDA)Na{OC(Ph)(4-*t*Bu-C_6H_5)](TMP)Zn(*t*Bu)].[135] Precedent also exists for cyclohexadienyl-Mn(I) complexes to undergo addition reactions with benzophenone but with a pre-lithiation step required.[136-138]

3.10. Reaction of $[Mn(CH_2SiMe_3)_2]_\infty$ 1 with 2, 4, 6-trimethylacetophenone

Reacting one molar equivalent of trimethylacetophenone with a hexane suspension of **1** afforded an instant homogeneous yellow/orange solution. Reduction of the solvent volume and storing the solution at room temperature, either in the refrigerator (at 5°C) or in the freezer (at -27°C) did not afford any solid product. The presence of the clear solution and the observed colour change are good indicators that a reaction has taken place. With no NMR available and no crystals available for X-ray crystallographic studies we can only speculate what type of reaction could have occurred. Trimethylacetophenone is known to undergo enolization reactions with organometallic reagents to form various oligomeric forms.[139] The methyl group directly attached to the carbonyl is relatively acidic and easily deprotonated to a CH_2 unit which is observed in its reaction with the mixed sodium-magnesium bases $NaMgBu_2$ and Na_2MgBu_4.[140] However **1** is a poor base so deprotonation is unlikely. If the $Mn[(CH_2SiMe_3)_2]_\infty$ starting reagent reacts in a similar way to previous reactions discussed before in this chapter, then we could envisage either a monomeric or dimeric complex to perhaps form with the ketone acting as a Lewis base (Figure 27). This reaction is still being investigated in the hope of obtaining a crystalline product in the near future.

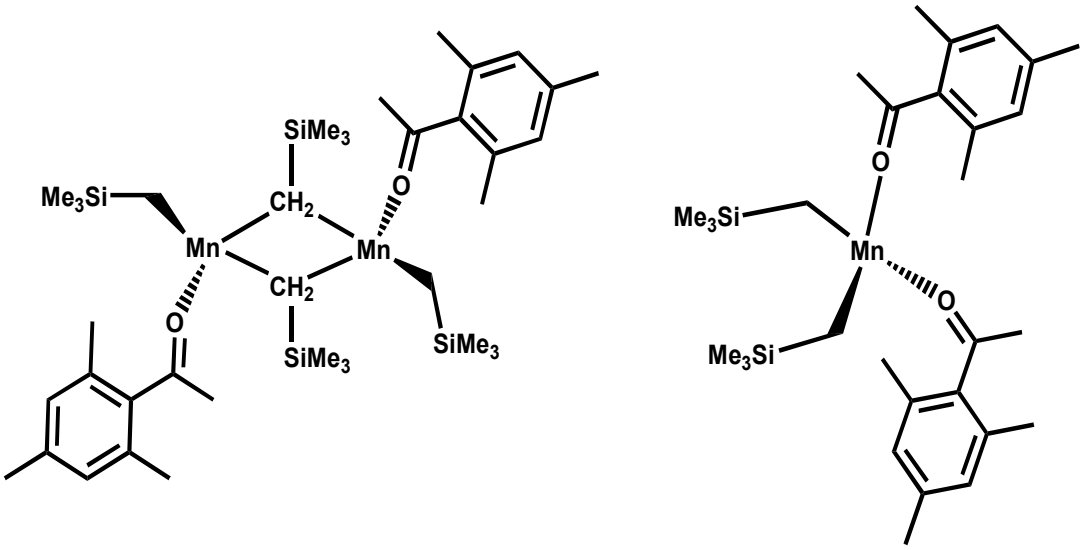

Figure 27: Proposed monomeric and dimeric complexes of the reaction between $[Mn(CH_2SiMe_3)_2]_\infty$ and 2, 4, 6-trimethylacetophenone.

3.11. Reaction of $[Mn(CH_2SiMe_3)_2]_\infty$ 1 with 2, 2, 2-trifluoroacetophenone

The last ketone we studied with reagent **1** was the strongly electron withdrawing 2, 2, 2-trifluoroacetophenone. In its reaction with **1**, again carried out in hexane solution, a colour change was immediately obvious going from light yellow/orange to deep orange. After stirring the solution for one day it was left at room temperature to crystallise. No crystals were obtained upon storage at room temperature, in the refrigerator (at 5°C) or in the freezer (at -27°C). Unfortunately, further reduction of the solvent volume still did not lead to crystals growth. As in the previous two reactions the instant colour change and solubilisation of all the components of the reaction indicate that a reaction has definitely occurred. Trifluoroacetophenone could react with **1** in two principal ways; i) via an addition reaction across the carbonyl group or ii) by coordination through the oxygen lone pair to generate a simple Lewis acid-Lewis base complex (Figure 28). However if you consider the steric crowding around the tertiary carbon in the addition product the coordination product seems the more likely possibility. Though too late for this report, the reaction is still being investigated with the hope of obtaining crystals in the near future.

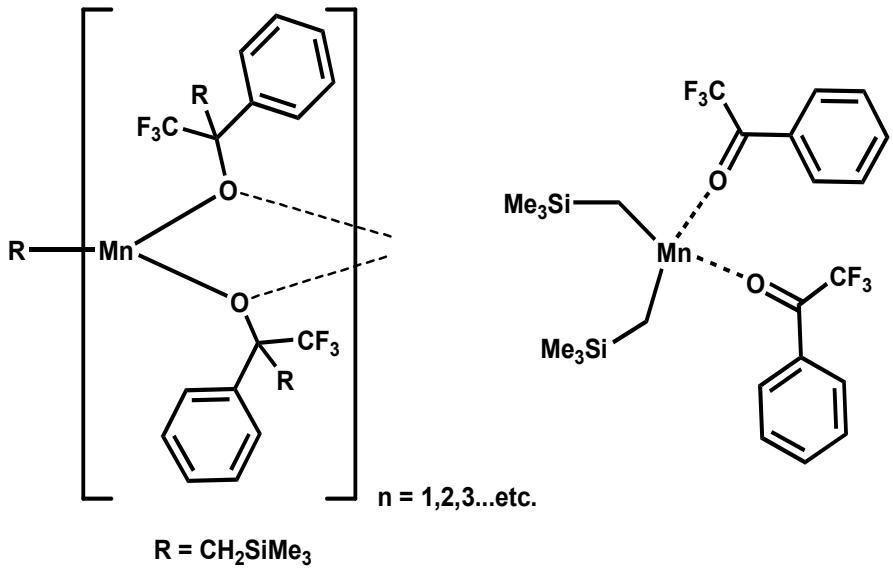

Figure 28: Proposed addition (LHS) and coordination (RHS) products from the reaction of $[Mn(CH_2SiMe_3)_2]_\infty$ with trifluoroacetophenone.

3.12. Conclusions

In conclusion this chapter has proved that the organometallic reagent $[Mn(CH_2SiMe_3)_2]_\infty$ **1** has a polymeric structure. Subjecting **1** to various donors including, TMEDA, pyridine and PPh_3 allows various monomeric $[TMEDA{\cdot}Mn(CH_2SiMe_3)_2]$ **2**, $[(pyridine)_2Mn(CH_2SiMe_3)_2]$ **3** and dimeric $[Mn(CH_2SiMe_3)_2PPh_3]_2$ **6** complexes to form. In contrast reactions of **1** with the weaker donor dioxane, **1** does not completely break down but gives new O-solvated polymeric arrangements; including the polymeric dimer subunit based $[\{(dioxane)[Mn(CH_2SiMe_3)_2]_2\}_\infty]$ **4** and monomeric sununit based $[\{(dioxane)[Mn(CH_2SiMe_3)_2]\}_\infty]$ **5** which propagate using the second O donor atom of the bifunctional cyclic ether. The versatility of **1** is displayed though its use as a deprotonation reagent with amines to give the trimeric complex $[(DippNH)_6Mn_3]$ **11** in which six molecules of $DippNH_2$ have been successfully deprotonated. Changing the substrate to ketones, a 1,2-addition reaction is seen when **1** is reacted with the sterically demanding benzophenone to give the heteroleptic trimer $[(Me_3SiCH_2)_2Mn_3\{\mu\text{-}OC(CH_2SiMe_3)Ph_2\}_4]$ **13**.

Chapter 4. Functionalised Arenes

This chapter will begin with a brief summary of each experiment attempted and the main results obtained from it. In particular, it will be stated whether the attempted metallation was achieved or not and, if so, the regioselectivity of deprotonation on the substrate will be discussed.

The initial aim of this part of the project was to investigate and quantify the reactivity of the new synergic sodium-manganese(II) base [(TMEDA)Na(TMP)(CH_2SiMe_3)Mn(TMP)] **16**. The general *ortho*-metallation of functionalised arenes has been known for many years and was discussed in detail in the introduction under the subheading D*o*M (Chapter 1). In this synergic base work the emphasis was on the hitherto unknown direct manganation of aromatic substrates.

4.1. Reaction of the manganate base 16 with anisole

The *ortho*-metallation (usually lithiation) of the alkyl-aryl ether anisole has been performed for many years.[52, 57] Anisole and its derivatives are widely used in organic synthesis in the pharmaceutical industry as building blocks to more complex molecules.[141-143] It is the presence of the methoxy group that lends anisole to metallation via D*o*M chemistry. The methoxy group is known as a weak *ortho*-director, which within our research group has been successfully magnesiated[144] and zincated[145] in previous reactivity studies. For this reason it was chosen as an ideal starting point to hopefully establish the first example of *ortho*-directed manganation of an aromatic ether.

Turning to the experimental work, a hexane solution of the synergic base **16** was reacted with one molar equivalent of anisole at room temperature to give a yellow/green solution. Large green cubic crystals were grown at room temperature over the course of twenty four hours. The crystals were subjected to X-ray crystallographic analysis which showed them to be the new *ortho*-manganated complex [(TMEDA)Na(TMP)(*o*-C_6H_4OMe)Mn(TMP)] **17** (Scheme 33) which was isolated in a high and reproducible crystalline yield of 76%.

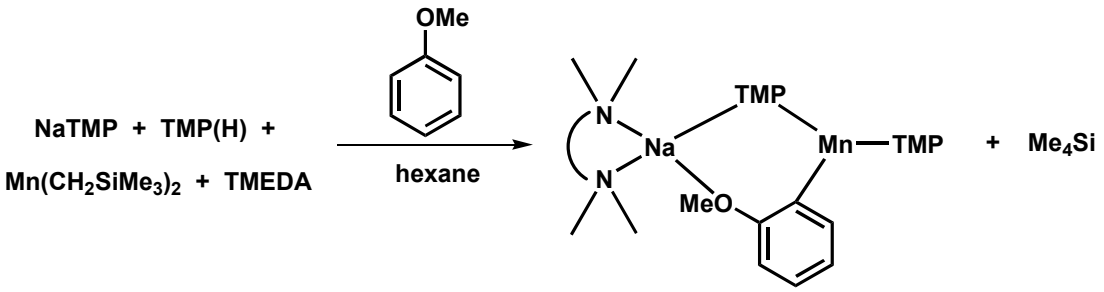

Scheme 33: Reaction of the synergic base **16** with anisole.

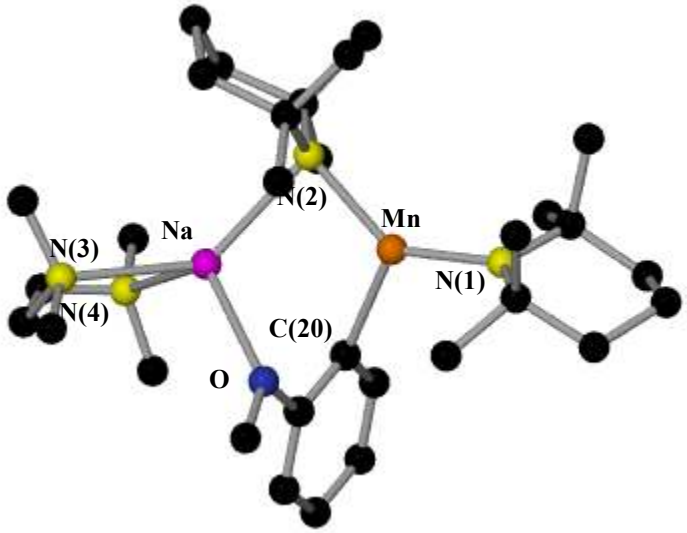

Figure 29: Molecular structure of **17**. Hydrogen atoms are omitted for clarity. Selected bond lengths [Å] and bond angles [º]: Mn-N(1), 2.0298(17); Mn-N(2), 2.0930(17); Mn-C(20), 2.189(2); Na-N(2), 2.5387(19); Na-O, 2.5357(16); Na-N(3), 2.573(2); Na-N(4), 2.530(2); N(1)-Mn-N(2), 133.36(6); N(1)-Mn-C(20), 115.44(7); N(2)-Mn-C(20), 11.19(7); N(2)-Na-N(3), 128.62(7); N(2)-Na-N(4), 131.46(7); N(2)-Na-O(1), 101.72(5); N(3)-Na-N(4), 73.53(7); N(3)-Na-O(1), 119.80(6); N(4)-Na-O(1), 98.48(6).

The molecular structure of **17** (Figure 29) can be classified as a contact ion pair ate compound with a CN_2 trigonal planar manganese coordination. This trigonal planar geometry is made up of one terminal TMP ligand [Mn-N(4), 2.0298(17) Å] and two bridging ligands, a TMP [Mn-N(1), 2.0930(17) Å] and an *o*-deprotonated anisole [Mn-C(20), 2.189(2) Å]. Defining this metallation as a manganation, the deprotonated *ortho*-C atom forms a σ-bond to the Mn atom, but does not interact with the Na atom. Instead the aryl ligand bridges to the Na through its O-heteroatom [Na-O, 2.5357(16) Å] to make a closed 6-atom 5-element central (NaNMnCCO) non-planar ring. Bidentate TMEDA completes the distorted tetrahedral (N,N,N,O) environment of sodium (mean

bond angle subtended at Na 108.9º). To the best of our knowledge this represents the first crystallographically characterised example of an *ortho*-manganated functionalised arene.

4.2. Reaction of the manganate base 16 with N, N-diisopropylbenzamide

Continuing the investigation of functionalised arenes the next substrate to be tested was N, N-diisopropylbenzamide. Again this substrate is used as a building block in many biologically important pharmaceutical compounds.[146, 147] Like anisole D*o*M chemistry can be applied in this case due to the presence of the strongly electron withdrawing carboxamido functional group. The carboxamido group is a strong *ortho*-directing group, the metallation of which by conventional metallating agents such as BuLi usually needs to be conducted at -78ºC in order to control the reaction regioselectivity and limit competitive nucleophilic attack of the carbonyl group.[148]

Thus the synergic base prepared *in situ* in hexane solution was reacted with one molar equivalent of N, N-diisopropylbenzamide at room temperature to give a bright orange solution. Thick orange needle crystals were grown from this solution at room temperature and analysed by X-ray crystallography to give the new *ortho*-manganated complex [(TMEDA)Na(TMP){*o*-[C(O)N(*i*Pr$_2$)]C$_6$H$_4$}Mn(CH$_2$SiMe$_3$)] **18** (Scheme 34). This reaction was repeated several times resulting in isolated crystalline yields ranging from 32-68%. The purity of the product was verified by reproducible microanalysis and melting point analysis.

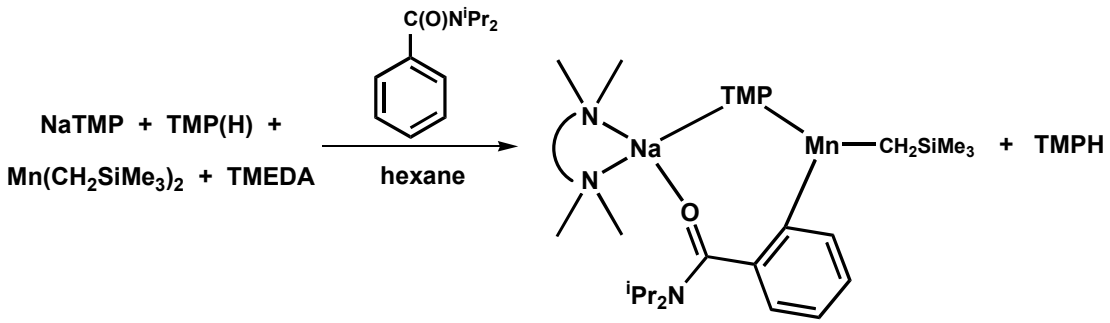

Scheme 34: Reaction of synergic base **16** with N, N-diisopropylbenzamide.

Complex **18** has two crystallographically independent molecules in its unit cell. As both are nearly identical only one is shown (Figure 30). Similar to complex **17**, the molecular structure of **18** can be classed as a contact ion pair ate arrangement. A distorted trigonal planar Mn(II) centre comprising a C_2N coordination is made up of [average bond angle around Mn 119.53º] a terminal alkyl group [Mn(1)-C(29), 2.158(5) Å], a bridging TMP [Mn(1)-N(1), 2.102(4) Å] and a bridging *o*-deprotonated benzamide molecule [Mn(1)-C(10), 2.171(5) Å]. In the core of the molecule lies a non-planar 7-atom, 5-element (MnCCCONaN) ring. The diisopropylbenzamide ligand has lost a proton in the *ortho*-position, which has been selectively replaced with a Mn(II) atom. The reaction can therefore be described as an alkali-metal-mediated manganation (AMM*Mn*), that is a direct hydrogen-manganese exchange process. In the coordination sphere of the sodium, there is a TMP bridge, a carbonyl oxygen atom from the diisopropylbenzamide and a bidentate chelating TMEDA ligand giving an overall distorted tetrahedral coordination (mean bond angle subtended at Na, 108.3º). Distortion is most pronounced at the N(3)-Na-N(4) [74.2(2)°] bond angle involving the TMEDA and at the N(1)-Na-N(3) [129.9(2)°] bond angle involving one TMEDA N atom and the TMP N atom.

To the best of our knowledge **17** and **18** represent the first examples of *ortho*-directed manganations. A search of the Cambridge Structural Database revealed **17** and **18** to be unique with no hits found for ether-substituted aryls with *ortho*-Mn(II) atoms[149] or indeed with any *ortho*-transition-metal atoms. Furthermore alkali-metal-arylmanganated structures of any type are surprisingly rare with no sodium examples at all (besides those previously made by AMM*Mn* and reported by our group).[55, 56] Three lithium examples, reported by Power[95] were synthesised via metathesis reactions with only one, the mesitylene derivative $[Li(THF)_4]$ $[MnMes_3]$ having a trigonal planar Mn centre similar to those in **17** and **18.** However this complex has a very different structural arrangement to **17** and **18** existing as a solvent-separated ion pair. The best comparison for **17** and **18** is provided by the unsubstituted phenyl analogue $[(TMEDA)Na(TMP)(C_6H_5)Mn(TMP)]$[56] (**19**). Unfortunately disorder in **18** limits the accuracy of its metrical parameters, though its connectivities are definite and the main features of its two independent molecules are similar to those seen in **17**. The smaller 4-membered (NaNMnC) ring due to lack of aryl-substitution in **19** has a marginally longer Mn-C bond (2.20(4) Å to the *ipso*-C; 2.189(2) Å *ortho*-C in **17**) made by the Mn(II) atom lying almost coplanar with the aryl ring (deviation from planarity 0.339 Å **19**,

0.558 Å in **17**; 0.221 and 0.220 Å in **18**). The long Na-ipso-C bond in **19** [2.731(4) Å] is substituted by a significantly shorter Na-(O)Me bond in **17** [2.5357(16) Å] which in part reflects the greater bond strength of donor-acceptor dative interactions versus cation-π interactions.[150] Even shorter Na-O bonds are seen in **18** at 2.313(6) and 2.309(5) Å, suggesting a relaxation of steric effects.

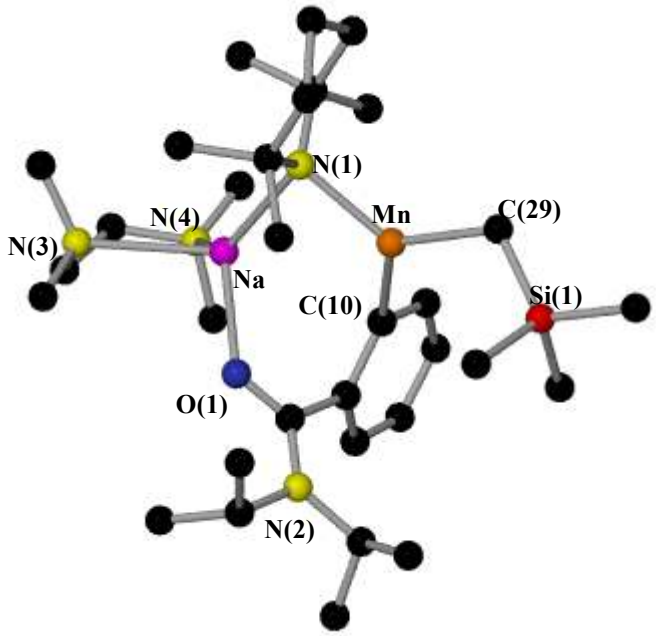

Figure 30: Molecular structure of [(TMEDA)Na(TMP){o-[C(O)N(*i*Pr$_2$)]C$_6$H$_4$}Mn(CH$_2$SiMe$_3$)] **18**. Only one of two crystallographically independent molecules is shown. Hydrogen atoms have been omitted for clarity. Selected bond lengths [Å] and bond angles [º]: Mn-C(29), 2.158(5); Mn-N(1), 2.102(4); Mn-C(10), 2.171(5); Na-O, 2.313(6); Na-N(1), 2.493(5); Na-N(3), 2.561(7) ; Na-N(4), 2.582(6) ; N(1)-Mn-C(29), 122.8(2); N(1)-Mn-C(10), 115.08(18); C(29)-Mn-C(10), 120.7(2); N(1)-Na-O(1), 106.5(2); N(1)-Na-N(3), 129.9(2); N(1)-Na-N(4), 122.4(2); O(1)-Na-N(3),116.7(2); O(1)-Na-N(4), 100.4(2); N(3)-Na-N(4), 74.2(2);

On closer inspection of the molecular structures of **17** and **18** there is seemingly a significant distinction in the reactivity of base **16** towards the different ether substituted aryl substrates. To explain **16** possesses a heteroleptic formulation which in theory means it could behave in an amido (TMP) or alkyl (Me_3SiCH_2) deprotonative fashion or indeed both. This alternative choice of basicity is observed in the reaction of **16** with anisole and N, N-diisopropylbenzamide or at least in the composition of the crystalline products isolated from solution. When **16** is reacted with anisole it functions ultimately as an alkyl base, generating tetramethylsilane as the co-product and the *ortho*-

manganated complex **17** which possesses a bisamido-monoaryl composition. In contrast, the reaction of **16** with N, N-diisopropylbenzamide shows the alternative basicity, acting as an amido base to give the heteroanionic monoalkyl-monoamido-monoaryl complex **18** with the concomitant loss of the amine TMP(H). These results establish that **16** is a versatile manganating agent with a ligand transfer switch, potentially tuneable to alkyl or amido basicity, dependent on the conditions and possibly the nature of the aromatic substrate. Clearly distinct mechanisms must therefore be available to **16** in its reactions with aromatic substrates. Monitoring possible reaction pathways via conventional NMR spectroscopy is not possible here owing to the paramagnetic nature of high spin d^5 Mn(II) in the isolated products/reaction mixtures. However, thermodynamically the loss of volatile Me_4Si from such manganations is likely to be greatly preferred.

Recently, investigations by Uchiyama *et al.*[33, 151-154] have shown that similarly composed lithium or sodium dialkyl-TMP-zincates examined through DFT calculations will preferentially deprotonate organic substrates in two steps (Scheme 35): in step 1, the TMP abstracts a proton from the substrate to form TMP(H); in step 2, TMP(H) is deprotonated to revert back to the TMP anion and rejoins (or never leaves) the heterometallic structure with an irreversible elimination of alkane, showing overall alkyl basicity.

Admittedly this zincate hypothesis cannot be directly compared to the manganate work discussed here as the heterobimetallic base used by Uchiyama *et al.* [LiZn(TMP)*t*Bu_2] possesses a 2:1 alkyl/amido stoichiometry in contrast to reagent **16**, where the stoichiometry is reversed. Recently, within our group this two-step mechanism has been tracked during the *ortho*-deprotonation of anisole by the potassium magnesiate base [(PMDETA)K(TMP)(CH_2SiMe_3)Mg(TMP)][155] (PMDETA = N,N,N',N'',N''-pentamethyldiethylenetriamine) by using a combination of X-ray crystallography and time dependent NMR spectroscopic studies. The findings of this study confirmed the two step hypothesis suggested by Uchiyama in that, the heteroleptic base first reacts kinetically through its TMP component to generate the *ortho*-magnesiated complex [(PMDETA)K(TMP)(*o*-C_6H_4OMe)Mg(CH_2SiMe_3)] which in turn then reacts through its alkyl component to generate the thermodynamic and final *ortho*-magnesiated anisole complex [(PMDETA)K(TMP)(*o*-C_6H_4OMe)Mg(TMP)]. This characteristic 'alkyl

versus amido' basicity will become a prominent feature throughout this thesis when the synergic base **16** is reacted with various other organic substrates.

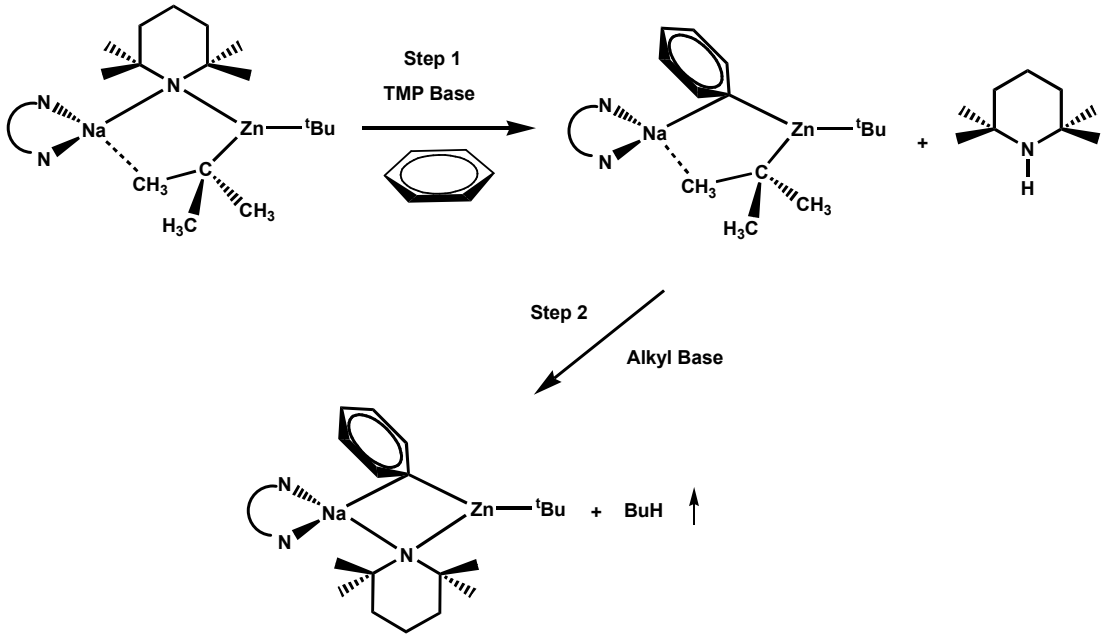

Scheme 35: Proposed two step AMM*Zn* reaction of benzene.

4.3. Reaction of 1 with anisole and N, N-diisopropylbenzamide

To establish whether these manganation reactions with both anisole and N, N-diisopropylbenzamide are examples of synergic reactivity both substrates were reacted with both individual metal components. With NaTMP in hexane no reaction was found in either case, showing that NaTMP on its own cannot *ortho*-metallate anisole nor N, N-diisopropylbenzamide even after twelve hours stirring at reflux temperature. Next we tested the dialkylmanganese compound $[Mn(CH_2SiMe_3)_2]_\infty$ reactivity towards both substrates. With anisole, even after 12 hours of heating the solution to reflux temperature the only product obtained was re-crystallised dialkylmanganese starting material **1**. However, when N, N-diisopropylbenzamide was reacted with the dialkylmanganese reagent the Lewis base/Lewis acid association complex $[Mn(CH_2SiMe_3)_2\{(iPr)_2NC(Ph)(=O)\}_2]$ **20** was obtained as bright orange plate crystals in a crystalline yield of 64% (Scheme 36).

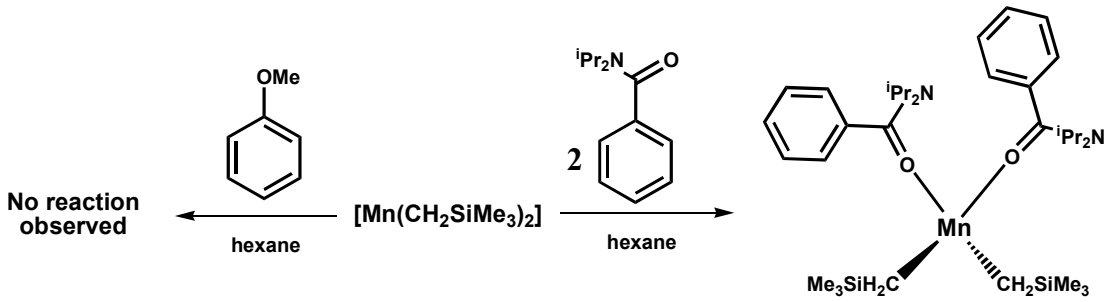

Scheme 36: Contrasting reactivity of dialkylmanganese reagent **1** towards anisole and N, N-diisopropylbenzamide.

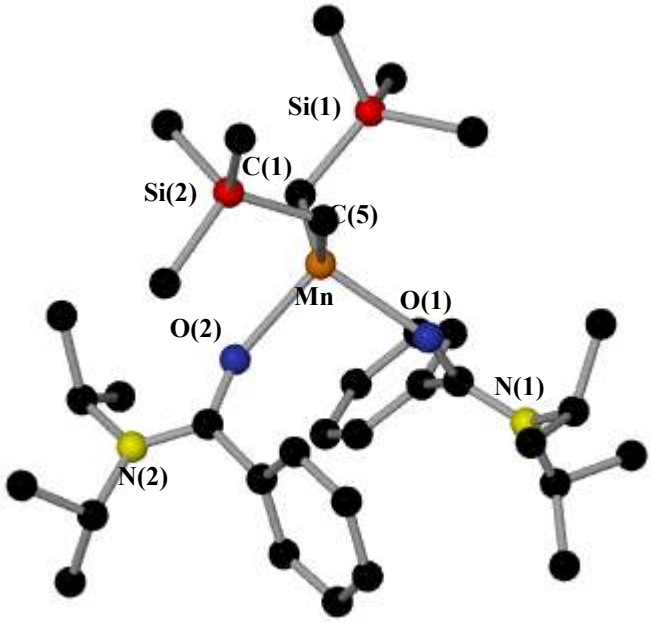

Figure 31: Molecular structure of $[Mn(CH_2SiMe_3)_2\{(iPr)_2NC(Ph)(=O)\}_2]$ **20**. Hydrogen atoms have been removed for clarity. Selected bond lengths [Å] and bond angles [º]: Mn-O(1), 2.1724(14); Mn-O(2), 2.1414(15); Mn-C(1), 2.159(2); Mn-C(5), 2.165(2); O(2)-Mn-C(1), 102.66(8); O(2)-Mn-C(5), 110.26(8); C(1)-Mn-C(5), 127.43(11); O(2)-Mn-O(1), 96.96(6); C(1)-Mn-O(1), 111.73(9); C(5)-Mn-O(1), 103.76(8).

The molecular structure of **20** (Figure 31) is a simple mononuclear arrangement. It shows a distorted tetrahedral Mn(II) centre made up of two alkyl groups and two neutral benzamide ligands, which coordinate to the metal through their oxygen atoms [Mn-O, 2.1724(14), 2.1415(15) Å]. To the best of our knowledge the only precedent for a crystallographically characterised homometallic compound containing a neutral tertiary aromatic amide coordinated to a metal is the tris(alkyl) gallium compound $[^tBu_3Ga(O=C(Ph)NMe_2)]$ reported by Bott and Barron.[156] The Mn-C bond lengths in

20 [2.159(2), 2.165(2) Å] compare favourably to the previously discussed TMEDA, pyridine and (-)sparteine[111] related complexes [2.1379(15) Å **2**; 2.146 Å **3**; 2.1582(18) Å, 2.165(17) Å **7** respectively] which also form mononuclear species. The inter alkyl separation in **20** has the narrowest angle 127.43º making it the most sterically crowded monomer [140.50º **2**; 138.69, 138.46º **3**; 132.84º **7**]. The formation of **20** helps to show the superior Lewis basicity of N, N-diisopropylbenzamide relative to that of the ether anisole, which does not cleave the polymeric manganese starting material $[Mn(CH_2SiMe_3)_2]_\infty$ **1**.

Following the X-ray crystallographic characterisation of **17** and **18** we became interested in utilising them in synthetically useful applications. Cahiez[157, 158] has had lots of success in achieving cross-coupling reactions between organo-manganese halides and functionalised aryl halides in the presence of a Pd-catalyst. However, to the best of our knowledge, no reports of catalysed cross-coupling reactions involving arylmanganate species have been reported up to now. Since **17** and **18** have covalent Mn-C(aryl) bonds within anionic ate-activated structures, we reasoned they could make excellent coupling agents. With the help of a fellow group member Ben Conway we carried out test reactions with iodobenzene in the presence of 2% $[PdCl_2(dppf)]$ (dppf = 1, 1'-bis(diphenylphosphino)ferrocene) of both crystalline and *in situ* hexane solutions of **17** and **18** (Scheme 37).

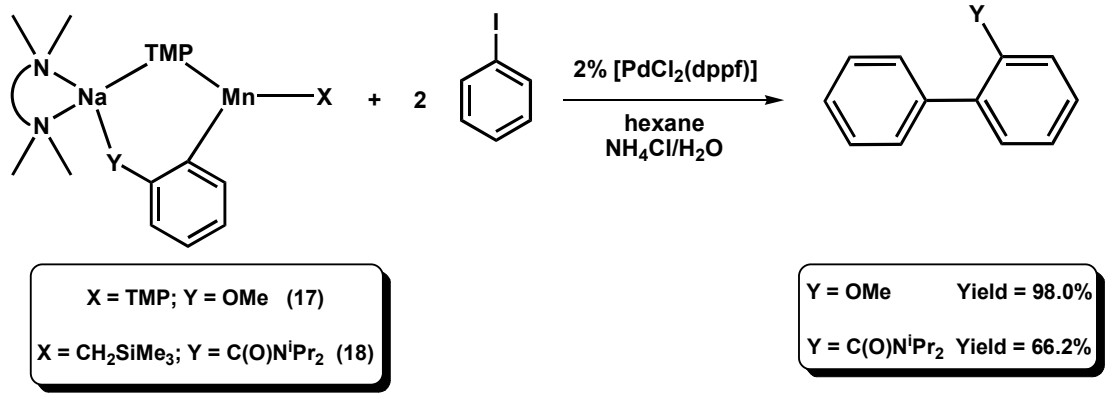

Scheme 37: Palladium catalysed cross-coupling reactions of 17 and 18 with iodobenzene.

Both reactions were successful and in the case of **17**, the coupled product 2-methoxybiphenyl was obtained in an impressive isolated yield of 98% while with **18** the product N,N-diisopropyl-2-phenylbenzamide could be obtained in a smaller yield of

66.2% after a standard aqueous/organic work-up and purification via SiO_2 column chromatography. Interestingly when the reactions were repeated in the absence of palladium catalyst direct coupling was still observed albeit in reduced yields of 32% and 42% for **17** and **18** respectively.

4.4. Reaction of the manganate base 16 with 2, 6-dimethylanisole

If *ortho*-positions next to the directing group on a substrate are blocked then obviously *ortho*-metallation cannot take place. In the case of 2, 6-dimethylanisole the *ortho*-positions are blocked by methyl groups resulting in an increased prospect of lateral metallation of the CH_3 groups. Experimentally this can be observed by conventional organolithium reagents such as *n*BuLi[159] (Scheme 38) however, yields tend to be moderate at best. With this in mind we decided to test the reactivity of the synergic base **16** with 2, 6-dimethylanisole in the hope of obtaining the first direct lateral metallation using a Mn(II) reagent.

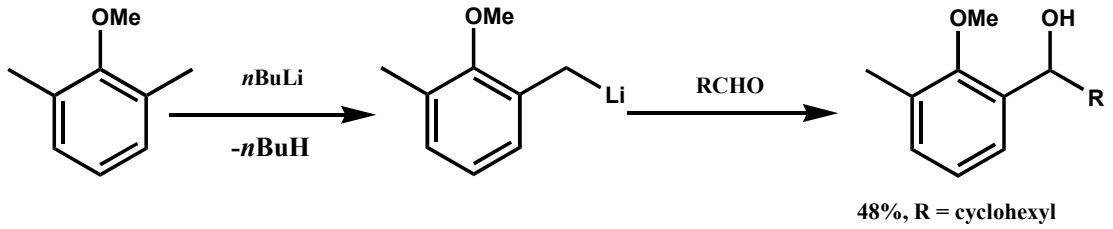

Scheme 38: Lateral metallation of 2,6-dimethylanisole by *n*BuLi.

Following the same protocol as before the synergic base **16** was reacted *in situ* in a hexane solution with one molar equivalent of 2, 6-dimethylanisole. An immediate colour change from light yellow to orange was observed and the reaction was allowed to stir at room temperature for 12 hours. Reduction of the solvent volume and placing the solution in the refrigerator (at 5ºC) or freezer (at -27ºC) did not afford any crystalline material nor did heating the reaction mixture to reflux temperature for several hours before cooling. The colour change of the reaction mixture from light orange to deep orange/brown suggests that a reaction had occurred, as indicated by obvious colour changes in the previous related reaction systems. Unfortunately due to the paramagnetic nature of Mn(II) no NMR monitoring of the reaction could be carried out and so it will require further investigation in the future with the aim of producing a crystalline solid.

4.5. Reaction of the manganate base 16 with N, N-dimethylaniline

Anilines are another class of functionalised aromatics that are relatively weak *ortho* directors in classical D*o*M chemistry using organolithium reagents. This is due primarily to delocalisation of the nitrogen lone pair into the aryl ring, decreasing the ability of the nitrogen to coordinate to an incoming organolithium molecule, which is not offset by an increase in the acidity of the ring protons through the inductive effect of the heteroatom. With regard to lithiation anilines tend to react more slowly or need higher temperatures than other aromatic substrates.[2] We selected anilines as a comparison to anisoles for this study as they have a similar directing effect and any differences in reactivity or selectivity towards the synergic base would be of interest.

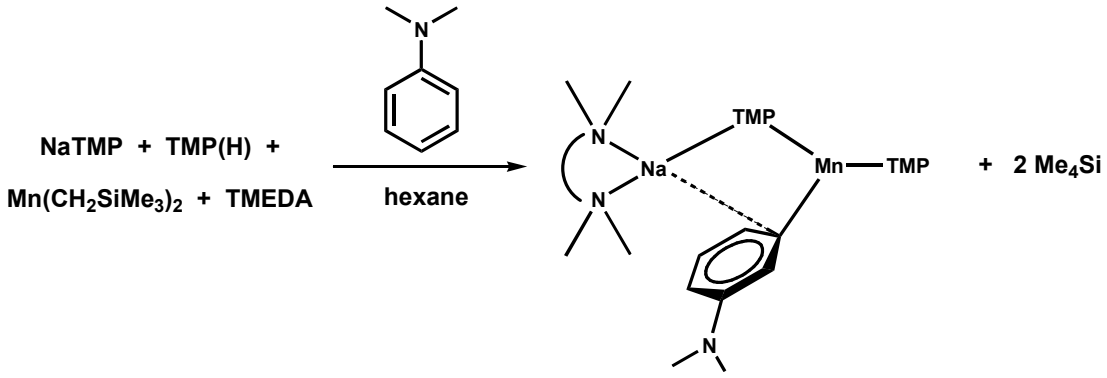

Scheme 39: Reaction of the synergic base with N, N-dimethylaniline showing the predominant *meta*-product.

Reacting an *in situ* hexane solution of the synergic base **16** with one molar equivalent of N, N-dimethylaniline at reflux temperature gave a dark brown/orange solution after two hours (Scheme 39). Light brown/orange crystals were observed in the solution at -27ºC and following their isolation were subjected to X-ray crystallographic analysis. This study revealed a mixture of *meta*- and *para*-manganated dimethylaniline isomers (in a 9:1 ratio) within the molecular structure of the product. For the purposes of this thesis only the predominant, meta-manganated dimethylaniline [(TMEDA)Na(TMP)(*m*-C_6H_4-NMe_2)Mn(TMP)] **21** will be discussed. It should be noted that the yield of **21** has not yet been definitely established. This reflects the difficulty of isolating its crystalline form, which melts rapidly during the filtration procedure.

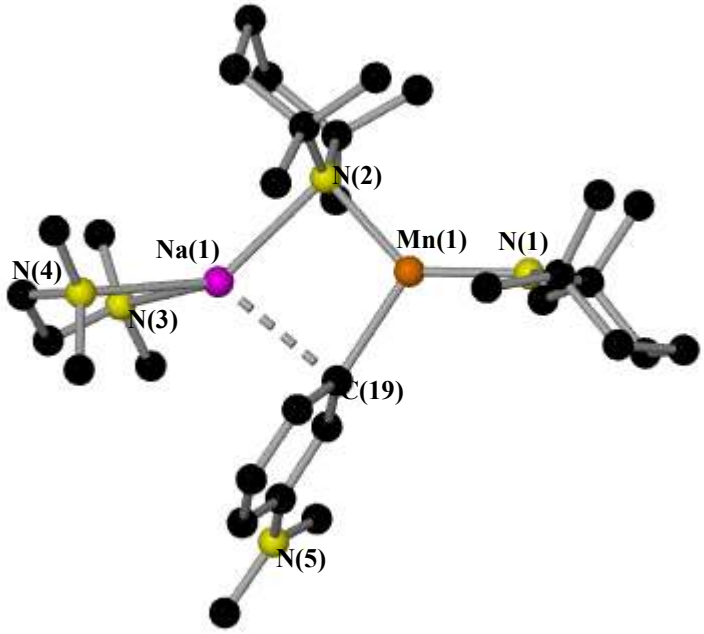

Figure 32: Molecular structure of **21** showing only the high yielding *meta*-deprotonated isomer. Hydrogen atoms have been omitted for clarity. Selected bond lengths [Å] and bond angles [º]: Mn(1)-N(1), 2.028(2); Mn(1)-N(2), 2.130(2); Mn(1)-C(19), 2.179(3); Na(1)-N(2), 2.497(2); Na(1)-N(3), 2.522(3); Na(1)-N(4), 2.544(3); Na(1)-C(19), 2.654(3); N(1)-Mn(1)-N(2), 133.76(9); N(1)-Mn(1)-C(19), 121.80(10); N(2)-Mn(1)-C(19), 104.41(10); N(2)-Na(1)-N(3), 129.96(9); N(2)-Na(1)-N(4), 130.43(9); N(3)-Na(1)-N(4), 74.39(8); N(2)-Na(1)-C(19), 82.69; N(3)-Na(1)-C(19), 124.64(10); N(4)-Na(1)-C(19), 121.44(11).

The molecular structure of **21** (Figure 32) shows a trigonal planar Mn atom coordinated to a terminal TMP [Mn(1)-N(1), 2.208(2) Å], a bridging TMP [Mn(1)-N(2), 2.130(2) Å] and a bridging dimethylaniline-based ligand [Mn(1)-C(19), 2.179(3) Å]. The dimethylaniline ligand has lost a proton from its *meta*-position on the aromatic ring, with the hydrogen replaced by a Mn(II) atom, making this reaction a C-H to C-Mn manganation. In the distorted tetrahedral coordination sphere of Na (mean bond angle, 110.57º), there is a bridging TMP [Na(1)-N(2), 2.497(3) Å], a bridging dimethylaniline [Na(1)-C(19), 2.654(3) Å] and a bidentate chelating TMEDA ligand. In the core of the structure there is a 4-atom (MnCNaN) ring, which is planar (sum of endocyclic bond angles 359.89º).

Due to the presence of the two distinct structures within the unit cell of **21** the bond lengths and angles cannot be usefully discussed nor compared. Nevertheless the connectivity within the complex is definite and can therefore be discussed in detail.

From the crystal structure, it can be observed that the deprotonation has occurred not in the *ortho* position as anticipated from the results of conventional metallation reactions, but surprisingly in the *meta*-position. Selectivity is not absolute but still exceptionally high as some molecules (10%) show deprotonation at the adjacent *para*-position. The origin of this special selectivity is not yet known for sure, but probably reflects the way the dimethylaniline substrate approaches the synergic base in the transition state of the reaction. With the nitrogen lone pair inactive for coordination, the π-system of the aryl ring probably interacts preferentially with the sodium atoms. Such π-arene···metal interactions could be the key to the unusual regioselectivities observed in AMM*M*, when the aromatic substituent is weakly directing. This result indicates that the synergic effect of the mixed-metal reagent has switched the orientation of deprotonation. Direct manganation is not usually possible using conventional manganese reagents showing that in this case the metallation observed is a result of the synergy fundamental to the new developing concept of alkali-metal-mediated manganation (AMM*Mn*).

Within our research group this interesting metallation pattern of dimethylaniline has been observed previously with zinc. Thus analogous, *meta*-deprotonated [(TMEDA)Na(TMP)($C_6H_4NMe_2$)Zn(*t*Bu)][160] was obtained, however, unlike the manganese example where a mixture of *meta*- and *para*-products were afforded, the zinc analogue gives *meta* deprotonation exclusively.

In the manganese reaction the starting reagent has reacted as an alkyl base towards N, N-dimethylaniline, with the TMP remaining in the terminal position on the Mn(II) atom post-metallation. Here the amido functional group on the aromatic ring does not interact with the alkali metal, unlike in the previous complexes **17** and **18** where instead the oxygen in the functional group on the aromatic ring coordinates to the Na resulting in a six or seven-membered ring. Instead a smaller four atom ring is seen in **21** with the Mn(II) atom lying close to the aryl plane and thus σ–bonding to the C atom; whereas Na lies almost perpendicular to this plane in more of a π–type contact.

4.6. Reaction of the manganate base with N, N-diisopropylaniline

Extending this study further we wanted to examine the effects on the metallation of adding steric bulk around the anilino nitrogen and so decided to investigate the reactivity of the synergic base with the more sterically demanding amine N, N-diisopropylaniline. Using the established synthetic protocol as before, **16** was reacted with one molar equivalent of diisopropylaniline in hexane solution. This resulted in a homogeneous yellow/orange solution. A crop of yellow needle crystals was deposited from the solution at room temperature which were subjected to X-ray crystallographic analysis to reveal the new *para*-manganated complex [(TMEDA)Na(TMP)(*p*-C_6H_4N*i*Pr_2)Mn(TMP)] **22** (Scheme 40) in an isolated crystalline yield of 69%.

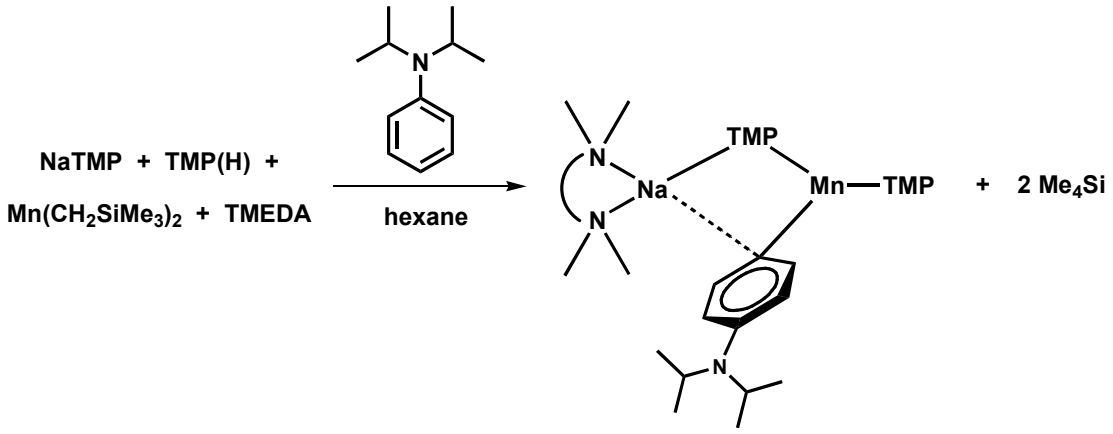

Scheme 40: Reaction of the synergic base with N, N-diisopropylaniline to yield *para*-manganated **22**.

Figure 33 shows the molecular structure of **22** retains the [(TMEDA)Na(TMP)Mn(TMP)] backbone of the synergic base but addition of a bridging diisopropylaniline-based unit allows the formation of a four membered (NaCMnN) rhomboidal ring at the centre of the structure. The Mn atom keeps its terminally coordinated TMP ligand [Mn-N(1), 2.024(8) Å] making this selective deprotonation the product of alkyl basicity, similar to that observed for complex **21,** with the loss of Me_4Si. However, the diisopropylaniline molecule has been selectively deprotonated in the unexpected *para*-position of the phenyl ring (compared to the *meta* cleavage in **21**). Defining this metallation as a manganation, the deprotonated *para*-C atom forms a strong σ-bond with the Mn atom [Mn-C(43), 2.153(7) Å] which lies co-planar with the plane of the aromatic ring; whereas the Na lies almost perpendicular to

this plane forming a longer π-arene type interaction with the *para* carbon of the aromatic ring [Na-C(43), 2.711(9) Å]. To the best of our knowledge this represents the first crystallographically characterised example of a *para*-manganated functionalised arene.

A search of the CCDB revealed **22** to be unique with no structural matches found for the *para*-metallation of N, N-diisopropylaniline even when the metal is changed to 'any metal' in the search. The Mn-C distance in **22** [2.153(7) Å] lies in the same range of those aforementioned closely related structures in this report [2.179(3) Å in **21,** 2.189(3) Å in **17**].

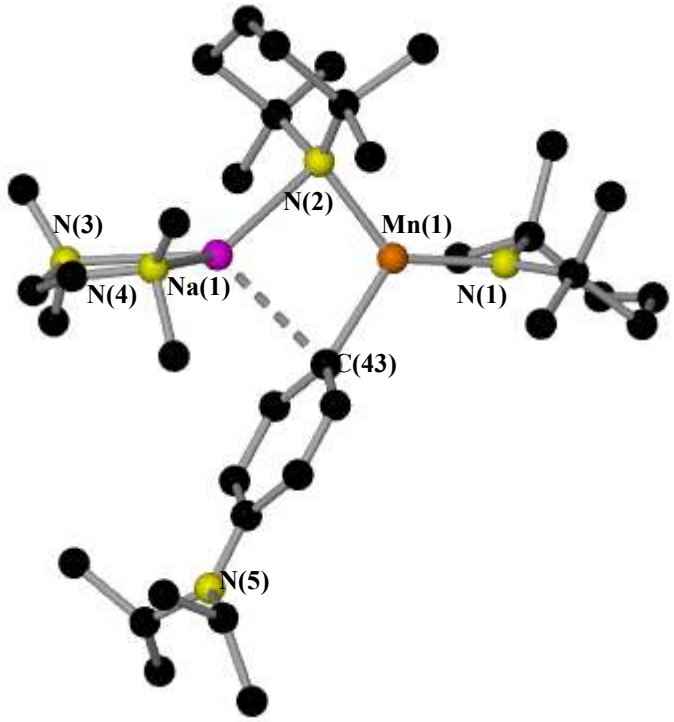

Figure 33: Molecular structure of **22** with hydrogen atoms omitted for clarity. Selected bond lengths [Å] and bond angles [º]: Mn(1)-N(1), 2.024(8); Mn(1)-N(2), 2.067(9); Mn(1)-C(34), 2.153(7); Na(1)-N(2), 2.495(10); Na(1)-N(3), 2.556(9); Na(1)-N(4), 2.408(12); Na(1)-C(34), 2.711(9); N(1)-Mn(1)-N(2), 131.3(4); N(1)-Mn(1)-C(34), 122.4(3); N(2)-Mn(1)-C(34), 106.2(4); N(4)-Mn(1)-N(2), 134.5(5); N(4)-Na(1)-N(3), 72.7(3); N(2)-Na(1)-N(3), 129.6(4); N(4)-Na(1)-C(34), 121.5(4); N(2)-Na(1)-C(34), 80.7(3); N(3)-Na(1)-C(34), 125.3(3).

After studying the reactivity of **16** with N, N-dimethylaniline and its diisopropyl analogue we can draw some conclusions about the effects of steric bulk on the position of metallation. With the less bulky methyl groups attached to the nitrogen metallation

takes place preferentially, although not exclusively, at the *meta*-position on the aromatic ring. However increasing the steric bulk to an isopropyl group directs the metalation in a different position, that is *para* on the aromatic ring. This delicate balance of *meta* versus *para* metalation must be in part due to the different ways the aniline substrate approaches the synergic base in the transition state of the reaction. A further range of substituted anilines would have to be further investigated before any definitive conclusions about the metallation site could be drawn.

4.7. Reaction of the manganate base 16 with toluene

Toluene has been metalated previously within the research group by both zinc and magnesium based synergic bases giving similar results. With magnesium the base [(TMEDA)Na(TMP)$_2$Mg(*t*Bu)][43] executes *meta* metallation of toluene leaving the more acidic methyl hydrogen atoms alone. With the zinc base [(TMEDA)Na(TMP)(*t*Bu)Zn(*t*Bu)][161] a mixture of *meta*:*para* metallation is observed in a 1.9:1 ratio leaving again the more acidic methyl group hydrogens untouched. Interestingly theoretical DFT calculations employing B3LYP method and the 6-311G** basis set of the magnesiation and zincation studies showed very little difference in the relative energies of the *meta* and *para* regioisomers,[43, 161] so it is not surprising that both are observed experimentally.

To examine what happens with manganese, as before a hexane solution of the synergic base **16** was reacted with one molar equivalent of toluene and refluxed for three hours to give an orange/red solution. Light orange/yellow crystals were observed at room temperature upon subsequent concentration of the reaction solution. Unfortunately the crystals were very sensitive and decomposed (within twelve hours) before adequate X-ray crystallography data could be collected.

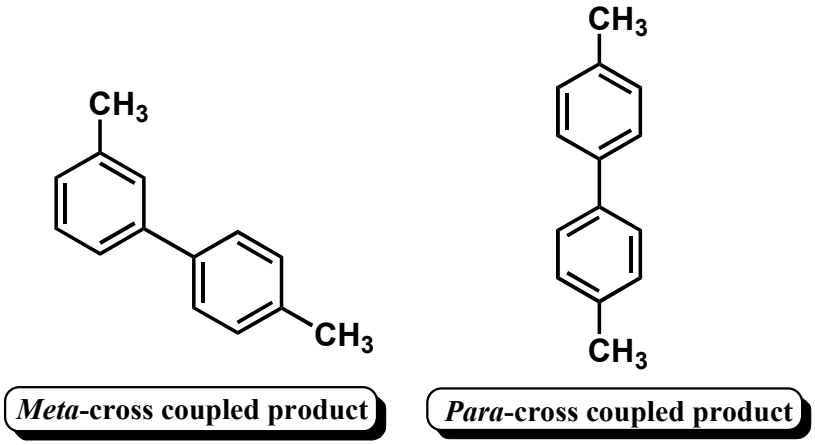

Figure 34: Examples of cross coupled products from reaction of manganated toluene with iodotoluene.

Looking to identify the resulting reaction product and with no NMR spectroscopy available due to the paramagnetic nature of Mn(II), we turned to other synthetic techniques that could help identify any present manganate products. With the collaboration of another group member Ben Conway, we decided to test the *in situ* reaction of **16** with toluene in a Pd-catalysed cross-coupling reaction with iodo-toluene to try and identify the intermediate manganated aromatic species. We anticipated the resulting cross coupled product would result in either a *meta*-cross coupled product exclusively or a mixture of *meta* and *para*-cross coupled products (Figure 34) which would match the metallation patterns observed for analogous magnesium and zinc synergic bases. Therefore to find the answer an *in situ* reaction of **16** with toluene was reacted with iodotoluene and the Pd catalyst [$PdCl_2$(dppf)] in 2 mol%. The orange/red solution was refluxed for 18 hours and after an aqueous/organic work up and purification by SiO_2 column chromatography using hexane as the eluent the resulting off white solid was analysed by NMR spectroscopy (Figure 35).

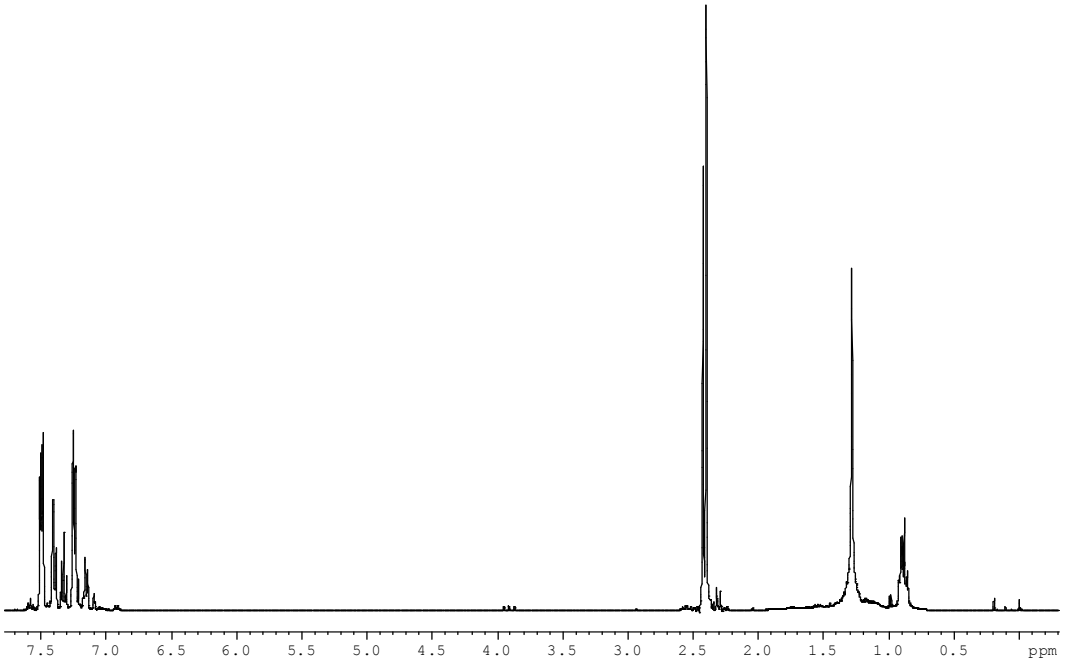

Figure 35: ^{1}H NMR spectrum in C_6D_6 solution of the solid from cross-coupling of manganated toluene with iodobenzene.

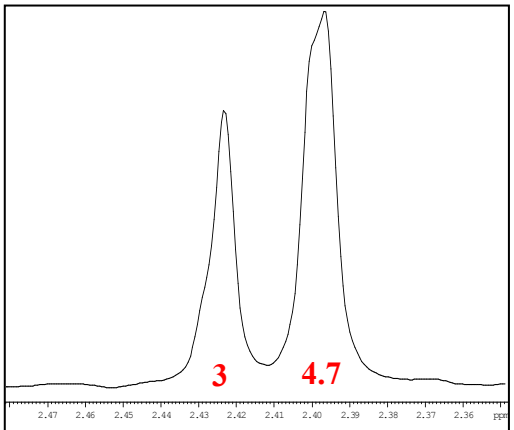

Figure 36

A *meta*-substituted toluene product would produce two different methyl singlets, as no plane of symmetry exists in the molecule. If we look to the aliphatic region of the ^{1}H NMR spectrum of the purified product then two signals for the methyl groups are seen along with some remaining solvent hexane (Figure 36) However, the integration of these two signals does not match up correctly, as you would expect the ratio to be 3 H : 3 H. The ratio in fact is 3 H : 4.7 H and when we look closely at the aromatic region there are also some signals that do not belong to the *meta*-product (Figure 37). By utilising COSY ^{1}H-^{1}H NMR spectroscopy a *meta* substituted pattern is observed. Proton H_c couples to H_b and H_d while a singlet, H_a, is found with the signal H_b. The other aromatic protons H_e and H_f can also be identified in the spectrum. Although all these proton signals integrate well, there still seems to be an extra proton under peaks H_e and H_f. Literature values for the aromatic resonances of the *para*-substituted compound at 7.45ppm and 7.21ppm would appear to match the unidentified peaks, meaning that both the *para*- and *meta*-products are observed in the

^{1}H NMR spectrum. It is no surprise that two products are present after purification as due to their similarities they must co-elute. The two products are isomers and so have the same molecular weight, giving a total overall product yield of 76%.

Next we had to try and determine the ratio of *meta* : *para* product. By using the methyl group region of the spectrum this can be easily achieved. Assuming the resonance at 2.42ppm is entirely due to the *meta*-isomer and the other resonance at 2.40ppm is due to both *meta*- and *para*-isomers then we can conclude that 22% of the isolated product is the *para* cross coupled product, 4, 4'dimethylbiphenyl and 78% is the *meta*-cross coupled product 3,4'dimethylbiphenyl. This result represents a similar finding as for the zincated toluene structure which exhibited a mixture of *para* and *meta* substituted products but in a less selective ration of 47% and 53% respectively.

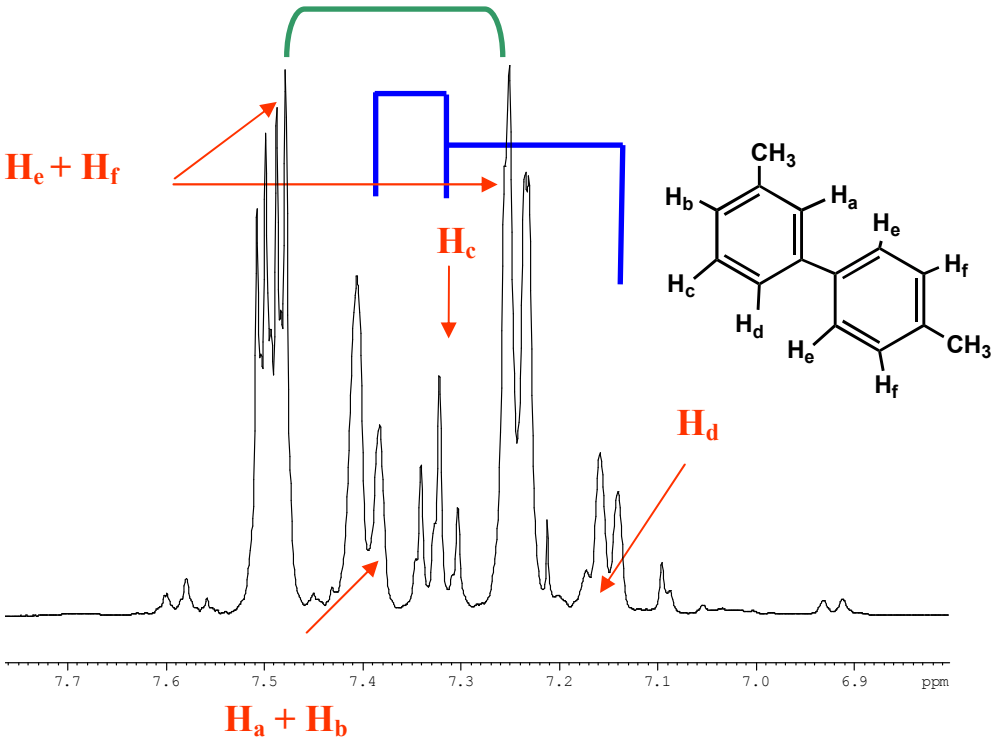

Figure 37: ^{1}H NMR of the aromatic region of the purified reaction product. Proton coupling is highlighted in blue and green.

4.8. Reaction of the manganate base with *ortho*-, *meta*-, and *para*-xylene

Following on with the theme of methyl substituted phenyl rings we wanted to further investigate the reactivity of the synergic base **16** with the three dimethyl substituted isomers *ortho*-, *meta*- and *para*-xylene (Figure 38). Usually increasing the number of

alkyl groups on an aromatic substrate can have a retarding effect on ring metallation due to the increased steric hindrance of the extra substituents. This can result in alternative lateral metallation of the methyl groups themselves which is what is commonly observed when common organometallic reagents such as *n*BuLi or LDA are employed.[162, 163]

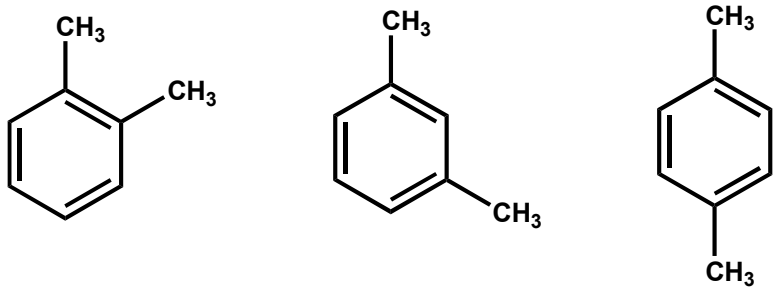

Figure 38: Series of *ortho*-, *meta*- and *para*-xylenes.

Turning to the experimental work, a hexane solution of base **16** was reacted with one molar equivalent of each of the xylene isomers in turn which in all three cases gave instant bright orange/brown solutions at room temperature. The resulting solutions were allowed to stir at room temperature for 12 hours before being filtered and stored at room temperature to allow crystallisation to occur (Scheme 41). Only the *meta*-xylene reaction mixture deposited a crop of crystals, yellow/orange cubes, that were subsequently identified by X-ray crystallographic analysis to be the new manganate [(TMEDA)Na(TMP){5-(1,3-$Me_2C_6H_3$)}Mn(TMP)] **23** (Figure 39). Unfortunately both the *ortho*- and *para*-xylene reactions produced no crystalline material (both at 5°C and -27°C), even after the reaction mixtures were heated to reflux for several hours. Again this must be stressed that solution state NMR spectroscopy cannot be used to investigate the composition of the reaction filtrates due to the paramagnetism of Mn(II). These two reactions will need further investigation in the hope of obtaining suitable crystalline material to identify any manganated products.

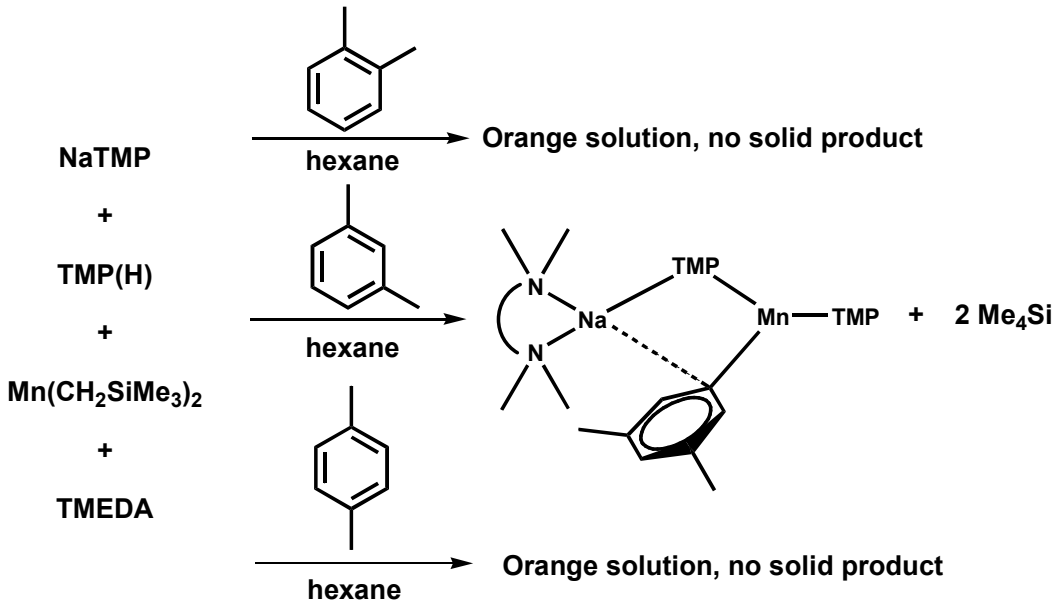

Scheme 41: Reactions of the synergic base with *ortho*-, *meta*-, and *para*-xylene.

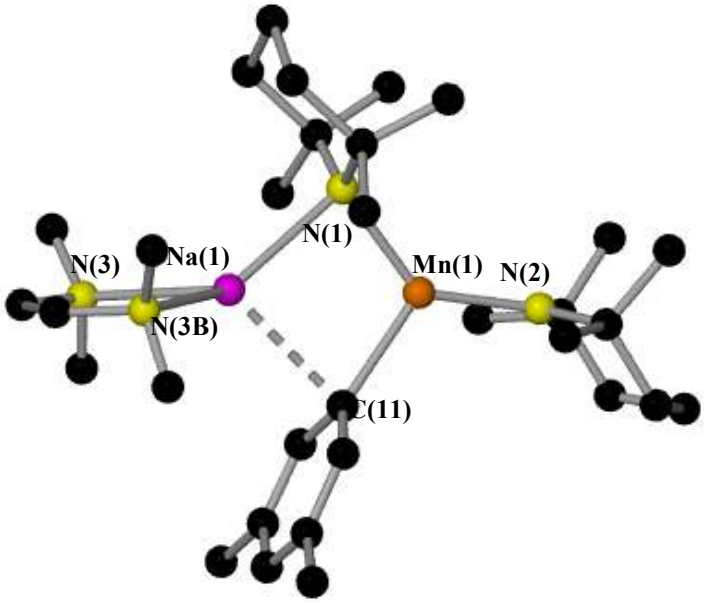

Figure 39: Molecular structure of **23**. Hydrogen atoms are omitted for clarity. Selected bond lengths [Å] and bond angles [º]: Mn(1)-N(1), 2.1109(18); Mn(1)-N(2), 2.0250(19); Mn(1)-C(11), 2.188(2); Na(1)-N(1), 2.459(2); Na(1)-C(11), 2.666(2), Na(1)-N(3), 2.589(9), Na(1)-N(3B), 2.461(9); N(2)-Mn(1)-N(1), 135.28(8); N(2)-Mn(1)-C(11), 117.17(8); N(1)-Mn(1)-C(11), 107.55(8); N(1)-Na(1)-N(3B), 137.05(15); N(1)-Na(1)-N(3), 127.74(16); N(1)-Na(1)-C(11), 85.07(7); C(11)-Na(1)-N(3B), 119.3(2); C(11)-Na(1)-N(3), 118.4(2); N(3)-Na(1)-N(3B), 74.01(17).

Complex **23** contains a trigonal planar Mn(II) centre comprising a terminal TMP ligand [Mn(1)-N(2), 2.0250(19) Å], a bridging TMP ligand [Mn(1)-N(1), 2.1109(18) Å] and a bridging deprotonated molecule of *meta*-xylene [Mn(1)-C(11), 2.188(2) Å]. The *meta*-xylene has lost a proton in the 5-position (*meta* to both methyl substituents), which has been selectively replaced with a Mn(II) atom defining this metallation as a manganation. In the coordination sphere of Na a bridging TMP is observed along with the chelating bidentate ligand TMEDA. Satisfying its coordination sphere the alkali-metal also interacts with the π–system of the aromatic substrate in a π-arene···metal type interaction [Na-C(11), 2.666(2) Å] to complete a central 4-membered ring.

The starting base **16** has functioned as an alkyl base towards *meta*-xylene, with the TMP ligand remaining at least ultimately in the terminal position on the Mn atom. This alkyl basicity is now common having been observed before in reactions of **16** with anisole, N, N-dimethylaniline and N, N-diisopropylaniline. Similar to the reaction of **16** with toluene, the more acidic methyl groups (in terms of pK_a) have been left untouched and metallation has taken place on the substituted benzene ring. In the case of **23**, direct manganation has occurred in the 5-position of the ring (*meta* to each of the methyl groups) which is the most favoured position in terms of reducing steric hindrance from the pair of methyl groups.

Previous studies with mixtures of K(HMDS) and $Zn(HMDS)_2$ within our group have shown that toluene, *meta*-xylene and mesitylene could be selectively deprotonated in the thermodynamic methyl site leaving the less favoured kinetic ring sites untouched.[164] In contrast, as mentioned previously, the TMP magnesiate [(TMEDA)Na(TMP)(*n*Bu)Mg(TMP)][43] selectively deprotonates toluene in the kinetic *meta*-position however, no reactivity studies were reported with any xylene substrates.

Searching the CCDB, it can be discerned that **23** represents the first structurally characterised complex to show direct manganation of *meta*-xylene in the 5-position. There exists several other main group In,[165] and Sn[166], and transition metal Ru,[167] Pt,[168] and Os[169] complexes containing a *meta*-xylene molecule with a metal in the 5-position, however these compounds are products of metal-halogen exchange or transmetallation reactions, and not direct metallation. Only does one example namely the organoplatinum(II) compound [PtMe{$HOB(C_6F_5)_3$}(DPK)] [DPK = di-2-pyridyl

ketone] directly deprotonate *meta*-xylene to give [Pt(5-{1,3-$CH_3C_6H_3$})$\{HOB(C_6F_5)_3\}$(DPK)][170] in which no products of *ortho* C-H or benzylic C-H bond activation were detected.

4.9. Naphthalenes and Functionalised Naphthalenes

With the success of metallating various functionalised aromatics the next logical step was to be more ambitious and extend this synergic metallation to non-activated aromatic molecules. Within our research group reagent **16** had proved successful in the manganation of benzene[55, 56] but aside from benzene the next most important compound of this type is naphthalene. This would also extend the work to polycyclic aromatic hydrocarbons.

Previous studies by Schlosser *et. a*l.,[21] into the metallation of naphthalene via a superbasic mixture of BuLi and K*t*BuO, commonly abbreviated to LiCKOR, yielded mixtures of both mono- and di-metallated products (characterised by electrophillic quenching but not isolated in their own right) with poor regioselectivity. In the case of di-metallated compounds mixtures containing up to 10 different metallation patterns were observed.[52, 171] With this in mind, the main aim of this section was to attempt to regioselectively metallate naphthalene with the new sodium-manganese synergic base.

4.10. Reaction of the manganate base 16 with naphthalene

The synergic reagent **16** was reacted *in situ* with one molar equivalent of naphthalene at room temperature to give a deep red solution after four hours stirring (Scheme 42). Deep red crystals were grown at room temperature overnight and following their isolation were analysed by X-ray crystallography. The product was established to be the new regioselectively C_2-manganated [(TMEDA)Na(TMP)($C_{10}H_7$)Mn(TMP)] **24**. Despite high isolated crystal yields of 88%, growing crystals suitable for X-ray study proved difficult as often microcrystalline solid was obtained and the reaction conditions had to be fine-tuned.

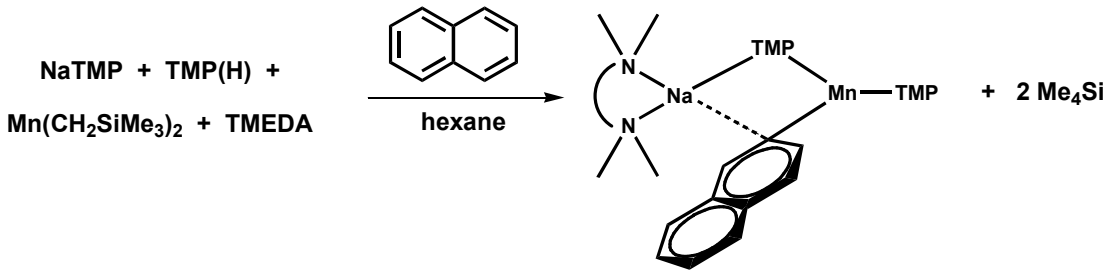

Scheme 42: Reaction of the synergic base **16** with naphthalene.

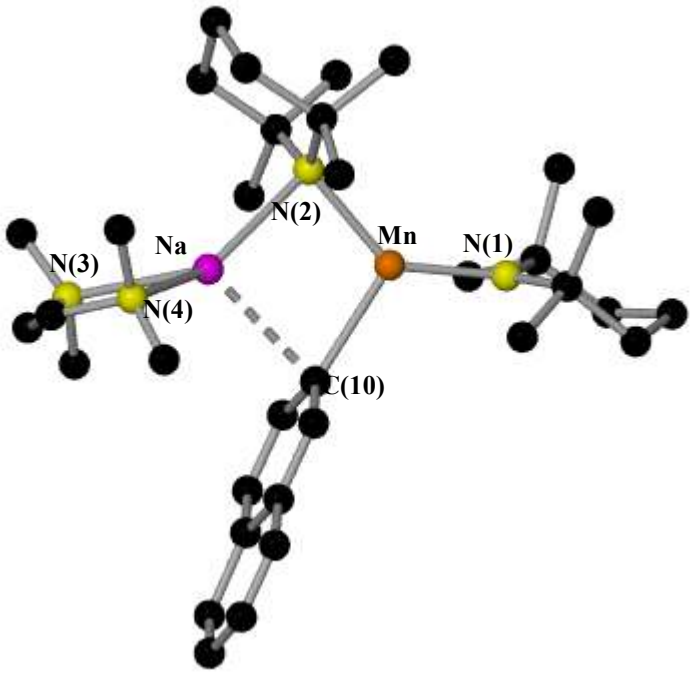

Figure 40: Molecular structure of **24**. Hydrogen atoms and one disorder component of the naphthyl ligand have been omitted for clarity.

Unfortunately due to 2-fold positional disorder of the naphthalene ligand in the crystal structure of **24**, which required constraints and restraints for its successful resolution, bond lengths and angles are less precise. However, the connectivity of **24** is definite and can therefore be discussed. Manganate **24** (Figure 40) can be categorised as a contact ion pair with the Mn(II) displaying its usual trigonal planar coordination made up of two TMP ligands, one terminal and one bridging, and a C(10) (2-position) deprotonated naphthyl ring system. Like the others in this chapter, this metallation can be defined as a manganation, as the deprotonated naphthyl atom C(10) makes a σ bond with the Mn(II) atom. The Na atom also engages with the deprotonated C(10) atom but in more of a perpendicular fashion to the π–system. This long range interaction allows a four-

element central ring (NaCNMn) to form. A chelating bidentate TMEDA ligand completes the ligand coordination around sodium.

To the best of our knowledge, **24** represents the first structurally characterised example of a Mn(II) metallated naphthalene molecule. A search of the Cambridge Structural Database revealed that only two other structures containing manganese and naphthalene have been structurally characterised, namely the arene carbonylmetalate complex PPN[Mn(η^4-$C_{10}H_8$)$(CO)_3$][172] [(PPN = Ph_3PNPPh_3)] and the mixed iron-manganese zwitterionic complex (η^4,η^6-napthalene)$Mn(CO)_3FeCp$.[173] However these two Mn(I) compounds are not products of direct (or indirect) metallation; instead, the Mn(I) is π–coordinated by the reductively activated naphthalene ligand, which retains all of its hydrogen atoms. Moreover there are only three previous mixed-metal structures containing sodium and naphthalene. Two are the closely related mono- and di-zincated complexes [(TMEDA)Na(TMP)(2-$C_{10}H_7$)Zn(*t*Bu)] and [$(TMEDA)_2Na_2(TMP)_2$(μ-2,6-$C_{10}H_6$)Zn_2(*t*Bu)$_2$][174] respectively, which show the same regioselective metallation of naphthalene in the 2-position, and in the dizincation case at the 6-position. There is also the remotely related lutetium complex [{[$(C_5Me_5Lu)_3(C_{10}H_8)(C_{10}H_7)$(H)]{[$Na(THF)_3$]}$_2C_{10}H_8$].[175]

Previously, within our group multi-deprotonation of naphthalene has been achieved via the synergic zincate base [(TMEDA)Na(TMP)(*t*Bu)Zn(*t*Bu)][51]. This begged the question "could the manganese base also poly-deprotonate naphthalene?" Therefore we repeated the initial reaction of **16** with naphthalene but changed the base: naphthalene ratio accordingly to 2:1. Various attempts at this reaction failed to di-deprotonate naphthalene, even when the reaction was heated for long periods at reflux temperature or the base stoichiometry was increased to a fourfold excess. The only crystals that were isolated from any of the reaction mixtures were the already discussed mono-manganated naphthalene complex **24**.

4.11. Reaction of the manganate base 16 with 1- or 2-methoxynaphthalene

Following the success of directly manganating the parent naphthalene it was decided to test the metallating ability of the synergic base towards the substituted naphthalene

isomers 1-methoxy- and 2-methoxy-naphthalene. In conventional metallation chemistry, the electron-donating functional group, here in the 1 or 3 position of the naphthalene ring, can (weakly) direct the metallation to two main positions, (i) *ortho* to the functional group, as the proton is sufficiently acidified by the inductive effect of the electronegative oxygen substituent as well as close enough to the lone pair of the oxygen to allow dative coordination of the metallating reagent, or (ii) *peri* to the functional group, which is possible only in the case of 1-methoxynaphthalene (Figure 41).

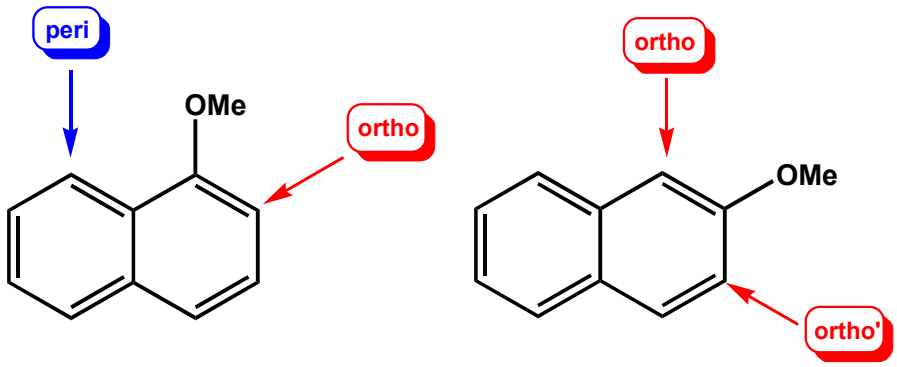

Figure 41: Possible metallation sites for 1-methoxynaphthalene (LHS) and 2-methoxynaphthalene (RHS).

When the synergic base **16** was reacted *in situ* with one molar equivalent of each methoxynaphthalene, in hexane solution, a colour change from light yellow to dark red was observed after four hours stirring at room temperature (Scheme 43). Crystallisation proved problematic as often, like that seen for the naphthalene reaction, microcrystalline solids were deposited that were unsuitable for X-ray analysis. However, increasing the solvent volume and allowing the reaction mixture to stand at room temperature or in a refrigerator for one week enabled the growth of X-ray quality red cubic crystals in both reactions. The structures were revealed to be the new *ortho*-manganated complexes [(TMEDA)Na(TMP){2-(1-OMe-$C_{10}H_6$)}Mn(CH_2SiMe_3)] **25** and [(TMEDA)Na(TMP){3-(2-OMe$C_{10}H_6$)}Mn(TMP)] **26**.

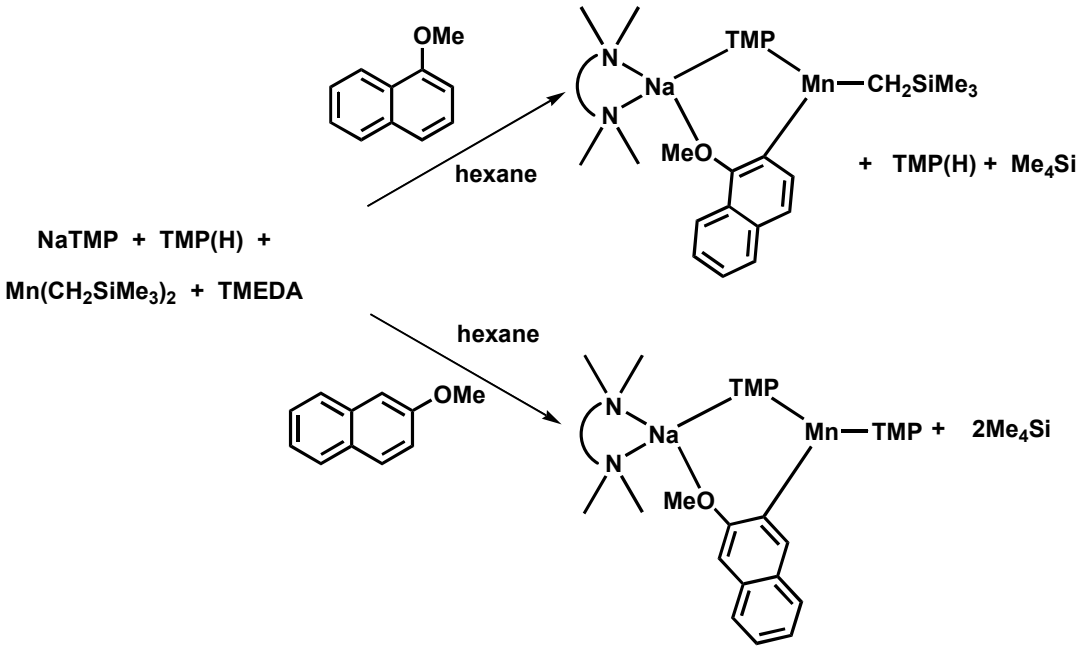

Scheme 43: Reaction of the synergic base with 1-methoxy- and 2-methoxynaphthalene.

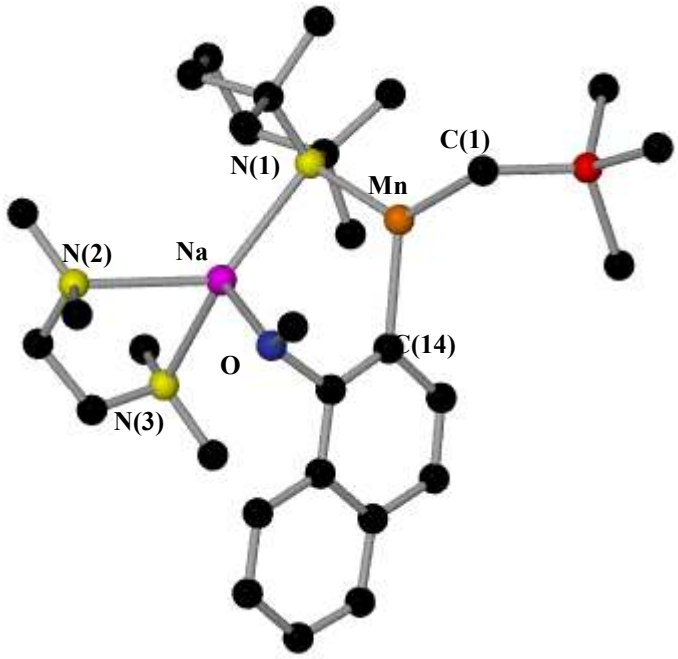

Figure 42: Molecular structure of **25**. Hydrogen atoms are omitted for clarity. Selected bond lengths [Å] and bond angles [º]: Mn-C(1), 2.141(2); Mn-C(14), 2.177(2); Mn-N(1), 2.0789(19); Na-N(1), 2.497(2); Na-N(2), 2.553(2); Na-N(3), 2.489(2); Na-O, 2.4174(18); C(1)-Mn-C(14), 118.31(9); C(14)-Mn-N(1), 111.60(8); C(1)-Mn-N(1), 129.29(9); O-Na-N(1), 104.99(6); O-Na-N(2), 98.87(7); O-Na-N(3), 106.98(7); N(2)-Na-N(3), 74.01(8); N(1)-Na-N(2), 129.47(8); N(1)-Na-N(3), 135.79(8).

The molecular structures of **25** and **26** (Figure 42 and Figure 43 respectively) can be classed as contact ion pairs sharing the common structural motif of a six-atom central ring. Made up of C_2N atoms in **25** and CN_2 atoms in **26,** the Mn adopts a trigonal planar coordination, comprising one terminal ligand (CH_2SiMe_3 in **25** and TMP in **26**) and two bridging ligands, a TMP and *ortho*-deprotonated methoxynaphthalene in both. The Mn atom forms a σ bond to the deprotonated C atom [C(14) in **25** in position 2; C(19) in **26** in position 3] of the naphthalene ring system, defining these reactions as manganations, that is Mn-H exchange reactions. In contrast Na interacts with the deprotonated naphthalene ligand though the O heteroatom of its methoxy-substituent to form a six-membered, five element ring (NaNMnCCO) in both **25** and **26**. The core of each structure is therefore made up of three fused rings, with **25** resembling a 5, 6, 7, 8-tetrahydrophenanthrene metallacycle and **26** a 1, 2, 3, 4-tetrahydroanthracene metallacycle (Figure 44).

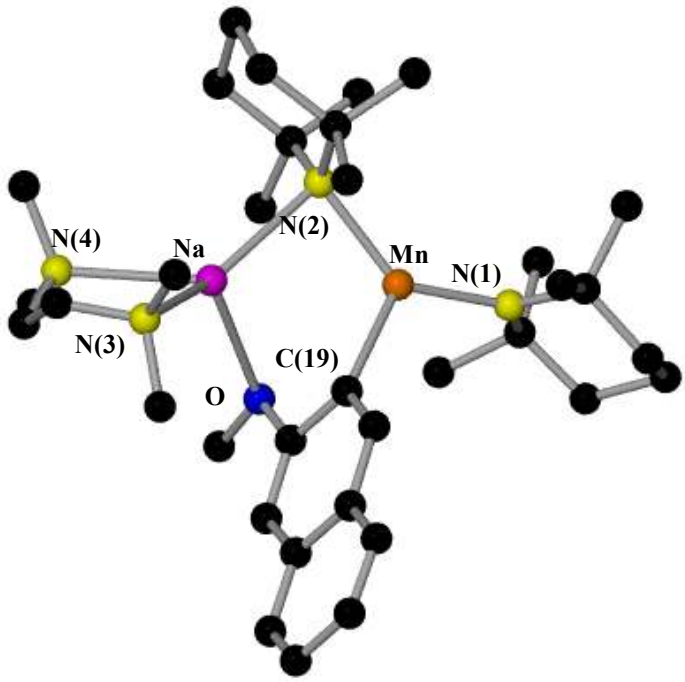

Figure 43: Molecular structure of **26**. Hydrogen atoms are omitted for clarity. Selected bond lengths [Å] and bond angles [º]: Mn-N(1), 2.0220(17), Mn-N(2), 2.1059(17); Mn-C(19), 2.201(2); Na-N(2), 2.4981(19); Na-N(3), 2.579(2); Na-N(4), 2.539(2); Na-O, 2.6843(19); N(1)-Mn-C(19), 114.12(8); N(2)-Mn-C(19), 110.84(7); N(1)-Mn-N(2), 134.96(7); O-Na-N(2), 93.49(6); O-Na-N(3), 120.00(6); O-Mn-N(4), 104.47(7); N(3)-Na-N(4), 73.37(7); N(2)-Na-N(3), 136.11(7); N(2)-Na-N(4), 128.01(8).

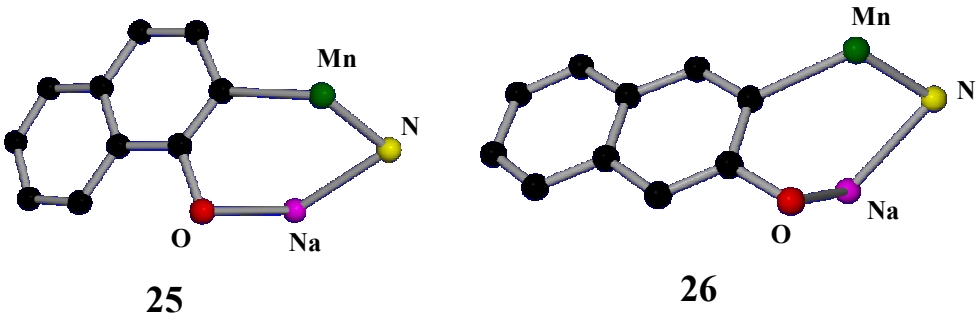

Figure 44: Metallacycle frameworks of **25** and **26**.

From these X-ray crystallographic results we again appear to observe a distinction in the reactivity of the synergic base **16** towards these functionalised naphthalenes. When **16** manganates 2-methoxynaphthalene it behaves ultimately as an alkyl base with loss of Me_4Si to give the thermodynamic product **25**. In contrast, when **16** is reacted with 1-methoxynaphthalene it shows the alternative basicity acting as an amido base resulting in the formation of the kinetic product **26** and with the loss of TMP(H). Clearly the factors governing whether an AMM*M* follows a kinetic or thermodynamic pathway are subtle and changing the substrate can lead to a modification in the transition structure, tipping the favour for one path over the other. It should also be stressed that these alternative reactions are based on the results of a few crystals only, and whether they apply to the bulk product of the reaction is still an open question. In addition a full series of substituted naphthalenes would have to be investigated before any definitive conclusions related to the nature of the substrate could be drawn.

To the best of our knowledge **25** and **26** represent the first structurally characterised examples of Mn(II) methoxynaphthalenes and in fact appear to be the first structurally characterised 2- or 3-metallated methoxynaphthalenes of any metal in the periodic table. There has been some literature by Mannschreck and Kielf[176] on the direct metallation of 1-methoxynaphthalene followed by Li-Mn(II) exchange and further reactions with electrophiles, where they propose an *ortho*-manganated 1-methoxynaphthalene as an intermediate; however they stress that the structures of these Mn(II) compounds are not yet known.

The best structural comparison for complexes **25** and **26** is provided by the *ortho*-manganated anisole [(TMEDA)Na(TMP)(*o*-C_6H_4OMe)Mn(TMP)] **17** previously

discussed in this chapter and the remotely related *peri*-lithiated dimer (1-methoxy-8-naphthylithium·THF)$_2$(THF)$_2$.[177, 178] The Mn-C(aryl) distance in **17** [2.189(2) Å] lies between that found in **25** [2.177(2) Å] and **26** [2.20(2) Å]. Compound **17** also has the same six-membered five-element ring (NaNMnCCO) as that found in **25** and **26**. These metallocyclic rings that make up the pseudo-phenanthrene and pseudo-anthracene arrangements are highly puckered; Na and N(1) lie out of the naphthyl ring plane by 2.373 and 1.976 Å, respectively in **25**, and Na and N(2) lie out of the naphthyl ring plane by 2.404 and 1.335 Å in **26**. In the lithiated dimer (1-methoxy-8-naphthylithium·THF)$_2$(THF)$_2$ the methoxy naphthalene is lithiated *peri* to the functional group with a Li-C(aryl) distance of 2.162(5) Å. This difference in metallation pattern causes a smaller five-membered central (OCCCLi) ring to form which lies coplanar with the naphthyl system.

Interestingly, the selective metallation of 1-methoxynaphthalene in either the 2- or 8-position (*ortho* and *peri* respectively) has been extensively studied by Shirley and Cheng.[179] They report that the metallation can be regioselectively controlled by changing the metallating reagent. By using an equimolar *n*BuLi/TMEDA mixture and quenching with solid CO_2, selectivity in greater than 99% carbonylation in position 2 is observed (note however the smaller overall yield of 59%) whereas changing the metallating reagent to *t*BuLi leads to greater than 98% carbonylation in the 8-position (but in a poorer 20-35% overall yield). When the selectivity of our synergic base **16** is compared to these precedent literature methods we also observe good regioselectivity in the 2-position with 1-methoxy naphthalene and in the 3-position with 2-methoxynaphthalene, with both complexes being isolated in decent crystalline yields up to 85% and 65% respectively. The metallation patterns of the three naphthalene complexes **24**, **25** and **26** were successfully confirmed by electrophilic quenching studies with iodine to give the respectively 2-iodonaphthalene, 2-iodo-1-methoxynaphthalene and 3-iodo-2-methoxynaphthalene compounds in isolated yields of 45%, 38% and 51% after aqueous workups.

4.12. Reaction of the manganate base 16 with N, N-dimethyl-1-naphthylamine

Continuing with the theme of substituted naphthalenes we next investigated the reactivity of the synergic base **16** with N, N-dimethyl-1-naphthylamine. Comparing this substrate with the already investigated N, N-dimethylaniline, where a mixture of *meta*- and *para*-manganation was observed, the only difference between them is the extended aromatic backbone. By investigating this reaction we can establish if the NMe_2 group has the same lack of directing ability when present on a polycyclic aromatic hydrocarbon (Figure 45).

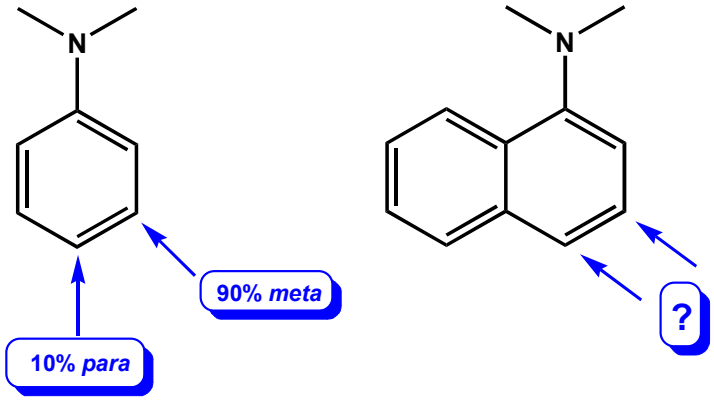

Figure 45: Comparison of N, N-dimethylaniline and N, N-dimethyl-1-naphthylamine metalation patterns.

Following the same procedure as before after forming the synergic base **16** *in situ* in hexane solution, one molar equivalent of N, N-dimethyl-1-naphthylamine was added to give a bright red solution after four hours stirring at room temperature (Scheme 44). Pale red crystals were grown from this solution at room temperature and subsequently subjected to X-ray crystallography. This revealed the product to be the new manganated complex [(TMEDA)Na(TMP){6-(1-Me_2N-$C_{10}H_6$)}Mn(TMP)] **27**.

The molecular structure of **27** (Figure 46) shows a trigonal planar three-coordinate Mn(II) atom with a terminal TMP, a bridging TMP and a bridging deprotonated dimethyl-1-naphthylamine ligand. The aromatic ligand has lost a hydrogen atom in the 6-position, which has been selectively substituted with a σ bonded Mn(II) atom. Therefore this selectivity, *meta* to the *peri*-position, is different to that previously

observed in the substituted aniline case. In the coordination sphere of the distorted tetrahedral Na, there is a bridging TMP, a bridging deprotonated dimethyl-1-naphthylamine ligand and a chelating bidentate TMEDA. The core of the structure displays a 4-atom, 4-element (MnCNaN) ring.

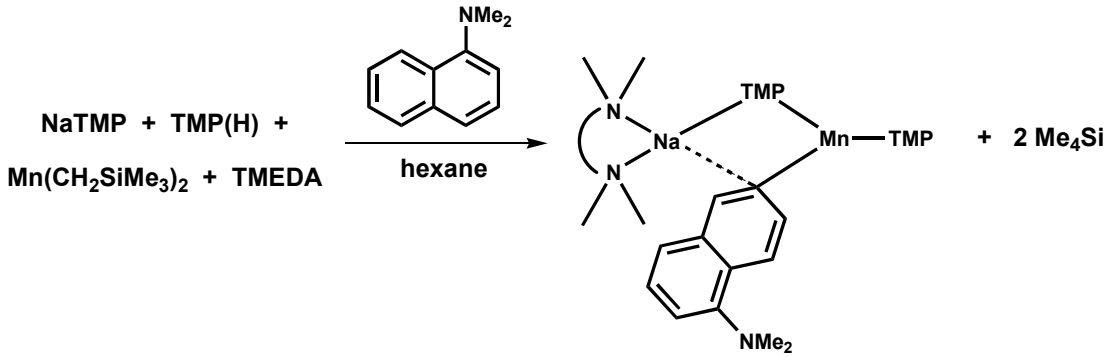

Scheme 44: Reaction of the synergic base with N, N-dimethyl-1-naphthylamine.

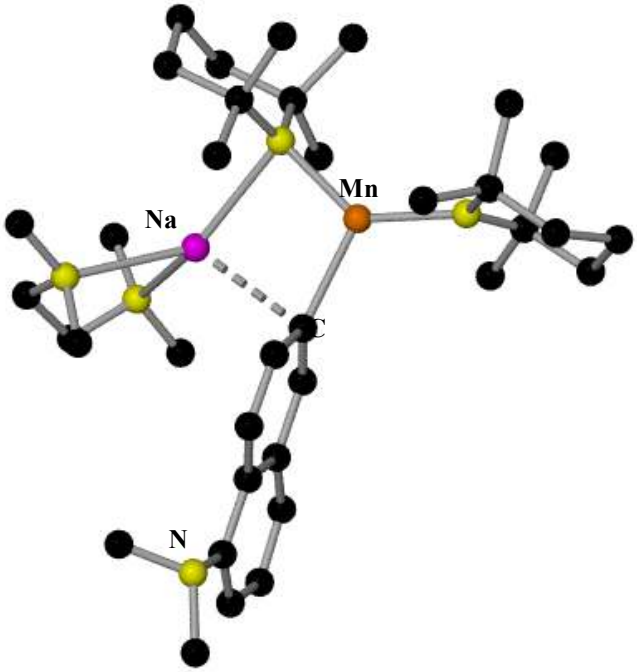

Figure 46: Molecular structure of **27**. Hydrogen atoms are omitted for clarity.

Unfortunately disorder in the crystal structure of **27** does not permit discussion of the bond lengths and bond angles, but the connectivity is nevertheless absolute. Various attempts to try and grow better quality crystals from different solvent systems and reaction conditions were not successful and disorder within the molecule was still

observed. Note that compound **27** is paramagnetic and thus not amenable to diagnostic NMR spectroscopy studies making further characterisation difficult.

Much previous work within the research group had focused on the reactivity of the magnesiate base [(TMEDA)Na(TMP)(*n*Bu)Mg(TMP)] which was mentioned earlier in the context of the selective *meta*-deprotonation of toluene. A major distinction between this magnesium base and our manganate **16**, apart from the change of the divalent metal, is the alkyl ligand, *n*-butyl and trimethylsilylmethyl respectively. It was therefore decided to synthesise a magnesium analogue of **16** and if successful to investigate its reactivity towards N, N-dimethyl-1-naphthylamine.

4.13. Synthesis of the magnesiate base 28

To synthesise the new trimethylsilylmethyl based magnesiate base, NaTMP was reacted with molar equivalents of TMP(H), $Mg(CH_2SiMe_3)_3$ and TMEDA to give a light yellow solution (
Scheme 45). Reduction of the solvent under vacuum and storage of the solution at room temperature allowed a crop of light yellow crystals to form (in a low isolated yield of 19%). X-ray crystallographic analysis of these crystals revealed them to be the anticipated magnesiate complex [(TMEDA)Na(TMP)(CH_2SiMe_3)Mn(TMP)] **28**. A low crystalline yield was observed due to the extremely soluble nature of the product however, analysis of the filtrate via ^{1}H NMR spectroscopy revealed the presence of **28** exclusively (Figure 47).

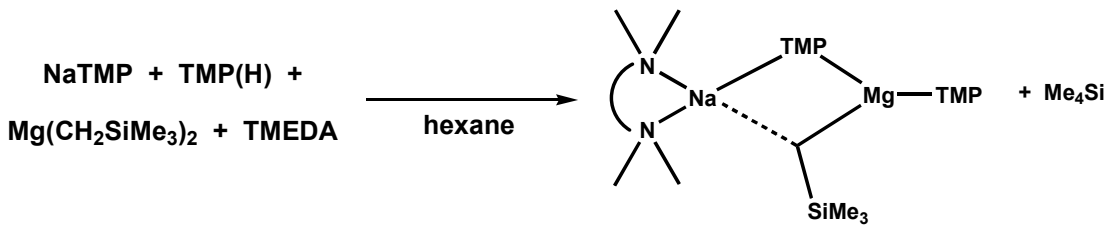

Scheme 45: Synthesis of the trimethylsilylmethyl-based magnesiate **28**.

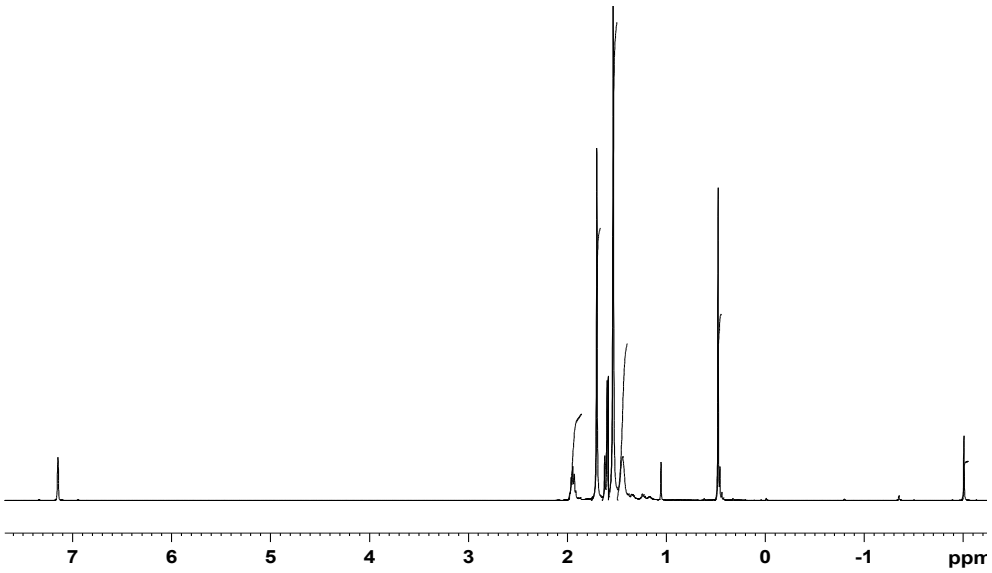

Figure 47: ^{1}H NMR in C_6D_6 solution of filtrate of magnesiate base **28**.

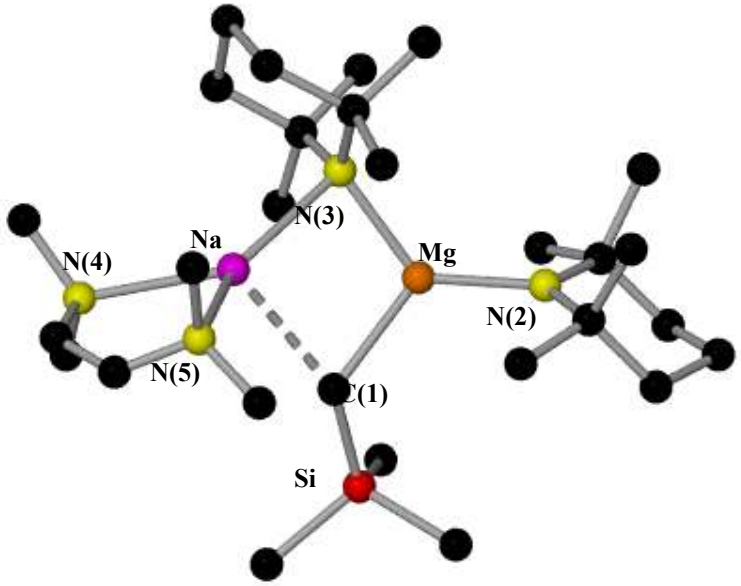

Figure 48: Molecular structure of **28**. Hydrogen atoms are omitted for clarity. Dashed line indicates agostic interaction. Selected bond lengths [Å] and bond angles [º]: Mg-N(2), 1.9895(18); Mg-C(1), 2.179(2); Mg-N(3), 2.068(3); Na-N(3), 2.454(4); Na-C(1), 2.678(2); Na-N(4), 2.433(2); Na-N(5), 2.488(3); C(1)-Mg-N(2), 123.36(10); C(1)-Mg-N(3), 106.67(13); N(2)-Mg-N(3), 128.70(14); N(4)-Na-N(3), 139.70(12); N(4)-Na-N(5), 75.48(12); N(3)-Na-N(5), 138.90(13); N(4)-Na-C(1), 115.49(10); N(3)-Na-C(1), 83.08(9); N(5)-Na-C(1), 100.81(12).

Isostructural to **16**, the molecular structure of **28** (Figure 48) exhibits a contact ion pair arrangement with a N_2C trigonal planar magnesium coordinated by two bridging ligands,

a TMP and trimethylsilylmethyl, and one terminal TMP ligand. As in many of the previously discussed structures, a ring motif, specifically here of a 4-atom, 4-element NaCMnN type, is a core feature. A chelating bidentate TMEDA molecule completes the distorted tetrahedral coordination around the Na. Table 2 compares the key corresponding dimensions within **28** and **16**.

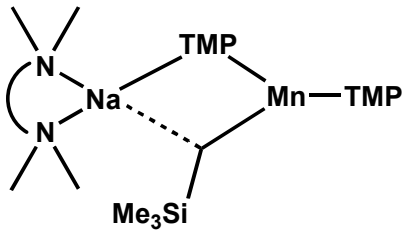

16

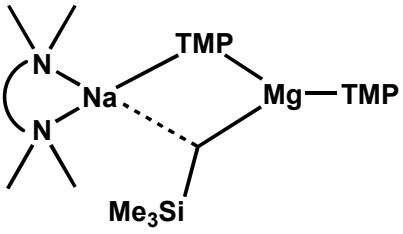

28

Figure 49: Chem-Draw representations of the manganese **16** and magnesium **28** synergic bases.

Table 2 Comparison of selected bond lengths [Å] and bond angles [º] for complexes **16** and **28**.

	16 (M= Mn)	**28** (M= Mg)
M-C(alkyl)	2.198(3)	2.179(2)
M-TMP	2.012(2)^{t} 2.109(2)^{b}	1.9895(18)^{t} 2.068(3)^{b}
Na-N (TMP)	2.435(3)	2.454(4)
Na-N (TMEDA)	2.425(6) 2.457(8)	2.433(2) 2.488(3)
N^{b}-M-N^{t}	129.43(12)	128.71(13)
N^{t}-M-C(alkyl)	123.68(12)	123.36(10)
N^{b}-M-C(alkyl)	105.70(10)	106.67(13)
Na-TMP-M	85.04(3)	85.42(11)
Na-C-M	77.77(9)	77.98(7)

key: t, terminal atom/bond; b, bridging atom/bond

When analysing the data in Table 2 the two isostructural compounds show no significant differences when Mn is substituted for Mg. The largest bond difference between them is in the M-TMP bridging distance at only 0.041Å while the largest angle difference is seen in the N^{b}-M-C angle at only 0.97º.

Next we wanted to investigate the reactivity of the new magnesiate **28**, to establish whether it followed the same reactivity patterns as that observed for its Mn analogue. Thus it was decided a good place to start would be with the metallation of N, N-dimethylnaphthylamine, as previously its reaction with **16** gave an interesting metallation position albeit with incomplete crystal data.

4.14. Reaction of the magnesiate base 28 with N, N-dimethyl-1-naphthylamine

After forming the magnesiate **28** *in situ* in hexane solution, one molar equivalent of N, N-dimethyl-1-naphthylamine was added to give a light orange/brown solution which was allowed to stir at room temperature for one day (
Scheme 46). Reduction of the solvent volume under reduced pressure and storage of the solution at room temperature furnished after three days, a crop of light orange/brown crystals in an isolated crystalline yield of 73 %. On the basis of X-ray crystallography and NMR spectral data, the crystals were found to be the new magnesiate complex [(TMEDA)Na(TMP){6-(1-Me_2N-$C_{10}H_6$)}Mg(TMP)] **29**.

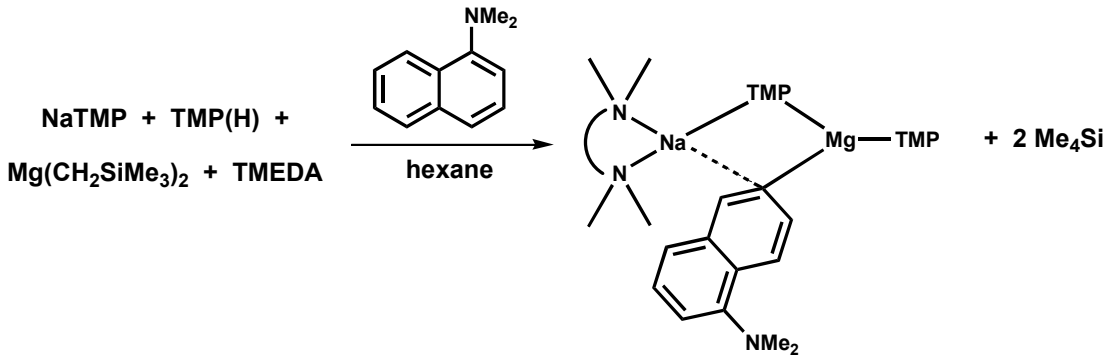

Scheme 46: Reaction of the magnesiate base **28** with N, N-dimethyl-1-naphthylamine.

In its gross structural features, magnesiate **29** (Figure 50) mirrors its manganate analogue **27**. A trigonal planar magnesium is surrounded by a terminal TMP [Mg-N(2), 2.002(5) Å], a bridging TMP [Mg-N(3), 2.049(5) Å] and a bridging dimethyl-1-naphthylamine ligand [Mg-C(1), 2.198(6) Å]. The alkaline-earth metal connects to the polycyclic aromatic ligand at the 6-position, where a hydrogen atom has been disconnected. In the coordination sphere of the distorted tetrahedral sodium, there is a bridging TMP [Na-N(3), 2.510(5) Å], a bridging dimethyl-1-naphthylamine [Na-C(1), 2.694(7) Å] and a bidentate chelating TMEDA molecule (mean Na-N, 2.486 Å) . The core of the structure contains a 4-atom (MnCNaN) ring which is essentially planar (sum of endocyclic bond angles 358.52º).

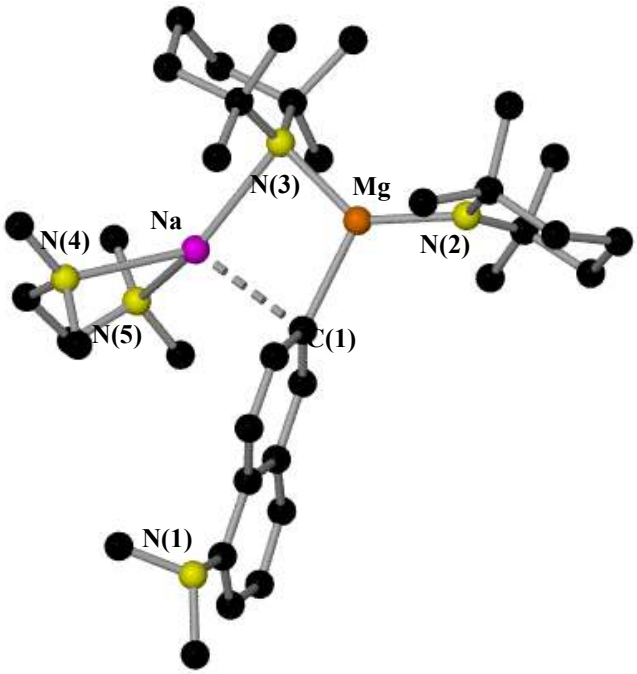

Figure 50: Molecular structure of **29**. Hydrogen atoms are omitted for clarity. Selected bond lengths [Å] and bond angles [°]: Mg-N(2), 2.002(5); Mg-N(3), 2.049(5); Mg-C(1), 2.198(6); Na-N(3), 2.510(5); Na-N(4), 2.489(6); Na-N(5), 2.483(6); N(2)-Mg-N(3), 133.46(19); N(2)-Mg-C(1), 117.2(2); N(3)-Mg-C(1), 108.9(2); N(5)-Na-N(4), 75.2(2); N(5)-Na-N(3), 135.9(2); N(4)-Na-N(3), 132.5(2); N(5)-Na-C(1), 118.3(2); N(4)-Na-C(1), 116.0(18); N(3)-Na-C(1), 83.12(7).

From the crystal structure it can be surmised that the synergic base **28** displays alkyl basicity towards N, N-dimethyl-1-naphthylamine. The terminal TMP remains bonded to the Mg while the trimethylsilyl group has been replaced selectively by a C_6-magnesiated aromatic ligand. The Mg lies in the plane of the naphthylamine ring forming a strong σ bond to the C_1 atom (at the 6-position). In contrast, Na lies nearly perpendicular to this plane interacting with the π-system of the naphthyl ring of the substrate, focusing its interaction on the C_1 atom on the ring.

As the divalent metal has been changed from manganese to magnesium, NMR spectroscopy is now available to study the solution chemistry of complex **29**. Recorded in C_6D_6 solution, the ^{1}H NMR spectrum of **29** (Figure 51 and
Figure 52). These assignments were made utilising COSY ^{1}H-^{1}H NMR spectroscopy. In the aliphatic section the resonance at 2.96 ppm can be assigned to the CH_3 groups of the amine, while the resonances at 1.89, 1.67 and 1.35 ppm can be assigned to the γ-CH_2, CH_3 and β-CH_2 of the TMP ligand respectively. The remaining resonances at 1.40 and

1.22 ppm can be assigned to the CH_3 and CH_2 hydrogen atoms of TMEDA respectively. The complex was also characterised by ^{13}C NMR spectroscopy the assignment details of which can be found in the experimental section of the thesis.

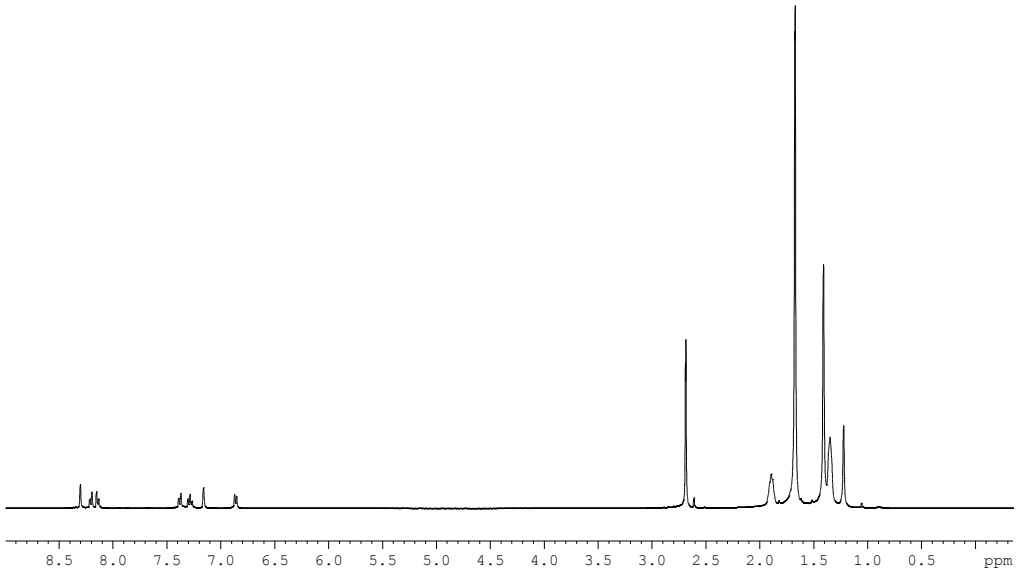

Figure 51: Full ^1H NMR spectrum of **29** in C_6D_6 solution.

A search of the Cambridge Structural Database revealed **27** and **29** to be unique with no hits found for the selective 6-position metallation of N, N-dimethyl-1-naphthylamine with manganese or magnesium or indeed for any metal in the periodic table. There are however some structural examples of metallation in the *peri*-position (8-position) of this specific molecule with the main group metals Al,[180-182] Ga,[180] and In[180] and the transition metals Mn[183] and Cu.[184] However, it should be mentioned that these related compounds were not prepared by direct metallation but are rather products of lithium-metal exchange reactions. There are also two structurally characterised examples of the products of direct *peri*-lithiation, namely the ether and THF solvated dimers [{1-(dimethylamino)-8-naphthyl}Li.Et_2O]$_2$[185-187] and [{1-(dimethylamino)-8-naphthyl}Li.THF]$_2$;[188] while examples of 6-position metallation are not found.

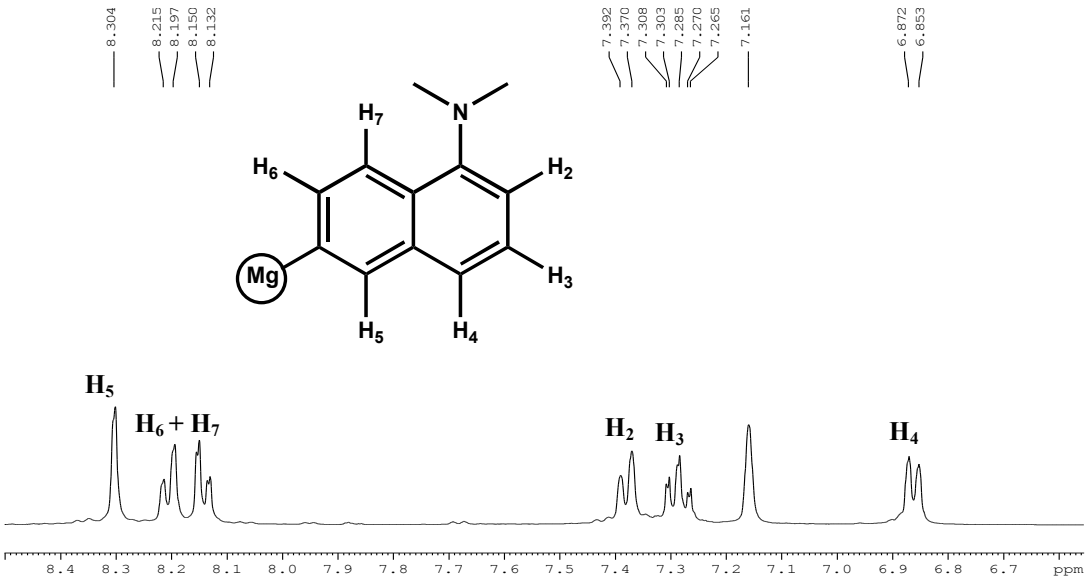

Figure 52: Expanded aromatic region of ^{1}H NMR spectrum of **29**.

To gain further understanding of this special 6-position directed magnesiation reaction of N, N-dimethyl-1-naphthylamine a theoretical study has been carried out. In collaboration with Dr Armstrong, density functional theory (DFT) calculations using the B3LYP functionals and the 6-311G** basis set were performed. Eight regioisomers of compound **29** were modelled (Figure 53) in which the naphthylene ring has been mono-metallated in the *ortho*, *meta*, *para*, 5, 6, 7, *peri* or methyl position. Reaction of **28** with the naphthylamine was found to be exothermic by -7.29 kcal mol^{-1} except in the case of the *peri*-position substitution where the reaction is endothermic and not favoured. The results of the DFT calculations show that the most stable theoretical structure is found to be the 7-position isomer closely followed by the 6-position isomer, which is only 0.16 kcal mol^{-1} less stable in energy. Although not in complete agreement with the experimental findings, where exclusive 6-position metallation is observed, the extremely very small difference in their relative energies suggest both metallation positions are possible and other factors must play a part in the final choice of metallation site. The next most stable theoretical model is the *meta* isomer (at 0.53 kcal mol^{-1}) closely followed by the *para* (1.85 kcal mol^{-1}) and 5-position (1.97 kcal mol^{-1}) isomers. The remaining *ortho* and *peri* isomers have increasingly higher relative energies of 6.17 kcal mol^{-1} and 8.86 kcal mol^{-1} respectively with finally the methyl isomer being the least stable of all (10.37 kcal mol^{-1}).

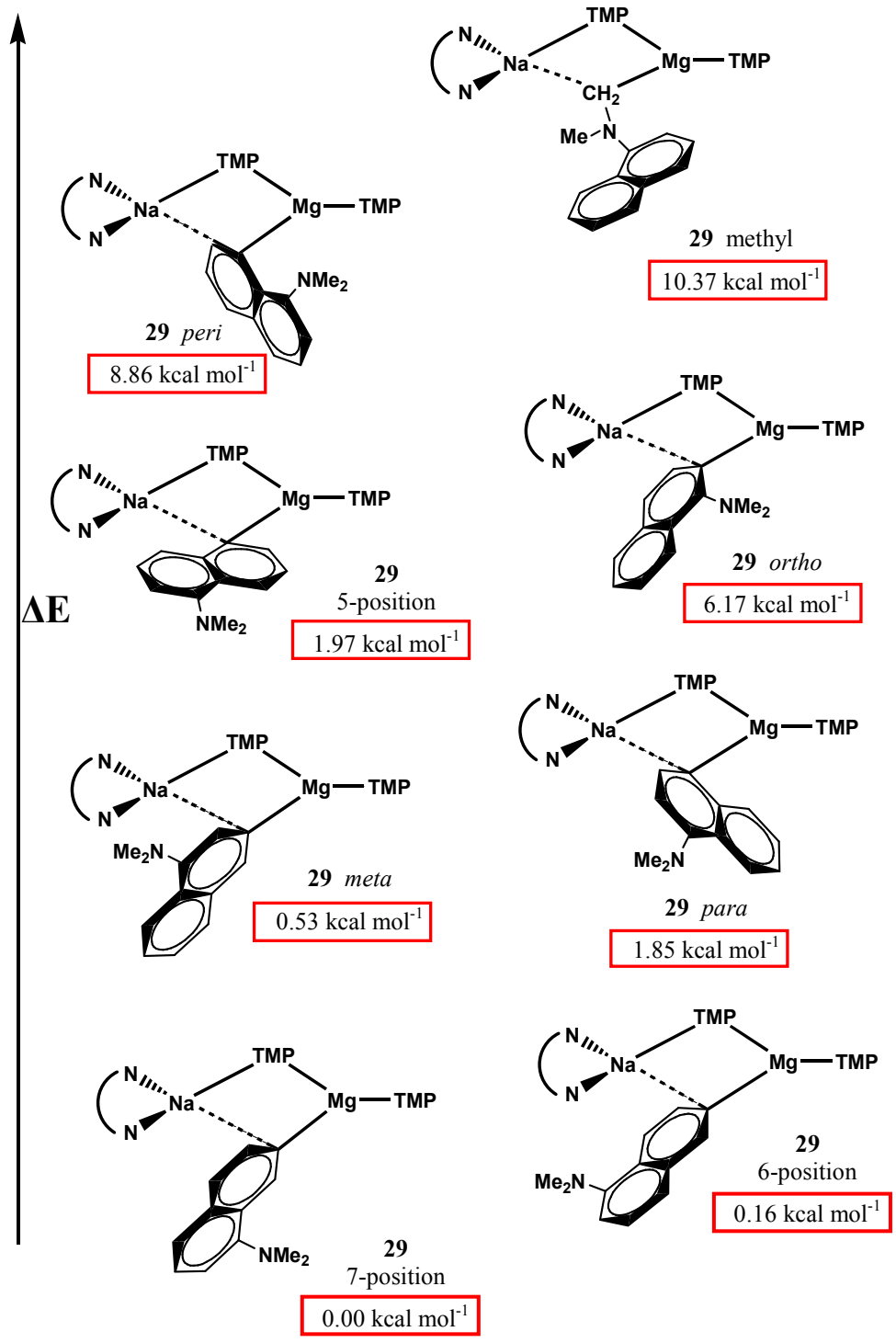

Figure 53: Theoretical structures of all possible isomers of **29** in order of decreasing stability.

We also carried out DFT calculations on the mono-metallation of the naphthylamine with the single metal systems Na and MgMe (results are displayed in Table 3). In both cases the most stable site of deprotonation was found in the *peri*-position (8 position) due to the additional interaction of the Na or Mg with the lone pair of electrons on the N centre of the NMe_2 group. The second most stable isomer in both reactions was the

ortho, which again could be rationalised due to the latter effect although the interaction is not as strong or significant. As aforementioned this result differs markedly to the mixed Na/Mg base findings with the naphthylamine in which the *peri*-position was one of the least stable isomers. Therefore the cooperative synergic effect of the two metals has reversed the order of the stability of the metallation products.

Table 3 Relative energies of the modelled sodium and methylmagnesium derivatives of N, N-dimethyl-1-naphthylamine.

Position of metallation	**Na (kcal mol^{-1})**	**MgMe (kcal mol^{-1})**
ortho	1.51	5.47
meta	7.56	16.16
para	6.89	15.66
5-position	6.95	15.85
6-position	7.64	16.14
7-position	7.90	16.21
peri	0.00	0.00
methyl (NMe_2)	6.61[a]	18.03[a]

key: a, an average of 6 positions.

The preference of the magnesiate base **28** to metallate the naphthylamine in the 6-position must be due in part to a kinetic effect as the marginally more thermodynamically stable 7-position is left untouched. This selectivity could also be due to a delicate balance of other contributing electronic or steric factors. The origin of this special selectivity could reflect the way the naphthylamine substrate approaches the synergic base in the transition state of the reaction. With the nitrogen lone pair inactive for coordination, the π-system of the naphthyl ring probably interacts preferentially with the sodium atom docking the substrate in close proximity to the metallator with the final choice of metallation site dependent on the closest hydrogen atom and most energetically stable conformation. These π-arene···metal interactions could be the key to the unusual regioselectivities observed in AMM*M*, especially when the aromatic substituent is weakly directing.

This result helps to strengthen the similarity of the two metals magnesium and manganese when applied to mixed-metal chemistry as both synergic bases **16** and **28**

display the same special regioselectivity (at the 6-position) when reacted with N, N-dimethyl-1-naphthylamine. Following this observed similarity we became interested in using the magnesiate base **28** to perhaps shed light on previous reactions involving **16** that failed to deposit any crystalline material. This would allow us to use NMR spectroscopy as a diagnostic tool and find out if and where metallation had taken place.

4.15. Reaction of magnesiate base 28 with 2, 6-dimethylanisole

Returning to the metallation of 2,6-dimethylanisole, we reacted the magnesiate base **28** *in situ* with one molar equivalent of the substrate to give an immediate colour change of the solution from light yellow to orange (like that observed with **16**). After 12 hours stirring at room temperature the solvent volume was reduced to furnish a crop of light yellow/orange crystals from the solution (
Scheme **47**). Analysis of these crystals by X-ray crystallography revealed them to be the new surprising sodium-magnesiate complex [(TMEDA)Na(TMP)(2,6-CH_3-OC_6H_3)Mg(TMP)] **30**, in which the anisole molecule has been converted to a phenoxide anion. Complex **30** could be isolated in crystalline yields of up to 55%.

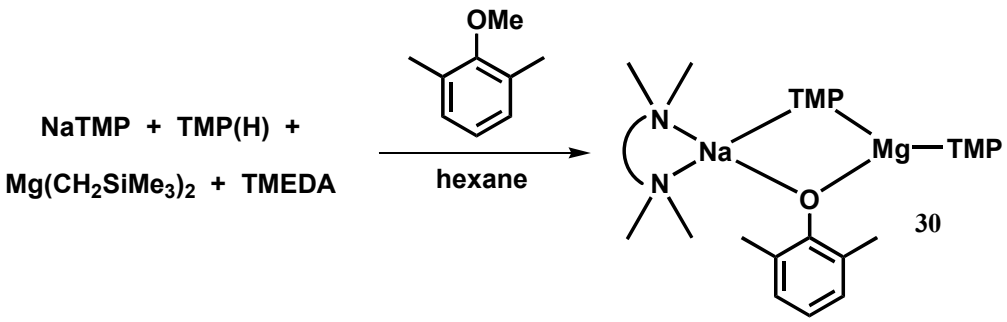

Scheme 47: Reaction of magnesiate base **28** with 2, 6-dimethylanisole.

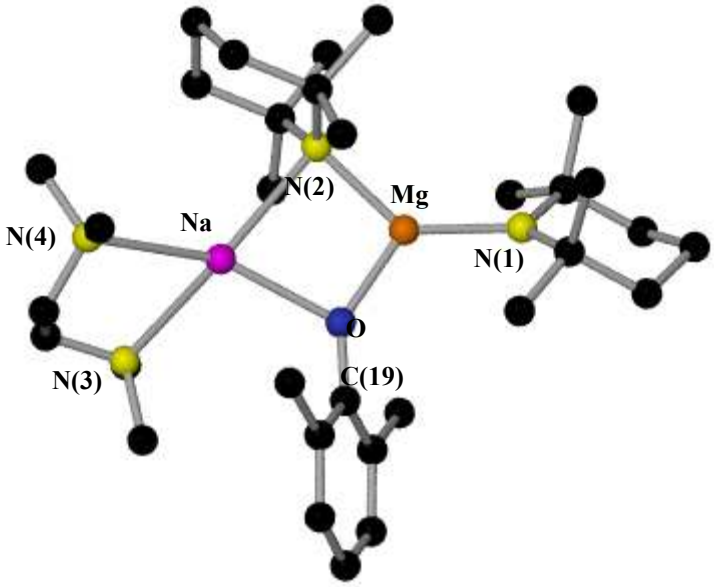

Figure 54: Molecular structure of **30**. Hydrogen atoms are omitted for clarity. Selected bond lengths [Å] and bond angles [º]: Mn-N(1), 1.9878(15); Mg-O, 1.9263(13); Mg-N(2), 2.0416(14); Na-N(2), 2.5776(16); Na-O, 2.2911(13); Na-N(3), 2.5476(17); Na-N(4), 2.5772(16); O-Mg-N(1), 124.91(6); N(1)-Mg-N(2), 134.85(6); O-Mg-N(2), 99.92(6); O-Na-N(2), 76.99(5); O-Na-N(3), 102.78(6); O-Na-N(4), 149.85(5); N(2)-Na-N(3), 143.39(5); N(2)-Na-N(4), 123.99(6); N(3)-Na-N(4), 73.70(6).

The molecular structure of **30** (Figure 54) shows a trigonal planar magnesium coordinated to a terminal TMP [Mg-N(1), 19878(15) Å], a bridging TMP [Mg-N(2), 2.0416(14) Å] and a bridging phenoxy ligand [Mg-O, 19263(1) Å]. The phenoxy ligand has originated from the cleavage of the methyl group attached to the oxygen within the 2, 6-dimethylanisole substrate. In the coordination sphere of the distorted tetrahedral Na, there is a bridging TMP [Na-N(2), 2.5776(16) Å], a bridging phenoxy ligand [Na-O, 2.2911(13) Å] and a bidentate chelating TMEDA ligand. The TMP and phenoxy ligand connect the Na and Mg to make a 4-atom, 4-element (NaOMgN) central ring which is essentially planar (sum of endocyclic angles 359.79º). Neither the magnesium nor sodium lie in the plane of the substrate with a Na-Mg-O-C(19) torsion angle of 179.9(2)º.

The ^{1}H NMR spectrum of **30** in C_6D_6 solution is shown in Figure 55. In the aromatic region of the spectrum there are two resonances belonging to the phenoxy ligand: a broad doublet at 7.13 ppm assigned to the equivalent protons H_A and $H_{A'}$ of the

aromatic ring and a triplet at 6.72 ppm that can be assigned to H_B of the aromatic ring. Turning to the aliphatic region of the spectrum a singlet at 2.35 ppm can be assigned to the two methyl groups in the 2- and 6-positions on the alkoxy ligand, while the two singlets at 1.62 and 1.56 ppm are assigned to the CH_3 and CH_2 groups of the chelating TMEDA respectively. The remaining multiplet at 1.88 ppm and two broad singlets at 1.43 and 1.40 ppm can all be assigned to the γ-CH_2, CH_3 and β-CH_2 protons of the TMP ligand respectively. Comparison of the ^{1}H NMR spectrum of the starting 2, 6-dimethylanisole substrate and that of complex **30** (shown in Figure 56) confirms the absence of the methyl signal belonging to the ether group OMe in **30**. Insignificantly a small amount of starting dimethylanisole is present.

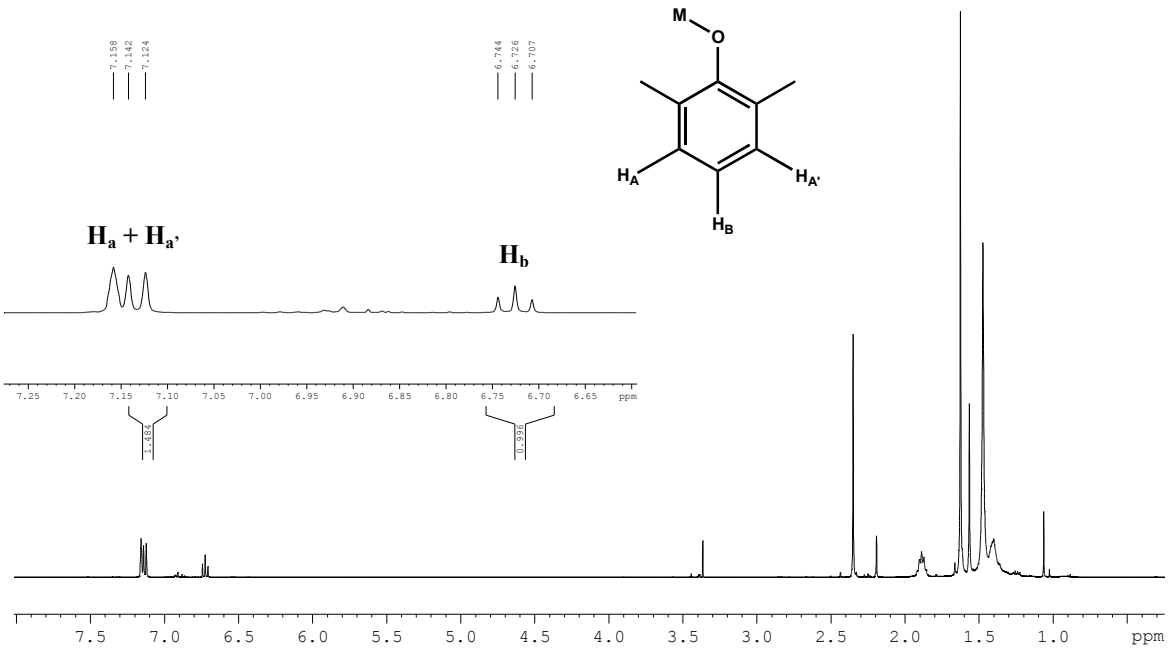

Figure 55: ^{1}H NMR spectrum in C_6D_6 solution of crystalline complex **30**, with aromatic region enhanced.

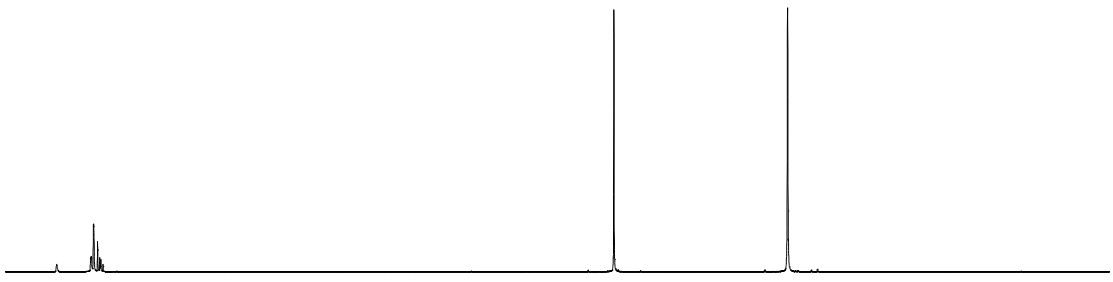

Figure 56: ^{1}H NMR spectrum in C_6D_6 solution of 2, 6-dimethylanisole.

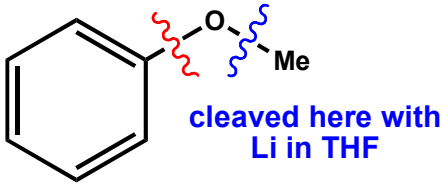

Figure 57

Compared to previous bimetallic products in this chapter, complex **30** is not the product of a metallation reaction, instead the methyl group belonging to the methoxy functional group has been cleaved leaving all the hydrogen atoms on the aromatic ring and the two methyl sidearms untouched. Ethers are commonly used in organic chemistry as a reaction medium due to their excellent solubilising properties and because they are unreactive towards many reagents including dilute acids and bases, halogens and nucleophiles.[189] However, in contrast when alkali-metal reagents are used to deprotonate substrates in metallation chemistry ether cleavage reactions are a relatively common occurrence giving rise to unselective products.[2, 190] In the context of anisole its cleavage to lithium phenoxide by lithium metal in the presence of biphenyl in refluxing THF solution has been known for some time.[191, 192] However different cleavage products are seen on changing the solvent to heptane, namely phenyllithium and lithium methoxide (Figure 57).[190] Cleavage reactions of substituted derivatives of anisole or other alkyl aryl ethers in general follow two pathways which are highly dependent on the solvent choice and steric bulk of the alkyl group. The alkyl-oxygen bond is cleaved when the alkyl group is bulky or if the reaction is carried out in THF;[190] while in contrast aryl-oxygen cleavage is promoted when the alkyl group is out of the plane of the aromatic ring or when the ether is an acetal (Figure 58).[193] In complex **30**, alkyl-oxygen cleavage has occurred even although the alkyl group is not sterically demanding. This has probably occurred as electronically, the phenoxide ion (PhO^-) is more thermodynamically stable in comparison to the formation of the methoxide ion (MeO^-).

Previous studies on the metallation of 2, 6-dimethylanisole have been carried out within our group using the synergic zinc reagent [(TMEDA)Na(TMP)(*t*Bu)Zn(*t*Bu)].[51] When a 1:1 stoichiometry was used lateral zincation of the methyl group was observed to give the benzylzincate complex [(TMEDA)Na(TMP)(C_6H_3OMe-2-CH_2-6Me)Zn(*t*Bu)]. Increasing the base stoichiometry to three molar equivalents gave a very different reaction product, namely the mixed alkyl-alkoxo complex [{(TMEDA)Na$(OMe)_2$Zn(*t*Bu)}$_2$][194] where the MeO ligands have originated from the

cleavage of 2, 6-dimethylanisole at the phenyl junction. However, it must be noted that the crystalline yield of this product was very low (7.7%) and no further optimisation studies were carried out. Both these zincate complexes show very different metallation or ether cleavage reactivity compared to that observed in complex **30**. In fact the products from the ether cleavage reactions show contrasting reactivities with the zincate cleaving the substrate at the aryl-oxygen bond while the magnesiate base breaks the more thermodynamically favoured alkyl-oxygen bond.

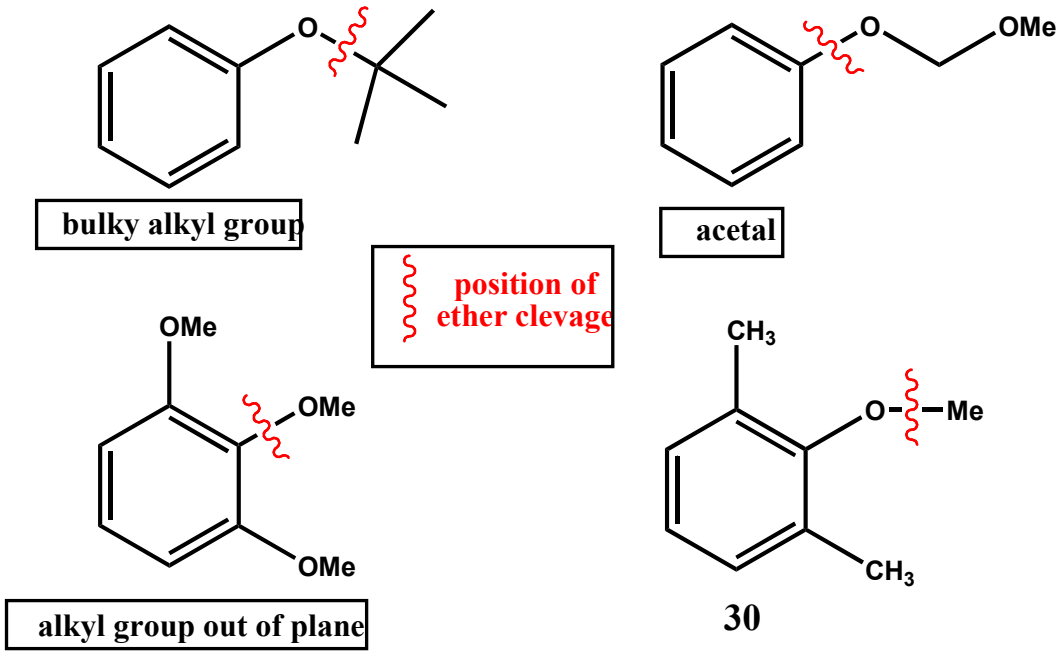

Figure 58: Comparison of ether cleavage positions of various ethers and complex **30**.

A search of the CCDB reveals only 16 hits for complexes containing the Na-O-Mg fragment with only one complex containing a phenoxy ligand system $[(EDBP)Na(OEt_2)Mg\textit{n}Bu]_2$[195] [EDBP = 2, 2'-ethylidenebis(4,6-di-tert-butylphenoxide)] which has Mg-O and Na-O bond lengths of 1.931(2) Å and 2.304 (2) Å respectively comparable to that in **30**. However it must be noted that this complex is formed from a deprotonation reaction of the starting phenol EDBP-H_2 and not an ether cleavage process.

4.16. Conclusions

One main aim of this work was to establish the effect of synergy in relation to the metallation of a range of functionalised and unfunctionalised aromatic substrates. The reactions studied are summarised in Figure 59. So far we have seen nine examples of the first reported direct manganations with a range of substrates including, anisole (**17**), N, N-diisopropylbenzamide (**18**), N, N-dimethylaniline (**21**), naphthalene (**24**), 1-methoxynaphthalene (**25**), 2-methoxynaphthylene (**26**), *m*-xylene (**23**), N, N-diisopropylaniline (**22**) and dimethyl-1-naphthylamine (**27**). All these results highlight the potency of the base system at achieving manganations of molecules that would not normally undergo metallations when standard manganese reagents are used (confirmed by carrying out some control reactions of the aromatic substrates with $[Mn(CH_2SiMe_3)_2]_\infty$ and Na(TMP) separately).

It has been established, from the reactions of the synergic base so far that, it reacts towards various substrates in different ways. We have observed the base react as both an alkyl and amido base, making it bifunctional in nature. However the reasons behind this basicity switch need to be investigated further to ascertain the bases true mode of function. A kinetic-thermodynamic distinction is likely

The versatility of the synergic base systems is highlighted by their ability to metallate functionalised aromatics in all three positions, namely *ortho*, *meta,* and *para*, depending on the functional group present on the aromatic ring. The potency of the synergic base **16** is best displayed when the unsubstituted (and therefore unactivated) naphthalene can undergo regioselective metallation at room temperature and in an almost quantitative yield of 88%. In some cases, demonstrated by the bicyclic substrate N,N-dimethyl-1-naphthylamine, new metallation positions, namely at the carbon atom 6, can be achieved.

Along with X-ray crystallographic characterisation of the compounds we have also shown that the manganated products can be applied in the synthetically invaluable procedure of carbon-carbon bond formations, both with (catalytically) and without the used of a palladium catalyst resulting in bi-aryl products in reasonable to excellent yields. This application has also proved useful in helping to identify reactive intermediates when X-ray crystallography was not available.

In conclusion, this chapter has through served examples established and elaborated the new concept of alkali-metal-mediated manganation AMM*Mn*. As this has not previously been accomplished, it represents the first direct method in the field of directed metallation with manganese in the II oxidation state. In addition these reactions have an important advantage over existing methods where low temperatures are nearly always required. In contrast, the synergic bases **16** and **28** react efficiently under mild conditions (25-50ºC) demonstrating a further advantage of the special synergic effect.

Chapter 5. Inverse Crowns and Ferrocenophanes

Another objective of this research programme was to try and synthesise new inverse crowns containing transition metal atoms. Until now the research group has successfully employed the synergic reaction mixture of "$Na_4Mn_2(TMP)_6(CH_2SiMe_3)_2$" to regioselectively 1, 4-dimanganate benzene and 3, 5-dimanganate toluene affording the inverse crown complexes $[(TMP)_6Na_4(1,4\text{-}Mn_2C_6H_4)]$ and $[(TMP)_6Na_4\{3,5\text{-}Mn_2C_6H_3(Me)\}]$[196] respectively. Most of the alkali-metal-manganese complexes in this area so far have involved the bulky cyclic amide TMP with the one exception being the silylamide, HMDS oxo-inverse crown $[Na_2Mn_2(HMDS)_4(O)]$.[197] Previous research involving magnesiates within our group has show that substituting the bulky secondary amide TMP for the slightly less bulky (and less basic) diisopropylamide (DA) produces surprisingly different chemistry. Unlike TMP and HMDS, DA contains β–hydrogen atoms that can undergo thermally induced β–hydride elimination reactions. It was this presence of β–hydrogens that resulted in the first example of "hydride encapsulated" inverse crown complexes, $[M_2Mg_2(\mu\text{-}H_2)\{N(i\text{Pr})_2\}_4(\text{toluene})_2]$[40, 198] (where M = Na or K). Perhaps even more remarkable is that the same synergic reaction mixture of BuNa, DA(H) and Mg*n*Bu_2 in a 1:3:1 stoichiometric ratio reacts with ferrocene to produce the spectacular 16-atom inverse crown $[\{Fe(C_5H_3)_2\}Na_4Mg_4\{i\text{Pr}_2N\}_8]$[49] in which ferrocene has been selectively four-fold deprotonated in the 1,1',3,3'-positions. The similarities between Mg and Mn(II), apparent in many of the structures previously mentioned, prompted us to try the ambitious goal of making a Mn(II) equivalent ferrocene inverse crown.

5.1. Synthesis of $[Na_2Mn_2(\mu\text{-}H)_2\{N(i\text{Pr})_2\}_4]\cdot(\text{toluene})_2$

Following on from the successful employment of DA(H) in AMM*Mg* we decided to attempt the synergic reaction of BuNa, $Mn(CH_2SiMe_3)_2$ and DA(H) in a 1:3:1 stoichiometric ratio with 0.25 molar equivalents of ferrocene. The resulting orange hexane/toluene solution was heated to reflux to give a deep red solution. On leaving the solution to cool to room temperature a crop of light pink needle crystals was deposited that were identified by X-ray crystallography not to be the anticipated "manganated" ferrocenophane, but surprisingly the unexpected sodium-manganese hydrido inverse

crown $[Na_2Mn_2(\mu\text{-}H)_2\{N(i\text{Pr})_2\}_4]\cdot(\text{toluene})_2$ **31**, note that no ferrocene is present in **31**. By omitting ferrocene from the synergic reaction mixture, **31** could be rationally synthesised in reproducible crystalline yields of up to 62% (Scheme 48).

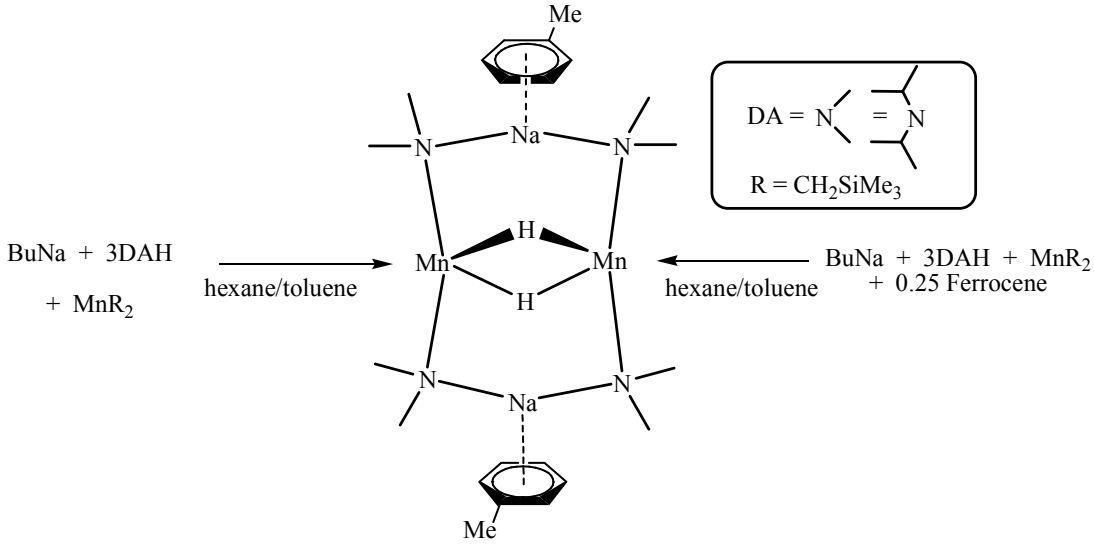

Scheme 48: Rational (LHS) and fortuitous (RHS) synthesis of the hydrido complex $[Na_2Mn_2(\mu\text{-}H)_2\{N(i\text{Pr})_2\}_4]\cdot(\text{toluene})_2$, **31**.

The molecular structure of **31** (Figure 60) is essentially isostructural to its magnesium congener $[Na_2Mg_2(\mu\text{-}H)_2\{N(i\text{Pr})_2\}_4]\cdot(\text{toluene})_2$ **32**. The centrosymmetric eight-atom ring of **31** adopts a chair conformation (Figure 61). The chair back, defined by N(3)Na(2)N(3B), is tilted at an angle of 155.8(1)º with respect to the essentially planar N(3)Mn(1)N(3C)····N(3A)Mn(1A)N(3B) chair seat. Two hydride anions straddle the centre of the cationic ring, bonding only to manganese in two separate Mn-H-Mn bridges. The hydride ions do not lie orthogonally above and below the chair seat, but in fact lean towards the chair back at an angle of 80.6(8)º. The Mn bonds strongly to the hydride ion with a Mn-H bond length of 1.869(13) Å, essentially the same within experimental error to that found for magnesium in **32** [1.86(2) Å]. The Mn-H distance also compares favourably with the average value of 1.893 Å[199] found in a range of manganese hydrides.[200] The shortest Na···H separation distance involving the hydride ion in **31** is 2.73(2) Å making it slightly longer than that observed for **32** [2.68(3) Å] and decidedly longer than those found in the crystal structure of NaH (2.44 Å),[201] in which there are direct Na-H interactions. Completing the structure of **31** are toluene molecules which weakly solvate the sodium cations (Na···centroid of toluene, 3.165 Å).

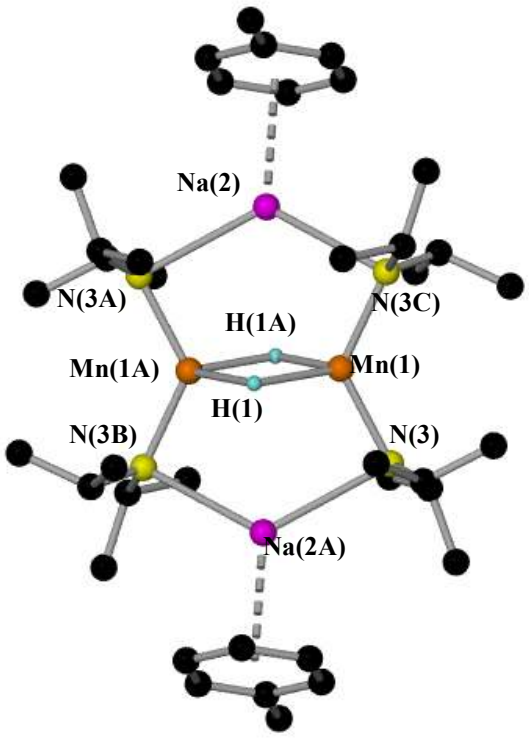

Figure 60: Molecular structure of **31**. Hydrogen atoms (except hydride ones) are omitted for clarity. Selected bond lengths [Å] and bond angles [º]: Mn(1)-N(3), 2.0970(8); Na(2)-N(3), 2.4620(9), Mn-H(1), 1.869(13), Na-*ipso*-C, 3.846(2); Na-*ortho*-C, 3.310(1); Na-*meta*-C, 3.587(2), Na-*para*-C, 3.731(2), Na-centroid, 3.165; Mn···Mn, 2.8267(6); Na···H, 2.73(2); N(3A)-Na(2)-N(3C), 133.20(5); N(3A)-Mn(1)-N(3B), 132.40(5); Mn(1)-H(1)-Mn(1A), 98.30.

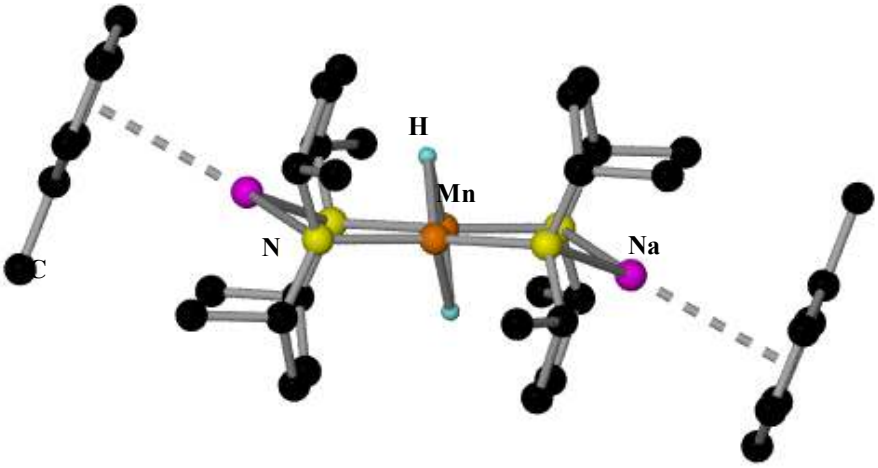

Figure 61: Alternative tilted view of the molecular structure of **31**. Hydrogen atoms (except hydride ones) have been omitted for clarity.

In the previously made Mn(II) inverse crowns $[(TMP)_6Na_4(1,4\text{-}Mn_2C_6H_4)]$[56], $[(TMP)_6Na_4\{3,5\text{-}Mn_2C_6H_3(Me)\}]$,[196] $[Na_2Mn_2(HMDS)_4(O)]$[197] and $[Li_2Mn_2(TMP)_4(O)]$,[197] Na-guest or Li-guest interactions (i.e., Na-arene, Na-O or Li-O interactions) are observed with no further solvation of the sodium or lithium centres required. However, in complex **31** the π–solvation of sodium in the host ring compensates for the absence of any significant Na-guest interactions making it a novel new feature for the Mn(II) inverse crown family.

To the best of our knowledge **31** represents the first structurally characterised example of a Mn(II) double hydride-bridged complex. On searching the CCDB, the only other double hydride-bridged complex that resembles **31** is the Mn(I) unsaturated phosphorus compound $[Mn_2(\mu\text{-}H)_2(CO)_6(\mu\text{-}Ph_2PCH_2PPh_2)]$[202] **33**. There are also two other heterobimetallic unsaturated Mn(I)/Ag[203] and Mn(I)/Au[204] complexes that contain a Mn-H-Mn bridge; however they also contain metal-metal Mn-M (M = Au or Ag) bonds. The Mn-H distances in **33**, ranging from 1.59(5) to 1.81(5) Å (mean 1.72 Å) are significantly shorter compared to the longer 1.869(13) Å observed in **31**. The Mn-H-Mn bond angles also differ in the two complexes with **31** having a bridging angle of 98.30(9)° while in **33**, which is not centrosymmetric, two independent angles of 107(3)° and 102(5)° are seen. Backing up the presence of the hydride ions in **31** the Mn=Mn double bond in **33** is significantly shorter [2.699(2) Å] than the observed Mn···Mn separation in compound **31** [2.8267(6) Å]. In fact this separation in **31** is more similar to the rather long single bonds found in the Mn(I)/Ag and Au complexes $[Ag_2Mn_4(\mu\text{-}H)_6(CO)_{12}(\mu\text{-tedip})_2]$ and $[AuMn_4(\mu\text{-}H)_5(CO)_{12}(\mu\text{-tedip})_{12}]$ (tedip = $(EtO)_2POP(EtO)_2$) (range: 2.860(2)-3.312(3) Å), which are indicative of a very small, direct bonding interaction being present between the Mn atoms.

While both magnesium and manganese diisopropylamide are known compounds, only the latter example has been structurally characterised using X-ray crystallography revealing its structure to be the dinuclear Mn(II) complex $[Mn_2(\mu\text{-}N\textit{i}Pr_2)_2(N\textit{i}Pr_2)_2]$.[205] Magnesium bis-diisopropylamide has been found to undergo thermally induced β-hydride elimination reactions (Scheme 49), which can be exploited synthetically to reduce aldehydes and ketones to alcohols.[206] Manganese bis-diisopropylamide also exhibits a similar thermal instability, as storage at -30ºC is essential to avoid its decomposition, which takes place at room temperature. On this basis one could

postulate that the presence of the hydride ions in **31** could have originated from a similar β–hydride elimination pathway in which the hydride ions have been encapsulated by the Lewis acidic bimetallic ring. The trapping of the hydride itself, in a reaction mixture that contains Na^+ ions, is surprising, as the more thermodynamically stable and insoluble NaH would be expected to form.[201]

However, using the synergic combination of sodium linked to manganese in the same complex triggers the elimination and subsequent capture of the hydride ions in the centre of an inverse crown complex. This highlights the powerful effects of cooperative cleave and capture chemistry.

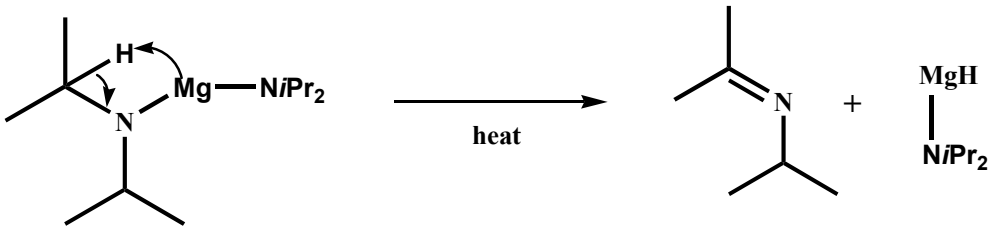

Scheme 49: Thermally induced β–hydride elimination from magnesium bis-diisopropylamide.

5.2. Synthesis of the ferrocenophane $[\{Fe(C_5H_4)_2\}_3\{Mn_3Na_2(NiPr_2)_2(HNiPr_2)_2\}]$

Returning to the original reaction of BuNa, $Mn(CH_2SiMe_3)_2$ and DA(H) in a 1:1:3 stoichiometric ratio with 0.25 molar equivalents of ferrocene and wanting to synthesise a ferrocene inverse crown, this time, to limit the possibility of β–hydride elimination the experiment was repeated but at 0ºC and the synergic reaction mixture subsequently stored in the refrigerator (at 4ºC). After three weeks a crop of red plate crystals was deposited that were latter identified by X-ray crystallography to be the new trimanganese, trinuclear ferrocenophane[207] $[\{Fe(C_5H_4)_2\}_3\{Mn_3Na_2(NiPr_2)_2(HNiPr_2)_2\}]$ **34**. Subsequently the rational synthesis of **34** could be achieved when one molar equivalent of ferrocene was used to give a much improved crystalline yield of 81%. Emphasising the synergy of AMM*Mn*, the corresponding homometallic reactions involving BuNa and diisopropylamine or $Mn(CH_2SiMe_3)_2$ and diisopropylamine failed to likewise promote metallation of ferrocene (Scheme 50).

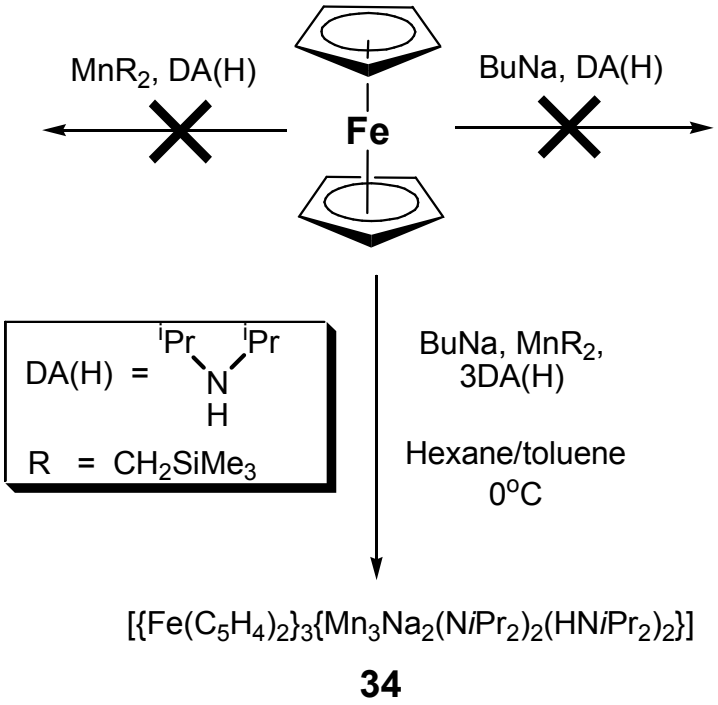

$[\{Fe(C_5H_4)_2\}_3\{Mn_3Na_2(NiPr_2)_2(HNiPr_2)_2\}]$

34

Scheme 50: Synergy of the alkali-metal-mediated manganation reaction with ferrocene.

Complex **34** proved problematic to recrystallise and so was often isolated from the solution as an insoluble red solid. As **34** is paramagnetic and thus not amenable to NMR spectroscopic studies, IR spectroscopy and melting point analysis were used to identify the red solid as a microcrystalline form of compound **34**. In addition to this, during repeat syntheses of **34** the hydride inverse crown **31** often crystallised preferentially, especially if any form of heat was applied to the reaction mixture. To stop this from occurring it was imperative that the addition of all the starting reagents was conducted at strictly 0ºC and that after the introduction of ferrocene all the hexane was removed in vacuo and subsequently replaced with cold toluene before the mixture was stored in the refrigerator at 4ºC. This observation of temperature dependence versus product formation suggests that the hydride inverse crown **31** is the final thermodynamic product, while the ferrocenophane **34** is the initial kinetically favoured product of the reaction mixture.

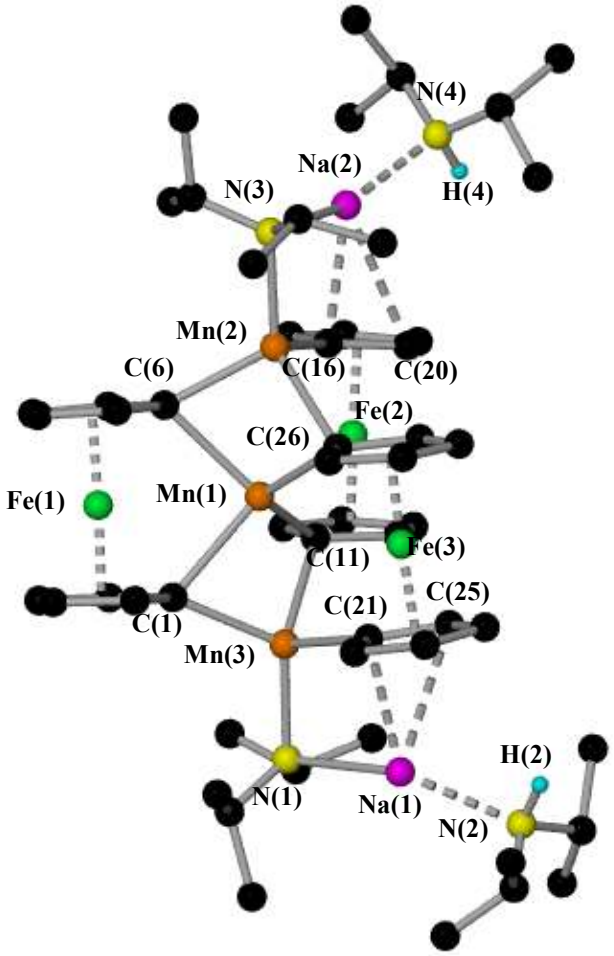

Figure 62: Molecular structure of **34** with selective atom labelling. Hydrogen atoms (except amine N-H ones) are omitted for clarity. Selected bond lengths [Å] and bond angles [°]: Mn(1)–C(1), 2.318(6); Mn(1)–C(6), 2.314(6); Mn(1)–C(11), 2.185(6); Mn(1)–C(26), 2.204(6); Mn(2)–C(6), 2.176(7); Mn(2)–C(16), 2.158(7); Mn(2)–C(26), 2.308(6); Mn(2)–N(3), 2.112(6); Mn(3)–C(1), 2.195(6); Mn(3)–C(11), 2.316(6); Mn(3)–C(21), 2.152(6); Mn(3)–N(1), 2.105(5); Na(1)–N(1), 2.409(6); Na(1)–C(21), 2.536(6); Na(1)–C(25), 2.817(7); Na(1)–N(2), 2.448(9); Na(2)–N(3), 2.405(7); Na(2)–C(16), 2.525(7); Na(2)–C(20), 2.867(7); Na(2)–N(4), 2.427(7); C(1)–Mn(1)–C(6), 92.9(2); C(1)–Mn(1)–C(26) 131.3(2); C(1)–Mn(1)–C(11), 94.5(2); C(6)–Mn(1)–C(26), 94.5(2); C(6)–Mn(1)–C(11), 131.7(2); C(26)–Mn(1)–C(11), 115.2(2); C(6)–Mn(2)–N(3), 115.3(2); C(6)–Mn(2)–C(16), 108.9(2); C(6)–Mn(2)–C(26), 95.4(2); N(3)–Mn(2)–C(16), 106.6(2); N(3)–Mn(2)–C(26), 126.4(2); C(16)–Mn(2)–C(26), 102.8(2); C(1)–Mn(3)–C(11), 94.0(2); C(1)–Mn(3)–C(21), 111.9(2); C(1)–Mn(3)–N(1), 117.4(2); C(11)–Mn(3)–C(21), 102.0(2); C(11)–Mn(3)–N(1), 125.7(2); C(21)–Mn(3)–N(1), 104.8(2).

The molecular structure of **34** (Figure 62) consists of three ferrocenyl dianions that have been selectively deprotonated in the 1- and 1'-positions. There are two distinct types of Mn atom in the complex; the core Mn(1) atom, which has a distorted tetrahedral geometry [range of bond angles, 92.9(2)-131.7(2)º] made up exclusively of contacts to ferrocenyl C atoms [range of bond lengths, 2.185(6)-2.318(6) Å]. One ferrocenyl ligand [containing Fe(1)] forms a chelate bridge to Mn(1) through C(1) and C(6); while the other two ferrocenyl ligands bind to it in a terminal manner through C(11) and C(26). The two remaining Mn atoms, Mn(2) and Mn(3), also have distorted tetrahedral environments, but their fourth coordination site is filled by an amido N atom, giving them overall C_3N coordination geometries. The ferrocenyl ligands bind in a terminal manner to these two Mn(2) and Mn(3) atoms. The structure is completed by Na atoms that lie at the 'top' and 'bottom' of the structure, forming four-atom CMnNNa rings solvated at Na by neutral diisopropylamine molecules with intact N-H bonds. Complex **34** represents only the second Mn(II)-containing ferrocenophane to be structurally characterised, with the first, also reported by our group, being the Mn/Li homoanionic ferrocenophane $[(TMEDA)_2Li_2Mn_2\{Fe(C_5H_4)_2\}_3]$[55] **35**, in which the ferrocenyl ligands have also been selectively deprotonated in the 1- and 1'-positions. An obvious significant difference between the two manganese(II) ferrocenophanes is the number of Mn atoms, in addition to the change of the alkali-metal partner, lithium or sodium. Ferrocenophane **34** contains three Mn atoms in contrast to the two present in **35**. This stoichiometric difference can be attributed to the fact that **34** retains two amido units of the parent synergic base mixture giving a heteroanionic arrangement and therefore an extra Mn(II) atom is needed for charge balance.

On searching the literature a closely related Mg analogue of compound **34** exists of the molecular formula $[\{Fe(C_5H_4)_2\}_3\{Mg_3Na_2(TMP)_2(TMP(H))_2\}]$,[208] in which the bulky cyclic amine TMP(H) was used in place of DA(H) in **34**. One distinction when comparing the Mg structure to **34**, apart from the different amines, is the symmetry relating the central divalent metal atoms. In **34** no such symmetry operation is present, whereas in the Mg complex a C_2 rotation axis passes through the central magnesium atom. Both complexes have distorted tetrahedral geometries about their three central Mg/Mn atoms with mean bond angles of 109.9º, 109.2º and 109.3º in **34** and 109.8º and 108.9º in the Mg complex. In **34** the presence of the less sterically demanding DA and DA(H) ligands does not significantly alter the Na-N bond lengths (average 2.42 Å)

when compared to the bond lengths in the TMP complex (average 2.44 Å). Another distinct difference is the mean M···M distance within the M···M···M segment, which in **34** at 2.658 Å is noticeably shorter than that of the Mg analogue (2.744 Å).

5.3. Synthesis of the inverse crown [{(TMEDA)Na(CH_2SiMe_3)(OBu)(*o*-C_6H_4OMe)Mn}$_2$]

High purity in the starting reagents and complete exclusion of oxygen in the system are crucially important for the success of these inert atmosphere metallation reactions. During the repeat synthesis of a few of our previous manganated products we obtained some new interesting inverse crown structures that appear to have occurred due to adventitious impurities in the starting reagents.

Retuning to the reaction that afforded **17**, the green *ortho*-manganated anisole complex [(TMEDA)Na(TMP)(*o*-C_6H_4OMe)Mn(TMP)], during one repeat experiment a sample of the *n*-butylsodium starting material was contaminated by *n*-butoxide, and this led to the formation of the orange, new inverse crown complex [{(TMEDA)Na(CH_2SiMe_3)(OBu)(*o*-C_6H_4OMe)Mn}$_2$] **36** (Scheme 51). Its unexpected feature is a butoxy group, presumably due to this contamination of *n*-butylsodium.

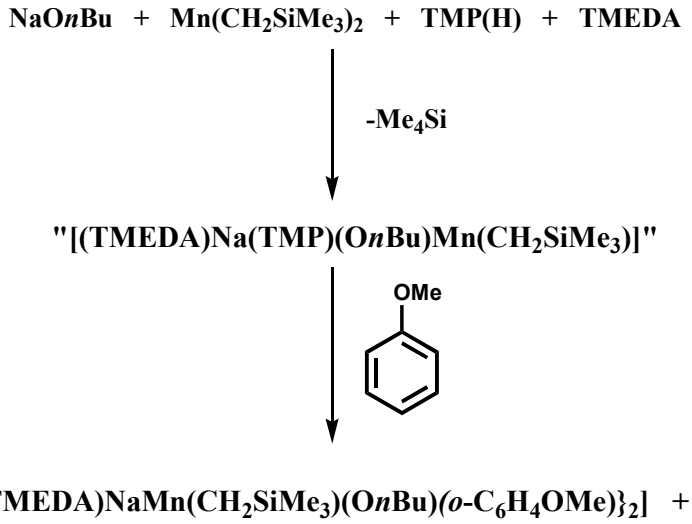

Scheme 51: Possible reaction pathway for the formation of butoxide containing **36**.

This new heteroanionic compound bears a resemblance to **17**, as both contain a selectively *ortho*-manganated molecule of anisole and a $[Na(TMEDA)]^+$ ion. However

they differ in the rest of the supporting anionic ligands coordinated to the Mn atom. In **17** there are two TMP ligands whereas in **36** there is an alkyl and a butoxide anion. One plausible pathway that would account for the synthesis of **36** would involve the initial formation of the heterotrileptic manganate species "[(TMEDA)Na(TMP)(O*n*Bu)Mn(CH_2SiMe_3)]" that could then react with the anisole as an amido base liberating TMP(H) as the co-product of the reaction. Unfortunately all attempts to prepare this potentially new mixed–metal reagent have been unsuccessful to date.

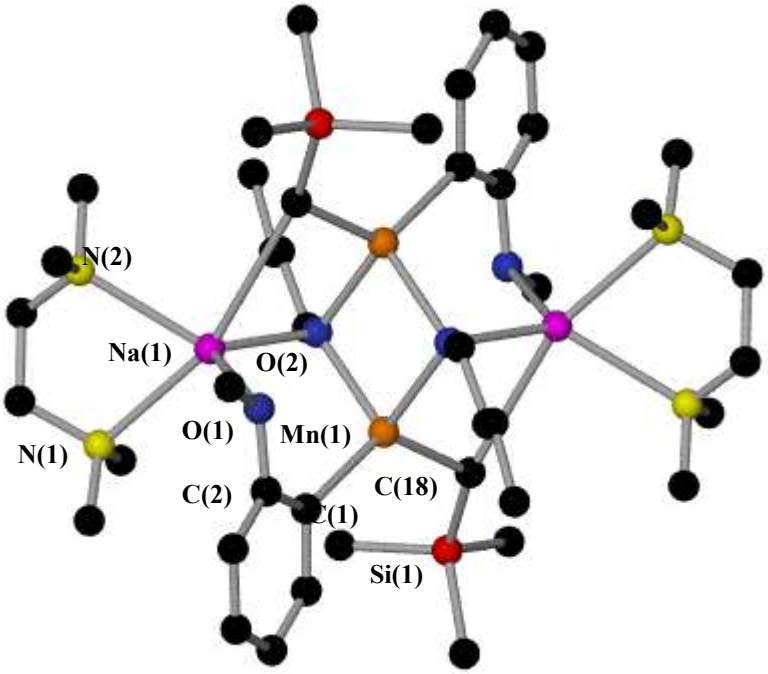

Figure 63: Molecular structure of **36** with selective atom labelling. Hydrogen atoms are omitted for clarity. Selected bond lengths [Å] and bond angles [°]: Mn(1)-C(1), 2.177(2); Mn(1)-C(18), 2.177(2); Mn(1)-O(2), 2.1333(15); Na(1)-N(1), 2.544(2); Na(1)-N(2), 2.530(2); Na(1)-O(1), 2.3997(18); Na(1)-O(2), 2.2982(17); Na-C(18A), 3.047(3); Mn(1)···Mn(1A), 3.1591(8); C(1)-Mn(1)-O(2), 110.05(7); C(1)-Mn(1)-O(2A), 115.92(7); C(1)-Mn(1)-C(18), 126.08(9); O(2)-Mn(1)-O(2A), 84.42(6); O(2)-Mn(1)-C(18), 110.10(8); O(2A)-Mn(1)-C(18), 102.37(7); N(1)-Na(1)-N(2), 72.64(8); N(1)-Na(1)-C(18A), 161.97(8); N(1)-Na(1)-O(2), 117.66(8); N(1)-Na(1)-O(1), 102.97(7); N(2)-Na(1)-C(18A), 89.98(8); N(2)-Na(1)-O(2), 131.57(8); N(2)-Na(1)-O(1); 121.17(8); C(18A)-Na(1)-O(2), 76.39(6); C(18A)-Na(1)-O(1), 81.64(7); O(2)-Na(1)-O(1), 107.68(6).

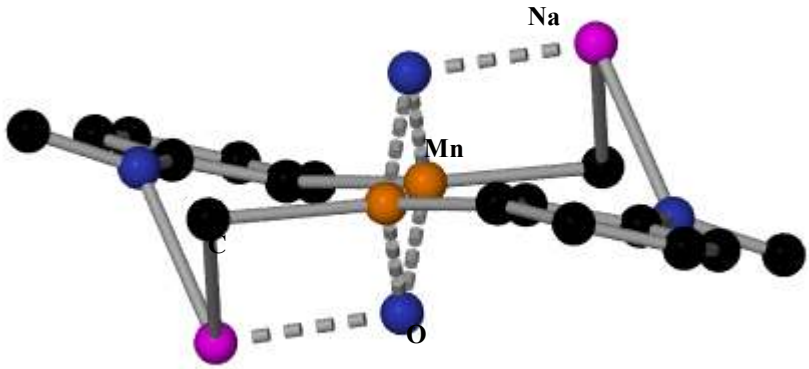

Figure 64: Core of **36** highlighting pseudo-chair conformation of $[(NaOCCMnC)_2]$ ring.

The centrosymmetric molecular structure of **36** (Figure 63) comprises two identical [(TMEDA)NaMn(OBu)(*o*-C_6H_4OMe)(CH_2SiMe_3)] units dimerised through a combination of alkoxide and alkyl bridges. The complex can be visualised as a cationic twelve-membered $[(NaOCCMnNC)_2]^{2+}$ ring hosting in the centre two butoxide ligands. This structural motif is reminiscent of that previously found for a series of inverse crowns complexes $[\{M^1M^2(NiPr_2)_2\}_2X_2]$ (M^1 = Li or Na; M^2 = Mg; X = OR, H),[39, 40] $[\{(TMEDA)MMg(Bu)_2\}_2(OtBu)_2]$ **37** (M = Na or K)[209] and $[K_2Ca_2\{OC(=CH_2)Mes\}]_6(THF)_2]$[210] previously made by our group as well as several other homometallic and heterometallic systems. These compounds exhibit an eight-membered cationic ring hosting two anionic ligands in the centre of the ring. In **36** due to the ambidentate nature of the *ortho*-manganated anisole ligand, C-bonding to Mn and O-bonding to Na, an expansion in ring size from eight atoms in **37** to twelve atoms in **36** is observed. This 12-atom ring adopts a pseudo-chair conformation (Figure 64) with the sodium atoms displaced on either side of the plane defined by C(1)Mn(1)C(18)···C(1A)Mn(1A)C(18A). The oxygen atoms belonging to the anisole are also marginally out of this plane as shown by the torsion angle O(1)-C (2)-C(1)-Mn(1), 17.1º. The sodium atoms achieve pentacoordination by bonding to two anionic (C of the alkyl; O of the alkoxide) ligands, the neutral O of the anisole and the two nitrogen atoms of the bidentate diamine TMEDA. The slight contraction of the Na-O(*n*Bu) bond length [2.2982(18) Å] relative to the Na-O bond length of the OMe of the anisole ligand [2.3997(18) Å] reflects the anionic nature of the former (that is, having a stronger electrostatic attraction) even although the latter oxygen has a lower coordination number. The Mn atom has a distorted tetrahedral environment [mean bond

angle, 108.14º] comprising of two O*n*Bu, one *ortho*-aryl C and one alkyl C atom. The Mn-C(anisole) bond length [2.177(2) Å] compares favourably to that found in complex **17** [2.189(2) Å]. The Mn-O bond lengths of 2.1333(15) and 2.1318(16) Å are modestly longer than the ones found in the mixed Li/Mn(II) alkoxides[211] [Li{Mn(N(SiMe$_3$)$_3$(OC*t*Bu$_3$)$_2$}] [2.019(4), 1.984(4) Å] and [Li$_2${MnBr$_2$(OC*t*Bu$_3$)$_2$(THF)$_2$}] [2.019(7) Å], which can be attributed to the dimeric nature of **36**, in which each butoxide ligand is tricoordinated, whereas the other structures have two-coordinate alkoxide ligands as they are monomeric.

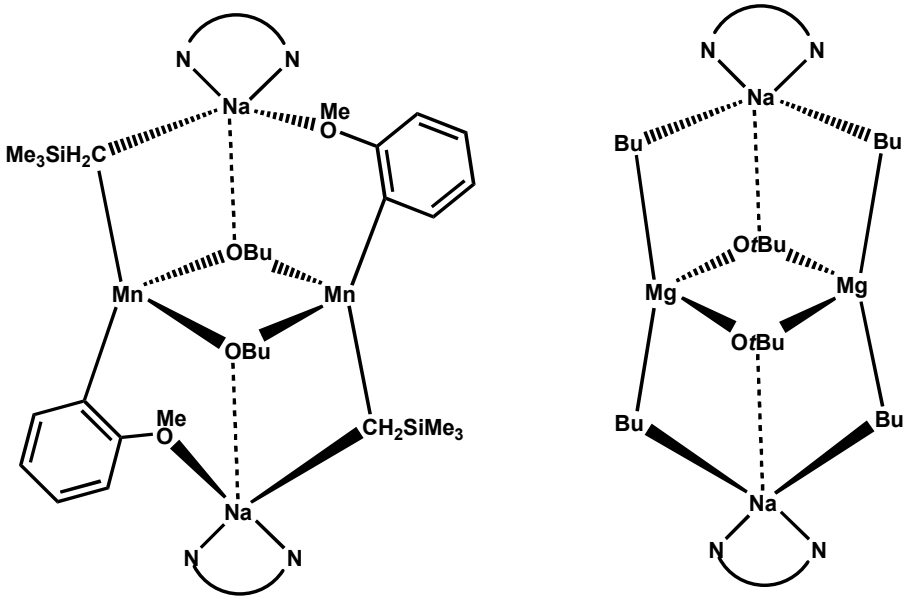

Figure 65: Comparison between the structural motifs of **36** and **37**.

This serendipitous encapsulation of *n*-butoxide or other oxo-related species such as alkoxides or peroxides is a widely recognised problem throughout organometallic chemistry. It has been experienced by previous members of our group, leading fortuitously to some interesting structures. For example, our group have reported the synthesis of the alkoxide-contaminated Mg complexes[212] [*t*BuMgO*t*Bu.THF], [*t*BuMg(O*t*Bu)(TMP)Mg(TMP)] and [Mg(O*n*Bu)HMDS.sol] (were sol = THF or Et$_2$O). Since neither the serendipitous nor rational synthesis via a BuNa/anisole/Mn(CH$_2$SiMe$_3$)$_2$/TMEDA/*n*BuO mixture has successfully reproduced complex **36** the reaction will need to be investigated further. However, satisfactory microanalysis results have been recorded. Hopefully in the future this framework of a twelve-membered ring could be a precedent for building a series of new inverse crowns.

5.4. Synthesis of $[(TMEDA)_2Na_2(TMP)_2(1,4\text{-}C_6H_4)Mn_2(TMP)_2]$

During one repeat synthesis of the naphthalenide complex **26** [(TMEDA)Na(TMP){3-(2-$OMeC_{10}H_6$)}Mn(TMP)] two types of crystalline material were observed, namely a crop of red block crystals and a few yellow needles (note that complex **26** is red). Using X-ray crystallography the red block crystals were confirmed to be the known complex **26**; however, surprisingly the yellow needles were determined to be the 1,4-dimetallated benzene species $[(TMEDA)_2Na_2(TMP)_2(1,4\text{-}C_6H_4)Mn_2(TMP)_2]$ **38**. The unexpected presence of a benzene derived molecule could be explained by trace amounts of benzene contaminating the starting material 2-methoxynaphthalene. More often than not, commercial aromatic compounds contain trace amounts of benzene, and due to **38** being the minor product of the reaction, this would seem the most plausible explanation for its presence. Unfortunately, all attempts to synthesise **38** rationally have lead to the exclusive formation of the previously reported monomanganated phenyl compound [(TMEDA)Na(TMP)(C_6H_5)Mn(TMP)],[56] even when a two- or four-fold excess of the synergic base is used.

The centrosymmetric molecular structure of **38** (Figure 66) contains a trigonal planar Mn(II) atom with a terminal TMP [Mn-N(2), 2.029(3) Å], a bridging TMP [Mn-N(1), 2.125(3) Å] and a bridging dideprotonated benzene ligand [Mn-C(1), 2.185(4) Å]. The benzene ligand had lost its two protons in the sterically optimal 1- and 4-positions, which are now occupied by Mn(II) atoms. In the coordination sphere of the Na, a bridging TMP [Na-N(1), 2.454(14) Å] is observed along with the chelating bidentate ligand TMEDA giving it an overall highly distorted tetrahedral geometry (mean bond angle, 110.42º). More ionic than Mn, the alkali-metal satisfies its coordination demands by also interacting electrostatically with the π-system of the benzene ring in a η^2-manner through the C(1) and C(2) positions [Na-C(1), 2.688(4) Å; Na-C(2), 2.859(4) Å], with the former bond inclined at an angle of 71.1º to the aromatic ring plane.

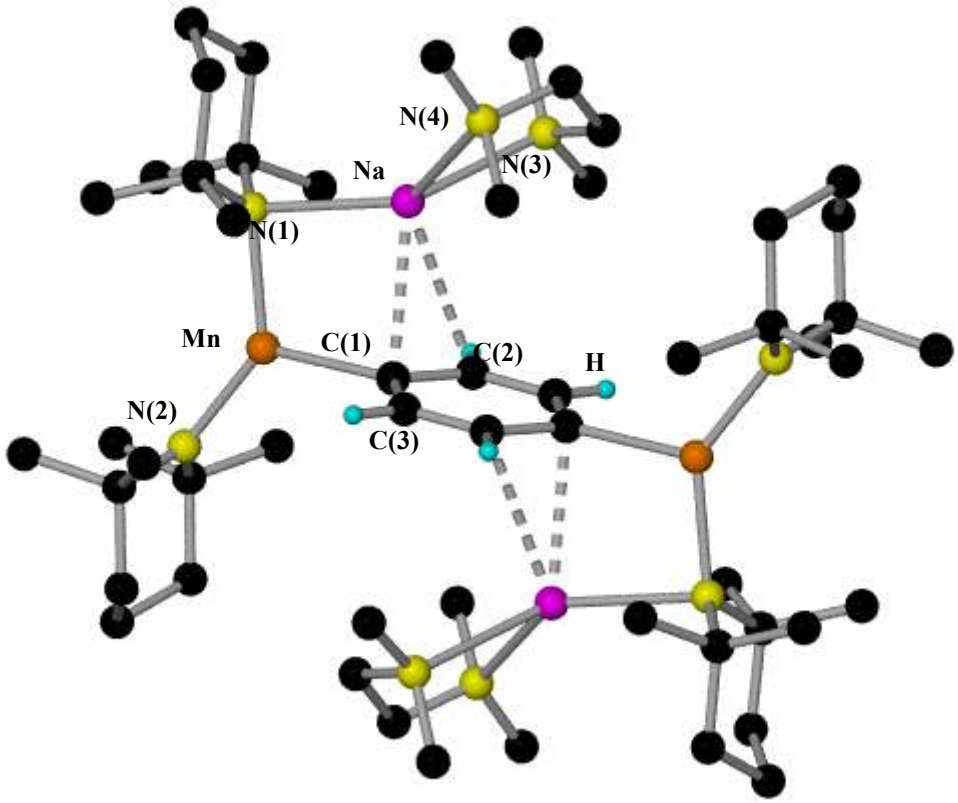

Figure 66: Molecular structure of **38** with selective atom labelling. Hydrogen atoms are omitted for clarity. Selected bond lengths [Å] and bond angles [°]: Mn-N(1), 2.125(3); Mn-N(2), 2.029(3); Mn-C(1), 2.185(4); Na-N(1), 2.454(4); Na-N(3), 2.524(4); Na-N(4), 2.516(4); Na-(C1), 2.688(4); Na-C(2), 2.859(4); N(1)-Mn-C(1), 104.75(13); N(1)-Mn-N(2), 135.13(14); N(2)-Mn-C(1), 120.12(14); N(1)-Na-N(3), 135.03(13); N(1)-Na-N(4), 130.86(13); N(3)-Na-N(4), 73.87(13); N(3)-Na-C(1), 118.81(14); N(4)-Na-C(1), 120.87(14); N(1)-Na-C(1), 83.08(12).

Complex **38** is isostructural to the magnesium $[(TMEDA)_2Na_2(TMP)_2(1,4\text{-}C_6H_4)Mg_2(TMP)_2]$ **39** and zinc $[(TMEDA)_2Na_2(TMP)_2(1,4\text{-}C_6H_4)Zn_2(TMP)_2]$ **40** complexes previously made within our laboratory.[213] Consistent with the relative metal sizes, the Mn-C-(aryl) distance in **38** [2.185(4) Å] compares favourably to the Mg-C(aryl) [2.179(4) Å] distance in **39** but is somewhat longer than its zinc counterpart in **40** [2.0657(18) Å]. In all three ate compounds the Na atom prefers to interact with the benzene ring in a η^2 fashion to give relatively short but weaker contacts to the C(1) and C(2) atoms of the benzene ring [Na-C average lengths: 2.774 Å (**38**), 2.772 Å (**39**) and 2.767 Å (**40**)]. The common motif in **38**, **39** and **40** can be interpreted as an "open

inverse crown" arrangement with the benzenediide [$(C_6H_4)^{2-}$] ring encapsulated in the centre. This structural arrangement differs from the conventional "inverse crown" motif where an additional two units of NaTMP allow the formation of a closed twelve-atom (NaNNaNMN) ring (M = Mn or Mg) containing the dideprotonated anionic guest (benzene in Figure 67). The dimanganation of benzene in the 1- and 4-positions has been previously reported by our group in the form of the inverse crown complex [$(TMP)_6Na_4(1,4\text{-}Mn_2C_6H_4)$] **41**.[56] The Mn-C(aryl) distances in both the "open" and "closed" structural arrangements vary little [2.185(4) Å in **38** and 2.201(2) Å in **41**] however, one noteworthy difference is in the TMP-Mn-TMP bond angle. In the closed inverses crown **41**, both the TMP ligands are bridging to give an angle of 145.74(17)º. In **38**, there is one bridging and one terminal TMP ligand which results in a significantly smaller angle of 135.13(14) º, a difference of 10.61°.

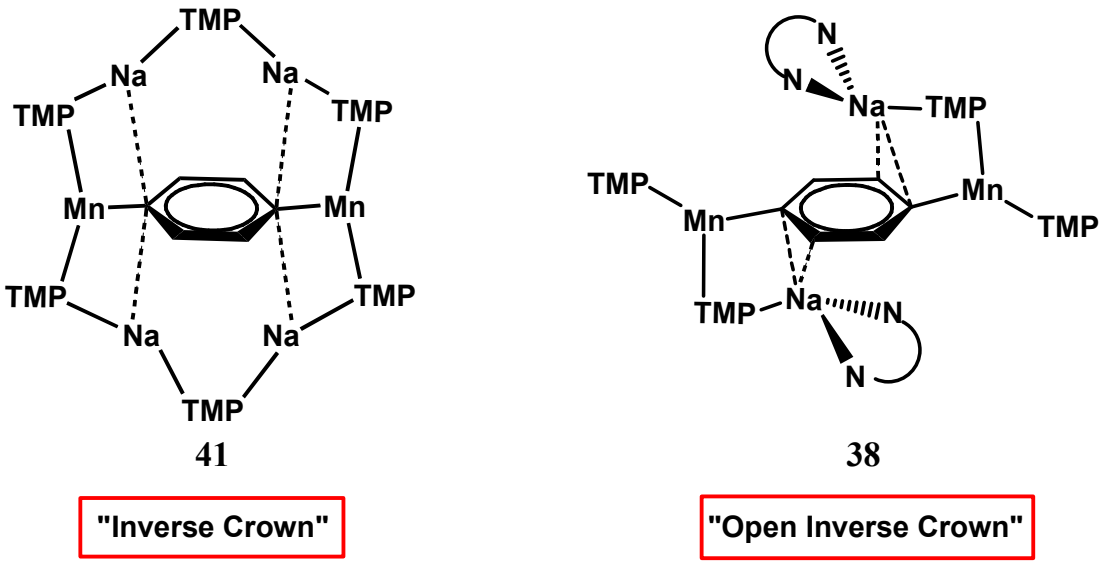

Figure 67: Comparison of benzene based "inverse crown" and "open inverse crown" motifs.

5.5. Conclusions

The main aim of the work detailed in this chapter was to extend the Mn(II) inverse crown family and to try and capture new anionic guest molecules. Three new manganese(II)-based inverse crowns have been successfully synthesised as well as an unexpected Mn(II) ferrocenophane complex. By introducing the diisopropylamido ligand to AMM*Mn* chemistry the doubly bridged hydride inverse crown complex **31**

and the trinuclear ferrocenophane **34** could both be successfully synthesised. The oxygen/moisture sensitivity of these organometallic mixed-metal-based reactions has been displayed in the serendipitous synthesis of the *n*-butoxide and 1, 4-dimanganated benzene inverse crown complexes **36** and **38** respectively. All three structures **31**, **36** and **38** show that different guests can be successfully encapsulated, within the host ring, ranging from the simple monoatomic hydride ion to the more complicated polyatomic benzenediide and *n*butoxide molecules. The advantage over other mixed-metal-based inverse structures when Mn(II) is used in place of magnesium or zinc is the new property of magnetism. As previously stated elsewhere in this thesis Mn(II) has a d^5 high spin electronic configuration making it paramagnetic. Although NMR spectroscopy cannot be used for characterisational purposes due to this paramagnetism, it does however introduce the new property of potential magnetism in new synthesised compounds. The magnetic fingerprints of all four compounds **31**, **34**, **36** and **38** will be discussed separately in Chapter 7.

Chapter 6. Synergic Ether Cleavage

The cleavage of ethers is commonly encountered in organometallic chemistry although it has been rarely studied in the context of new bimetallic reagents. Recently our group has investigated the reactivity of the trimethylsilylmethyl sodium-zincate base [(TMEDA)Na(TMP)(CH_2SiMe_3)Zn(CH_2SiMe_3)] with the cyclic ether THF. Astonishingly the base can directly α-zincate THF to give the intermediate complex [(TMEDA)Na(TMP)(OC_4H_7)Zn(CH_2SiMe_3)][214] which remains intact at room temperature without any opening of its zincated heterocyclic THF ring. This exciting result prompted us to investigate the reactivity of the similarly composed manganate and magnesiate bases **16** and **28** respectively with THF.

6.1. Reaction of the manganate base 16 and magnesiate base 28 with THF

In situ hexane solutions of **16** and **28** were reacted separately with one molar equivalent of THF. The resulting light yellow or light orange solutions respectively, were allowed to stir at room temperature overnight. Reduction of the solvent volume under reduced pressure and storage of the solutions at room temperature furnished an initial crop of needle crystals for both reactions, colourless for magnesium and bright orange/red for manganese. Both sets of crystals were subsequently identified by X-ray crystallography to be the di-metallated butadiene complex [[(TMEDA)Na(TMP)}$_2${1, 4-[M(TMP)]$_2$-C_4H_4}] where M = Mn in **42** or Mg in **43**. Upon removal of the initial needle crystals via filtration a second crystalline product was grown from the mother liquors. Observed as colourless plates from the magnesium liquors and light pink plates from the manganese liquors, both crystalline products were subsequently identified by X-ray crystallography to be the oxo-inverse crown complex [$Na_2M_2(TMP)_4O$] where M = Mn in **44** or Mg in **45** (Scheme 52). Based on the quantity of THF consumed in each of the reactions, the yields of **42** and **44** in the manganese case and **43** and **45** in the magnesium case are close to quantitative with the relative proportions of the two distinct products being approximately 50% : 50% (see experimental for full details). Both reactions proved to be reproducible with the different crystalline products, namely needles and plates, easily distinguishable by the naked eye.

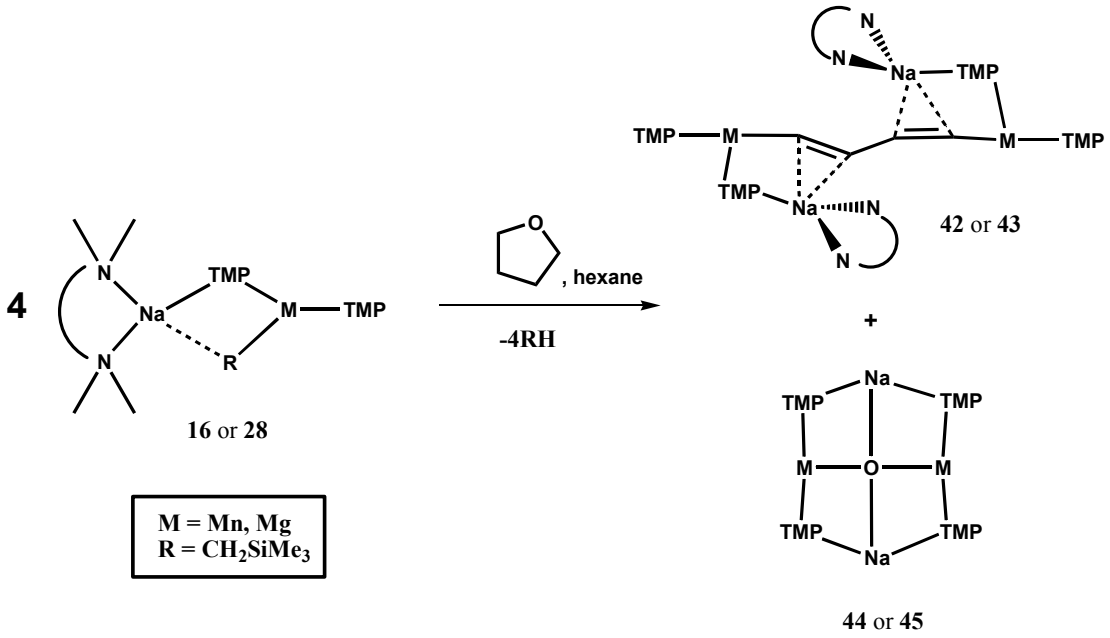

Scheme 52: Synthesis of 1, 4-dimetallated butadienes **42** (M =Mn) and **43** (M = Mg) and inverse crown ethers **44** (M =Mn) and **45** (M = Mg).

The dimetallated butadienes **42** and **43** are isostructural. Unfortunately disorder in manganate **42** does not allow a discussion of its dimensions although its connectivity is absolute. Full characterisation of **42** is also hindered by its paramagnetic nature which rules out informative NMR spectroscopic studies. However, in contrast magnesiate **43** has been successfully characterised by both X-ray crystallography and solution NMR spectroscopic studies. Its molecular structure (Figure 68) is centrosymmetric with an inversion centre in the middle of the s-trans-1, 3-butadiene fragment. Formally a dianion, the C_4H_4 chain has been trapped at each end with a (TMEDA)Na(TMP)Mg(TMP) cationic base residue. Magnesium bonds to the butadiene via a σ-bond [Mg-C(25), 2.1687(12) Å] lying almost co-planar with the C_4 chain [deviation from the plane 0.26 Å, C(26A)-C(26)-C(25)-Mg(1), 172.35(12)º]. The magnesiated butadiene has alternating bond lengths within its C_4 chain [C(25)-C(26), 1.232(17) Å, C(26)-C(26A), 1.485(2) Å] verifying the localised double bond-single bond-double bond pattern of the trapped dienyl fragment. In contrast to magnesium, sodium interacts with the butadiene fragment via a π-type contact with the C=C bonds of the allyl chain [Na-C(25), 2.6430(12) Å, Na-C(26), 2.8838(12) Å] lying almost perpendicular to the C_4 chain [C(26A)-C(26)-C(25)-Na(1), 110.3(2)º]. This σ/π synergic bonding is a signature feature of products formed via AMM*M* of aromatic or alkene substrates,[215, 216] with this being the first example involving a diene. The structure is

completed by a TMP nitrogen bridging the two distinct metals [Na-N(2), 2.4541(10) Å, Mg-N(2), 2.0801(10) Å], a chelating TMEDA on sodium [Na-N(3), 2.4889(11) Å, Na-N(4), 2.5256(10) Å] and a terminally bound TMP on magnesium [Mg-N(1), 1.9954(10) Å].

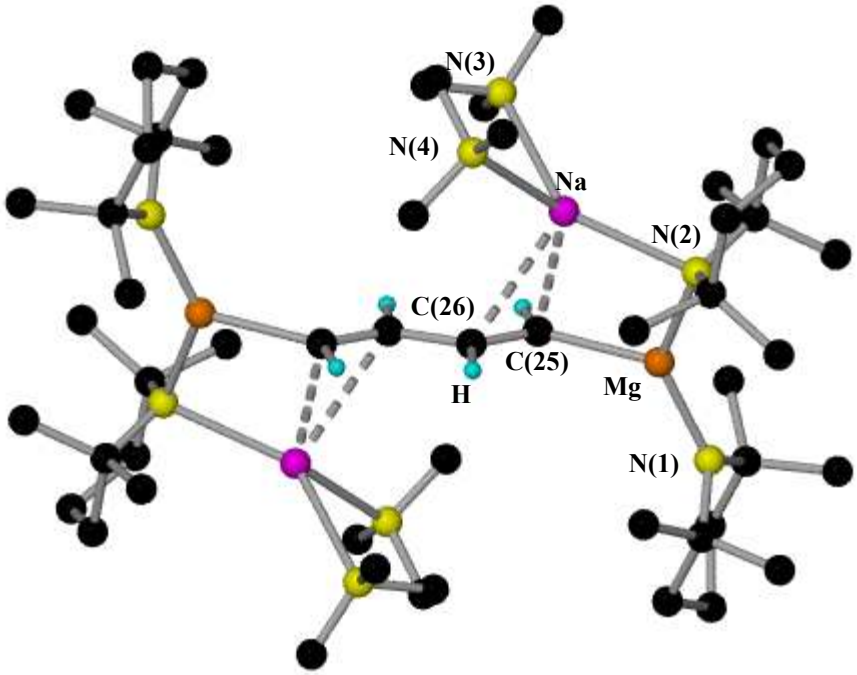

Figure 68: Molecular structure of **43** with selective atom labelling. Hydrogen atoms except butadiene ones are omitted for clarity. Selected bond lengths [Å] and bond angles [°]: Mg-N(1), 1.9954(10); Mg-N(2), 2.0801(10); Mg-C(25), 2.1687(12); Na-N(2), 2.4541(10); Na-N(3), 2.4889(11); Na-N(4), 2.5256(10); Na-C(25), 2.6430(12); Na-C(26), 2.8838(12); C(25)-C(26), 1.3212(11); C(26)-C(26A), 1.485(2); N(1)-Mg-N(2), 134.52(4); N(1)-Na-C(25), 119.87(4); N(2)-Mg-C(25), 105.62(4); N(2)-Na-N(3), 138.36(4); N(2)-Na-N(4), 131.46(3); N(3)-Na-N(4), 73.99(3); N(2)-Na-C(25), 83.14(3); N(3)-Na(1)-C(25), 105.84(4); N(4)-Na-C(25), 129.02(4).

Complex **43** was fully characterised in solution by a battery of NMR spectroscopic studies. A ^{1}H spectrum recorded at room temperature in C_6D_6 solution (Figure 69) revealed characteristic resonances at 2.18 and 2.06 ppm for the CH_2 and CH_3 groups of TMEDA and at 1.68 and 1.49 ppm, belonging to the CH_3, γ-CH_2 and β-CH_2 groups of TMP. There was also an additional singlet downfield at 6.64 ppm which integrated to 4 hydrogens which we assigned to the metallated butadienyl fragment.

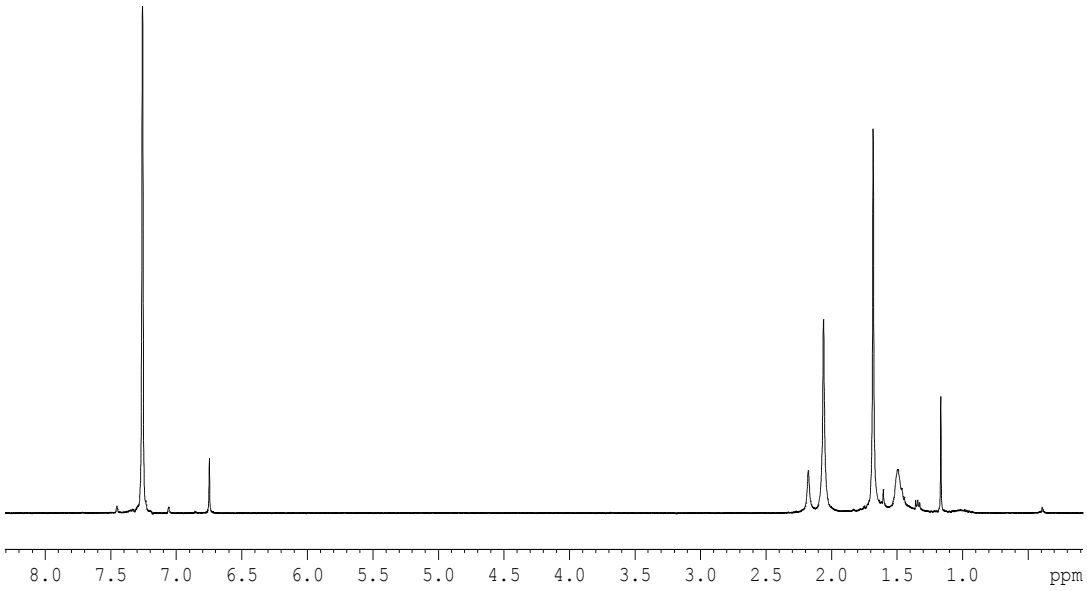

Figure 69: ^{1}H NMR spectrum in C_6D_6 solution of butadienyl complex **43**.

The presence of a singlet surprised us as we expected two different chemical shifts for the two unique types of butadienyl hydrogens present in complex **43**. However, after a thorough literature search we found a convincing precedent in 1,4-bis(dicarbonyl-π-cyclopentadienyliron)buta-1,3-diene, which in certain spectra also exhibited degeneracy of its C(H)=C(H)-C(H)=C(H) proton resonances to give a single peak.[217-220] The presence of the single signal was finally attributed to a combination of small chemical shift differences and a relatively large coupling constant. By hydrolysing the NMR sample of **43** with D_2O we proved the singlet at 6.64ppm belonged to the C_4H_4 chain and observed the loss of the single resonance and the appearance of two new doublets at 6.25 and 5.09 ppm signifying the formation of a 1,4-deuterated modification of 1, 3-butadiene (Figure 70).

By changing the NMR solvent from C_6D_6 to d_8-THF the ^{1}H NMR spectrum of **43** revealed a pair of doublet of triplets at about 6.50 ppm (Figure 71). This splitting pattern revealed we had an AA'BB'-spin system in our butadiene fragment where Hb and Hb' are chemically equivalent but not magnetically equivalent causing the doublet to split further into a triplet. Furthermore ^{13}C spectra revealed two distinct signals at 163.32 and 154.99 ppm for the two chemically different carbon atoms of the C_4H_4 butadiene chain. By utilizing 2D NMR spectroscopy COSY and HSQC techniques the signal at 163.22

and 6.35 ppm could be straightforwardly assigned to C_b and H_b respectively while the signals at 154.99 and 6.49 ppm could be assigned to C_a and H_a respectively.

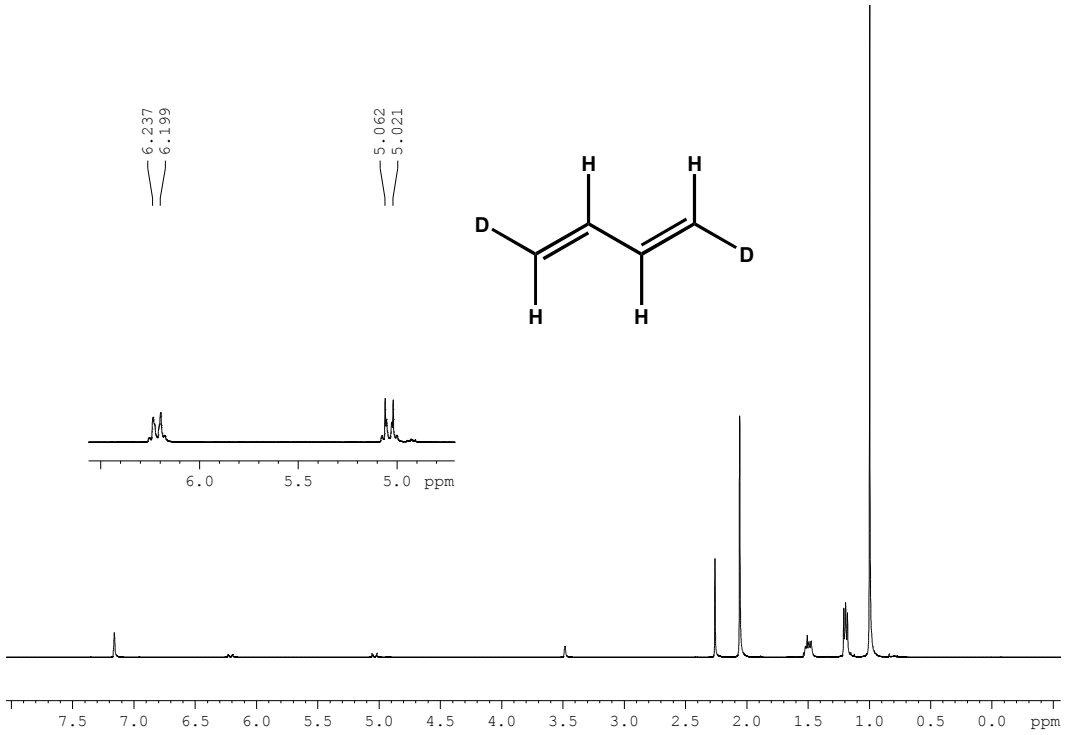

Figure 70: ^{1}H NMR of **43** after hydrolysis with D_2O.

The next question we wanted to answer "was the C_4H_4 butadiene chain in **43**, and by extrapolation in **42**, coming from the cleavage of THF?" The simplest experiment to find this answer was to repeat the synthesis of **43** using d_8-THF instead of protic THF. Following the same synthetic protocol as before the magnesiate base **28** was reacted with one molar equivalent of d_8-THF in hexane solution. A crystalline product was obtained as before but only after 5 days which was noticeably longer than it took to grow than its protic analogue. Analysing the crystals by ^{1}H-NMR in C_6D_6 solution showed an essentially identical spectrum to that of **43** but critically missing the single resonance at 6.64ppm (Figure 72). On running the complementary ^{2}D NMR spectrum of the deuterated crystalline product in C_6D_6 solution, the single resonance 'reappears' at a marginally more downfield shift of 6.81ppm (Figure 73 LHS). Hydrolysing this sample with H_2O gave a ^{2}D spectrum consistent with (H)DC=CD-CD=CD(H) to give two new resonances at 6.21 and 5.04 ppm that can be assigned to the two unique types of D atom in the structure (Figure 73 RHS). From these complementary NMR studies it is definite

that the C_4H_4 chain in **43** and the C_4D_4 chain in its deuterium analogue are derived from THF and d_8-THF respectively

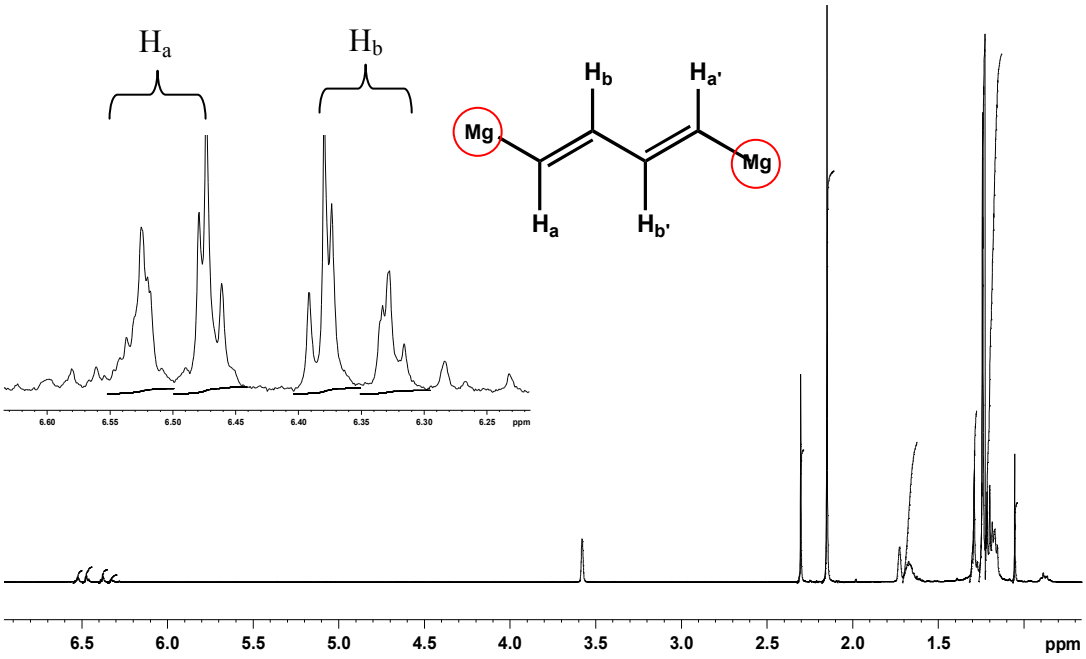

Figure 71: ^{1}H NMR spectrum in d_8-THF of butadiene complex **43**. Inset shows enhanced aromatic region.

Considering the other crystalline product of the reaction, namely the oxo-inverse crown, magnesiate **45** has been previously reported by our Group in 2003.[38] However its synthesis did not involve THF, instead the captured oxide was assumed to come from adventitious oxygen or moisture present in the air sensitive reaction mixture of BuNa, *n*BuMg and TMP(H).[38] Although the molecular structure of **45** is already known, we have characterised it further by analysing its NMR spectroscopic data in C_6D_6 solution. Interestingly two distinct types of TMP CH_3 resonance are observed at 1.26 and 1.47 ppm in the ^{1}H spectrum (Figure 74), which pair up with the two distinct CH_3 resonances at 34.3 and 39.1 ppm in the ^{13}C spectrum. This observation is in keeping with the endo- and exo- positioning of the CH_3 groups of the TMP with respect to the $(NaNMgN)_2$ host ring in the molecular structure of **45**.

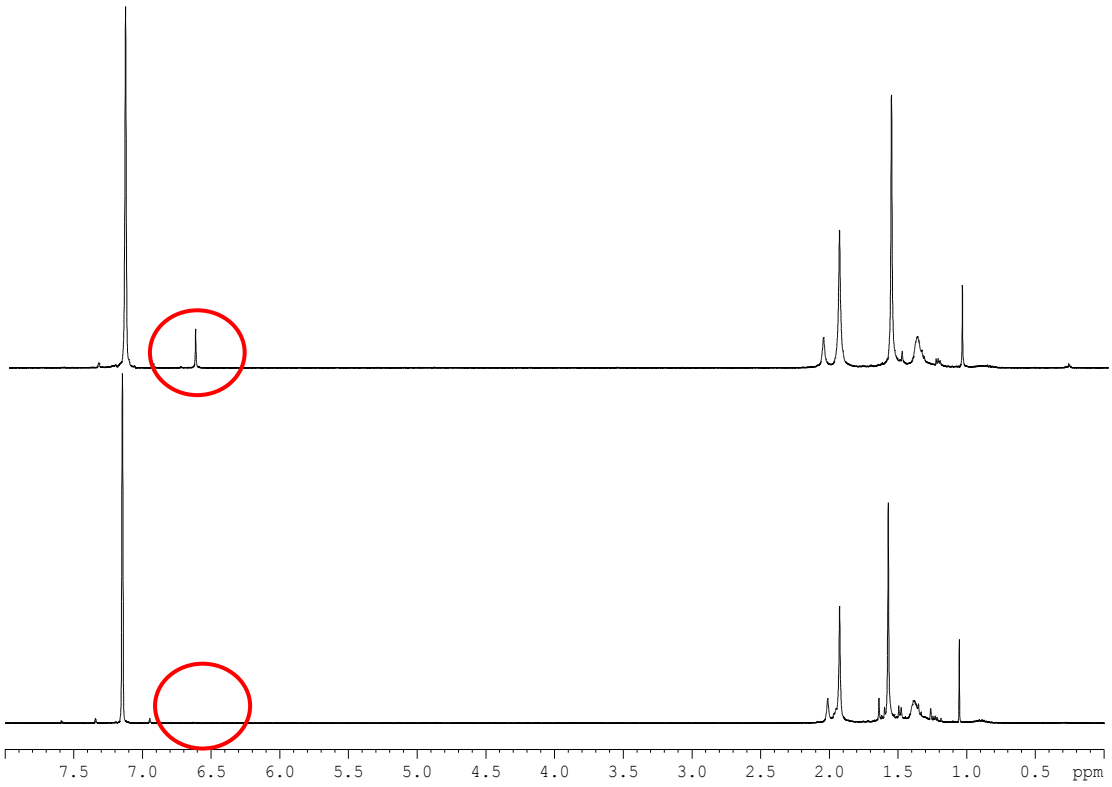

Figure 72: Comparison of ^{1}H NMR spectra of **43** in C_6D_6 solution with cleaved THF (top spectrum) and d_8-THF (bottom spectrum). **Red circle** shows presence / absence of butadienyl CH resonance.

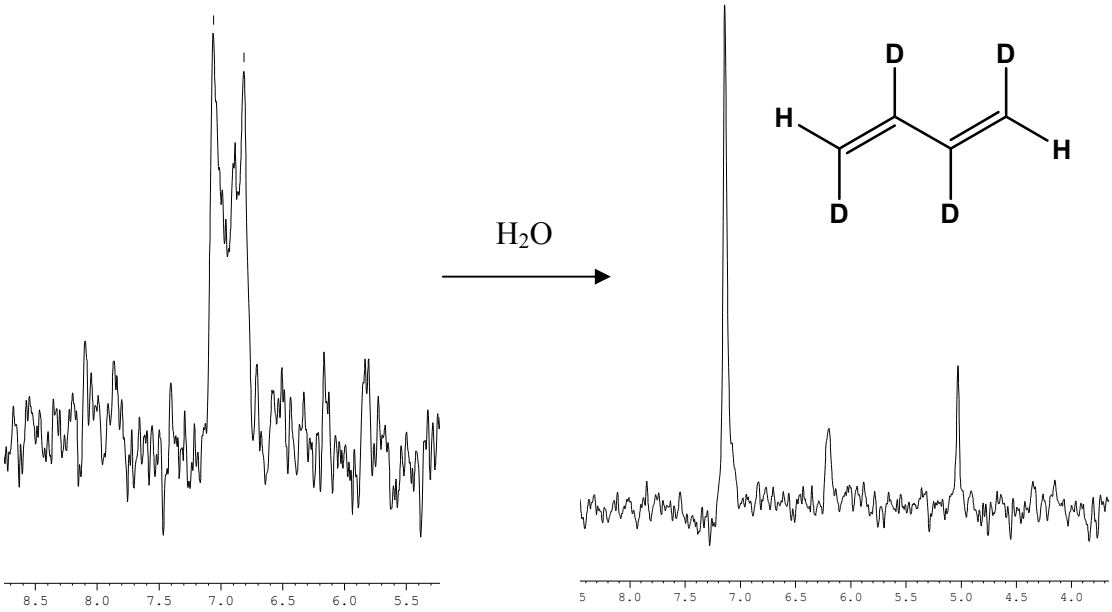

Figure 73: ^{2}D-NMR spectrum of crystalline C_4D_4 magnesiate complex (LHS). Hydrolysed sample to give new $C_4D_4H_2$ trans-butadiene compound (RHS).

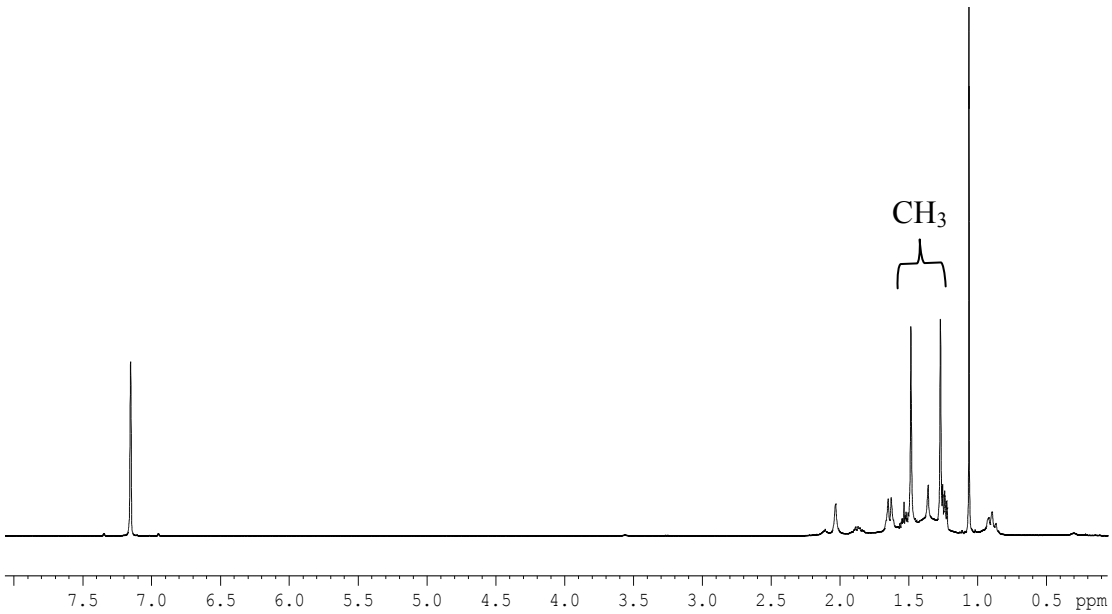

Figure 74: ^{1}H NMR spectrum in C_6D_6 solution of complex **45**.

The manganate inverse crown ether **44** is unfortunately not amenable to diagnostic NMR spectroscopic studies due to its paramagnetic nature; however, its structure was fully determined by X-ray crystallographic studies. Isostructural to the magnesiate **45**, the molecular structure of **44** (Figure 75) is centrosymmetric comprising alternating Na and Mn atoms linked through N bridges to form a $(NaNMnN)_2$ octagonal ring. Captured in the centre of the cationic ring is a guest oxide (O^{2-}) ion that lies coplanar with the eight-membered ring. The smaller Mn atoms approach the oxide core more closely with shorter Mn-O [1.9484(5) Å] and longer Na-O [2.2448(10) Å] bond lengths. Similarly the Mn-N bond lengths are shorter [mean 2.081 Å] than their Na-N counterparts [mean 2.465 Å]. These shorter Mn-O/N bond lengths mirror those found in **45,** when Mn is substituted for Mg [corresponding values 1.8672 (9) Å, 2.2405(10) Å, 2.047 Å, 2.508 Å], though the Mn bond lengths are systematically slightly longer that their Mg analogues.[38]

Published by our group, the only other reported sodium/manganese oxo-inverse crown is the HMDS complex $[Na_2Mn_2\{N(SiMe_3)_2\}_4O]$[197] **46** made from the 1 :1 :1 reaction mixture of NaHMDS, $Mn(CH_2SiMe_3)_2$ and HMDS(H). Its formation was attributed to a redox mechanism, where oxidative coupling of two Me_3SiCH_2 ligands gave the ethane silyl-substituted $Me_3SiCH_2CH_2SiMe_3$ and **46**. Several attempts were made at the time to try and synthesis the new manganese inverse crown **44** through deliberate oxidation (via

air) or hydrolysis of the starting precursors, however, all efforts failed. This contrasts with the marked reproducibility of complex **44** via the direct THF reaction. While we cannot explicitly rule out the alternative oxidative or hydrolytic pathway for at least some of the formation of the oxo-inverse crown population in **44** or **45**, these observations along with the near-quantitative yields of **44** and **45** that match up with those in **42** and **43** strongly suggest the consumption of one THF molecule, which lends strong support for the THF being the direct source of the oxide in these inverse crown ethers.

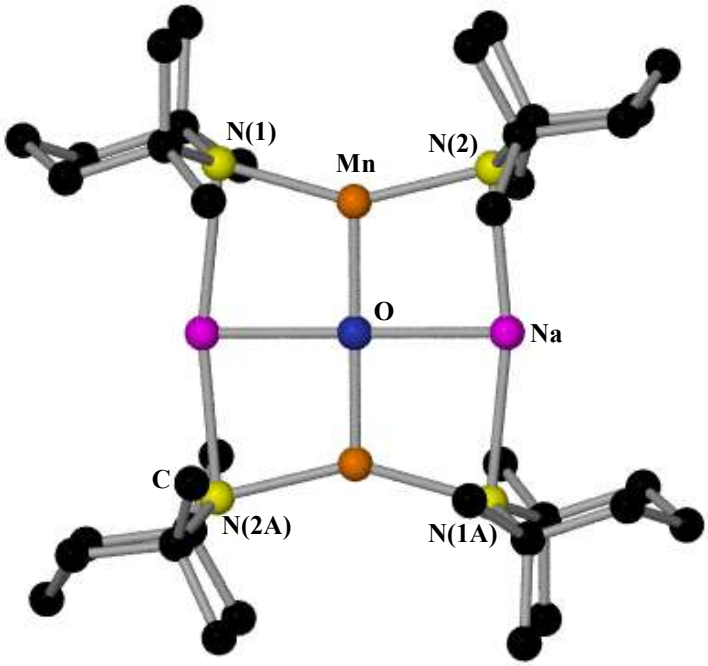

Figure 75: Molecular structure of **44** with selective atom labelling. Hydrogen atoms are omitted for clarity. Selected bond lengths [Å] and bond angles [°]: Mn-N(1), 2.1046(13); Mn-N(2), 2.0717(12); Mn-O, 1.9451(4); Na-N(1A), 2.4400(14); Na-N(2), 2.5318(14); Na-O, 2.2548(7); N(1)-Mn-N(2), 150.60(5); N(2)-Na-N(1A), 169.04(5); Na-O-Mn, 90.47(2); Mn-O-Na(A), 89.53(2); Na-N(2)-Mn, 80.33(4); Na-N(1)-Mn, 81.11(4).

All these experimental findings, both X-ray crystallographic and NMR based have lead us to believe that both the butadiene fragment and the oxide anion have originated from the cyclic ether THF. Organometallic reagents tend to have a general lack of stability in ether solvents, especially THF, with ether cleavage reactions dominating THF decomposition.[190] Wittig[221] and Gilman[222] are two of many renowned contributors to this area of organometallic based ether cleavage. Reactivity studies have shown that

alkyl lithium reagents commonly deprotonate THF by abstracting a proton in the C2 position, α to the oxygen atom in THF. This α-lithiated furyl anion then undergoes a reverse [3 + 2] cycloaddition to generate ethene and lithium enolate[223] (Scheme 53). In very rare cases an alternative pathway is seen, for example through a *t*BuLi and HMPA mixture, THF is cleaved open but retains its full complement of five ring atoms within a lithium but-3-en-1-oxide chain.[224, 225] One possible explanation for the observation of this unusual ether chain complex is via a deprotonation reaction at the C2 atom followed by an α-elimination and a 1, 2-H shift. Previously mentioned, the last and newly developed direct α-zincation of THF by a bimetallic zinc/sodium synergic base can also be surprisingly achieved without the cyclic THF ring opening or being cleaved.[214]

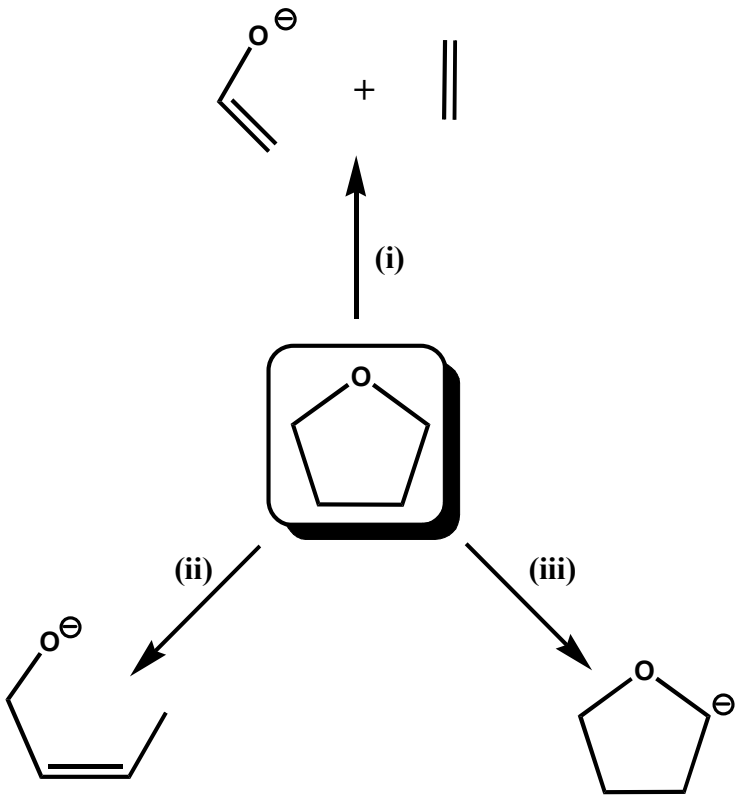

Scheme 53: Known outcomes of THF metallation reactions: i) lithium enolate of acetaldehyde via LiR (R = Me, *t*Bu, *n*Bu); ii) lithium but-3-en-1-oxide via *t*BuLi/HMPA; and iii) intact α–deprotonated anion via [(TMEDA)Na(TMP)(CH_2SiMe_3)Zn(CH_2SiMe_3)].

6.1.1. Mechanistic considerations

In total contrast to all the documented ether deprotonative reactions discussed above our reaction could be considered as a new synergic cleavage of THF, in that the C_4H_8 backbone of THF is cleaved and deprotonated four times to give the captured metallated butadiene fragment while the O^{2-} anion is expelled and captured in the form of a mixed-metal inverse crown. The reactions that produce **42**, **43**, **44** and **45** must be extremely complex as their solution mixtures contain various metals, different bases and different solvents making it an exceptionally challenging and time consuming task to establish precise mechanisms. However, by looking to the literature and making some reasonable assumptions we can postulate the mechanistic steps involved in these complex reactions. The most likely first step would involve the α-deprotonation of THF, especially with the specific precedent of the aforementioned α-zincation reaction. A second α'-deprotonation could then follow as the same synergic magnesium base has previously α, α'-deprotonated the heterocycle furan (C_4H_4O) to form a sub-porphyrin type structure (see page 150). With two deprotonations at either side of the oxygen on the THF the build up of charge could then encourage its expulsion to give an oxide (O^{2-}) inverse crown motif. At this point the C_4 fragment of the THF would be left as a neutral dicarbene that could rearrange through 1, 2-hydrogen shifts to give a 1, 3-butadiene molecule (Figure 76). Given the vast excess of mixed-metal base molecules within in the reaction mixture, capable of dual σ-/π-bonding, the butadiene is unlikely to be 'free' in solution. As we have recently reported that non-activated ethene can be deprotonated by a related potassium-zinc base,[214] the twofold deprotonation of a butadiene species appears to be a feasible conclusion to the reaction sequence. Overall a total of four deprotonations has been accomplished, a feat not unknown in mixed-metal magnesiate chemistry where fourfold deprotonations of metallocenes[49, 117] is precedented.

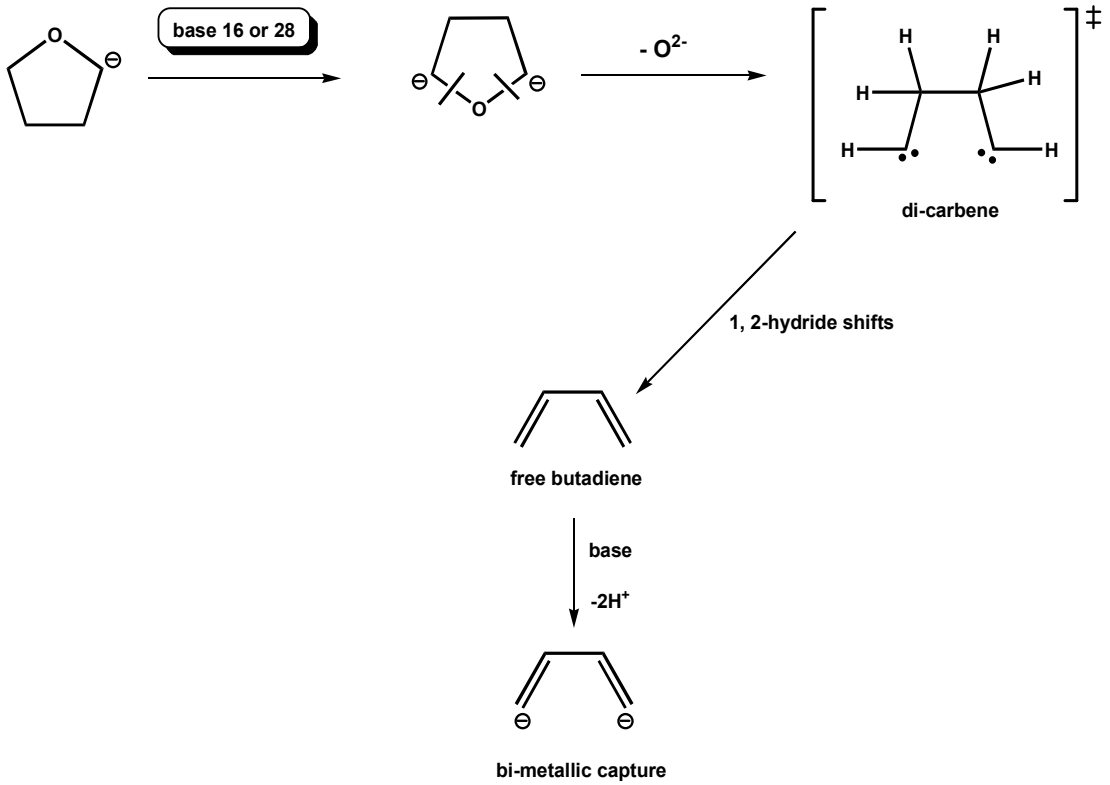

Figure 76: Proposed reaction pathway of synergic cleavage of THF.

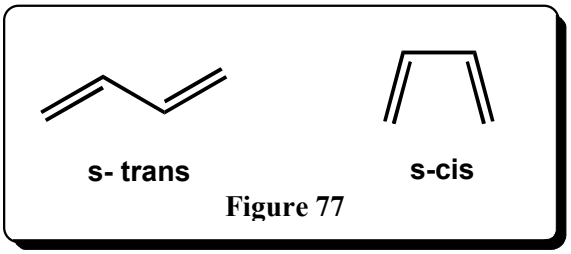

Figure 77

The first reactions in which a metallated butadiene was isolated but not structurally characterised were made by Schlenk in 1928 from a mixture of tolan (Ph-C≡C-Ph) and lithium metal.[226] However, the true nature of this reaction was not realised until thirteen years later in 1941 when a 1, 4-dilithiated butadiene structure was predicted.[227] On searching the CCDB one can find about 60 structurally characterised complexes containing 1, 4-dimetallated or structures that contain a M-C=C-C=C-M moiety. In the complexes that contain a butadiene fragment two conformations can exist, the s-cis or s-trans (Figure 77), with the latter being by far the more common conformation. Most of the compounds have the same metal attached to each end of the butadiene chain with a large variety of ligand systems and metals including; Fe,[228-234] Ru,[235-237] Os,[238] Ni,[239-242] Pt,[243] Pd, [244] Ge,[245] Al[246] and Li.[247-249] The vast majority of these structures contain some sort of alkyl or ligand substitution on the butadiene backbone and are synthesised from a variety of different routes including C-H activation, metal-halogen exchange reactions, transmetallations and reductions. For example, the

dilithium complex $[(DME)_2Li_2C_4Ph_4]$[247] (DME = 1,2-dimethoxyethane), made from the reaction of diphenylacetylene and Li powder, has four phenyl groups substituted on its cis-butadiene framework, whereas the aluminium butadiene complex $[\{(Me_3C)_2Al\}_2(Me_3SiC{=}CH\text{-}C{=}CSiMe_3)]$,[246] made from the addition reaction of di(*tert*-butyl)aluminium hydride to the diyne 1,4-bis(trimethylsilyl)-1,3-butadiyne, has no alkyl substitution on its bridging trans-butadiene motif. There are no reported structural examples of magnesiated or manganated butadiene complexes reported in the literature nor is there any precedent for the formation of a butadiene fragment from an ether cleavage reaction of THF or any other ether. These structures of **42** and **43** therefore give unprecedented insight into the complex and unpredictable blackbox chemistry that is ether cleavage.

6.2. Reaction of the synergic bases 16 and 28 with tetrahydrothiophene

Having established this reaction works well for THF we wanted to test the synergic bases reactivity towards its sulphur analogue tetrahydrothiophene (THT). Following a similar protocol as before one molar equivalent of THT was reacted with each of the bases separately in hexane solution. With manganate **16** an initial colour change from light yellow to orange was observed for the solution that after 20 minutes at room temperature precipitated a bright orange solid. Both heat and various solvent combinations did not afford a homogeneous solution and no crystalline product could be grown (at 25°C, -5°C or -27°C). Turning to the magnesiate base **28**, its reaction with THT produced a light yellow transparent solution that after 24 hours stirring at room temperature was placed in the refrigerator (at -5ºC) to furnish a crop of colourless plate crystals (Scheme 54). Analysis of these crystals by X-ray crystallography revealed them to be the new magnesiate [(TMEDA)Na(TMP)(α-C_4H_7S)Mg(TMP)] **47** (crystalline yield, 34%). The complex is extremely soluble at room temperature so isolating it in a high crystalline yield proved difficult. However, checking the filtrates by ^{1}H NMR spectroscopy showed the major product to be the isolated complex **47**.

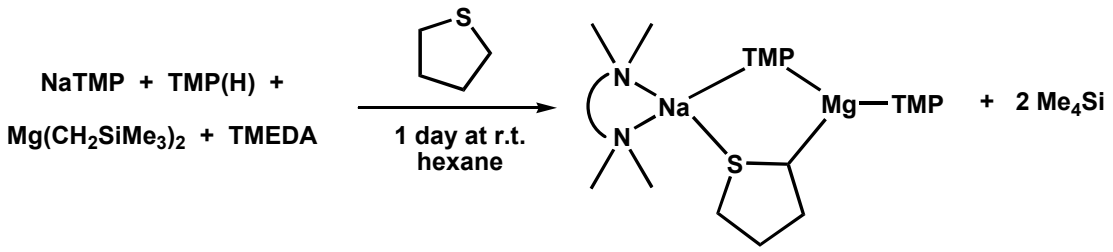

Scheme 54: Reaction of the magnesiate base **28** with the cyclic thioether THT.

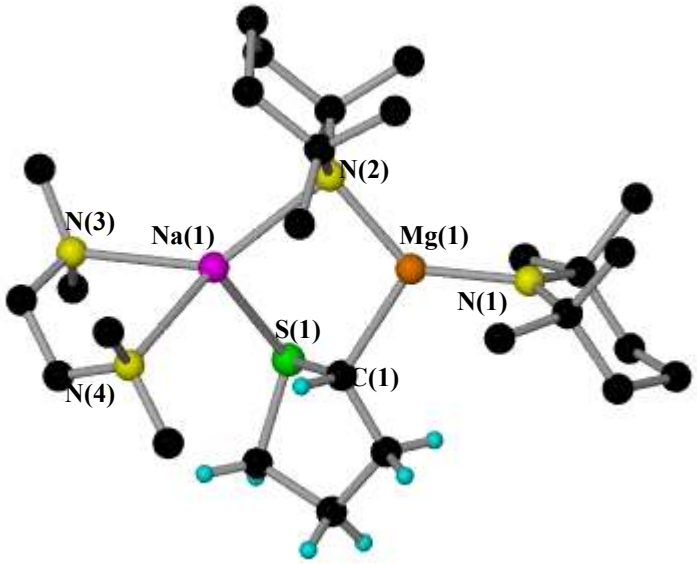

Figure 78: Molecular structure of **47** with selective atom labelling. Hydrogen atoms except THT ones are omitted for clarity. Selected bond lengths [Å] and bond angles [°]: Mg(1)-N(1), 1.9879(17); Mg(1)-N(2), 2.0824(16); Mg(1)-C(1), 2.189(2); Na(1)-N(3), 2.478(3); Na(1)-N(2), 2.4925(17); Na(1)-N(4), 2.5834(19); Na(1)-C(1), 2.835(2); Na(1)-S(1), 2.8713(9); N(1)-Mg(1)-N(2), 134.46(7); N(1)-Mg(1)-C(1), 117.60(8); N(2)-Mg(1)-C(1), 107.83(8); N(2)-Na(1)-S(1), 96.19(4); N(2)-Na(1)-N(4), 135.88(6); N(2)-Na(1)-N(3), 136.21(10); S(1)-Na(1)-N(4), 107.45(5); S(1)-Na(1)-N(3), 105.32(9); N(4)-Na(1)-N(3), 72.63(9).

Figure 78 shows the molecular structure of **47** with its most important feature being the magnesiated molecule of THT which has lost one hydrogen atom from the α-C position which has been selectively replaced by a magnesium atom [Mg-C(1), 2.189(2) Å]. This substitution makes the α–C(1) atom a stereogenic centre (note overall the crystals are racemic) with a distorted tetrahedral coordination of C, H, S and Mg atoms (mean bond angle 109.39º). The rest of the complex adopts the common (TMEDA)Na(μ-TMP)Mg(TMP) backbone with the Na atom additionally stabilising the deprotonated

THT molecule through a Na-S bond [Na-S, 2.8713(9) Å]. Ultimately magnesiate **28** has behaved as an alkyl base towards THT with the loss of tetramethylsilane. The two TMP molecules are retained with one acting as a bridge between Na and Mg [Mg-N(2), 2.0824(16) Å; Na-N(2), 2.4925(17) Å] while the other remains terminally bound to Mg [Mg-N(1), 1.9879(17) Å].

The structure of **47** observed in the crystal fits the ^{1}H (Figure 79) and ^{13}C NMR data collected in C_6D_6 solution. Most revealingly all seven hydrogen atoms can be detected individually in the ^{1}H NMR spectrum and quantitatively assigned using ^{1}H-^{1}H COSY NMR techniques (Figure 80). For example the signal furthest upfield at 0.93 ppm can be assigned to H_a, the single hydrogen remaining on the α-C of the THT molecule which has been deprotonated by the magnesium. This appears as a doublet of doublets.

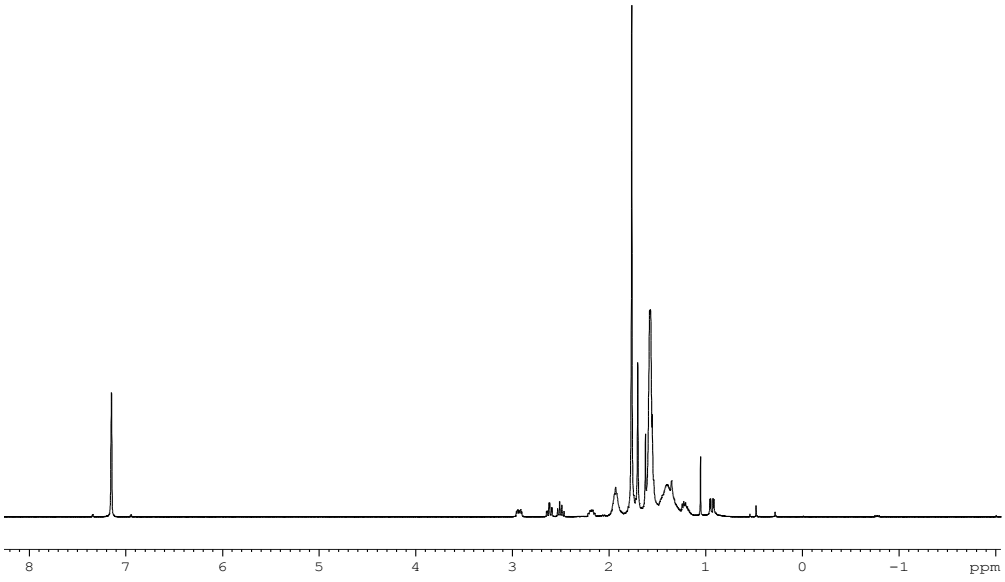

Figure 79: ^{1}H NMR spectrum in C_6D_6 solution of complex **47**.

To the best of our knowledge **47** represents the first structurally characterised example of an α-magnesiated tetrahydrothiophene. In fact on searching the literature and CCDB, examples of structurally characterised metallated THT molecules appear to be extremely rare. Only one structurally characterised THT complex, the trinuclear osmium complex $[Os_3(CO)_{10}(C_4H_7S)(\mu\text{-}H)]$[250] is known, which was isolated as an intermediate during the ring opening of THT by a triosmium cluster under high temperatures. Its M-α-C(THT) distance of 2.33(2) Å is significantly longer than that found in compound **47** [Mg-C(1), 2.189(2) Å]. There are also two related 2, 3-

dihydrothiophene (DHT) platinum $[Pt(PEt_3)_2(DHT\text{-}H)]PF_6$ and osmium $[HOs_3(CO)_9(PPh_3)(DHT\text{-}H)]$[251] complexes that have been structurally characterised which were both isolated during investigations into the hydrodesulphurisation of thiophene.

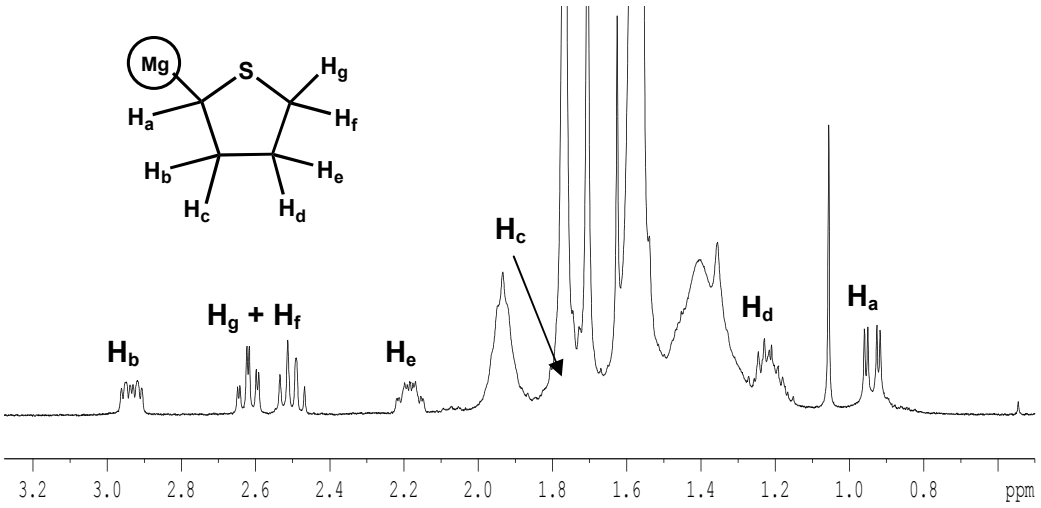

Figure 80: ^{1}H NMR spectrum in C_6D_6 solution of complex **47** expanding the aliphatic region.

During one repeat synthesis of complex **47**, but allowing the reaction mixture to stir at room temperature for three weeks, a different crystalline product was isolated from the solution in the form of colourless needles (note in contrast complex **47** crystallises as plates). Interested in what these needles could be we analysed them by ^{1}H NMR spectroscopy in C_6D_6 solution. The spectrum revealed signals for TMP and TMEDA as well as a single signal downfield at 6.64ppm. We have seen this signal before in the NMR spectrum of the aforementioned di-magnesiated butadiene complex **43**, which we assigned to the four protons belonging to the butadiene fragment. Here a similar reaction has occurred with the sulphur analogue THT, where again a butadiene fragment has been captured and twofold deprotonated. Hoping to recover a second crystalline product, as seen before with the THF reaction, we removed the butadiene crystals from the solution to leave the mother liquor. Unfortunately reducing the solvent volume or storing the solution in the refrigerator (at -5C) or freezer (at -27C) did not afford any more crystalline nor solid material. Analysis of this filtrate by NMR spectroscopy showed a mixture of species including a small amount of the butadiene complex, TMP, TMEDA and some residual complex **47**. The reaction was repeated on many occasions where it was found that the solution mixture was extremely sensitive. On most repeat

syntheses if the solution was allowed to stir for three weeks or longer at room temperature, the butadiene complex **43** could be isolated from the solution as the main product. However, on some occasions complex **47** was isolated instead. Wanting to develop a quicker route to the butadiene complex from THT we decided to heat the reaction mixture to reflux temperature for 8 hours. Unfortunately no crystalline products could be isolated from this solution and analysis of it by ^{1}H NMR spectroscopy showed a complicated mixture of products that were unassignable.

Looking to the literature, previous investigations by Adams *et al*. [250] have shown that THT can undergo ring opening reactions with trinuclear osmium cluster complexes. An initial CH activation reaction gave the α-metallated THT complex $[Os_3(CO)_{10}(SC_4H_7)(\mu\text{-}H)]$[250] which undergoes a ring-opening cleavage reaction of one of the C-S bonds to give the new 3-butenethiolate complex $[Os_3(CO)_9\{S(CH_2)_2CHCH_2\}(\mu\text{-}H)]$. Interestingly, heating this complex above 205ºC releases butene. Comparing these findings to our own synergic system suggest that one possible pathway to the formation of butadiene **43** from THT could involve a C-S cleavage reaction after the initial α-magnesiation of THT. Further work would have to be carried out in order to unravel the full mechanism.

From these results it seems that this new synergic cleavage reaction is applicable to both THF and THT when using the magnesiate base **28**. With THF the reaction proceeds straight to fragmentation with two separate crystalline products being isolated, namely, a metallated butadiene complex **43** and an oxo-inverse crown **45**, recovering and capturing all the component parts of the THF ring. In contrast, the reaction with THT can be stopped at the α-metallation stage, prior to cleavage, allowing the isolation and characterisation of complex **47**. Only after weeks stirring at room temperature does the fragmentation of THT occur to give only one isolated crystalline product, namely, the di-metallated butadiene **43** with the filtrate showing a complicated mixture of residual species. The isolation of the α-magnesiated THT **47** helps to strengthen our previous argument that the reaction pathway firstly proceeds through an initial α-metallation step. Further work would need to be carried out in order to investigate where the sulphur from the fragmented THT resides at the end of the complicated process.

A stereogenic α-C atom is obtained following the α-magnesiation of THT which interested us. We wondered that by somehow making the magnesiate base chiral "would we be able to isolate just one of the stereoisomers?" Preliminary studies within our group are investigating the use of chiral ligands, specifically the bulky alkaloid (-)-sparteine, in our mixed-metal base systems on metallation reactions. (-)-Sparteine has been successfully used in alkyllithium systems[252, 253] with good stereoselectivity being achieved in deprotonation, oxidation and addition reaction systems.[254-256] In view of this, we decided to try and synthesise a new chiral magnesiate base using (-)-sparteine in place of TMEDA in the hope of testing its reactivity with THT.

6.3. Synthesis of the chiral magnesiate base 48

To synthesise the new (-)-sparteine based magnesiate, equimolar amounts of NaTMP, TMP(H), $Mg(CH_2SiMe_3)_2$, and (-)-sparteine, in hexane solution, were reacted together to give a light yellow solution. Reduction of solvent volume under reduced pressure allowed the deposition of a crop of pale yellow plate crystals (Scheme 55). Analysis of these crystals by X-ray crystallography revealed the complex to be the (-)-sparteine complexed magnesiate [{(-)-sparteine}Na(TMP)(CH_2SiMe_3)Mg(TMP)] **48** (isolated crystalline yield, 58%).

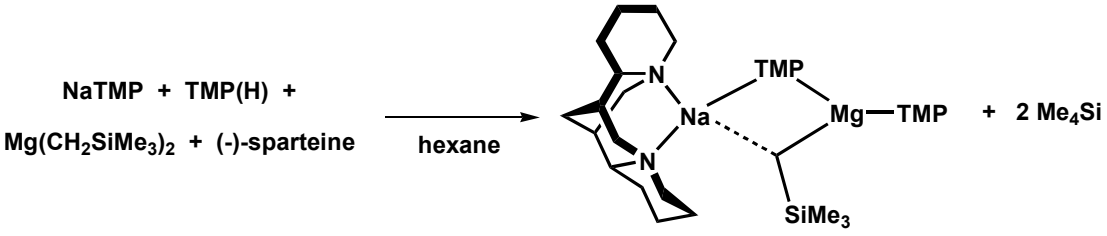

Scheme 55: Synthesis of the new chiral magnesiate base **48**.

As in the similarly composed magnesiate **28**, the molecular structure of **48** (Figure 81) exhibits a contact ion pair arrangement made up of a N_2C trigonal planar magnesium coordinated by a bridging TMP [Mg(1)-N(31), 2.098(2) Å], a terminal TMP [Mg(1)-N(21), 2.013(2) Å] and a bridging alkyl ligand [Mg(1)-C(1), 2.195(2) Å]. Like many of the structures discussed in this report a central motif, specifically here of a 4-atom, 4-element (NaCMgN) type is a core feature. A molecule of (-)-sparteine coordinates to the Na atom through its two N atoms [Na(1)-N(41), 2.484(2) Å; Na(1)-N(416), 2.487(2) Å]

to complete its distorted tetrahedral coordination. Table 4 compares the key corresponding dimensions within complexes **48** and **28**.

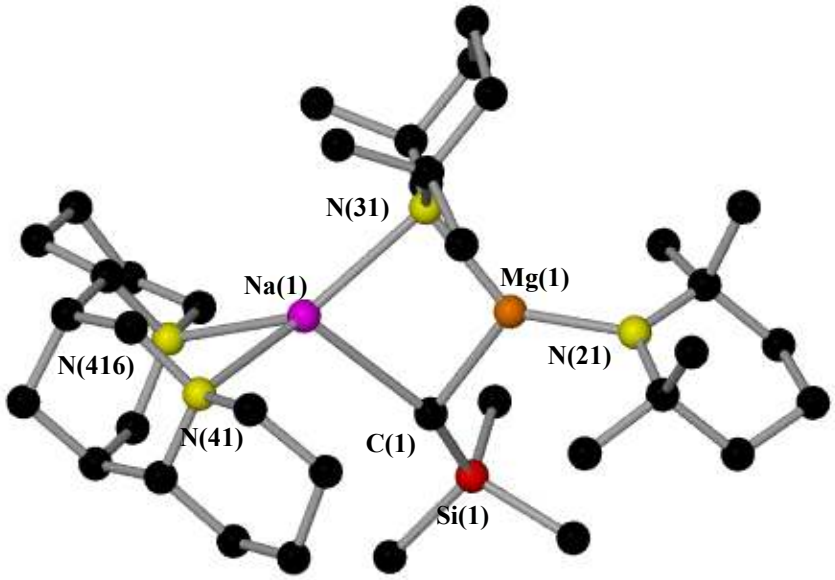

Figure 81: Molecular structure of **48** with selective atom labelling. Hydrogen atoms are omitted for clarity. Selected bond lengths [Å] and bond angles [°]: Mg(1)-N(21), 2.013(2); Mg(1)-N(31), 2.098(2); Mg(1)-C(1), 2.195(2); Na(1)-N(41), 2.484(2); Na(1)-N(416), 2.487(2); Na(1)-N(31), 2.505(2); Na(1)-C(1), 2.738(2); N(41)-Na(1)-N(416), 72.94(7); N(41)-Na(1)-N(31), 139.55(8); N(416)-Na(1)-N(31), 138.79(8); N(41)-Na(1)-C(1), 117.29(9); N(416)-Na(1)-C(1), 106.64(7); N(31)-Na(1)-C(1), 81.91(7); N(21)-Mg(1)-N(31), 130.51(8); N(21)-Mg(1)-C(1), 122.15(9); N(31)-Mg(1)-C(1), 106.54(9).

Table 4 Comparison of selected bond lengths [Å] and bond angles [°] within complexes **28** and **48**.

	28	**48**
Mg-C(alkyl)	2.179(2)	2.195(2)
Mg-TMP	1.9895(18)^{t} 2.068(3)^{b}	2.013(2)^{t} 2.195(2)^{b}
Na-N (TMP)	2.454(4)	2.505(2)
Na-N^{a}	2.433(2) 2.488(3)	2.484(2) 2.487(2)
Na-C(alkyl)	2.678(2)	2.738(2)
N^{b}-Mg-N^{t}	128.71(13)	130.51(8)
N^{t}-Mg-C(alkyl)	123.36(10)	122.15(9)
N^{b}-Mg-C(alkyl)	106.67(13)	106.54(9)
Na-TMP-Mg	85.42(11)	86.94(7)
Na-C-Mg	77.98(7)	79.44(7)
N^{a}-Na-N^{a}	75.48(12)	72.94(7)

key: t, terminal atom/bond; b, bridging atom/bond; a, TMEDA or (-)-sparteine N atom.

Analysing the data in Table 4 reveals that the pertinent dimensions involving the magnesium in **48** are, within experimental error, essentially the same as their counterparts in **28**. This indicates that changing TMEDA for (-)-sparteine produces no noticeable alteration of the divalent metal's geometry. The Na atom dimensions in **48** also compare favourably to those in **28** with the most notable difference being the N-Na-N bite angle which is 2.54º more acute than the corresponding angle in the TMEDA complex **28**. The majority of other bond angles are within 2º of each other.

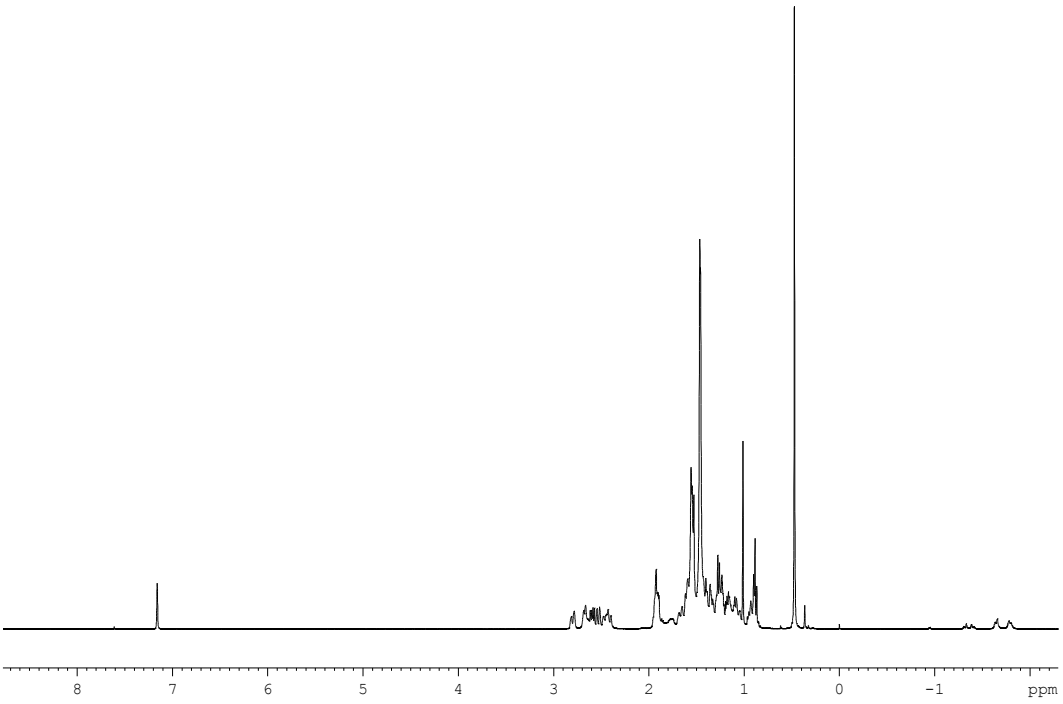

Figure 82: ^{1}H NMR spectrum in C_6D_6 of complex **48**.

Investigating **48** by NMR spectroscopy in C_6D_6 solution (Figure 82) matches up with its structure in the solid state suggesting that (-)-sparteine remains coordinated to the metallic framework in solution [evidenced by the shift of the ligand signals relative to free, uncoordinated (-)-sparteine]. Most revealingly the methylene Me_3SiCH_2 atoms are diastereotopic, appearing as two distinct broad doublets at -1.64 and -1.76 ppm. This is a consequence of the interaction from the Na atom which has a molecule of chiral (-)-sparteine complexed to it. There are also corresponding signals for TMP and the methyl groups of the CH_2SiMe_3 ligand, however the vast majority of the signals in the spectrum belong to (-)-sparteine. On closer inspection of the ^{1}H NMR spectrum there is a second set of diastereotopic methylene Me_3SiCH_2 signals at -1.31 and -1.39 ppm which could belong to a residual impurity or the complex reacting with the deuterated benzene

solvent. Inspecting the ^{13}C NMR spectrum a forest of peaks are observed with most of them again belonging to (-)-sparteine. There are two distinct separate signals for the methylene carbon CH_2SiMe_3 at 1.83 and -1.83ppm, that pair up with the two sets of signals observed in the ^{1}H NMR spectrum, however only one set of (-)-sparteine and TMP signals are seen, suggesting that only one type of (-)-sparteine containing complex is present in solution.

Within our research group a similarly composed *n*butyl based sodium/magnesium complex [{(-)-sparteine}Na(TMP)(*n*Bu)Mg(TMP)][257] was recently synthesised. The bond lengths and bond angles of both complexes **48** and the aforementioned *n*Bu analogue are identical within experimental error indicating no major differences in the complex when substituting a *n*Bu group for a trimethylsilyl ligand. Unfortunately no reactivity studies of this (-)-sparteine complexed *n*Bu base have so far been carried out.

6.4. Reaction of the magnesiate synergic base 48 with THT

Wanting to test if **48** could enantioselectively deprotonate a substrate we tested its reactivity towards THT. Thus an *in situ* hexane solution of **48** was reacted with one molar equivalent of THT affording a light yellow solution. After 12 hours stirring at room temperature the solution was filtered and its solvent volume reduced under vacuum. Storage of the solution at room temperature deposited a crop of colourless plate crystals that were subsequently analysed by X-ray crystallography to be [{(-)-sparteine}Na(TMP)(α-C_4H_7S)Mg(TMP)] **49** in a 48% crystalline yield (Scheme 56).

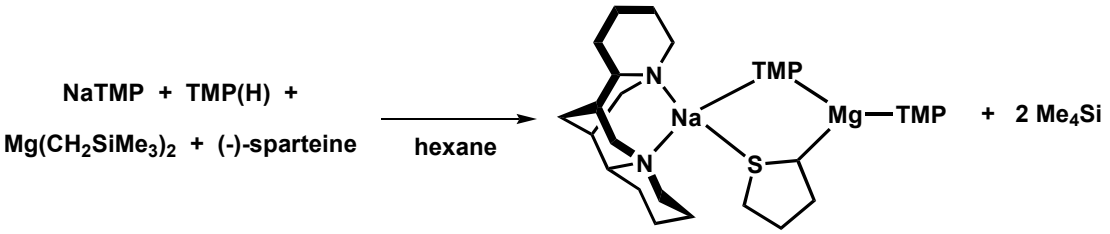

Scheme 56: Reaction of the magnesiate base **48** with THT.

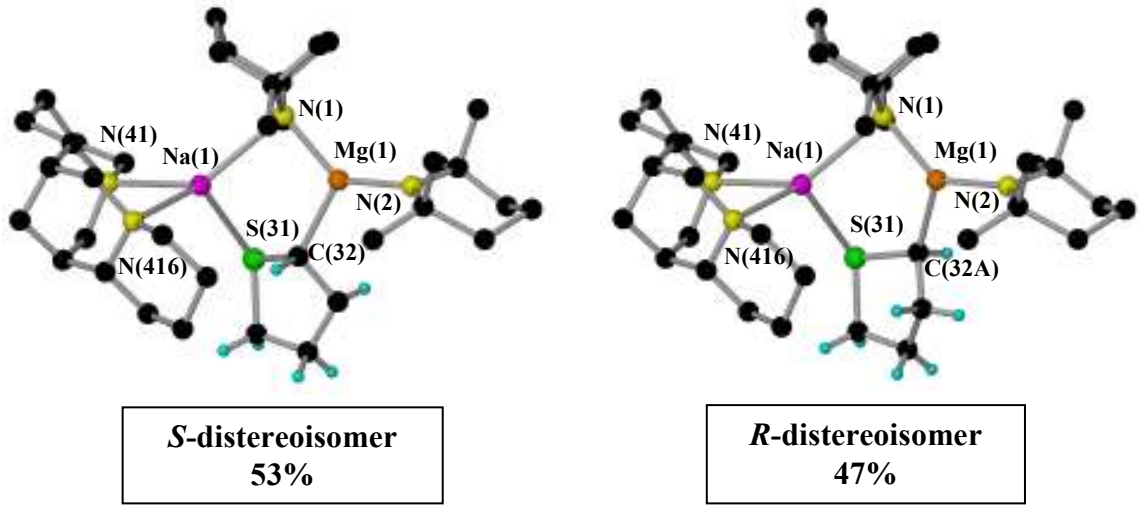

Figure 83: Molecular structures of **49** with selective atom labelling. Hydrogen atoms except THT ones are omitted for clarity. Only one of two independent molecules is shown in both its *R* (RHS) and *S* (LHS) forms. Selected bond lengths [Å] and bond angles [°]: Na(1)-N(416), 2.500(2); Na(1)-N(41), 2.542(3); Na(1)-N(1), 2.667(2); Na(1)-S(31), 2.8779(14); Mg(1)-N(2), 1.993(2); Mg(1)-N(1), 2.073(2); Mg(1)-C(32), 2.212(7); Mg(1)-C(32A), 2.216(6); N(416)-Na(1)-N(41), 73.34(8); N(416)-Na(1)-N(1), 135.04(8); N(41)-Na(1)-N(1), 131.45(8); N(416)-Na(1)-S(31), 99.12(6); N(41)-Na(1)-S(31), 120.15(7); N(1)-Na(1)-S(31), 96.22(6); N(2)-Mg(1)-N(1), 130.86(10); N(2)-Na(1)-C(32), 117.5(2); N(1)-Mg(1)-C(32), 110.5(2); N(2)-Mg(1)-C(32A), 111.26(19); N(1)-Mg(1)-C(32A), 117.61(18).

The crystal structure of the α-magnesiated THT complex **49** (Figure 83) has two crystallographically independent molecules in its unit cell. As both molecules are nearly identical only one will be discussed in detail. However within this one molecule there are two diastereoisomeric forms, namely the *S* and *R* forms that after refinement of the crystals structure were found to be present in a 53:47% ratio. As in previously discussed structures, the magnesium adopts a pseudo trigonal planar geometry (average bond angle for **49*S*,** 119.60°; **49*R*,** 119.91°) coordinating to a α-C of a deprotonated THT molecule and two TMP nitrogen atoms, one of which is terminal, and another which bridges asymmetrically between sodium and magnesium. The sodium atom is held in a distorted tetrahedral geometry (average bond angle 109.2°) by the bridging TMP nitrogen, the bidentate (-)-sparteine ligand and the sulphur atom of the metallated THT substrate. As in many of the previous structures, a ring motif, specifically here of a 5-atom, 5-element (NaSCMgN) type, is a core feature. This ring is fused to both the thiophenyl ring and via the spiro sodium atom to the (-)-sparteine ligand.

Our aim of selectively deprotonating the THT substrate has been achieved using the (-)-sparteine magnesium base **48** however, disappointingly no enantiomeric selectivity was observed as both *R* and *S* forms are present. The percentage of each enantiomer in the crystal composition is almost 50 (*R*) : 50 (*S*) showing poor ee. From this result it would seem that attaching the chiral (-)-sparteine ligand to the sodium has no effect on the outcome of the metallated product and does not allow for only one enantiomer to be isolated. Perhaps the chiral ligand is too far removed from the metallation site and therefore cannot control the enantiomeric outcome.

As mentioned before structures containing a metallated THT molecule are extremely rare with only one previously reported osmium complex $[Os_3(CO)_{10}(SC_4H_7)(\mu\text{-}H)]$[250] and our previously discussed α-magnesiated THT complex [(TMEDA)Na(TMP)(α-C_4SH_7)Mg(TMP)] **47** available for comparison. The Mg-αC bond distances in **47** and **49** compare favourably [**47**, 2.189(2) Å; **49*S***, 2.212(7) Å; **49*R***, 2.216(6) Å] while those in the osmium complex are significantly longer [2.33(2) Å]. One slight difference in complexes **47** and **49** are the Mg-α-C-S bond angles with that in **47** being approximately 10º less obtuse that those in **49** [**47**, 111.13(11)º; **49*S***, 122.7(4)º; **49*R***, 120.9(3)º].

Unfortunately no NMR data of complex **49** has been collected as this reaction was intended to be a 'test reaction' for base **48**. Due to time constraints at the end of this research project the reaction was never repeated and clearly further investigation is required into this reaction and its interesting stereogenic products.

After our success in reacting magnesiate **28** with both THF and THT we decided to focus our investigations on the related but unsaturated heterocycle furan. The furan framework features frequently in a variety of natural products, fragrances and pharmaceuticals as well as in various synthetic precursors to other important chemicals.[258] All these aspects make its metallation chemistry an essential avenue for investigation and development. Contrary to the large body of literature on the lithiation of furan[259] there is limited knowledge of magnesiofuran compounds.[260] Within our group previous studies with the magnesiate base [(TMEDA)Na(TMP)(*n*Bu)Mg(TMP)][46] and furan allowed the isolation of an α-furyl (2-C_4H_3) complex [{{$(THF)_2Na_2$}{$(TMEDA)Mg_2$}$(2\text{-}C_4H_3O)_6$}$_\infty$][261] which established a new type of inverse crown architecture composed of a 12-atom $(NaOCMgCO)_2$ ring

hosting the furyl guests in the centre. The 12-membered rings formed a larger polymeric chain linked together by TMEDA bridges. We wanted to investigate the reaction of magnesiate **28** with furan to see if changing the alkyl group in the base from *n*Bu to Me_3SiCH_2 would have a significant effect.

6.5. Reaction of the magnesiate synergic base 28 with furan

With the expectation of a similar outcome, an *in situ* hexane solution of **28** was treated with one molar equivalent of furan. The light yellow solution was heated for five minutes, which upon cooling to room temperature deposited a crop of large colourless needle crystals. Subsequent analysis of these crystals revealed the unexpected complex $[\{(TMEDA)_3Na_6Mg_3(CH_2SiMe_3)(2,5\text{-}C_4H_2O)(2\text{-}C_4H_3O)_5\}_2]$ **50** (Scheme 57). Despite the complicated looking formulation of **50**, its synthesis proved entirely reproducible in typical isolated crystalline yields of 48%, or even higher in powder form (approximately 75%). We originally thought that a disproportionation pathway seemed the most likely route to the formation of complex **50**, however the retention of some monosilyl ligands and the large number of furan deprotonations needed for its existence rules this out. Instead the magnesiate base **28** must act as a dual alkyl-amido base as depicted in Scheme 57.

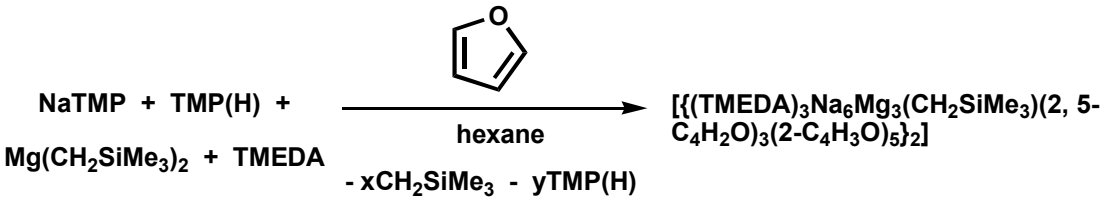

Scheme 57: Synthesis of complex **50**.

X-ray crystallographic studies revealed **50** to be the highest nuclearity molecular structure uncovered for any bimetallic product synthesised through AMM*Mg* as it possesses 12 Na and 6 Mg atoms. The complexity of structure **50** means it is best viewed as a Chem Draw representation (Figure 84). It is a centrosymmetric dimer with an inversion centre located halfway along the Mg(3)···Mg(3'), Na(2)···Na(2'), and Na(5)···Na(5') connections. It contains 10 α-mono-deprotonated furyl anions and 6 α,α'-twofold-deprotonated furyl dianions, giving a remarkable total of 22 furan

deprotonations. Since there are only 6 Mg atoms in the structure, equating to 12 deprotonations, the reaction producing **50** must involve a combination of magnesiation and sodiation.

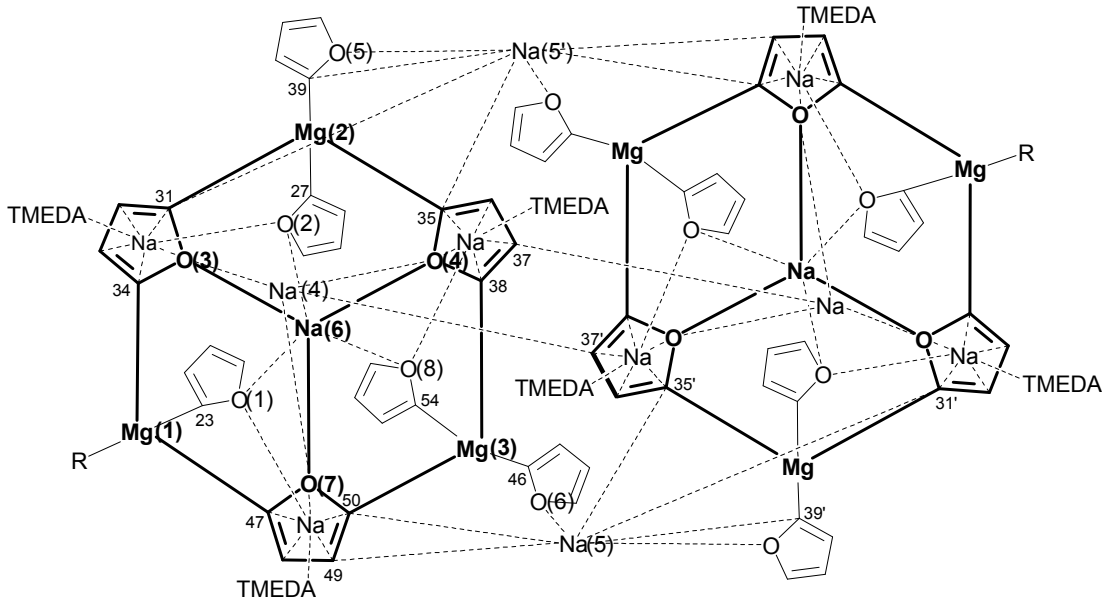

Figure 84: ChemDraw representation of **50** showing labelling scheme.

The molecular structure of the monomeric unit of **50** is shown in Figure 85. The most prominent feature is the trinuclear fusion of 3 Mg atoms and 3 fur-di-yl dianions through a 12 atom $(MgCOC)_3$ ring (highlighted by the shaded area). This 12 membered ring is severely puckered with each Mg atom forming, with respect to the fur-di-yl planes, one near in-plane and one out-of-plane bond to the deprotonated α-C atoms. Outside the ring system, Mg(1) carries a terminal unreacted CH_2SiMe_3 ligand [Mg(1)-C(19), 2.177(3) Å], while Mg(2) and Mg(3) carry terminal α-deprotonated furyl anions [Mg(2)-C(39), 2.156(4) Å; Mg(3)-C(46), 2.149(4) Å]. In addition all three Mg atoms carry another α-furyl monoanion, disposed endo with respect to the 12-atom ring, making them overall 4-coordinate. Turning to the Na atoms, four distinct types exist in **50**. Na(1), Na(2) and Na(3) all cap the electron rich faces of the fur-di-yl dianions in η^5-OC_4 interactions and are chelated by a TMEDA molecule. On the same side of the 12-

atom ring to Na(1)-(3), Na(6) is positioned directly above

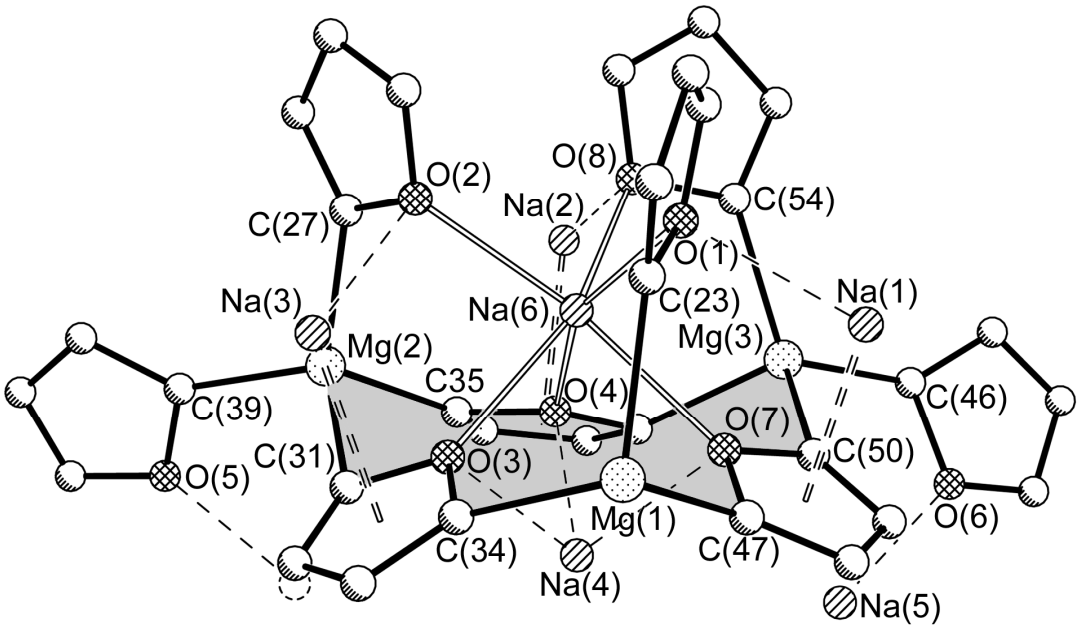

Figure 85: Monomeric unit of **50** with hydrogen atoms, TMEDA, CH_2SiMe_3 and disordered groups omitted for clarity. The $(MgCOC)_3$ ring is shaded. Mg(1)-C(34), 2.214(3); Mg(1)-C(47), 2.203(3); Mg(2)-C(31), 2.216(3); Mg(2)-C(35), 2.202(4); Mg(3)-C(38), 2.237(4); Mg(3)-C(50), 2.187(3); Mg(1)-C(23), 2.272(3); Mg(2)-C(27), 2.185(3); Mg(2)-C(39), 2.156(4); Mg(3)-C(46), 2.149(4); Mg(3)-C(54), 2.202(3); Na(1)-O(1), 2.456(2); Na(2)-O(8), 2.440(2); Na(3)-O(2), 2.480(2); Na(4)-O(3), 2.343(2); Na(4)-O(4), 2.470(2); Na(4)-O(7), 2.349(3); Na(6)-O(1), 2.364(2); Na(6)-O(2), 2.410(2); Na(6)-O(3), 2.440(2); Na(6)-O(4), 2.621(2); Na(6)-O(7), 2.466(2); Na(6)-O(8), 2.397(2); Na(5)-O(5), 2.343(4); Na(5')-O(6), 2.314(4); Na(1)-CT, 2.469; Na(2)-CT, 2.496; Na(3)-CT, 2.484 (CT = Centroid).

this ring forming a distorted trigonal pyramid to its 3 heteroatoms [O(3), O(4) and O(7)] and a distorted O_6 octahedral coordination overall counting the contacts to the 3 *endo*-disposed α-magnesiated furyls. Lying on the opposite side of the 12-atom ring to Na(6) to which it is almost eclipsed, Na(4) also binds to the 3 same heteroatoms of this ring [O(3), O(4) and O(7)]. It also forms a short intermolecular contact to a β-C atom [C(37')] of a neighbouring fur-di-yl dianion along with several longer intra- and inter-monomer Na-C contacts. The major dimerisation junction found at Na(5) has five main points of contact. It engages intramolecularly with O(6), belonging to a monoanion, and with a C=C bond [C(49)-C(50)] belonging to a dianion. Intermolecularly it engages with O(5A) and an α-C atom [C(39)] of a monoanion and two α-C atoms [C(31), C(35)] of two dianions making seven contacts in total. The shortest metal-carbon bond in **50** is

found in the sole terminal Mg(1)-C(19) involving the sp^3 alkyl group [2.177(3) Å], while the mean Mg-C(sp^2) bond length is 2.20 Å. Reflecting the more ionic nature of the bonding, the shortest Na-contact [Na(4)-C(37')] at 2.546(3) Å does not include a deprotonated C atom, instead a β-C(H) atom of a fur-di-yl dianion is involved. One interesting feature of the Na η^5-interaction with the dianion face, is its unsymmetrical contacts. Looking at Na(1) as an example the Na-contacts are biased towards one O-αC edge [Na(1)-O(7), 2.588(3) Å; Na(1)-C(47), 2.629(4) Å: *cf.* mean for other 3C atoms, 2.829 Å].

The ^{1}H NMR spectrum of complex **50** was recorded in d_8-THF solution (Figure 86). Four distinct resonances in the aromatic region are revealed: a sharp singlet at 6.22 ppm that can be assigned to the equivalent H atoms of the (OC_4H_2) dianions, while the broad resonances at 7.48, 6.22 and 6.00 ppm can be assigned to the H_3, H_4 and H_5 atoms respectively of the (OC_4H_3) monoanions. The integration ratios of all four peaks, for the two different furyl anions, match well with the stoichiometry found in the crystal structure. There are also corresponding peaks for TMEDA at 2.30 and 2.15 ppm, and CH_2SiMe_3 at -0.10 and -1.62 ppm found in the spectrum. The set of resonances belonging to the monoanion compare favourably with those of the OC_4H_3 monoanions in $[\{\{(THF)_2Na_2\}\{(TMEDA)Mg_2\}(2\text{-}C_4H_3O)_6\}_\infty]$[261] which have corresponding shifts of 7.58, 6.37 and 6.11 ppm. The sharp/broad distinction of the aromatic resonances in **50** implies a greater mobility of the OC_4H_3 monoanions compared to the OC_4H_2 dianions. This is logical as the dianions are held firmly on two sides by short, strong Mg-C bonds as opposed to only one Mg-C bond for the monoanions. The ^{13}C NMR spectrum recorded in d_8-THF showed six separate peaks in the aromatic region of the spectrum matching up with the six different furyl carbon atoms seen in the crystal structure. Recording the ^{1}H NMR spectra of **50** in C_6D_6 solution makes the spectrum significantly more complicated with a forest of resonances in the aromatic region. It is likely that the structure of **50** is retained in the weakly coordinating arene solvent, but broken down, at least partially, in strongly coordinating THF. One possibility is that THF ligation replaces the intermolecular contacts and TMEDA ligands to de-aggregate **50** to a monomeric form.

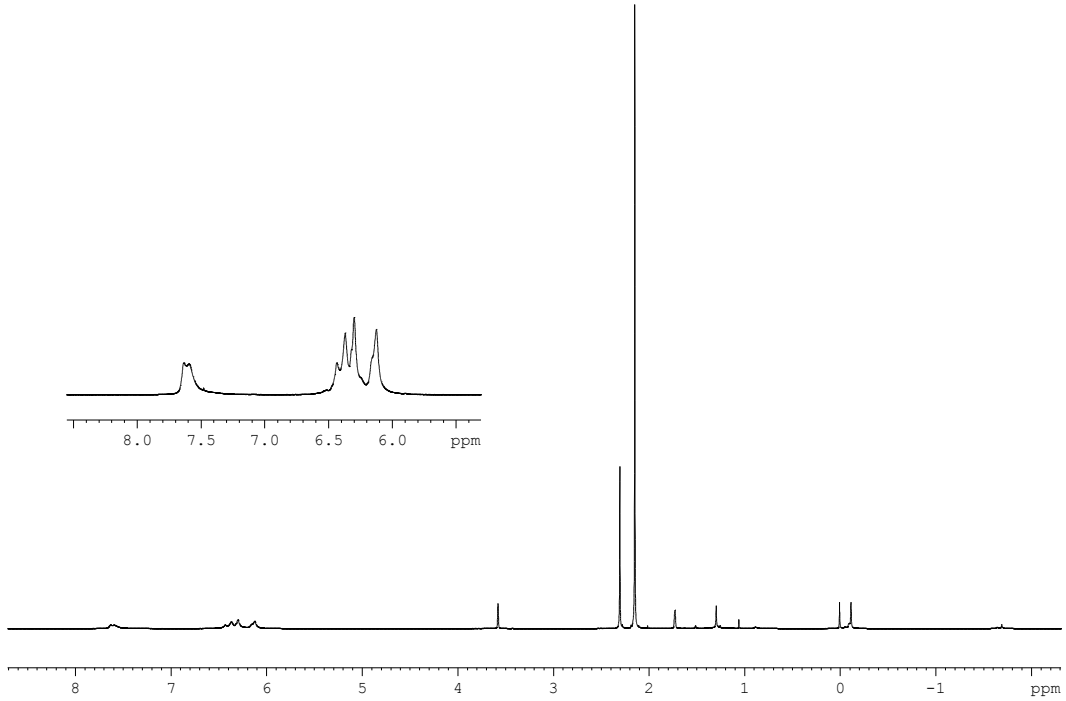

Figure 86: ^{1}H NMR spectrum in d_8-THF solution of complex **50** with inset showing expanded aromatic region.

Furan metallation by alkyl lithium reagents has been documented for some time with α-metallation being achieved in high yields with *n*BuLi in refluxing Et_2O.[262] Using the same base it can also be performed in THF solution either with[263] (at room temperature) or without[264] (at -78ºC) the presence of TMEDA. More recently lithium magnesiates Bu_3MgLi and Bu_4MgLi_2 have been shown to deprotonate a range of functionalised and unfunctionalised furan molecules, via *in situ* quench reactions, in reasonable to high yields.[11] We decided to test our metallated furan complex **50** in a series of electrophilic quench reactions with iodine and trimethylsilylchloride. Unfortunately no reaction was observed in both cases. This observation supports the view that **50** must retain high nuclearity in THF solution making it therefore inter-penetrable by incoming electrophiles. On the other hand, complex **50** can be broken down into its component parts upon the addition of D_2O to an NMR sample. The ^{1}H NMR spectrum (Figure 87) reveals two signals at 7.45 and 6.35 ppm integrating to 1 : 3.2 H respectively. This integration matches the expected ratio of 10 : 32 H expected for 10 mono-deuterated furans and 6 di-deuterated furan molecules within complex **50**.

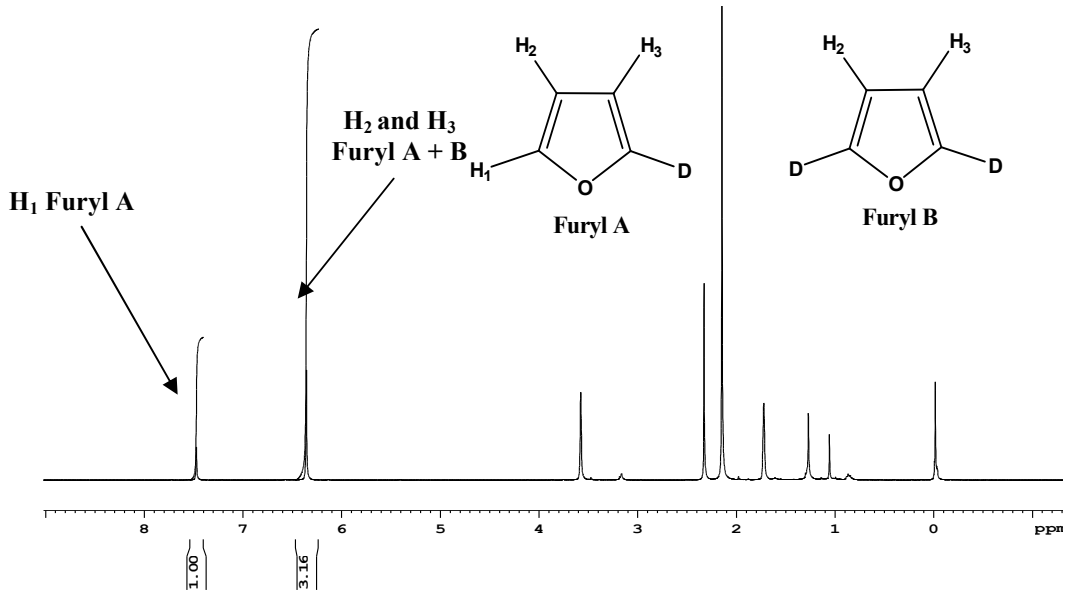

Figure 87: ^{1}H NMR spectrum in d_8-THF solution of **50** hydrolysed with D_2O.

With no apparent future in molecular functionalisation chemistry for our furan complex **50** we became interested in its potential as a building block for supramolecular systems.[265] We realised the central motif of **50** closely resembled that of a subporphyrin, a class of synthetic macrocycle belonging to the larger porphyrin family, that exhibits non-planar aromaticity of current interest in the supramolecular area. A comparison of the central motif in **50** and a subporphyrin can be seen in Figure 88. In **50** the Mg bridges and O heteroatoms mimic the CH bridges and N heteroatoms seen in the subporphyrin. Both have central Lewis acidic atoms in their central trigonal cavities, a sodium atom in **50** and a boron atom in the subporphyrin.

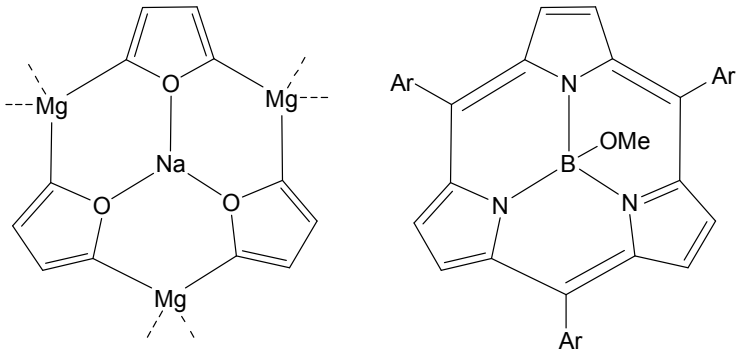

Figure 88: Comparison of the central motif of **50** (LHS) and a subporphyrin (RHS).

A search of the CCDB revealed several examples of mono-metallated furan complexes with a range of metals including Sn,[266] Ru,[267, 268] and Os.[269] However, only two of these complexes were prepared via a direct metallation route; the previously discussed magnesiated furan complex $[\{\{(THF)_2Na_2\}\{(TMEDA)Mg_2\}(2\text{-}C_4H_3O)_6\}_\infty]$[261] synthesised via AMM*Mg* by our group and the yttrocene 2-furyl complex $[Cp^*_2Y(C_4H_3O)(THF)]$[270] ($Cp^* = C_5\text{-}Me_5$) made from the direct reaction of $(Cp^*_2YH)_2$ with excess furan. The same paper reports two yttrocene 2-furyl ate complexes $[Cp^*_2Y(C_4H_3O)(\mu\text{-}Cl)Li(THF)_2]$ and $[Cp^*_2Y(C_4H_3O)_2Li(TMEDA)]$ made from the reaction of $[[Cp^*_2Y(\mu\text{-}Cl)_2Li(Et_2O)_2]$ with one and two molar equivalents of 2-lithiofuran respectively.

These results, here on the magnesiation of furan, highlight the importance of gaining structural information of metallated intermediates. The self-assembly of such a large supramolecular structure could not have been predicted from such a 'simple' metallation, nor could the incorporation of both a mono- and di-metallated species into the same structural product. We have also shown that by simply changing the alkyl ligand in the magnesiate base from *n*Bu to Me_3SiCH_2, vastly different structural and metallation chemistry can be achieved.

6.6. Reaction of the magnesiate synergic base 28 with thiophene

Staying with the current theme of unsaturated heterocycles, we decided to investigate the reaction of the magnesiate base **28** with thiophene. Unlike its π-deficient analogue furan, thiophene is π-excessive with the sulphur atom providing a strong acidifying effect on the ring. Hoping to obtain a similar thiophene based supramolecular structure like **50** an *in situ* hexane solution of **28** was reacted with one molar equivalent of thiophene to give a light yellow solution. After stirring at room temperature for one day the solution was concentrated *in vacuo* and placed in the refrigerator (at 5ºC) where after two days a crop of colourless plate crystals were deposited. Subsequent analysis by X-ray crystallography revealed them to be the new *ortho*-magnesiated complex $[(TMEDA)Na(C_4H_3S)_3Mg(TMEDA)]$ **51** isolated in a 26% crystalline yield. The subsequent rational synthesis of **51** could be easily achieved by reacting equimolar amounts of BuNa and $[Mg(CH_2SiMe_3)_2]_\infty$ with two molar equivalents of TMEDA and

three equivalents of thiophene to give an increased crystalline yield of 53% (Scheme 58).

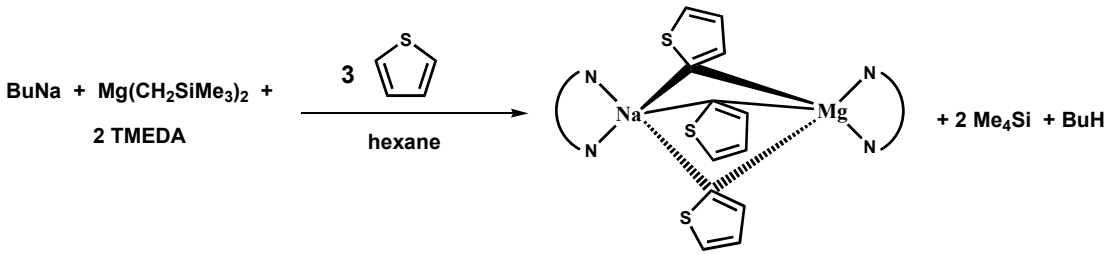

Scheme 58: Rational synthesis of thiophene complex **51**.

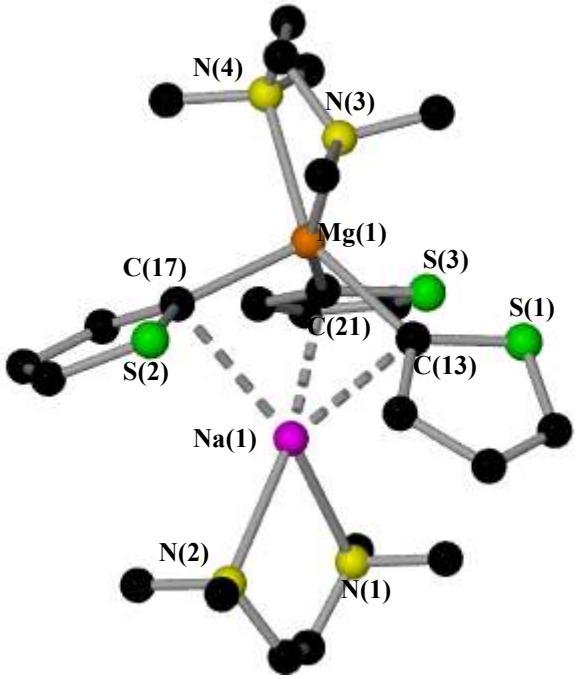

Figure 89: Molecular structure of **51** with selective atom labelling. Hydrogen atoms are omitted for clarity. Selected bond lengths [Å] and bond angles [°]: Na(1)-C(13), 2.778(2); Na(1)-C(17), 2.907(2); Na(1)-C(21), 2.628(2); Na(1)-N(1), 2.495(2); Na(1)-N(2), 2.473(2); Mg(1)-C(13), 2.263(2); Mg(1)-C(17), 2.217(2); Mg(1)-C(21), 2.236(2); Mg(1)-N(3), 2.4583(19); Mg(1)-N(4), 2.2589(19); N(2)-Na(1)-N(1); 73.43(7); N(2)-Na(1)-C(21), 165.03(8); N(1)-Na(1)-C(21), 103.08(8); N(2)-Na(1)-C(13), 119.49(8); N(1)-Na(1)-C(13), 118.15(7); C(21)-Na(1)-C(13), 75.20(7); N(2)-Na(1)-C(17), 102.14(7); N(1)-Na(1)-C(17), 165.74(7); C(21)-Na(1)-C(17), 77.62(7); C(13)-Na(1)-C(17), 75.96(7); C(17)-Mg(1)-C(21), 102.62(9); C(17)-Mg(1)-N(4), 104.69(8); C(21)-Mg(1)-N(4), 150.13(8); C(17)-Mg(1)-C(13), 102.74(9); C(21)-Mg(1)-C(13), 94.36(9); N(4)-Mg(1)-C(13), 91.24(8); C(17)-Mg(1)-N(3), 105.08(7); C(21)-Mg(1)-N(3), 86.24(8); N(4)-Mg(1)-N(3), 75.22(7); C(13)-Mg(1)-N(3), 151.34(7).

The molecular structure of **51** (Figure 89) contains a penta-coordinated N_2C_3 magnesium atom in a distorted trigonal bipyramidal geometry connected to three α-deprotonated thiophene molecules [Mg(1)-C(13), 2.263(2); Mg(1)-C(17), 2.217(2); Mg(1)-C(21), 2.236(3)] and a bidentate chelating molecule of TMEDA. Each α-magnesiated thiophene is further coordinated to a sodium atom via a Na-α-C bond [Na(1)-C(13), 2.778(2); Na(1)-C(17), 2.907(2); Na(1)-C(21), 2.628(2)]. Each Na-α-C bond interaction is distinct with a difference of 0.279 Å between the shortest and longest bonds. The coordination sphere around sodium is also completed by a chelating molecule of TMEDA making it overall penta-coordinated in a distorted trigonal bipyramidal geometry. In the rational synthesis that produced **51** a total of three deprotonations has taken place, one on each thiophene substrate. Since there is only one Mg atom in the complex, the atom-economical reaction that produces **51** must involve a mixture of magnesiation and sodiation.

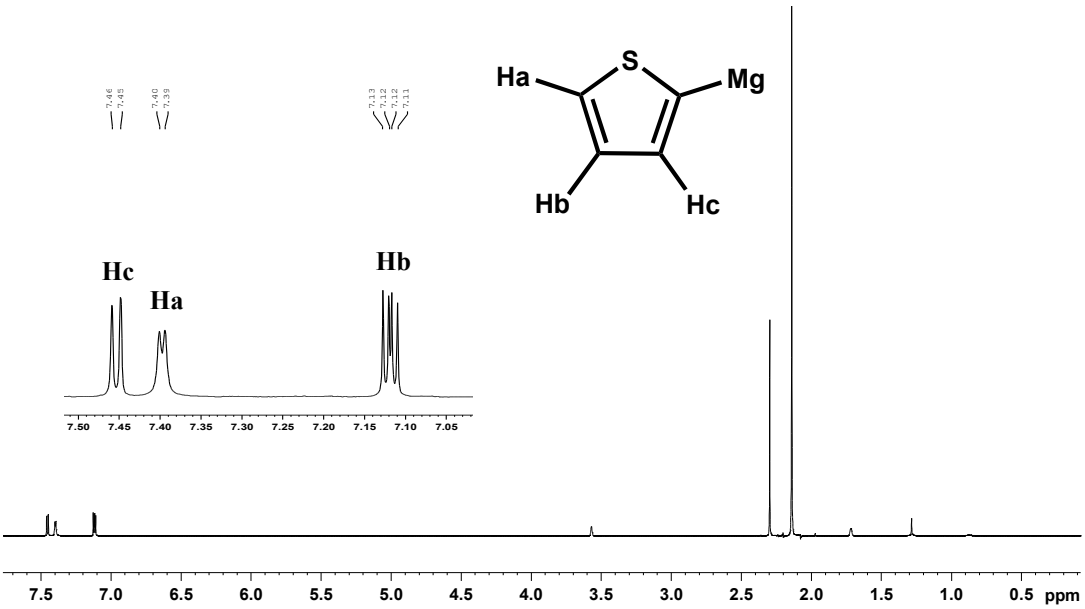

Figure 90: ^{1}H NMR spectrum in d_8-THF solution of complex **51**. Inset shows expanded with aromatic region.

The crystal structure composition of **51** was confirmed by ^{1}H NMR spectroscopy in d_8-THF solution (Figure 90). The three signals furthest downfield at 7.45, 7.40 and 7.12 ppm can be assigned to the three remaining hydrogen atoms of the α-metallated thiophene, while the two signals at 2.30 and 2.19 ppm can be assigned to the CH_2 and CH_3 groups of the TMEDA ligand respectively. The initial set of thienyl resonances

compare favourably with those of the C_4H_3S monoanions in the proposed "lithium tri(2-thienyl)magnesiates.TMEDA" with corresponding chemical shifts of 7.45, 7.39, 7.14 ppm.[9]

Known since 1949, the α-metallation of thiophene by *n*BuLi[271, 272] has been extensively studied,[273] however, most of the metallation patterns are confirmed only indirectly via *in situ* electrophilic quenching studies and have to be performed at low temperatures with only a few published[272, 274, 275] and some privately reported[276-279] crystal structures of lithiated examples. On searching the CCDB two examples of α-magnesiated thiophene structures can be found, namely the six coordinate trans-$[Mg(C_4H_3S)_2(THF)_4]$[280] **52** synthesised from the reaction of magnesium turnings with 2-bromo-thiophene and the octahedral Grignard reagent $[(C_4H_3S)MgBr(DME)_2]$[280] **53** which contains a chiral Mg centre. The Mg-α-C(thienyl) distance in complexe **52** [2.290(6) Å] is in the same range as those in **51** [average Mg-α-C(thienyl) bond length: 2. 238 Å] while the bond length in complex **53** is slightly shorter at 2.171(7) Å. Recently, Mongin *et. al.*[9, 281] have shown through mixed lithium magnesiate and lithium cuprate work that thiophene can be initially α-metallated *in situ* before being systematically trapped via quenching studies with various electrophiles in yields varying from 48-77%. However no structural information on the composition of these mixed lithium magnesiate or lithium cuprate bases are reported. In contrast to our previously discussed sulphur containing α-magnesiated THT complexes **47** and **49**, where the sodium bonds to the sulphur atom, complex **51** displays a different bonding pattern and prefers to bond to the α-magnesiated C atom with an average bond length of 2.771 Å. There is a large steric preference for this distinction as in **47** and **49** the Mg-αC bond is shielded effectively by two sterically demanding TMP ligands, whereas in **51** Mg-αC bonds are much more exposed.

Continuing with the theme of cyclic ethers the sodium-zincate base $[(TMEDA)Na(TMP)(CH_2SiMe_3)Zn(CH_2SiMe_3)]$ was also successful in selectively α-zincating the larger saturated ether tetrahydropyran (THP) furnishing $[(TMEDA)Na(TMP)(\alpha\text{-}C_5H_9O)Zn(CH_2SiMe_3)]$.[214] We have already observed in the THF reaction that changing the metal from zinc to magnesium results in a different reaction pathway and cleavage of the THF is observed instead of metallation. This prompted us to study the reactivity of the magnesiate base **28** towards THP.

6.7. Reaction of the magnesiate synergic base 28 with tetrahydropyran

Following the same synthetic protocol as before an *in situ* hexane solution of **28** was reacted with one molar equivalent of THP to give a light brown solution that was stirred at room temperature for 4 days. After filtration and reduction of the solvent volume under reduced pressure a crop of colourless needle crystals were deposited. Subsequent analysis by X-ray crystallography revealed this product to be the unexpected polymeric pentadienyl complex $[\{(TMEDA)Na(\eta^4\text{-}C_5H_7)Na\{OMg(TMP)\}_2(Na_2\eta^3\text{-}\eta^3\text{-}C_5H_7)\}_2]_\infty$.(hexane) **54**. Unfortunately attempts to resynthesise **54** were unsuccessful and often the base **28** would preferentially crystallise. Using an excess of THP and heating the reaction mixture to reflux temperature did not furnish pure **54** and often dark brown oils were formed. Due to this difficulty a yield for complex **54** was never obtained.

Owing to the complex nature of complex **54** its full molecular structure is best viewed as a Chem draw representation (Scheme 59). In total **54** contains 8 Na atoms, 4 Mg atoms, 4 O atoms, 4 pentadienyl ligands, 4 TMP ligands and 2 chelating molecules of TMEDA. The O atoms and the pentadienyl ligands are in a 1:1 ratio and are thought to have originated from the cleavage and deprotonation of the THP substrate. In the centre of complex **54** an 8-atom distorted cube is observed consisting of alternating Mg and O atoms. A total number of 12 deprotonations has taken place as a consequence of three from each pentadienyl fragment (i.e., $C_5H_{10}O$ to C_5H_7). Moreover since there are 4 remaining TMP ligands and only 4 Mg atoms in the structure, equating to 8 deprotonations, the reaction that produces **54** must involve a combination of magnesiation and sodiation. The complex adopts a 1-D polymeric arrangement chain through Na-η^3-pentadienyl linkages.

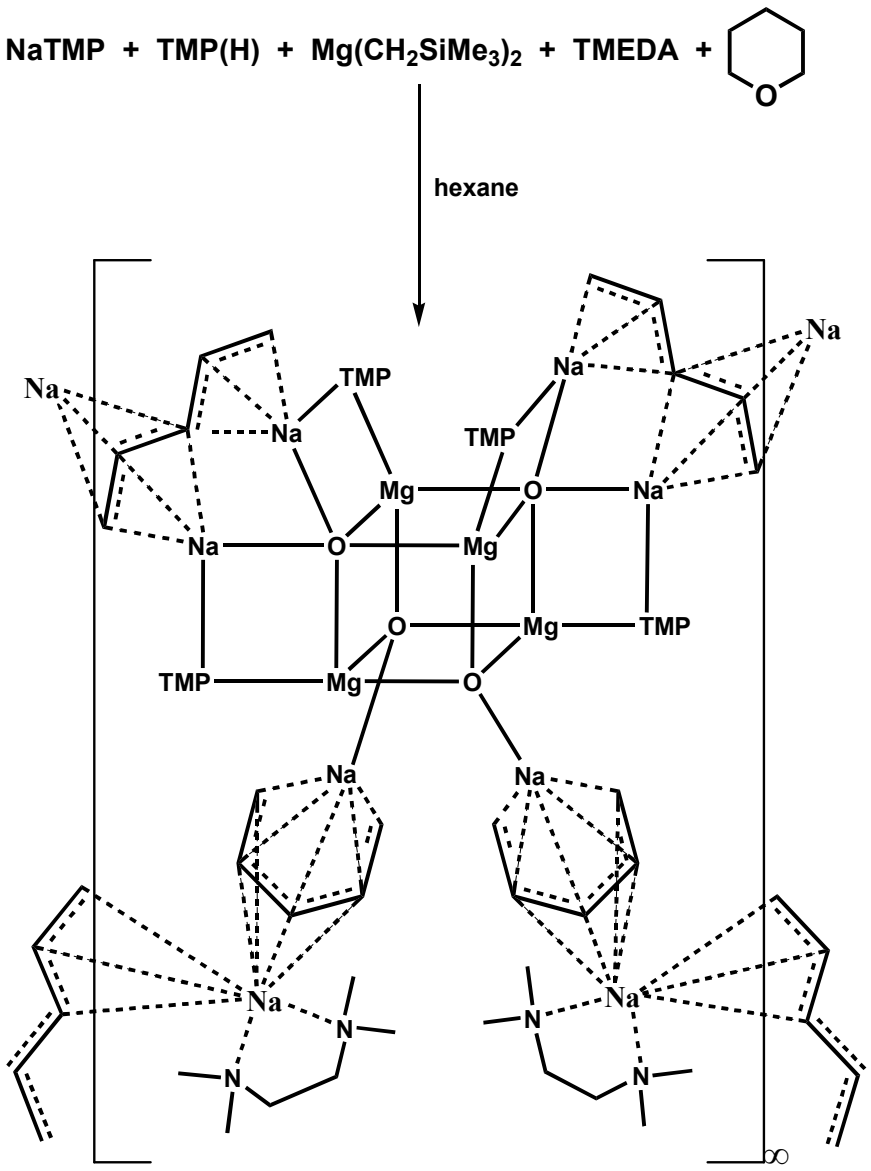

Scheme 59: Reaction of the magnesiate base **28** with THP affording **54**.

The molecular structure of **54** is a dimer with a rotation axis through the Mg_4O_4 central cube. The asymmetric unit of **54** (Figure 91) contains two different conformations of the pentadienyl fragment. Its main feature is a central planar 4-atom (MgOMgO) ring (sum of endocyclic bond angles, 359.75º). Each Mg atom adopts a distorted tetrahedral NO_3 coordination consisting of a TMP ligand [Mg(1)-N(1), 2.076(4) Å; Mg(2)-N(2), 2.083(4) Å] and three O atoms [Mg(1)-O(1), 2.044(3) Å; Mg(1)-O(2), 1.987(3) Å; Mg(1)- O(2A), 1.992(3) Å; Mg(2)-O(1), 2.030(3) Å; Mg(2)-O(2), 1.995(3) Å; Mg(2)-O(1A), 1.997(3) Å]. Each O atom of the ring displays a different bonding environment; O(1) forms two short bonds to two Na [O(1)-Na(1), 2.257(3) Å; O(1)-Na(2), 2.314(3) Å] and three Mg

atoms making it overall penta-coordinated, while O(2) adopts a tetra-coordinated environment forming three Mg-O bonds and one short Na-O bond [O(2)-Na(3), 2.161(3) Å]. A further two 4-atom, 4-element NaNMgO rings are formed at either side of the main Mg_2O_2 ring through the interaction of each TMP ligand with Na(1) and Na(2) [Na(1)-N(1), 2.431(4) Å; Na(2)-N(2), 2.442(4) Å]. There are three distinct types of Na cation present in **54**. Na(1) and Na(2) cap the electron rich 'W-shaped' pentadienyl ligand in two separate Na-(η^3-C pentadienyl) interactions [average Na-C(pentadienyl) bond length, 2.7235 Å] with the shortest Na-C bond lengths belonging to Na(2)-C(2) [2.620(6) Å] and Na(1)-C(4) [2.634(6) Å]. In contrast Na(3) and Na(4) cap the bottom and top of a 'U-shaped' pentadienyl ligand, respectively, in two separate Na-(η^4-pentadienyl) interactions with a similar average Na-C(pentadienyl) bond length of 2.764 Å for Na(3) and 2.839 Å for Na(4). The C-C bond distances of the pentadienyl ligands have an average distance of 1.358 Å for the 'W-shaped' and 1.377 Å for the 'U-shaped' forms consistent with an allyl based ligand system. The coordination sphere around Na(3) is completed by a short Na-O bond [2.161(3) Å] making it overall six-coordinate. A chelating molecule of TMEDA and three further η^3 Na-C contacts to a second 'W-shaped' pentadienyl anion [Na(4)-C(3B), 2.838(5) Å; Na(4)-C4B), 2.857(6) Å; Na(4)-C(5B), 2.942(7) Å] complete the coordination sphere around Na(4), with the latter allowing **54** to adopt a polymeric chain (Figure 92).

We were able to characterise complex **54** by ^{1}H NMR spectroscopy in d^8-THF solution (Figure 93). The three downfield multiplets, at 6.33 (two overlapping resonances) and 3.53 ppm and the broad multiplet at 3.47 ppm can be assigned to the two different pentadienyl ligand systems present in **54**. The two singlets at 2.31 and 2.15 ppm can be assigned to the CH_2 and CH_3 groups of the TMEDA respectively while the three signals at 1.69, 1.29 and 1.06 ppm can be assigned to the γ-CH_2, β-CH_2 and CH_3 units of the TMP ligand respectively. Resonances corresponding to the pentadienyl ligands compare well to literature values for several alkali-metal bound pentadienyl complexes, as for example 3.45, 6.23 and 3.55 ppm for 'U-shaped' K(C_5H_7) in d^8-THF solution[282] and 2.79, 6.13 and 4.35 ppm for 'W-shaped' K(C_5H_7) in liquid ammonia.[283-286] Unfortunately due to the problems in the re-synthesis of **54** no ^{13}C NMR spectrum could be recorded.

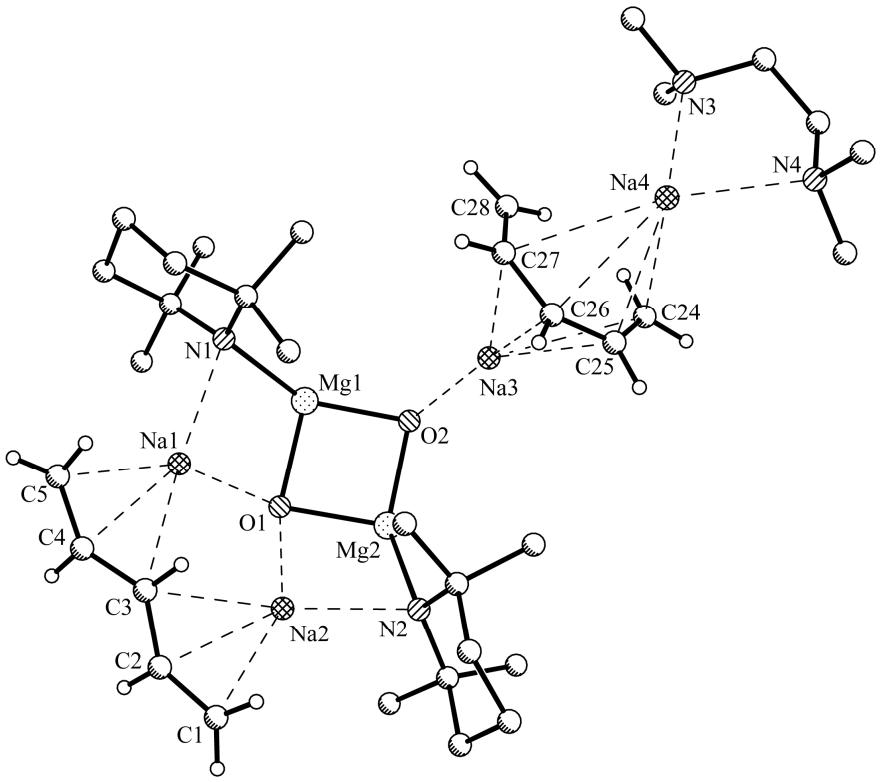

Figure 91: Asymmetric unit of **54** with selective atom labelling. Hydrogen atoms except for pentadienyl ones are omitted for clarity. Selected bond lengths [Å] and bond angles [°]: Mg(1)-O(1), 2.044(3); Mg(1)-O(2), 1.987(3); Mg(1)-N(1), 2.076(4); Mg(2)-O(1), 2.030(3), Mg(2)-O(2), 1.995(3); Mg(2)-N(2), 2.082(4); Na(1)-O(1), 2.257(3); Na(1)-N(1), 2.431(4); Na(1)-C(3), 2.949(6); Na(1)-C(4), 2.634(6); Na(1)-C(5), 2.654(6); Na(2)-O(1), 2.314(3); Na(2)-N(2), 2.442(4); Na(2)-C(1), 2.640(6); Na(2)-C(2), 2.620(6); Na(2)-C(3), 2.847(6); Na(3)-O(2), 2.161(3); Na(3)-C(24), 2.926(7); Na(3)-C(25), 2.751(7); Na(3)-C(26), 2.664(6); Na(3)-C(27), 2.716(6); Na(3)-C(28), 2.861(7), Na(4)-N(3), 2.506(6); Na(4)-N(4), 2.522(5); Na(4)-C(3B), 2.838(5); Na(4)-C(4B), 2.857(6); Na(4)-C(5B), 2.942(7); Na(4)-C(24), 2.906(6); Na(4)-C(25), 2.760(6), Na(4)-C(26), 2.780(6); Na(4)-C(27), 2.760(7); C(1)-C(2), 1.326(8); C(2)-C(3), 1.397(8); C(3)-C(4), 1.381(8); C(4)-C(5), 1.328(8); C(24)-C(25), 1.376(9); C(25)-C(26), 1.372(9); C(26)-C(27), 1.397(10); C(27)-C(28), 1.366(9); O(1)-Mg(1)-O(2), 91.690(13); O(1)-Mg(1)-O(2A), 93.84(12); O(1)-Mg(1)-N(1), 106.34(15); O(2)-Mg(1)-O(2A), 92.44(12); O(2)-Mg(1)-N(1), 139.24(15); O(2A)-Mg(1)-N(1), 121.54(15); O(1)-Mg(2)-O(1A), 93.16(12); O(1)-Mg(2)-O(2), 91.90(12); O(1A)-Mg(2)-O(2), 95.22(12); O(1)-Mg(2)-N(2); 110.43(15); O(1A)-Mg(2)-N(2), 123.93(13); O(2)-Mg(2)-N(2), 131.95(14); N(3)-Na(4)-N(4), 73.65(19); O(1)-Na(1)-O(1), 89.33(12); N(2)-Na(2)-O(1), 90.43(12).

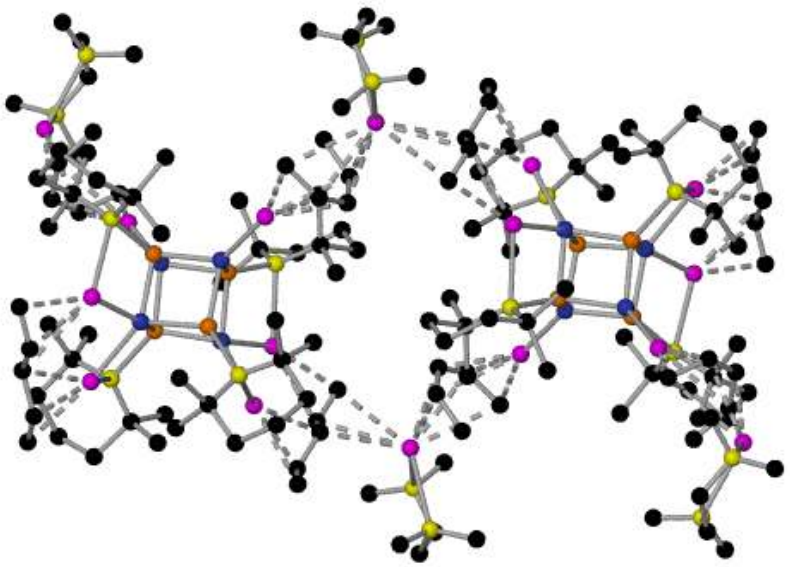

Figure 92: Extended polymeric framework of complex **54**.

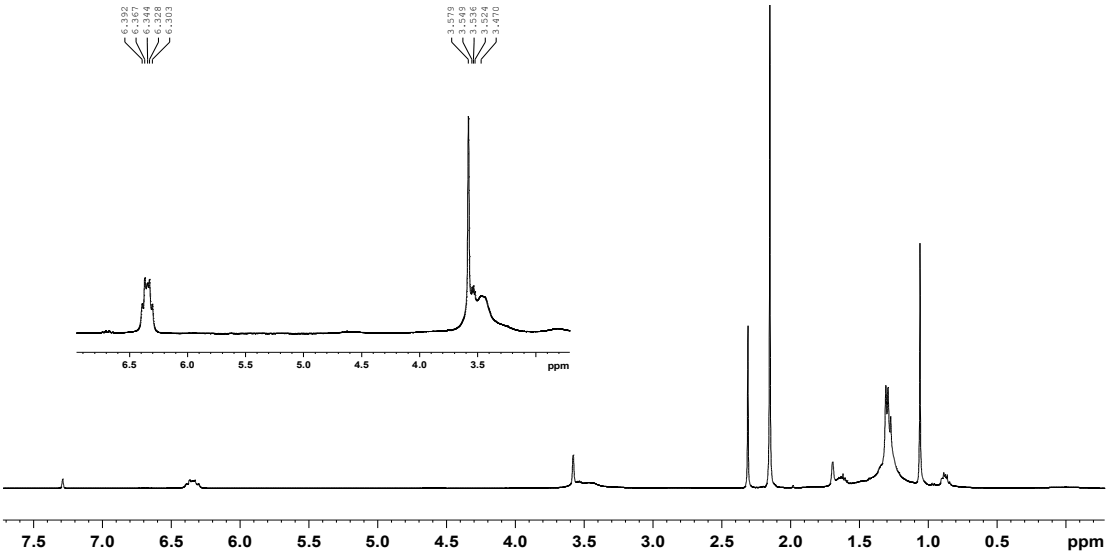

Figure 93: ^{1}H NMR spectrum of complex **54** in d^{8}-THF solution. Inset shows downfield region.

In line with the previously discussed synergic ether cleavage of THF here the same magnesiate base **28** executes a similar synergic cleavage reaction of THP. The oxygen atom from the THP is cleaved and captured by the Mg atoms to form a central Mg_4O_4 cube in complex **54**. The remaining C_5H_{10} backbone of the THP is then deprotonated three times to furnish a C_5H_7 pentadienyl fragment that is synergically trapped in the complex by the Na and O atoms in both a 'W- and U-shaped' conformation. In contrast

to the THF reaction, where two separate oxide- and diene-based crystal structures were obtained, here, remarkably, both components of THP are trapped within the same molecular structure.

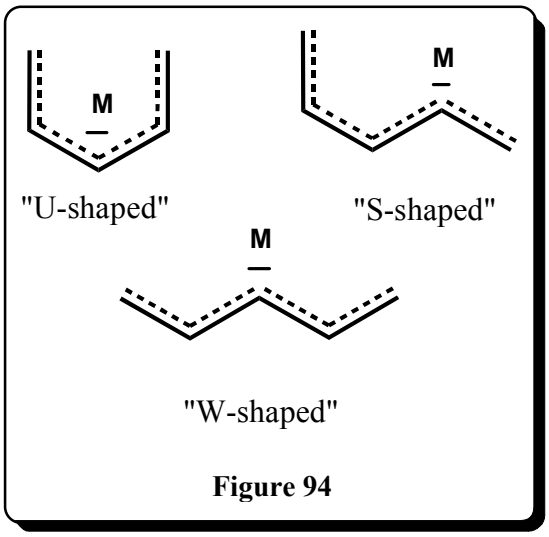

Figure 94

Metal pentadienyl chemistry has been studied for many years with cyclopentadienyl C_5H_5 being one of the most common and important stabilising ligands in inorganic and organometallic chemistry.[287] In comparison, the metal chemistry of the open five-membered pentadienyl ligand has not been as extensively studied. When complexed to a transition metal, the pentadienyl anion has been reported to adopt several conformations including 'U-', 'S-' and 'W-shapes' with the zigzag 'W-shape' being the most thermodynamically stable (Figure 94).[282, 287] On searching the CCDB there are a total of 22 hits for complexes that contain a pentadienyl ligand with all of them containing a transition metal partner. The most common structurally reported conformation of the pentadienyl anion in these transition metal complexes is the horseshoe 'U-shape'. One rare example exists of a mixed 'U- and W-shaped' pentadienyl iron complex [(η^5-pentadienyl)(η^3-pentadienyl)Fe(PEt_3)][288] synthesised from the reaction of K(C_5H_7) and $FeCl_2(PEt_3)_2$ and a similarly rare di-nickel complex [bis(μ_2-η^3,η^3-pentadienyl)Ni_2][289] exists with two 'W-conformation' C_5H_7 anions. However to the best of our knowledge **54** represents the first structurally characterised mixed-metal complex containing a pentadienyl ligand as well as the first non-transition metal containing example. There are no reported structural examples of magnesiated pentadienyl complexes reported in the literature nor is there any precedent for the formation of a pentadienyl fragment from an ether cleavage reaction of THP or any other ether.

6.8. Conclusions

The main aim of this chapter was to investigate the reactivity of both the manganese **16** and magnesium bases **28** with the cyclic ether THF and its sulphur analogue tetrahydrothiophene. In the case of the THF substrate a new type of cleavage reaction was observed. The C_4 backbone of the THF is cleaved at both of its C-O junctions and fourfold deprotonated to furnish a trapped 1, 4-dimetallated butadiene fragment as one isolable crystalline product **42** and **43**, while the THF O atom is also synergically captured separately in the inverse crown complexes **44** and **45**. Through experimental and NMR studies it has been proved that both the butadiene ligand and the oxide atom originate from the initial intact THF substrate. In the case of the sulphur analogue THT, a slightly different reaction outcome was observed with at first, an initial α-magnesiated THT complex being isolated. However, leaving the reaction to stir at room temperature for three weeks allowed the same synergic cleavage of the C_4 THT backbone to occur with a di-magnesiated butadiene complex finally being isolated. A full mechanism for these complicated reactions has not yet been unravelled, through the observation of the initial α–magnesiated THT complex, suggests α–metallation is an early step.

Continuing this new synergic cleave and capture chemistry to the larger 6-membered cyclic ether THP, disclosed a comparable cleavage reaction. Similar to the THF reaction the aliphatic C_5 backbone of the THP substrate was cleaved and deprotonated to give a captured larger pentadienyl fragment. However, unlike the THF reaction in which the O atom is trapped in a separate complex, here, the O atom belonging to the THP is captured in the same crystalline complex as the pentadienyl fragment in the form of a central Mg_2O_2 cubane, with the overall complex **54** forming a polymeric chain, the structure of which is unprecedented.

Extending the chemistry to the unsaturated analogues furan and thiophene allowed the isolation of two very different structurally composed complexes. Reaction of magnesiate **28** with furan allowed the isolation of an unexpected, highly complicated 18 metal atom cluster **50**, containing both mono- and di-magnesated furyl ligands which represents the largest mixed-metal complex synthesised so far through AMM*Mg*. In contrast **28** reacted with thiophene to give a simpler monomeric mixed-metal complex

51 which contains three α-magnesiated thiophene ligands which have originated through a combination of magnesiation and sodation.

We have also discussed enantiomeric deprotonations in this chapter using the chiral ligand (-)-sparteine in place of TMEDA to enable the synthesis of the new chiral magnesiate base **48**. Test reactions of **48** with THT allowed the isolation of the α-magnesiated THT complex **49**, which contained both enantiomeric *R* and *S* forms in its crystal composition, showing unfortunately poor ee. However, further work within our group is currently investigating this concept further in the hope of designing a chiral base capable of selective enantiomeric deprotonations.

Chapter 7. Magnetic Studies

As aforementioned Mn(II) has a high spin d^5 electronic configuration making it paramagnetic. This paramagnetism allows the magnetic properties of several of the compounds synthesised to be explored by variable temperature magnetisation experiments. Appropriate collaboration with another group was sought due to our lack of appropriate equipment needed to carry out such magnetic analysis. Thus we established a formal collaboration with Professor Rentschler's group in Johannes-Gutenberg University in Mainz Germany, to investigate the magnetic properties of our relevant Mn(II) complexes.

Due to this being a new specialisation within the group, at present our understanding of magnetism is still developing and we rely heavily on the expertise of Professor Rentschler and her group. However the basic principles underpinning magnetism will be discussed next in relation to our compounds.

7.1. Magnetism

The term magnetism is used to describe how materials respond on the microscopic level to an applied magnetic field. In most atoms, electrons occur in pairs and spin in opposite directions. Therefore when electrons pair together, their opposite spins cause their magnetic fields to cancel each other out so no net magnetic field is created. Alternatively, materials which contain unpaired electrons respond to an external magnetic field resulting in them having a net measurable magnetic field. Most material in this category can be classified as either paramagnetic or ferromagnetic.

7.1.1. Diamagnetic Compounds

Diamagnetic metal compounds have a very weak and negative susceptibility to magnetic fields making them slightly repelled by a magnetic field. As a consequence the material does not retain magnetic properties when the external magnetic field is removed. Diamagnetic materials in which all their electrons are in a paired state result in no permanent net magnetic moment per atom. It is the realignment of the electron

orbitals under the influence of an external magnetic field that allows the diamagnetic properties to arise. Most elements in the periodic table exhibit diamagnetic magnetism.

7.1.2. Paramagnetic Compounds

On the other hand, paramagnetic metal compounds contain unpaired electrons and have a small and positive susceptibility to a magnetic field. When an external magnetic field is applied, these magnetic moments tend to align themselves in the same direction as the applied field, thus reinforcing it. Although these metals are attracted by the magnetic field, the attraction is not strong enough for the material to retain the magnetic properties when the external field is removed.

7.1.3. Ferromagnetic Compounds

A ferromagnet, similar to a paramagnetic substance, contains unpaired electrons and has a large and positive susceptibility to an external magnetic field. They exhibit a strong attraction to the magnetic field and in some cases are able to retain their magnetic properties even after the external field has been removed. Their strong magnetic properties arise due to the presence of the magnetic moments aligning parallel to each other as well as aligning parallel to the applied field which collectively makes the magnetic force strong.

When more than one metal is present in a compound, interesting magnetic properties can occur if the two metal centres are close enough to interact with each other. It should also be noted that if the complexes have adjoining ligands that link the two metals together then this ligand can sometimes allow the two metal centres to communicate with each other magnetically. This type of magnetism is known as superexchange (see below).

7.1.4. Exchange Coupling

The exchange mechanism is dependent on the direct overlap of the relevant orbitals at the two magnetic sites, which can lead to antiferromagnetic or ferromagnetic ordering

according to the circumstances. However, this simple mechanism cannot always account for very substantial coupling that is known to exist in many substances.

7.1.5. Superexchange

Superexchange is the dominant source of dipolar coupling in transition metal complexes. This indirect mechanism is dependent on the simultaneous covalent bonding of the metal ions with their ligand bridges. It commonly leads to antiferromagnetic ordering (see below).

7.1.6. Antiferromagnetic coupling through superexchange

It is best to consider a linear metal ligand array such as $M^{n+}–O^{2-}–M^{n+}$ and assume that the indirectly coupled metal ions both possess just one electron. If we consider the system in Figure 95, the overlap between each metal *d*-orbital and the filled *p*-orbital of the intervening ligand leads to partial back donation of electron density to the metal site. The exchange is mediated by σ–bonding with *p*-orbitals on the bridging ligand. One-centre exchange effects dictate through covalency, an antiferromagnetic coupling between the spins of the bridged cations. The strength of superexchange coupling via the bridging ligand also proves highly dependent on the M-L-M bond angle.[290] Antiferromagnetic superexchange is weakened when the bond angle is reduced toward 90°. Concomitantly, the opportunity for a significant ferromagnetic interaction arises.

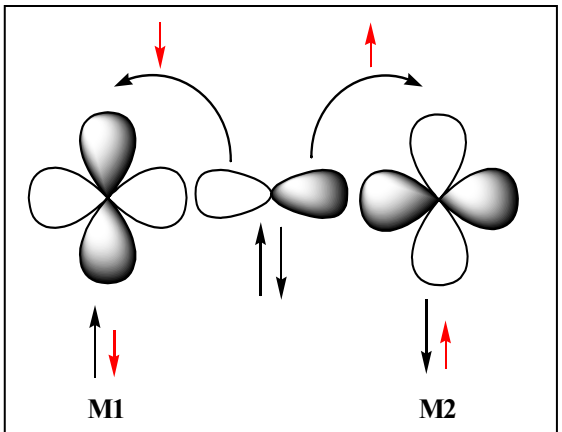

Figure 95: Depiction of antiferromagnetic coupling.

7.1.7. Ferromagnetic coupling through superexchange

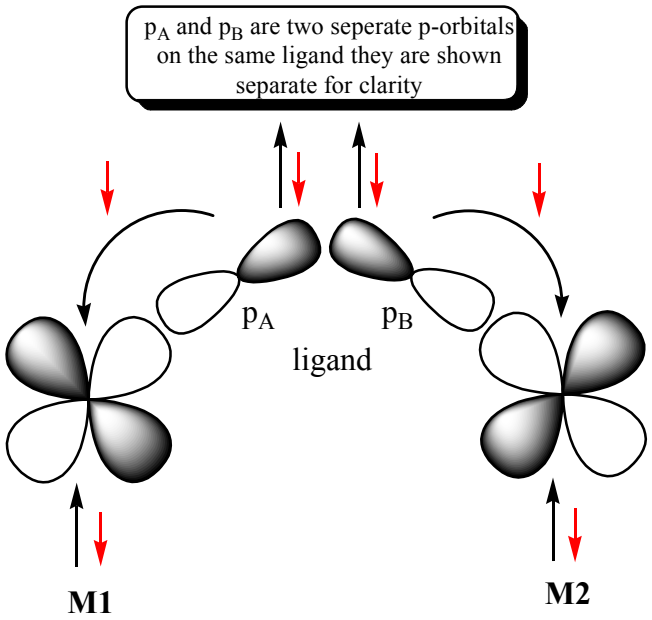

Figure 96: Depiction of ferromagnetic coupling.

Certain circumstances exist where superexchange leads to ferromagnetic coupling rather than an antiferromagnetic interaction between the metal cations. One such possibility alluded to before when this can occur is when the M-L-M bond angle is 90°. Assuming, again that the cations only carry one *d* electron for simplicity Figure 96 depicts what can take place. The metal *d*-orbitals now overlap with different *p*-orbitals on the ligand due to the 90° disposition of the ligand. Here the one centre exchange effects thus come into operation to promote ferromagnetic coupling.[290]

Turning to our own complexes, the variable temperature magnetic properties of the starting reagent bis(alkyl)manganese $Mn(CH_2SiMe_3)_2$ **1**, the trimeric homoleptic amido-manganese complex **11** and heteroleptic benzophenone addition complex **13** were measured along with the doubly bridged hydride inverse crown **31**, the *n*butoxide inverse crown **36**, the trinuclear ferrocenophane **34**, and the manganated butadiene **42**. Each of these compounds will be discussed in turn following general considerations.

7.2. General Procedure and Considerations

The magnetic susceptibility data of all seven compounds were collected in a temperature range of 2 – 300 K under an applied field of 1 Tesla on powdered microcrystalline samples using a SQUID magnetometer (MPMS-7, Quantum Design). Experimental susceptibility data were corrected for the underlying diamagnetism using Pascal's constants. The temperature dependent magnetic contribution of the glass holder

was experimentally determined and subtracted from the measured susceptibility data. The resulting molar susceptibility data was plotted in χ_M *vs.* T and χ_MT *vs*. T. The program julx31 was used for spin Hamiltonian simulations of the data.[291][292] For compounds **11** and **13** the magnetic data were simulated satisfactorily by using the Hamiltonian $\hat{H} = -2\, \boldsymbol{J}_{ij} \Sigma\, \hat{\mathbf{S}}_i \bullet \hat{\mathbf{S}}_j$, with $\hat{S}_1 = \hat{S}_2 = S_3 = 5/2$.

7.3. Magnetic Measurements of $[Mn(CH_2SiMe_3)_2]_\infty$ 1

Complex **1** is paramagnetic showing typical dependence of magnetic susceptibility as a function of temperature (Figure 97). At room temperature the $\chi_M T$ product reaches a value of 0.62 cm^3 K mol^{-1}, considerably below the expected value for an uncoupled manganese(II) species in a high spin state. A sharp decrease of the $\chi_M T$ product with decreasing temperature indicates a significant interaction between the manganese ions along the chain. Simulating the high-temperature magnetic data down to 50 K, an exchange coupling constant of J = -45 cm^{-1} is obtained. This value is in accordance with an exchange coupling constant of less than -70 cm^{-1} estimated by Wilkinson *et al*. on frozen solutions by EPR studies and J = -42.5 cm^{-1} as measured for the dinuclear species $[(Me_3SiCH_2)(\mu\text{-}CH_2SiMe_3)Mn(THF)]_2$[105, 123] The Fischer equation was used to calculate the exchange interaction within a classical Heisenberg chain model and obtained J = -51.4 cm^{-1} as the best fit to the overall experimental data as shown in Figure 97 (solid line on the graph).

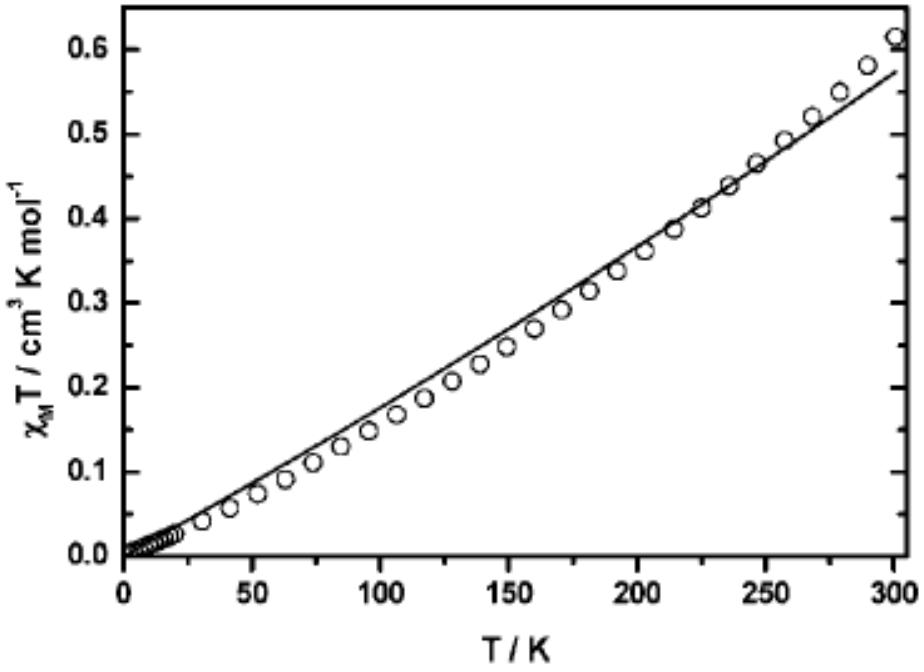

Figure 97: $\chi_M T$ vs T (○) for homometallic Mn(II)compound **1**.

We therefore propose that an effective through-space interaction between the manganese(II) ions due to the short Mn-Mn distance of about 2.89 Å has to be taken into consideration operating at low temperatures together with the superexchange mechanism via the $Me_3SiCH_2^-$ bridging ligands to explain the antiferromagnetic interaction that is observed along the chain.

7.4. Magnetic Measurements of [(DippNH)$_6$Mn$_3$] 11

The behaviour of the magnetic susceptibility of tri-nuclear complex **11** as a function of temperature shows the presence of an intramolecular antiferromagnetic exchange (Figure 98). The χ_MT product at room temperature (300 K) reaches a maximum value of 6.54 cm^3 K mol^{-1} which is markedly lower than the expected spin only value of 13.13 cm^3 K mol^{-1} for $S_1 = S_2 = S_3 = {}^5/_2$ with only a small decrease of the χ_MT product upon lowering the temperature. At 100 K the χ_MT value reaches a plateau and remains nearly constant down to 10 K at which point a rapid decrease of the χ_MT product is observed where at 2 K a minimum value of 3.42 cm^3 K mol^{-1} is finally reached. The noticeable small χ_MT value at room temperature indicates a strong dominating antiferromagnetic coupling between the three manganese(II) centres.

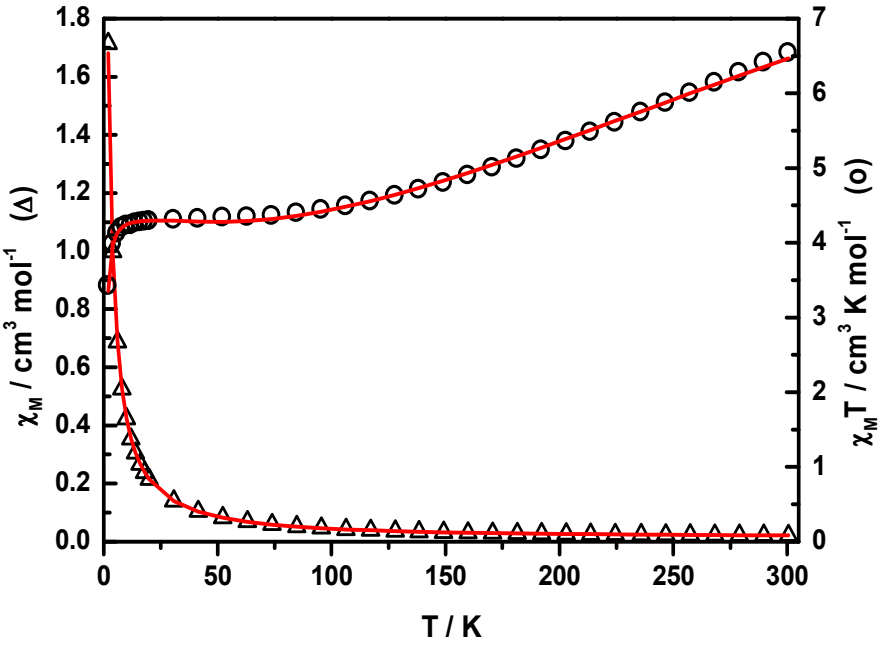

Figure 98: Molar susceptibility (○) and $\chi_M T$ (Δ) versus T for complex **11**.

A satisfactory simulation of the magnetic data can be obtained by using two different coupling constants. The dominating antiferromagnetic coupling with J = -20.36 cm^{-1} accounts for the nearest neighbours interactions in the linear Mn···Mn···Mn arrangement of the ions and is reasonable for the double μ_3-nitrogen bridging amido-ligand. An additional small coupling with a value of J = -0.97 cm^{-1} considers the next nearest neighbour interaction between the external Mn(II) ions. The g-value is 1.99 for all three manganese ions and is very close to the g-value of a free electron. To the best of our knowledge there are no pertinent examples of tri-manganese N-bridged complexes to compare the magnetic data of complex **11**. However, there is a dinuclear N(pyrrolide) complex [{1,1-(μ-C_4H_3N)(C_4H_3N)C_6H_{10}]Mn$(THF)_2\}_2$·2(THF)[123] which is reported as exhibiting intramolecular antiferromagnetic exchange through N atom bridges, similar to **11**, with a moderately higher coupling constant of J = -23.2 cm^{-1}.

7.5. Magnetic Measurements of [$(Me_3SiCH_2)_2Mn_3\{\mu$-$OC(Me_3SiCH_2)Ph_2\}_4$] 13

The magnetic susceptibility data for the tri-nuclear complex **13** found the $\chi_M T$ product to be 9.89 cm^3 K mol^{-1} at 300 K which is considerably below the expected spin only

value of 13.13 cm^3 K mol^{-1} predicted for three independent manganese(II) centres with $S_1 = {}^5/_2$ each. This indicates an already significant antiferromagnetic interaction between the Mn(II) metal ions. With reducing the temperature the $\chi_M T$ product decreases further, reaching a plateau at 20 K with a value of 4.36 cm^3 K mol^{-1} (Figure 99). Decreasing the temperature more a further drop of the $\chi_M T$ product is observed, which can be explained simply by saturation effects of the non-zero magnetic moment.

For simulating the magnetic data of compound **13** a coupling scheme with two interactions and only one coupling constant was used (Mn1 ·· J_1 ·· Mn2 ·· J_1 ·· Mn3). The best simulation is obtained with an antiferromagnetic coupling of J = -7.35 cm^{-1} and a g-value of 2.00. This coupling constant is in the expected order of magnitude and reasonable for manganese (II) ions bridged by two μ_3-oxygens.

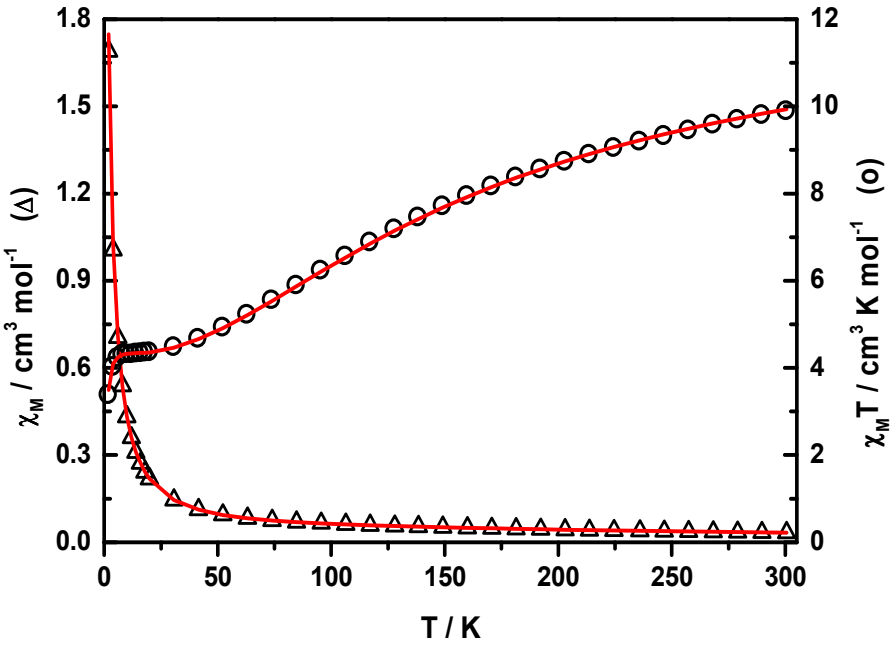

Figure 99: Molar susceptibility (○) and $\chi_M T$ (Δ) versus T for complex **13**.

As far as we can ascertain the only other previous magnetic investigations reported for an oxygen bridged tri-manganese(II) compound is for the alkoxy bridged complex $[Mn_3(OCH\text{-}tBu_2)_6]$.[133] Similar to complex **13**, the alkoxide is reported as being antiferromagnetic with a magnetic susceptibility of 5.2 μ_B (determined via the Evans method).[293, 294] Unfortunately no coupling constants are reported in this earlier study.

7.6. Magnetic Measurements of $[Na_2Mn_2(\mu\text{-}H)_2\{N(iPr)_2\}_4]\cdot(toluene)_2$ 31

Variable temperature magnetic measurements on paramagnetic mixed amido-hydrido complex **31** found a $\chi_M T$ value of 3.45 cm^3 K mol^{-1} at room temperature (Figure 100), which is remarkably lower than the expected theoretical value of 8.75 cm^3 K mol^{-1} for two uncoupled manganese(II) ions with a g value of 2.00. Upon lowering the temperature a considerable decrease in $\chi_M T$ is observed, indicating a strong antiferromagnetic coupling between the two manganese(II) ions. Using the spin Hamiltonian $\hat{H} = -2\, \boldsymbol{J}\, \hat{\mathbf{S}}_1 \bullet \hat{\mathbf{S}}_2$ the susceptibility data were simulated satisfactorily with $\hat{\mathbf{S}}_1 = \hat{\mathbf{S}}_2 = 5/2$, $\boldsymbol{J} = -28.37$ cm^{-1} and $g_1 = g_2 = 2.00$. An additional paramagnetic impurity of 9.1% corresponding to an $S = 5/2$ species had to be taken into account.

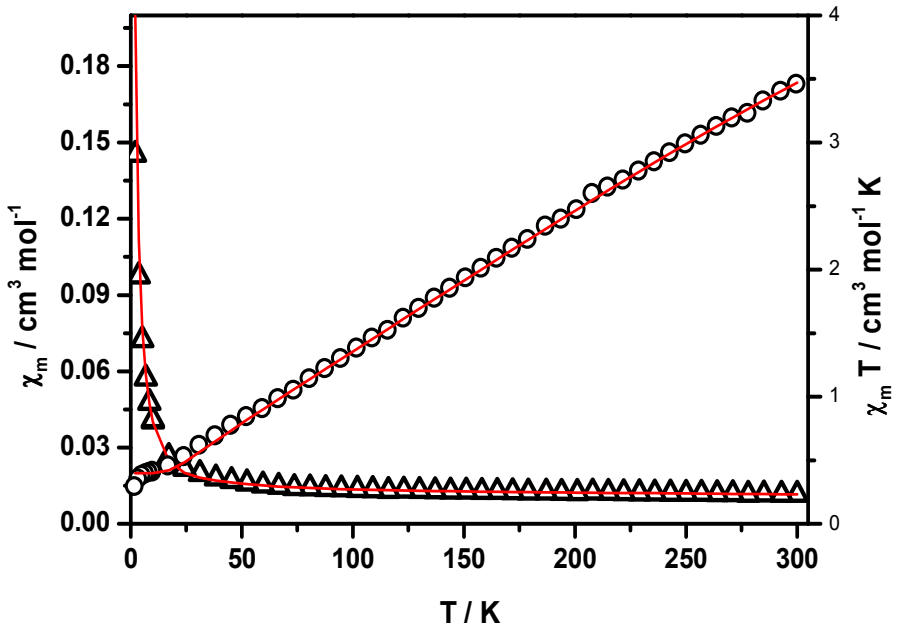

Figure 100: Molar susceptibility (○) and $\chi_M T$ (Δ) versus T for complex **31**.

In complex **31** the magnetic interactions can operate *via* the two hydride bridges by a superexchange mechanism as well as by direct overlap of the manganese orbitals. Both interactions are expected to be antiferromagnetic in nature, as observed in the actual experiment; however, there is no possibility to determine the relative importance of each individual pathway. However, recently DFT studies on complex **31** by Alberola and Polo have found that the exchange coupling is of a direct type between the two Mn(II) centres without the participation of the hydride bridge.[295]

To the best of our knowledge there is only one reported compound bridged by hydride ions for which magnetic data has been previously collected. In the chromium complex $[\{(Ph_2PCH_2\text{-}SiMe_2)_2N\}Cr]_2(\mu\text{-}H)_2$[296] the chromium ions are also bridged by two hydride ions and overall the complex shows an extremely strong antiferromagnetic coupling of $J = -139$ cm^{-1}. In comparison to that in **31**, the two chromium(II) ions have a short metal–metal distance of 2.642(1) Å and also shorter bond lengths to the hydrides [1.78(3) and 1.76(3) Å]. Because of the better overlap of the metal-metal orbitals and of the metal-hydride orbitals this five-fold increase in the coupling constant is not remarkable. In this case the direct metal-metal overlap is expected to make the biggest contribution to the increase in the magnetic interaction.

7.7. Magnetic Measurements of $[\{Fe(C_5H_4)_2\}_3\{Mn_3Na_2(N\textit{i}Pr_2)_2(HN\textit{i}Pr_2)_2\}]$ 34

For trinuclear ferrocenophane **34**, variable-temperature magnetic studies indicated that the room-temperature value of $\chi_M T$ was 4.06 cm^3 K mol^{-1} which lies dramatically below the expected value of 13.13 cm^3 K mol^{-1} for three isolated paramagnetic manganese(II) ions (Figure 101). The expected value can even be larger if the iron(II) ions are not considered to be in the low-spin state having only a diamagnetic contribution. In the temperature range 300–8 K the $\chi_M T$ value is approximately constant with only a small decrease observed. Further cooling leads to a sharp decrease of the $\chi_M T$ product. The otherwise approximately constant $\chi_M T$ value indicates a very small coupling between the magnetic centres, and the sharp drop is ascribed to intermolecular antiferromagnetic coupling and/or saturation effects.

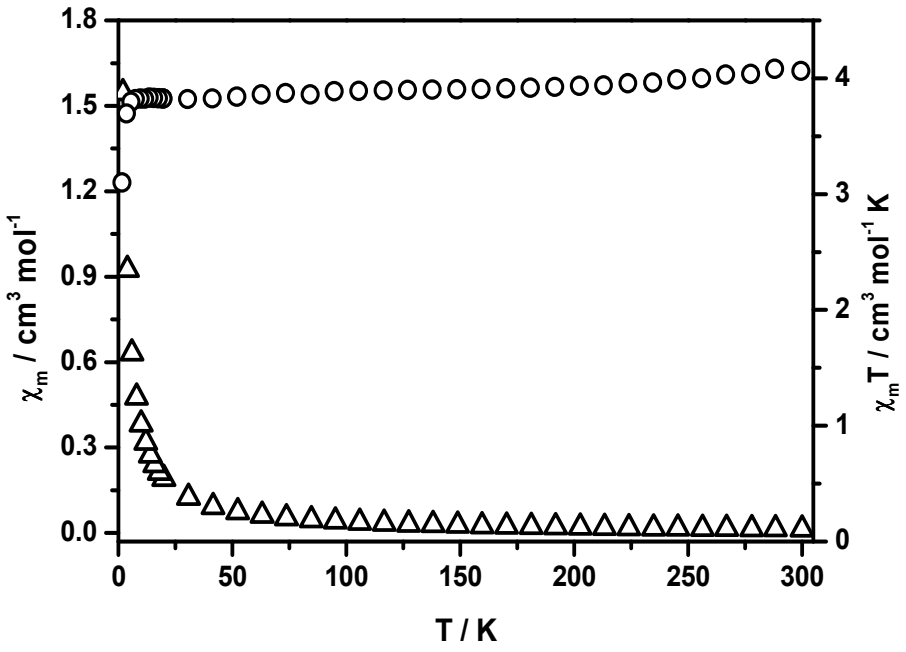

Figure 101: Molar susceptibility (○) and $\chi_M T$ (Δ) versus T for complex **34**.

No satisfactory simulation of **34** can be made with three manganese(II) centres in a high-spin state. The magnetic properties of the aforementioned Mn(II) complex $[(TMEDA)_2Li_2Mn_2\{Fe(C_5H_4)_2\}_3]$ **35**[55] were also recently explored by our group and similar unexplained results were obtained, with χT found to be lower than the expected value for two isolated Mn(II) paramagnetic centres.

7.8. Magnetic Measurements of [{(TMEDA)Na(CH_2SiMe_3)(OBu)(*o*-C_6H_4OMe)Mn_2}$_2$] 36

The χ_MT product at 300 K for butoxide bridged compound **36** is 4.69 cm^3 K mol^{-1} which is significantly below the expected spin only value of 6.00 cm^3 K mol^{-1} for $S_1 = S_2 = {}^5/_2$ and a g-value of 2.00. With reducing temperature the χ_MT product decreases reaching a final value of 0.33 cm^3 K mol^{-1} at 2 K. The shape of the curve and not reaching the spin only value at room temperature indicates an antiferromagnetic coupling between the two manganese(II) centres (Figure 102). The magnetic data can be simulated satisfactorily by using the spin Hamiltonian $\hat{H} = -2\ \boldsymbol{J}_{12}\ \hat{\mathbf{S}}_1 \bullet \hat{\mathbf{S}}_2$ including a temperature independent paramagnetic impurity. The best simulation is obtained with an antiferromagnetic coupling of -9.48 cm^{-1} and a g-value of 2.00. An additional

impurity of 14.3 % with a Spin value of S = 2 based on the molecular weight of the complex was included.

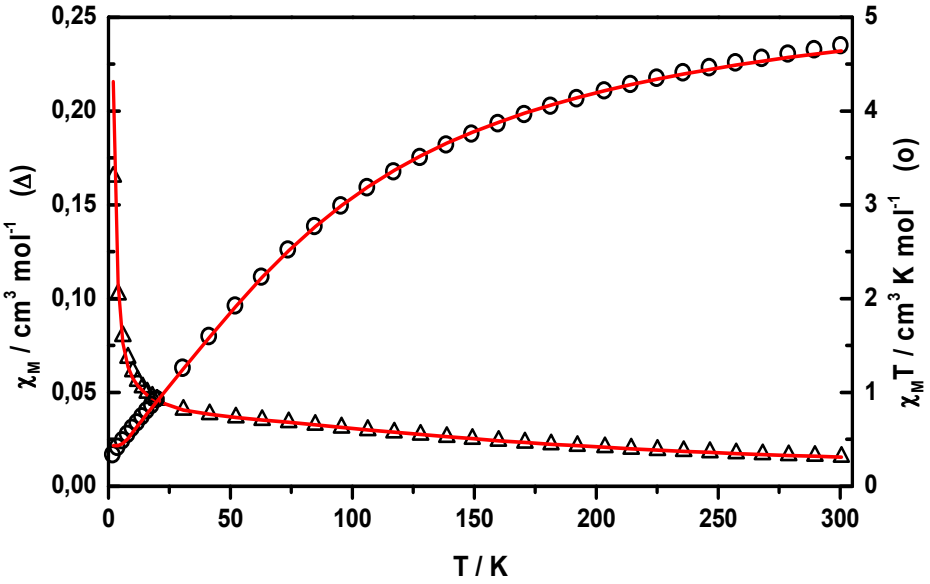

Figure 102: Molar susceptibility (○) and $\chi_M T$ (Δ) versus *T* for complex **36**.

7.9. Magnetic Measurements of [{(TMEDA)Na(TMP)}$_2${1, 4-[Mn(TMP)]$_2$-C_4H_4}] 42

The variable-temperature magnetic investigation of benzenediide compound **42** found the χ_MT product to be 8.42 cm^3 K mol^{-1} at 300 K (Figure 103) which is close to the calculated spin only value of 8.75 cm^3 K mol^{-1} for $S_1 = S_2 = {}^5/_2$. Upon lowering the temperature to 100 K only a small decrease of the χ_MT produced was observed. Additional cooling leads to a considerable decrease of the χ_MT product reaching the lowest recorded value of 0.34 cm^3 K mol^{-1} at 2 K. These results indicate a small antiferromagnetic coupling between the two Mn(II) centres.

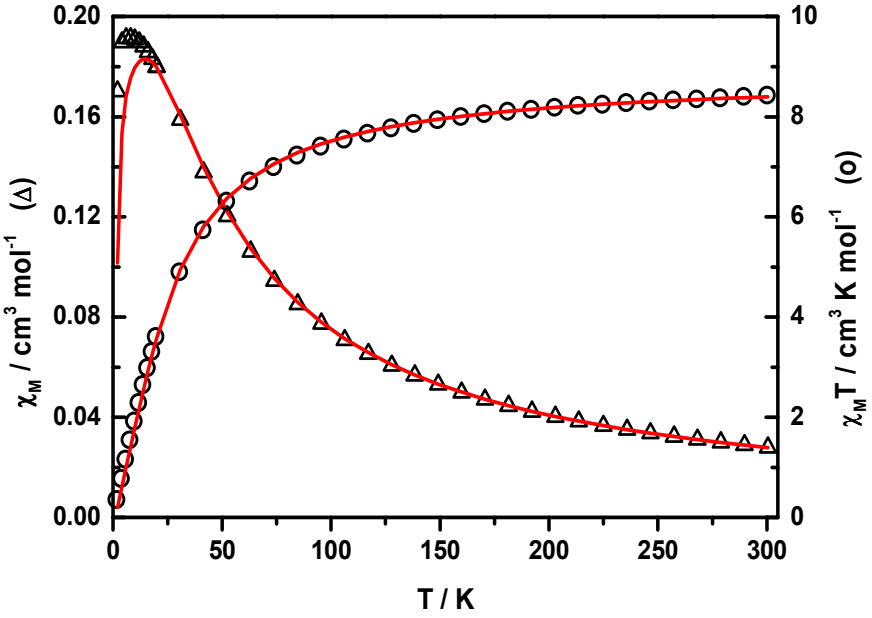

Figure 103: Molar susceptibility (○) and $\chi_M T$ (Δ) versus T for complex **42**.

The magnetic data are satisfactorily simulated using the spin Hamiltonian $\hat{H} = -2\,\boldsymbol{J}\,\hat{\mathbf{S}}_1 \bullet \hat{\mathbf{S}}_2$, with $\hat{S}_1 = \hat{S}_2 = 5/2$. The best simulation is obtained with an antiferromagnetic coupling of $J = -1.787$ cm^{-1} and a g-value of 2.01. The antiferromagnetic coupling *via* the butadiene bridge occurs by a polarisation mechanism. The strength of the coupling observed is high with respect to the number of atoms included in the bridge. To the best of our knowledge there are no reported magnetic data studies for butadiene as a bridging ligand. However, our group has recently reported the magnetic data of two C_4 bridged Mn(II) complexes, namely, the deprotonated benzene and toluene inverse crown compounds $[(TMP)_6Na_4(1,4\text{-}Mn_2C_6H_4)]$[56] **41** and $[(TMP)_6Na_4\{3,5\text{-}Mn_2C_6H_3(Me)\}]$[196] **54** respectively. Like complex **42**, both **41** and **54** are antiferromagnetic with coupling constants of $J = -0.70$ and -0.10 cm^{-1} respectively with the strength of the coupling in both **41** and **54** being weaker than that observed here in **42**.

7.10. Summary of Magnetic Data

All seven compounds **1**, **11**, **13**, **31**, **34**, **36** and **42** displayed antiferromagnetic coupling with varying strengths seemingly dependent on the number of Mn(II) atoms present and the chemical nature of the bridging ligand. The strongest antiferromagnetic coupling

interaction was found for the polymeric bis(alkyl)manganese complex **1** which exhibits a coupling constant of J = -45.0 cm^{-1} and bridging alkyl ligands. In contrast the weakest coupling constant was found for complex **42**, the di-manganated butadiene, which has a coupling constant of J = -1.787cm^{-1} and a C_4 alkyl bridge. Table 5 summarises the magnetic findings of all seven compounds as well as the additional magnetic measurements conducted on the di-manganated benzene and toluene inverse crown complexes **41** and **54**.

Table 5 Magnetic data of all complexes

Compound	Mn-X-Mn Bridge	Coupling J (cm^{-1})	Observed coupling
$[Mn(CH_2SiMe_3)_2]_\infty$ **1**	X = C	- 45.0	antiferromagnetic
$[(DippNH)_6Mn_3]$ **11**	X = N	- 20.36	antiferromagnetic
$[(Me_3SiCH_2)_2Mn_3\{\mu\text{-}OC(Me_3SiCH_2)Ph_2\}_4]$ **13**	X = O	- 7.35	antiferromagnetic
$[Na_2Mn_2(\mu\text{-}H)_2\{N(iPr)_2\}_4]\cdot(toluene)_2$ **31**	X = H	- 28.37	antiferromagnetic
$[\{Fe(C_5H_4)_2\}_3\{Mn_3Na_2(N\textit{i}Pr_2)_2(HN\textit{i}Pr_2)_2\}]$ **34**	X = C	n/a	antiferromagnetic
$[\{(TMEDA)Na(CH_2SiMe_3)(OBu)(\textit{o}\text{-}C_6H_4OMe)Mn_2\}_2]$ **36**	X = O	-9.8	antiferromagnetic
$[[(TMEDA)Na(TMP)\}_2\{1,4\text{-}[Mn(TMP)]_2\text{-}C_4H_4\}]$ **42**	X = C (allyl)	- 1.787	antiferromagnetic
$[(TMP)_6Na_4(1,4\text{-}Mn_2C_6H_4)]$[56] **41**	X = C (aromatic)	-0.70	antiferromagnetic
$[(TMP)_6Na_4\{3, 5\text{-}Mn_2C_6H_3(Me)\}]$[196] **54**	X = C (aromatic)	-0.10	antiferromagnetic

Chapter 8. General Experimental Techniques

8.1. Inert-Atmosphere Schlenk Techniques

Owing to the acute sensitivity of all the organometallic starting materials and products to both moisture and oxygen, all manipulations (including analytical preparations) were undertaken under a dry and inert atmosphere (argon blankets were generally utilised). Most of the synthetic work was carried out using high-vacuum, Schlenk techniques on a vacuum/argon double manifold (Figure 104) and an argon filled glove box.

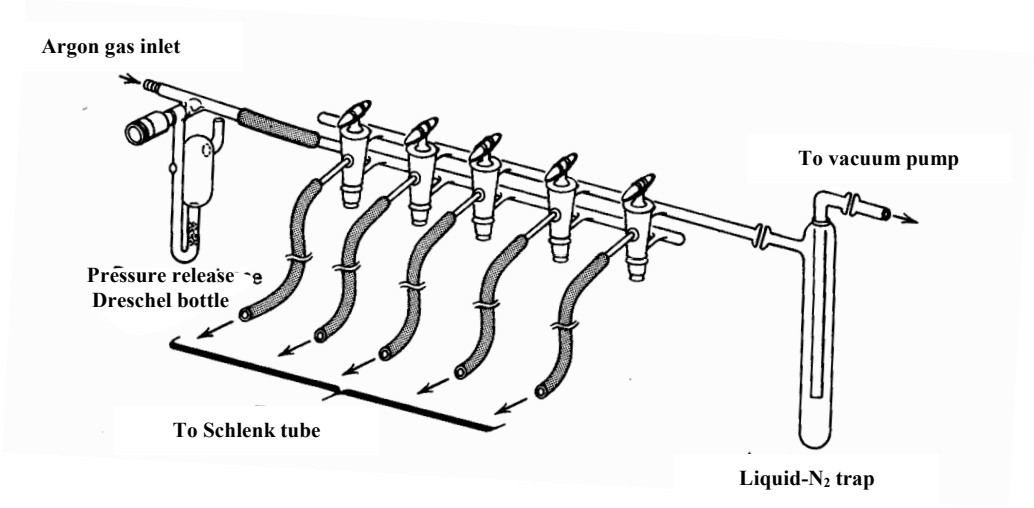

Figure 104: Diagram of a Schlenk vacuum/argon line.

The Schlenk line follows two independent paths: one connected to a vacuum pump; and the other connected to a supply of dry oxygen-free argon. Five independent positions link the Schlenk line to the appropriate apparatus. At each position the glass taps can be switched to open to either vacuum or argon, allowing the influx or removal of gas to the system. Taps and joints within the system are all lubricated with high vacuum grease and gas overpressure is prevented by the addition of and outlet oil Dreschel bottle. A Dewar flask filled with liquid nitrogen placed around the vacuum trap prevents contamination of the vacuum pump by solvents removed from the reaction media. Prior to each experiment air from the Schlenk tube was removed in vacuo and substituted by inert argon gas. This evacuation and inert gas flushing was repeated three times to make absolutely certain that all oxygen had been removed from the apparatus.

8.2. Glove Box Techniques

Manipulations of air sensitive reagents and metal-based products (for example, determination of reaction material weights, product yields, preparation of NMR, IR nujol mull and microanalysis samples) had to be performed in a glove box in order to prevent their decomposition. The glove box model employed was a MBraun MB10 compact composed of steel with two evacuable ports that were fitted with butyl rubber gloves. The integrity of the argon atmosphere in the box was maintained by gas circulation, in which the working gas was constantly circulated between the glove box and the H_2O/O_2 gas purification system. Moisture and oxygen levels in ppm were monitored via the LCD control panel. The box was regenerated as often as necessary (usually once every 2-3 months). To avoid contamination when transferring air sensitive compounds in and out of the box, the port is evacuated for a minimum of 10 minutes to ensure all traces of oxygen and moisture have been removed before filling it with argon. This evacuation-argon fill procedure is repeated twice before the inner door can be safely opened without fear of the introduction of moisture or oxygen.

8.3. Purification of Solvent and Liquid Reagents

As many commercial solvents, liquid amines, and alcohols contain trace amounts of dissolved moisture and oxygen, all were distilled and degassed (where applicable) prior to use in reactions.

Distillation of solvents (hexane, THF, toluene, and ether) was carried out under an inert nitrogen blanket over a sodium metal and benzophenone solution until the solution turned blue. The sodium metal reacts with excess water to form sodium hydroxide with release of hydrogen gas. Excess sodium will react with benzophenone to form the blue ketal radical. The presence of this blue colour indicates the solvent is therefore dry. Amines and alcohols were distilled in the presence of calcium hydride (CaH_2) under a nitrogen/argon blanket. All distillates were stored over flame dried 4Å-molecular sieves to ensure the removal of all moisture.

Degassing of solvents and amines was carried out using freeze-pump-thaw[297] methodology to remove any dissolved oxygen. This involved freezing the solvent/amine in a liquid nitrogen bath prior to thawing to room temperature under vacuum. Finally, all degassed solvents/amines were stored over 4Å-molecular sieves to avoid contamination by moisture.

8.4. Preparation of Glassware

All glassware was cleaned using a commercial cleaner and a basic solution of KOH in propan-2ol, before rinsing it with hot water and acetone. The sintered glass frits of filter sticks were cleaned by washing with nitric acid followed by water and then acetone. All glassware was placed in an oven at approximately 130°C for at least 2 hours, preferably overnight, prior to use. After cooling the glassware, any moisture within it was removed by heating the assembled apparatus with a hairdryer whilst under a high vacuum.

8.5. Reagents Used

The bulk of reagents used employed purchased from the Aldrich Chemical Company including *n*BuLi (1.6M in hexanes) and neat Me_3SiCH_2Cl. The alkoxide NaO*t*Bu and TMEDA were purchased from Lancaster Chemicals and TMP(H) from Acros Organics. Unless otherwise stated, other reagents used during this project were bought from the Aldrich Chemical Company at the highest purity available.

8.6. Standardisation of *n*-butyllithium

Commercial solutions of organometallic compounds such as *n*-butyllithium react rapidly with trace amounts of air and moisture and can lose solvent over time. Standardisation is therefore a necessity to obtain an accurate molarity prior to employing them in reactions. This standardisation can be carried out by titration of the relevant organometallic compound with salicylaldehyde phenylhydrazone in dry THF.[298] The yellow solution formed turns red when the end point is reached. The

molarity of the *n*BuLi solution can then be calculated using the normal procedure for acid-base titrations.

8.7. Instrumentation

8.7.1. Nuclear Magnetic Resonance (NMR) Spectroscopy

All samples for NMR spectroscopy were prepared under an argon atmosphere either in the glove box or on the Schlenk line. Compounds were dissolved in deuterated solvents which had been pre-dried over 4A molecular sieves and the NMR tubes were made air-tight using a combination of caps and Parafilm®. NMR spectra were recorded on either a Bruker DPX 400 MHz or 500 MHz spectrometer machine operating at 400.03 MHz or 500.13 for ^{1}H and 100.62 MHz for ^{13}C.

8.7.2. Infrared Spectroscopy

Infrared spectra of starting materials and selected products were obtained as Nujol mulls on NaCl plates. Mulls were prepared in the glove box using anhydrous Nujol, which was dried over sodium metal under argon, and then transferred to the spectrometer in a desiccator. Spectra were recorded on a Nicolet 360 FTIR spectrometer spanning range 4000-400cm^{-1}.

8.7.3. Melting Point Determinations

The melting points of selected new products synthesised and of starting materials were determined as follows. A small sample of crystalline/powdered material was loaded into a melting point tube in the glove box. This tube was then sealed with Plasticine® before removal from the glove box. The melting point was then determined in the usual manner using a Buchi Melting Point B-545 apparatus.

8.7.4. Microanalysis Measurements

Microanalyses were performed in order to obtain percentage values of the elemental composition of the compounds synthesised. A Perkin-Elmer 2400 elemental analyser was used in determining the carbon, nitrogen and hydrogen elemental percentages of samples. Microanalysis samples were prepared in the glove box and sealed in an air tight box before being removed for the subsequent analysis. However sometimes it was not possible to obtain reliable analysis for certain the compounds synthesised due to their highly air-sensitive nature.

8.7.5. X-Ray Diffraction

Crystals suitable for X-ray diffraction studies were grown in Schlenk tubes under an argon atmosphere, at various temperatures. The majority of the mother liquor was removed and the crystals were either analysed by a Bruker SMART 1K diffractometer (Prof. W. Clegg, University of Newcastle) or an Oxford Diffraction Xcalibur S diffractometer (Dr. A. Kennedy, University of Strathclyde).

8.8. Preparation of Starting Materials

Preparation of the common starting materials *n*BuNa, $Mg(CH_2SiMe_3)_2$ and $Mn(CH_2SiMe_3)_2$ will be detailed in this section. These preparations were carried out numerous times throughout the course of this PhD programme.

8.8.1. Preparation of *n*BuNa

The pyrophoric sodium alkyl *n*BuNa was prepared according to the literature method reported by Schleyer.[299] Thus, NaO*t*Bu (1.92 g, 20 mmol) was suspended in 50mL of dried hexane and the suspension placed in an ultrasonic bath for 10 minutes to give a white uniform dispersion. This suspension was placed in an ice bath while *n*BuLi (12.5 mL, 20 mmol) was added slowly dropwise to it. The resulting thick white suspension was allowed to stir at room temperature overnight. Filtration of the suspension yielded a white solid (BuNa) which was washed with hexane (50mL) before being dried under

high vacuum and transferred for storage in the glove box. It was assumed that this solid was pure *n*BuNa, though it may contain trace amounts of other products (*n*BuLi, NaO*t*Bu, LiO*t*Bu). Typical crude yield = 1.20 g, 75%.

8.8.2. Preparation of $[Mg(CH_2SiMe_3)_2]_\infty$

To a 500mL round bottomed flask equipped with a condenser and a dropping funnel, magnesium fillings (3 g, 12.3 mmol) were added and the system flushed three times before 100 mL of dried ether was introduced. A solution of Me_3SiCH_2Cl (12.5mL, 9mmol) in 50mL of dry ether was added dropwise via the dropping funnel. The reaction was allowed to reflux for 1-2 hrs to which dried dioxane (8 mL, 9.3 mmol) in 50 mL of dried ether was added dropwise to afford a thick grey suspension. Next the reaction stirred for 2-3 days at room temperature before it was filtered through Celite and washed with 2 x 40 mL of ether to give a homogeneous solution. All the solvent was removed under vacuum leaving an off-white solid. The solid was purified via sublimation (180°C) to yield a crystalline white solid that was transferred to the glove box for storage. During one repeat synthesis large enough crystals were obtained during the sublimation for X-ray diffraction to be carried out on them. Typical yields = 7-8 g (40- 45%).

8.8.3. Preparation of $[Mn(CH_2SiMe_3)_2]_\infty$ Compound 1

$Mg(CH_2SiMe_3)_2$ (3 g, 15 mmol) and $MnCl_2$ (1.91 g, 15 mmol) were suspended in 60 mL of dry ether and allowed to stir for 2-3 days at room temperature. All the solvent was removed under vacuum to give a dull orange solid. Subsequently 160 mL of dried toluene was introduced and with vigorous heating to boiling an orange solution with a white precipitate ($MgCl_2$) was observed. The solution was filtered hot and the bright orange filtrate allowed to cool to room temperature before storage of the solution in the freezer (-27°C) enabled crystallisation to occur. Orange needle-like crystals were observed and the solvent was removed via cannular and the remaining orange solid dried under vacuum for 2 hrs. The orange crystalline compound was then transferred to the glove box for storage. In order to obtain suitable crystals for an X-ray diffraction experiment, a sample of $Mn(CH_2SiMe_3)_2$ was sublimed *in vacuo* at 150°C to give larger

orange cubic crystals (2.50-2.80 g, 73-81 %). ν_c(nujol): 2776.1cm^{-1} (C-H). Elemental analysis calcd (%) for $C_8H_{22}MnSi_2$ (229.38): C 41.89, N 0.00, H 9.67; found: C 41.89, N 0.00, H 9.79. M.p. 152°C (decomp.).

8.9. Synthesis of [Mn(CH$_2$SiMe$_3$)$_2$TMEDA] Compound 2

$Mn(CH_2SiMe_3)_2$ (0.23 g, 1 mmol) was suspended in 20 ml of dry hexane. TMEDA (0.15 mL, 1 mmol) was added to give an orange/yellow solution which was allowed to stir at room temperature for 12 hrs. The solution was filtered and concentrated by removing some solvent under vacuum. Storage of the solution at room temperature afforded a crop of orange crystals after two days (0.11 g, 32%). ν_c(nujol): 2799.5cm^{-1} (C-H). Elemental analysis calcd (%) for $C_{10}H_{27}N_2MnSi_2$ (345.58): C 48.66, N 8.11, H 11.08; found: C 48.66, N 7.92, H 10.90. M.p. 93°C.

8.10. Synthesis of [(C$_5$H$_5$N)$_2$Mn(CH$_2$SiMe$_3$)$_2$] Compound 3

$Mn(CH_2SiMe_3)_2$ (0.23 g, 1 mmol) was suspended in 20 ml of dry hexane. Pyridine (0.08 mL, 1 mmol) was added and the reaction mixture was stirred at room temperature for 2 hours. The bright orange solution obtained was filtered and the solvent volume reduced under vacuum. Storage of the solution in the refrigerator (at 4°C) afforded a crop of bright orange plate crystals (0.12 g, 62%).

8.11. Synthesis of [{(dioxane).[Mn(CH$_2$SiMe$_3$)$_2$]}$_\infty$] Compound 4

In the usual protocol, $Mn(CH_2SiMe_3)_2$ (0.23 g, 1 mmol) was suspended in 20 ml of dry hexane. Dioxane (0.09 mL, 1 mmol) was then added to give a light brown solution which was allowed to stir at room temperature for 12 hrs. The solution was filtered and concentrated by removing some solvent under vacuum. Storage of the solution at room temperature afforded a crop of pink needle crystals after two days (0.30 g, 56%). M.p. 156°C. ν_c(nujol): 2770.6cm^{-1} (C-H). Elemental analysis calcd (%) for $C_{20}H_{52}Mn_2O_2Si_4$ (546.86): C 45.39, N 0.00, H 9.53; found: C 45.39, N 0.00, H 9.88.

8.12. Synthesis of [{(dioxane).[$Mn(CH_2SiMe_3)_2$]}$_\infty$] Compound 5

$Mn(CH_2SiMe_3)_2$ (0.23 g, 1 mmol) was suspended in 20 ml of dry hexane. Dioxane (0.09 mL, 1 mmol) was added to give a light brown solution which was allowed to stir at room temperature for 12 hrs. The solution was filtered and concentrated by removing some solvent under vacuum. Storage of the solution in the freezer (at -27°C) afforded a crop of colourless plate crystals after two days (0.19g, 60 %). Elemental analysis calcd (%) for $C_{12}H_{30}MnO_2Si_2$ (317.48): C 45.40, N 0.00, H 9.52; found: C 45.40, N 0.00, H 9.99. M.p. 153°C.

8.13. Synthesis of [$(CH_2SiMe_3)(PPh_3)Mn(CH_2SiMe_3)]_2$ Compound 6

$Mn(CH_2SiMe_3)_2$ (0.23 g, 1 mmol) was suspended in 15 ml of dry hexane. Triphenylphosphine, PPh_3 (0.26 g, 1 mmol) was added and the reaction allowed to stir at room temperature overnight. A white precipitate was observed which when heated gave a clear red/pink solution. The pink solution was filtered and upon concentration of the solution under vacuum pink rhombic crystals were obtained (0.38g, 39%).

8.14. Synthesis of $Mn_3(NHDipp)_6$ Compound 11

$Mn(CH_2SiMe_3)_2$ (0.23 g, 1 mmol) was suspended in 15 ml of dry hexane. Freshly distilled primary amine NH_2Dipp (0.38 ml, 2 mmol) was introduced to the reaction mixture to give a yellow /green solution. The solution was allowed to stir at room temperature overnight resulting in a cloudy solution. The solution was heated gently to give a clear green solution, filtered and the solvent volume reduced under vacuum. Storage of the solution at room temperature resulted in a crop of yellow green crystals (0.66g, 55%).

8.15. Synthesis of [$(Me_3SiCH_2)_2Mn_3\{\mu\text{-}OC(CH_2SiMe_3)Ph_2\}_4$] Compound 13

$Mn(CH_2SiMe_3)_2$ (0.23 g, 1 mmol) was suspended in 15 ml of dry hexane, to which benzophenone (0.18 g, 1 mmol) was added. At this point a red solution was observed. The reaction mixture was allowed to stir at room temperature for 5 hrs and was subsequently left to stand at room temperature to induce crystallisation. A crop of light pink rectangular crystals were obtained (0.26g, 74%).

8.16. Synthesis of [(TMEDA)Na(TMP)(CH_2SiMe_3)Mn(TMP)] Compound 16

BuNa (0.16 g, 2 mmol) was suspended in 20 mL of dry hexane and the Schlenk tube was placed in an ultrasonic bath for 10 minutes to ensure a fine dispersion was achieved. TMPH (0.68 mL, 4 mmol) was then added and the reaction mixture was allowed to stir at room temperature for 1 hr. $Mn(CH_2SiMe_3)_2$ (0.46 g, 2 mmol) and TMEDA (0.31 mL, 2 mmol) were added to afford a pale yellow solution. Concentration of the solution under vacuum and storage in a refrigerator led to the formation of a crop of light pink plate crystals (0.60g, 53%).

8.17. Synthesis of [(TMEDA)Na(TMP)(*o*-C_6H_4-OMe)Mn(TMP)] Compound 17

Freshly prepared BuNa (0.16 g, 2 mmol) was suspended in 20 mL of dry hexane and placed in an ultrasonic bath for 10 minutes to ensure a fine dispersion was achieved. To this suspension TMPH (0.68 mL, 4 mmol) was added and the reaction was allowed to stir at room temperature for 1 hr and then $Mn(CH_2SiMe_3)_2$ (0.46 g, 2 mmol) was introduced. Subsequently a molar equivalent of TMEDA (0.31 ml, 2 mmol) was added and the pale yellow solution was stirred for 30 minutes at room temperature. Next, anisole (0.22 mL, 2 mmol) was added and the resulting yellow solution allowed to stir at room temperature overnight. The reaction solution was filtered and the yellow filtrate concentrated *in vacuo*. The solution was left to crystallise overnight at room temperature and a crop of green/yellow crystals was obtained (0.76g, 76%) M.p. 128 °C

(decomp); elemental analysis calcd (%) for $C_{31}H_{59}MnN_4NaO$ (581.75): C 64.00, H 10.22, N 9.63; found: C 64.00, H 10.45, N 9.23.

8.18. Synthesis of [(TMEDA)Na(TMP){o-[C(O)N(*i*Pr$_2$)]C$_6$H$_4$}Mn(CH$_2$SiMe$_3$)] Compound 18

Following the same methodology described for **17**, the mixed-metal reagent [(TMEDA)Na(TMP)(CH_2SiMe_3)MnTMP] was prepared *in situ* by reaction of NaTMP (2 mmol), TMPH (0.34mL, 2 mmol), Mn(CH_2SiMe_3) (0.46 g, 2 mmol) and TMEDA (0.31 ml, 2 mmol) affording a yellow solution. *N, N*-diisopropylbenzamide (0.41 g, 2 mmol) was then introduced and the resulting bright orange solution was stirred at room temperature overnight. The solution was filtered and the filtrate concentrated *in vacuo*. A crop of bright orange needles was deposited at room temperature (0.40 g, 32%). M.p. 148 °C (decomp); IR (nujol): ν =1592.7 cm^{-1}(C=O); elemental analysis calcd (%) for $C_{32}H_{63}MnN_4NaOSi$ (625.88): C61.41, H 10.15, N 8.95; found: C 61.40, H 10.08, N 8.45.

8.19. Synthesis of [Mn(CH$_2$SiMe$_3$)$_2${(*i*Pr)$_2$NC(Ph)(=O)}$_2$] Compound 20

$Mn(CH_2SiMe_3)_2$ (0.23 g, 1 mmol) was suspended in 20 ml of dry hexane. N, N-diisopropylbenzamide (0.41 g, 2 mmol) was added to give an orange solution that was allowed to stir at room temperature for 5 hrs. Standing the solution at room temperature overnight furnished a crop of yellow crystals (0.40 g, 64%). M.p. 79.2 °C; elemental analysis calcd (%) for $C_{34}H_{60}N_2O_2$ (639.96): C 63.81, H 9.44, N 4.37; found: C 63.81, H 9.38, N, 4.57.

8.20. Synthesis of [(TMEDA)Na(TMP)(*m*-C$_6$H$_4$-NMe$_2$)Mn(TMP)] Compound 21

Following the same methodology described for **17**, the mixed-metal reagent [(TMEDA)Na(TMP)(CH_2SiMe_3)MnTMP] was prepared *in situ* by reaction of NaTMP (2 mmol), TMPH (0.34 mL, 2mmol) Mn(CH_2SiMe_3) (0.46 g, 2 mmol) and TMEDA (0.31 ml, 2 mmol) affording a yellow solution. Next N, N-dimethylaniline, $NMe_2C_6H_5$

(0.25 ml, 2 mmol) was added to give a light orange solution. The solution was heated to reflux temperature (60-65°C) for 12 hrs, allowed to cool to room temperature and filtered. The dark orange/brown filtrate was subsequently stored in the freezer (at -27°C) to afford a crop of colourless cubic crystals. No yield has yet been recorded due to the temperature sensitive nature of the product as the crystals readily melt at room temperature.

8.21. Synthesis of [(TMEDA)Na(TMP)(*p*-$C_6H_4N^iPr_2$)Mn(TMP)] Compound 22

Following the same methodology described for **17**, the mixed-metal reagent [(TMEDA)Na(TMP)(CH_2SiMe_3)MnTMP] was prepared *in situ* by reaction of NaTMP (1 mmol), TMPH (0.17mL, 1 mmol), Mn(CH_2SiMe_3) (0.36 g, 1 mmol) and TMEDA (0.15 ml, 1 mmol) affording a yellow solution. Next, N, N-diisopropylaniline (0.19 ml, 1 mmol) was added to give a orange/yellow solution. The reaction mixture was allowed to stir at room temperature overnight, filtered and the solvent volume reduced in vacuo. Storage of the orange solution at room temperature for 4 days allowed a crop of yellow needle crystals to be deposited (0.45g, 69%).

8.22. Cross-coupling of manganated toluene with 4-iodotoluene

Following the same methodology described for **17**, the mixed-metal reagent [(TMEDA)Na(TMP)(CH_2SiMe_3)MnTMP] was prepared *in situ* by reaction of NaTMP (1 mmol), TMPH (0.17mL, 1 mmol), Mn(CH_2SiMe_3) (0.36 g, 1 mmol) and TMEDA (0.15 ml, 1 mmol) affording a yellow solution. Next toluene (,1mmol) was added and the reaction allowed to stir at room temperature overnight. To this crude hexane solution 4-iodotoluene (0.22g, 2mmol) and [$PdCl_2$(dppf)] (16.3mg, 0.02mmol) was added and the reaction heated to reflux for 18 hours. The mixture was quenched with a saturated NH_4Cl (5 ml) solution, hexane (10 ml) and distilled water (10 ml). The crude bilayer was filtered through Celite into a separating funnel with the aqueous layer subsequently discarded. The organic layer was then washed with distilled water (3 x 10 ml), dried over anhydrous $MgSO_4$ for 1 hour and then filtered to give a clear orange solution. The solvent was removed in vacuo and the resulting orange oil was dissolved in the minimum ammout of hexane and purified by SiO_2 column chromatography

(eluent: hexane) to give a mixture of 4,4'dimethylbiphenyl (22%) and 3,4'dimethylbiphenyl (78%) (0.28g, 76% total yield).

^{1}H NMR of 4,4'dimethylbiphenyl (400MHz, $CDCl_3$, 300K): δ 7.49 (4H, m, aromatic H), 7.25 (4H, m, aromatic H), 2.40 (6H, s, CH_3).

^{1}H NMR of 3,4'dimethylbiphenyl (400MHz, $CDCl_3$, 300K): δ 7.49 (2H, m, aromatic H), 7.41 (2H, m, aromatic H), 7.32 (1H, t, aromatic H), 7.15 (1H, d, aromatic H), 7.25 (2H, m, aromatic H), 2.42 (3H, s, CH_3), 2.40 (3H, s, CH_3).

8.23. Synthesis of [(TMEDA)Na(TMP){5-(1,3-$Me_2C_6H_3$)}Mn(TMP)] Compound 23

Following the same methodology described for **17**, the mixed-metal reagent [(TMEDA)Na(TMP)(CH_2SiMe_3)MnTMP] was prepared *in situ* by reaction of NaTMP (1 mmol), TMPH (0.17mL, 1 mmol), Mn(CH_2SiMe_3) (0.36 g, 1 mmol) and TMEDA (0.15 ml, 1 mmol) affording a yellow solution. Next, *m*-Xylene (0.12 mL, 1 mmol) was added to give a bright yellow solution that after 2hrs stirring at room temperature afforded a yellow precipitate. Gently heating the mixture re-dissolved the precipitate to give a bright yellow solution that upon cooling to room temperature deposited a crop of yellow cubic crystals (0.40g, 69%).

8.24. Synthesis of [(TMEDA)Na(TMP)(2-$C_{10}H_7$)Mn(TMP)] Compound 24

NaTMP was prepared *in situ* by reaction of *n*BuNa (0.16 g, 2 mmol) with TMPH (0.34 mL, 2 mmol) in 20 mL of dry hexane. Mn(CH_2SiMe_3)$_2$ (0.46 g, 2mmol), TMPH (0.34 mL, 2 mmol) and TMEDA (0.30 mL, 2 mmol) were then introduced and the mixture was stirred for 15 min to afford a light yellow/orange solution. Naphthalene (0.256 g, 2 mmol) was subsequently added, affording an orange solution that was stirred at room temperature for 12 hours. A colour change to red was observed and the solution was concentrated by removal of some solvent under vacuum. Storage of the solution at room temperature afforded a crop of red plate crystals (0.76g, 88%). M.p. 156.1°C; elemental

analysis calcd (%) for $MnNaC_{34}H_{59}N_4$ (601.78): C 67.85, H 9.88, N 9.31; found C 67.12, H 10.09, N 8.98.

8.25. Synthesis of [(TMEDA)Na(TMP)(2-(1-$MeOC_{10}H_6$))Mn(CH_2SiMe_3)] Compound 25

Following the usual protocol, NaTMP was prepared *in situ* by reaction of BuNa (0.16 g, 2 mmol) with TMPH (0.34 mL, 2 mmol) in 20 mL of dry hexane. $Mn(CH_2SiMe_3)_2$ (0.46 g, 2 mmol), TMPH (0.34 mL, 2 mmol) and TMEDA (0.30 mL, 2 mmol) were then introduced and the mixture was stirred for 15 min to afford a light yellow/orange solution. 1-Methoxynaphthalene (0.29 mL, 2 mmol) was added and a colour change to red was seen immediately. The reaction mixture was stirred at room temperature for 12 hours. The resultant deep red solution was filtered and the filtrate concentrated by removal of some solvent under vacuum. A crop of red block crystals (0.75g, 65%) was deposited upon storage of the solution in the refrigerator (5°C). M.p. 122.2°C; elemental analysis calcd (%) for $MnNaOSiN_3C_{30}H_{54}$ (578.78): C 62.26, H 9.40, N 7.26; found C 62.33, H 9.87, N 6.94.

8.26. Synthesis of [(TMEDA)Na(TMP)(3-(2-$MeOC_{10}H_6$))Mn(TMP)] Compound 26

NaTMP was prepared *in situ* by reaction of freshly prepared BuNa (0.16 g, 2 mmol) with TMPH (0.34 mL, 2 mmol) in 20 mL of dry hexane. $Mn(CH_2SiMe_3)_2$ (0.46 g, 2 mmol), TMPH (0.34 mL, 2 mmol) and TMEDA (0.30 mL, 2 mmol) were then introduced and the mixture was stirred for 15 min to afford a light yellow/orange solution. Next 2-methoxynaphthalene (0.32 g, 2 mmol) was added and a colour change to red was observed. The reaction mixture was stirred at room temperature for 12 hours, the reaction mixture was filtered and the filtrate concentrated by removal of some solvent under vacuum. A crop of red block crystals (1.07 g, 85%) was deposited upon storage of the solution at room temperature. M.p. 147°C; elemental analysis calcd (%) for $MnNaOC_{35}H_{61}N_4$ (631.81): C 66.54, H 9.73, N 8.87; found C 66.13, H 10.12, N 8.56.

8.27. Synthesis of [(TMEDA)Na(TMP){6-(1-$NMe_2C_{10}H_6$)}Mn(TMP)] Compound 27

Following the same methodology described for **17**, the mixed-metal reagent [TMEDA.Na(TMP)(CH_2SiMe_3)MnTMP] was prepared *in situ* by reaction of NaTMP (1 mmol), TMPH (0.17 mL, 1 mmol), Mn(CH_2SiMe_3) (0.36 g, 1 mmol) and TMEDA (0.15 ml, 1 mmol) affording a yellow solution. Next N, N-dimethylnaphthylamine (0.16 mL, 1 mmol) was added and a colour change to bright orange was observed. The orange solution was allowed to stir at room temperature for 3 days. The resulting red solution was filtered and the solvent volume concentrated by about half under vacuum. Storage of the solution for 3 days at room temperature allowed the growth of a crop of red plate crystals (0.37g, 57%).

8.28. Synthesis of [(TMEDA)Na(CH_2SiMe_3)(TMP)Mg(TMP)] Compound 28

TMPH (0.34 mL, 2 mmol) was added to a suspension of BuNa (0.08 g, 1 mmol) in dry n-hexane (20 mL) and the resultant mixture was allowed to stir at room temperature for 1 hour. Mg(CH_2SiMe_3)$_2$ (0.2 g, 1 mmol) and TMEDA (0.15 mL, 1 mmol) were added to give a light yellow/orange solution and the resultant solution was allowed to stir for 12 hours at room temperature. The reaction mixture was filtered and subsequent removal of some solvent *in vacuo* gave a crop of large light brown crystals (0.1g, 19%); m.p. 143°C (decomp).

^{1}H NMR (400MHz, d_6-benzene, 300K): δ1.95 (q, 4H, γ-C$\underline{H}_2$, TMP) 1.70 (12H, C$\underline{H}_3$, TMEDA), 1.60 (s, 4H, C$\underline{H}_2$, TMEDA), 1.52 (s, 24H, C$\underline{H}_3$ TMP), 1.44 (s (br), β-C$\underline{H}_2$, TMP), 0.48 (s, 12H, C$\underline{H}_3$, CH_2SiMe_3), -2.00 (s, 2H, C$\underline{H}_2$, CH_2SiMe_3).

8.29. Synthesis of [(TMEDA)Na(TMP){6-(1-$NMe_2C_{10}H_6$)}Mg(TMP)] Compound 29

TMPH (0.34 mL, 2 mmol) was added to a suspension of BuNa (0.08 g, 1 mmol) in dry n-hexane (20 mL) and the resultant mixture was allowed to stir at room temperature for 1 hour. Mg(CH_2SiMe_3)$_2$ (0.2 g, 1 mmol) and TMEDA (0.15 mL, 1 mmol) were added

to give a light yellow solution. To this N, N-dimethylnaphthylamine (0.16 mL, 1 mmol) was added to give a light yellow solution that was allowed to stir at room temperature for 3 days. The yellow solution was filtered and the solvent volume reduced by half under vacuum. Storage of this solution at room temperature yielded a crop of colourless plate crystals (0.45g, 73%).

^{1}H Numbering Scheme for 29

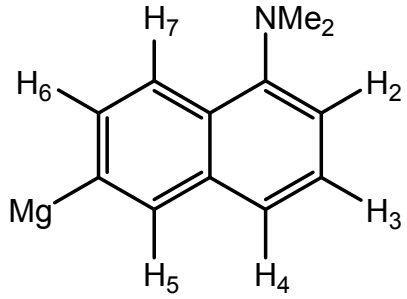

^{1}H NMR (400MHz, d_6-benzene, 300K): δ 8.30 (s, 1H, H_5), 8.20 (d, 1H, H_7), 8.13 (d, 1H, H_8), 7.38 (d br, 1H, H_2), 7.28 (td, 1H, H_3), 6.86 (d, 1H, H_4), 2.96 (s, 3H, C$\underline{H}_3$-N), 1.89 (m, 4H, C$\underline{H}_2$-γ-TMP), 1.67 (s, 24H, C$\underline{H}_3$-TMP), 1.40 (s, 12H, C$\underline{H}_3$-TMEDA), 1.35 (m, 8H, β-C$\underline{H}_2$-TMP), 1.22 (s, 4H, C$\underline{H}_2$-TMEDA).

^{13}C Numbering Scheme for 29

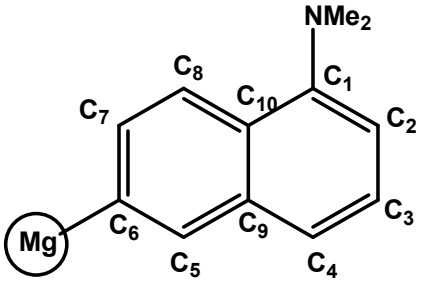

^{13}C NMR (400MHz, d_6-benzene, 300K): δ 170.31 (C_6), 151.21 (C_1), 139.62 (C_5), 138.30 (C_7 and C_8), 135.36 (C_9), 124.69 (C_3), 122.55 (C_2), 121.74 (C_{10}), 112.19 (C_4), 56.50 ($\underline{C}H_2$-TMEDA), 52.23 (α-$\underline{C}$, TMP), 45.83 ($\underline{C}H_3$-TMEDA), 45.12 (N-$\underline{C}H_3$), 42.38 (β-$\underline{C}H_2$, TMP) 35.87 ($\underline{C}H_3$-TMEDA), 20.32 (γ-$\underline{C}H_2$, TMP).

8.30. Synthesis of [(TMEDA)Na(TMP)(2,6-$Me_2C_6H_3O$)Mg(TMP)] Compound 30

As in the previous reaction, TMPH (0.34 mL, 2 mmol) was added to a suspension of BuNa (0.08 g, 1 mmol) in dry n-hexane (20 mL) and the resultant mixture was stirred at room temperature for 1 hour. $Mg(CH_2SiMe_3)_2$ (0.2 g, 1 mmol) and TMEDA (0.15 mL, 1 mmol) was added to give a light yellow solution. Dry 2, 6-dimethylanisole (0.14 mL,

1 mmol) was added and the reaction allowed to stir at room temperature overnight. The light orange solution was filtered and the solvent volume reduced under vacuum. Storage of the solution for 2 days at room temperature allowed a crop of light orange cubic crystals to grow (0.31 g, 55%).

^{13}C Numbering Scheme for 30

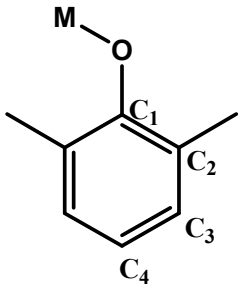

^{1}H NMR (400MHz, d_6-benzene, 300K): δ 7.13 (d, br, 2H, Ar-H), 6.72 (t, 1H, Ar-H), 2.34 (s, 6H, Ar-CH_3), 1.88 (m, 4H, γ-CH_2, TMP), 1.62 (s, 12H, CH_3, TMEDA), 1.56 (s, 4H, CH_2, TMEDA), 1.47 (s (br), 24H, CH_3 TMP), 1.39 (s (br), 8H, β-CH_2, TMP).

^{13}C NMR (400MHz, d_6-benzene, 300K): δ 162.12 (C_1), 128.65 (C_3), 125.41 (C_2), 115.52 (C_4), 57.14 (CH_2-TMEDA), 51.90 (α-C-TMP), 45.94 (CH_3-TMEDA), 41.29 (β-CH_2, TMP), 36.05 (CH_3-TMP), 20.93 (γ-CH_2, TMP), 19.19 (Ar-CH_3).

8.31. Synthesis of $[Na_2Mn_2\{N(^iPr)_2\}_4(\mu\text{-}H)_2.(toluene)_2]$ Compound 31

Freshly made BuNa (0.16 g, 2 mmol) was suspended in 20 mL of dry hexane and placed in an ultrasonic bath for 10 minutes to ensure a fine dispersion was achieved. To this mixture diisopropylamide (0.84 ml, 6 mmol) was added and the reaction allowed to stir at room temperature for 1 hr. Next $Mn(CH_2SiMe_3)_2$ (0.46 g, 2 mmol) was introduced to give a light orange solution. The solution was heated to reflux for 45 minutes causing the precipitation of an off white/pink solid. Hexane was removed from the solution *in vacuo* and 10ml of dry hot toluene was added. Upon heating almost all of the solid dissolved to give an orange solution. The solution was filtered hot and the filtrate slowly reduced in volume *in vacuo*. Red needle crystals formed at room temperature (0.70g, 62%).

8.32. Synthesis of [{Fe(C_5H_4)$_2$}$_3${Mn_3Na_2(N*i*Pr$_2$)$_2$(HN*i*Pr$_2$)$_2$}] Compound 34

Solid BuNa (0.16 g, 2 mmol) was suspended in 20 mL of dried hexane and placed in an ultrasonic bath for 10 minutes to ensure a fine dispersion was achieved. To this dispersion diisopropylamine (0.84 ml, 6 mmol) was added and the reaction mixture allowed to stir at room temperature for 1 hour. The reaction was mixture was cooled to 0°C and Mn(CH_2SiMe_3)$_2$ (0.46 g, 2 mmol) and ferrocene (0.37 g, 2 mmol) were added to give a translucent bright orange solution. All the hexane was removed in vacuo and 40 mL of dry toluene was introduced. Subsequent storage in the refrigerator (at 5°C) for 3 weeks furnished compound **4** as a crop of bright red/orange plate crystals (0.63 g, 81%).

8.33. Synthesis of [{(TMEDA)Na(CH_2SiMe_3)(OBu)(*o*-C_6H_4OMe)Mn_2}$_2$] Compound 36

Following the same experimental procedure as described for **17**, compound **36** was prepared in situ by reaction of BuNa (0.16 g, 2 mmol), TMPH (0.68 mL, 4 mmol), Mn(CH_2SiMe_3)$_2$ (0.46 g, 2 mmol) and TMEDA (0.31 mL, 2 mmol). N, N-diisopropylbenzamide (0.41 g, 2 mmol) was then added and the mixture was stirred for 18 hours affording a bright orange homogeneous solution. The solution was filtered and the solvent volume concentrated under vacuum. Storage of this solution at room temperature afforded a crop of orange crystals after two days. (0.41 g, 31%). M.p. 148°C (decomp); IR (nujol): ν =1592.7 cm^{-1} (C=O); elemental analysis calcd (%) for $MnNaC_{32}H_{63}N_4OSi$ (625.88): C 61.41, H 10.15, N 8.95; found: C 61.40, H 10.08, N 8.45.

8.34. Synthesis of [(TMEDA)$_2$$Na_2(TMP)_2$(1,4-$C_6H_4$)$Mn_2(TMP)_2$] Compound 38

Following the same synthetic procedure as described for **26**, compound **38** was fortuitously obtained from one repeat synthesis. Two types of crystals were observed, the major product being red block crystals identified as **26,** combined with a minor crop

of yellow needle crystals identified as **38**. Unfortunately all attempts to prepare **38** by rational means have so far been unsuccessful.

8.35. Synthesis of [[(TMEDA)Na(TMP)}$_2${1,4-[Mn(TMP)]$_2$-C_4H_4}] Compound 42 and [$Na_2O(TMP)_4Mn_2$] Compound 44

TMPH (0.34 mL, 2 mmol) was added to a suspension of BuNa (0.08 g, 1 mmol) in dry n-hexane (20 mL) and the resultant mixture was allowed to stir at room temperature for 1 hour. $Mn(CH_2SiMe_3)_2$ (0.23 g, 1 mmol) and TMEDA (0.15 mL, 1 mmol) was added to give a light orange solution. Next, THF (0.08 mL, 1 mmol) was added and the solution allowed to stir at room temperature for 12 hours. The red solution was filtered and concentrated slightly under vacuum. Allowing the solution to stand at room temperature for 1 week afforded red/orange needle crystals of **42** (0.25g, 49.9%). The mother liquor was further concentrated in vacuum to furnish light pink plate crystals of **44** (0.16g, 43.6%).

8.36. Synthesis of [[(TMEDA)Na(TMP)}$_2${1, 4-[Mg(TMP)]$_2$-C_4H_4] Compound 43 and [$Na_2O(TMP)_4Mg_2$] Compound 45

TMPH (0.34 mL, 2 mmol) was added to a suspension of BuNa (0.08 g, 1 mmol) in dry n-hexane (20 mL) and the resultant mixture was allowed to stir at room temperature for 1 hour. $Mg(CH_2SiMe_3)_2$ (0.20 g, 1 mmol) and TMEDA (0.15 mL, 1 mmol) were added to give a light yellow solution. Next, THF (0.08 mL, 1 mmol) was added and the colourless solution was gently heated for 5 minutes. Upon cooling to room temperature large colourless needle crystals of **43** (0.23g, 48.9%) were deposited. The mother liquor was subsequently further concentrated under vacuum and upon standing at room temperature colourless plate crystals of **45** were obtained (0.14g, 41.7%).

^{1}H NMR (400MHz, d_6-benzene, 300K) Compound 43: δ 6.75 (s, 4H, $C_4\underline{H}_4$), 2.18 (s, 8H, $C\underline{H}_2$, TMEDA), 2.06 (s, 24H, $C\underline{H}_3$, TMEDA), 1.68 (s (br), 48H, $C\underline{H}_3$ TMP), 1.49 (s (br), 24H, γ-$C\underline{H}_2$, TMP & β-$C\underline{H}_2$, TMP).

^{1}H NMR (400MHz, d_8-THF, 300K) Compound 43: δ 6.50 (m, 2H, $C_4\underline{H}_4$), 6.36 (m, 2H, $C_4\underline{H}_4$), 2.30 (s, 8H, $C\underline{H}_2$, TMEDA), 2.15 (s, 24H, $C\underline{H}_3$, TMEDA), 1.67 (m, 8H, γ-$C\underline{H}_2$, TMP), 1.24 (s (br), 48H, $C\underline{H}_3$ TMP), 1.16 (m (br), 16H, β-$C\underline{H}_2$, TMP).

^{13}C NMR (400MHz, d_8-THF, 300K) Compound 43: 163.32 (C_B, $\underline{C}_4H_4$), 154.99 (C_A, $\underline{C}_4H_4$), 58.94 ($\underline{C}H_2$-TMEDA), 52.62 (α-$\underline{C}$-TMP), 46.23 ($\underline{C}H_3$-TMEDA), 42.57 (β-$\underline{C}H_2$, TMP), 35.82 ($\underline{C}H_3$-TMP), 20.75 (γ-$\underline{C}H_2$, TMP).

^{1}H NMR (400MHz, d_6-benzene, 300K) Compound 45: δ 1.98 (m, 1H, γ-$C\underline{H}_2$, TMP), 1.74 (d (br), 3H, γ-$C\underline{H}_2$, TMP & β-$C\underline{H}_2$, TMP), 1.47 (s, 6H, $C\underline{H}_3$ TMP), 1.26 (s, 6H, $C\underline{H}_3$ TMP), 1.00 (m (br), 2H, β-$C\underline{H}_2$, TMP).

^{13}C NMR (400MHz, d_6-benzene, 300K) Compound 45: δ 51.80 (α-$\underline{C}$-TMP), 43.3 (β-$\underline{C}H_2$, TMP), 39.1 ($\underline{C}H_3$-TMP), 34.3 ($\underline{C}H_3$-TMP), 19.9 (γ-$\underline{C}H_2$, TMP).

8.37. Synthesis of [{(TMEDA)Na(TMP)}$_2${1, 4-[Mg(TMP)]$_2$-C_4D_4}] Compound 43-*d_4*

TMPH (0.34 mL, 2 mmol) was added to a suspension of BuNa (0.08 g, 1 mmol) in dry n-hexane (20 mL) and the resultant mixture was allowed to stir at room temperature for 1 hour. $Mg(CH_2SiMe_3)_2$ (0.20 g, 1 mmol) and TMEDA (0.15 mL, 1 mmol) was added to give a light yellow solution. Next, d_8-THF (0.08 mL, 1 mmol) was added and the colourless solution was gently heated for 5 minutes. Upon cooling to room temperature large colourless needle crystals were deposited. (0.18g, 38.2%).

^{1}H NMR (400MHz, d_6-benzene, 300K): δ 2.18 (s, 8H, $C\underline{H}_2$, TMEDA), 2.06 (s, 24H, $C\underline{H}_3$, TMEDA), 1.68 (s (br), 48H, $C\underline{H}_3$ TMP), 1.49 (s (br), 24H, γ-$C\underline{H}_2$, TMP & β-$C\underline{H}_2$, TMP).

^{2}H NMR (400MHz, C_6H_6-benzene, 300K): δ 6.90 (s (br), C_4D_4)

8.38. Synthesis of [(TMEDA)Na(TMP)(α-C_4H_7S)Mg(TMP)] Compound 47

TMPH (0.34 mL, 2 mmol) was added to a suspension of BuNa (0.08 g, 1 mmol) in dry n-hexane (20 mL) and the resultant mixture was stirred at room temperature for 1 hour. $Mg(CH_2SiMe_3)_2$ (0.20 g, 1 mmol) and TMEDA (0.15 mL, 1 mmol) were then introduced to give a light yellow solution. Tetrahydrothiophene, THT (0.08 mL, 1 mmol) was added and the solution was allowed to stir at room temperature for 1 hour. The light yellow solution was filtered and placed directly in the refrigerator (at 5°C). After 1 week colourless block crystals were obtained (0.18 g, 34%).

Numbering Scheme for thiophene ring in 47

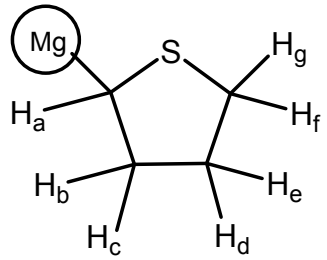

^{1}H NMR (d_8-THF): δ 2.93 (m, 1H, H_d-THT), 2.62 (td, 1H, H_g-THT), 2.49 (m, 1H, H_f-THT), 2.18 (m, 1H, H_e-THT) 1.93 (s, br, 4H, γ-TMP), 1.77 (s, 13H, CH_3-TMEDA + H_c-THT), 1.71 (s, 4H, CH_2-TMEDA), 1.58 (d, br, 24H, CH_3-TMP), 1.41 (s, br, 8H, β-TMP), 1.91 (m, br, 1H, H_d-THT), 0.93 (dd, 1H, H_a-THT).

8.39. Synthesis of [{(TMEDA)Na(TMP)}$_2${1,4-[Mg(TMP)]$_2$-C_4H_4}] from THT

TMPH (0.34 mL, 2 mmol) was added to a suspension of BuNa (0.08 g, 1 mmol) in dry n-hexane (20 mL) and the resultant mixture was stirred at room temperature for 1 hour. $Mg(CH_2SiMe_3)_2$ (0.20 g, 1 mmol) and TMEDA (0.15 mL, 1 mmol) were added to give a light yellow solution. Tetrahydrothiophene (0.08 mL, 1 mmol) was added and the solution was allowed to stir at room temperature for 2 weeks. The light yellow solution was filtered and the solvent volume was reduced under vacuum. Storage of the solution in the refrigerator (at 5°C) deposited a crop of colourless needle crystals (0.21g, 44%).

NMR (400MHz, d_6-benzene, 300K): δ 6.75 (s, 4H, $C_4\underline{H}_4$), 2.18 (s, 8H, $C\underline{H}_2$, TMEDA), 2.06 (s, 24H, $C\underline{H}_3$, TMEDA), 1.68 (s (br), 48H, $C\underline{H}_3$ TMP), 1.49 (s (br), 24H, γ-$C\underline{H}_2$, TMP & β-$C\underline{H}_2$, TMP).

8.40. Synthesis of [{(-)-sparteine}Na(TMP)(CH_2SiMe_3)Mg(TMP)] Compound 48

TMPH (0.34 mL, 2 mmol) was added to a suspension of BuNa (0.08 g, 1 mmol) in dry *n*-hexane (20 mL) and the resultant mixture was allowed to stir at room temperature for 1 hours. $Mg(CH_2SiMe_3)_2$ (0.20 g, 1 mmol) and (-)-sparteine (0.23 mL, 1 mmol) was added to give a light yellow solution that was allowed to stir at room temperature for 8 hours. The yellow solution was filtered and the solvent volume reduced slightly under vacuum upon which a crop of light yellow plate crystals was deposited (0.38g, 58%).

^{1}H NMR (400MHz, d_6-benzene, 300K): δ 1.92 (m, 4H, γ-$C\underline{H}_2$, TMP), 1.56 (s (br), 8H, β-$C\underline{H}_2$, TMP), 1.47 (s (br), 24H, $C\underline{H}_3$, TMEDA), 0.48 (s, 9H, $C\underline{H}_3SiCH_2$), -1.35 (m, 1H, $C\underline{H}_2SiMe_3$), -1.76 (m, 1H, $C\underline{H}_2SiMe_3$), 2.80, 2.67, 2.59, 2.55, 2.52, 2.43, 1.77, 1.66, 1.60, 1.36, 1.26, 1.17, 1.09, 0.94, 0.89 (m, 26H, (-)-sparteine).

^{13}C NMR (400MHz, d_6-benzene, 300K) : δ 41.38 (β-$\underline{C}H_2$-TMP), 36.20 ($\underline{C}H_3$-TMP), 20.27 (γ-$\underline{C}H_2$-TMP), 5.17 ($\underline{C}H_3SiCH_2$), 1.83 ($\underline{C}H_2SiCH_3$), -1.83 ($\underline{C}H_2SiCH_3$), 67.50, 62.10, 57.39, 54.74, 52.38, 42.24, 40.07, 38.46, 34.66, 31.93, 30.07, 28.21, 26.37, 25.40, 24.72, 23.01, 14.29 (α-$\underline{C}$-TMP & $\underline{C}$ (-)-sparteine)

8.41. Synthesis of [{(-)-sparteine}Na(TMP)(α-C_4H_7S)Mg(TMP)] Compound 49

TMPH (0.34 mL, 2 mmol) was added to a suspension of BuNa (0.08 g, 1 mmol) in dry *n*-hexane (20 mL) and the resultant mixture was allowed to stir at room temperature for 1 hour. Next, $Mg(CH_2SiMe_3)_2$ (0.20 g, 1 mmol) and (-) sparteine (0.23 mL, 1 mmol) was added to give a light yellow solution. Tetrahydrothiophene (0.09 mL, 1 mmol) was subsequently delivered to the solution to give a clear bright yellow solution that was allowed to stir at room temperature for 8 hours. The resultant light orange solution was

filtered and the solvent volume reduced slightly under vacuum. A crop of colourless plate crystals was deposited (0.31g, 48%).

8.42. Synthesis of [{(TMEDA)$_3$Na$_6$Mg$_3$(CH$_2$SiMe$_3$)(2,5-C$_4$H$_2$O)$_3$(2-C$_4$H$_3$O)$_5$}$_3$] Compound 50

Following the usual procedure, TMPH (0.36 mL, 2 mmol) was added to a suspension of BuNa (0.08 g, 1 mmol) in dry n-hexane (20 mL) and the resultant mixture was allowed to stir at room temperature for 1 hour. Mg(CH$_2$SiMe$_3$)$_2$ (0.2 g, 1 mmol), TMEDA (0.15 mL, 1 mmol) and furan (0.07 mL, 1 mmol) was added. The resultant cloudy solution was gently heated for 5 minutes and allowed to cool to room temperature where upon it deposited a crop of large colourless crystals (0.07g, 48%). Repeating the reaction but allowing the solution to stir at room temperature for 12 hours, afforded a white solid that be isolated in a higher yield (0.11g, 75%) this solid analysed the same as the crystalline modification; M.p. 189°C (decomp).

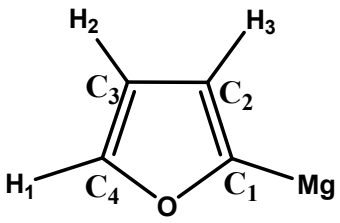

Furyl A

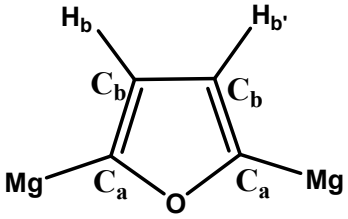

Furyl B

Numbering Scheme for furyl ring units in 50

^{1}H NMR (500MHz, d$_8$-THF, 300K): δ7.61 (s (br), 10H, H$_3$-furyl A), 6.37 (t, 10H, H$_2$-furyl A), 6.29 (s, 12H H$_{b+b'}$ furyl B), 6.12 (s (br), 10H, H$_1$-furyl A), 2.30 (s, 24H, C<u>H</u>$_2$, TMEDA), 2.15 (s, 75H, C<u>H</u>$_3$, TMEDA), -0.10 (s, 9H, C<u>H</u>$_3$, CH$_2$SiMe$_3$), -1.62 (s 2H, C<u>H</u>$_2$, CH$_2$SiMe$_3$).

^{13}C NMR (500MHz, d$_8$-THF, 300K): 200.71, 199.82 (C-Mg from C$_1$, furyl A + C$_a$, furyl B) 142.45 (C$_2$, furyl A), 120.54 (C$_b$, furyl B), 119.58 (C$_4$, furyl A), 107.16 (C$_3$, furyl A).

8.43. Synthesis of [(TMEDA)Na(C$_4$H$_3$S)$_3$Mg(TMEDA)] Compound 51

BuNa (0.08 g, 1 mmol) was suspended in 20 mL of dry n-hexane and placed in an ultrasonic bath for 10 minutes to ensure an even dispersion. Next, $Mg(CH_2SiMe_3)_2$ (0.2 g, 1 mmol), was added along with TMEDA (0.31 mL, 2 mmol) to give a colourless, homogeneous clear solution. Thiophene (0.24 mL, 3 mmol) was subsequently added and the resultant light yellow solution allowed to stir at room temperature for 3 hours. The light yellow solution was filtered and the solvent volume reduced slightly under vacuum before storage of the solution in the refrigerator (at 5°C). After 2 weeks a crop of colourless plate crystals were deposited (0.28g, 53%).

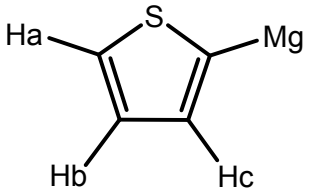

Numbering Scheme for 51

^{1}H NMR (500MHz, d^8-THF, 300K): 7.45 (d, 1H, H_c-thiophene), 7.40 (m, 1H, H_a-thiophene), 7.12 (m, 1H, H_b-thiophene), 2.30 (s, 8H, C$\underline{H}_2$-TMEDA), 2.19 (s, 24H, C$\underline{H}_3$-TMEDA).

8.44. Synthesis of $[\{(TMEDA)Na(\eta^4\text{-}C_5H_7)Na\{OMg(TMP)\}_2(Na_2\eta^3\text{-}\eta^3\text{-}C_5H_7)\}_2]_\infty$.(hexane) Compound 54

TMPH (0.34 mL, 2 mmol) was added to a suspension of BuNa (0.08 g, 1 mmol) in dry n-hexane (20 mL) and the resultant mixture was allowed to stir at room temperature for 1 hour. Next, $Mg(CH_2SiMe_3)_2$ (0.20 g, 1 mmol) and TMEDA (0.15 mL, 1 mmol) to give a clear light yellow solution. Pyran (0.09 mL, 1 mmol) was added and the resultant orange brown solution was allowed to stir at room temperature for 4 days. The brown solution was filtered and the solvent volume reduced under vacuum. Storage of the solution at room temperature allowed light brown needle crystals to grow. Unfortunately no yield was obtained for complex **54** due to poor reproducibility.

^{1}H NMR (500MHz, d$_8$-THF, 300K): 6.33 (m, H, two overlapping resonances of C_5H_7) 3.53 (m, H, C_5H_7) 3.47 (m br, H, C_5H_7), 2.31 (s, H, C$\underline{H}_2$-TMEDA), 2.15 (s, H, C$\underline{H}_3$-TMEDA), 1.69 (m, H, γ-C$\underline{H}_2$-TMP), 1.29 (m, H, β-C$\underline{H}_2$-TMP) and 1.06 (s, H, C$\underline{H}_3$-TMP).

Future Work

Looking to the future the synergic sodium-manganese(II) alkyl-amido base [(TMEDA)Na(TMP)(CH_2SiMe_3)Mn(TMP)] **16**, needs further investigation with a more substantial and varied range of organic substrates to gain a better understanding of its synthetic utility. For example functionalised aromatic substrates containing functional groups of molecules such as alcohols, aldehydes, esters, ketones, acetanilides, nitriles, and carboxylic acids could be tested as well as a range of heteroaromatic (pyridines, pyrimidines etc.) substrates. Initial results within this research project have shown that the manganated products can be used in the synthetically invaluable procedure of carbon-carbon bond formation both with (catalytically) and without a Pd catalyst. The latter observation is especially significant as it could lead to more efficient cross-coupling with, aryl halides, which is why mechanistic studies should be carried out in the future to ascertain how the methodology can be tuned and improved. This poses the intriguing question, "could AMM*Mn* rival established methods such as Negishi, Stille or Suzuki-Miyaura coupling?"

During the investigations of the manganese base **16**, we developed a new isostructural magnesium base [(TMEDA)Na(TMP)(CH_2SiMe_3)Mg(TMP)] **28**. Used mainly as a substitute base for comparison purposes towards the end of the research project it displayed near-identical reactivity to that of manganate **16**. Clearly the reactive potential of **28** needs to be fully investigated which could constitute a full research project on its own

Turning to the inverse crown work, it has been shown that the transition metal Mn(II) can be incorporated into such frameworks playing host to various guest molecules from the hydride to the more complex *n*-butoxide and benzene. It would be advantageous to continue to investigate the range of different guests that can be placed into these inverse crown frameworks as well as increasing ring sizes which might lead to interesting magnetic properties.

The unique, unexpected synergic cleavage of THF, tetrahydrothiophene and THP needs further examination to try and decipher the precise reaction mechanisms that lead to the

cleave and capture of the reactive substrate fragments produced during these complex reactions. The reaction would also benefit from a full reactivity study on a wider range of ethereal based substrates to see if similar cleavage products can be obtained. Further development of the chiral magnesium base [{(-)sparteine}Na(TMP)(CH_2SiMe_3)Mg(TMP)] **48** with a wider range of prochiral substrates such as the ketones 4-*t*butylcyclohexanone or 2,6-dimethylcyclohexanone is needed to establish whether it could have synthetic use in enantiomeric deprotonation reactions.

Recently, we have found within our group that changing the alkali-metal partner in these mixed-metal base systems can have a significant effect on the reactivity leading to new interesting complexes. To date manganese has only been paired with either lithium or sodium, with no reactivity studies at all conducted with the heavier alkali-metal potassium. This virgin territory of the possibility of potassium-mediated manganation could lead to new and exciting chemistries and structures as well as to polymanganese complexes, which would be extremely interesting from a magnetic perspective.

A new avenue of investigation that comes to light with using the transition metal ion Mn(II) is the prospect of interesting magnetochemistry. A major aim in this regard, highlighted previously, is the synthesis of polymanganese complexes. If complexes can be made where the metal centres are in close proximity to each other or joined by a small bridging ligand then potentially multiple interactions could occur and thus interesting magnetic behaviour could be obtained.

The most challenging aim of the future project would be to make AMM*Mn* reactions catalytic. The sequence of amide to amine to amide may be an important factor in such an ambitious task.

References:

[1] R. E. Mulvey, F. Mongin, M. Uchiyama, Y. Kondo, *Angew. Chem. Int. Ed.* **2007**, *46*, 3802.
[2] J. Clayden, *Organolithiums: Selectivity for Synthesis, Vol. 23*, Pergamon, Oxford, **2002**.
[3] J. A. Wanklyn, *Ann.* **1858**, *108*, 67.
[4] G. Wittig, F. Bickelhaupt, *Chem. Ber.* **1958**, *91*, 865.
[5] E. Weiss, U. Schumann, *Angew. Chem.* **1988**, *100*, 573.
[6] G. Wittig, F. J. Meyer, G. Lange, *Justus Liebigs Ann. Chem.* **1951**, *571*, 167.
[7] G. Wittig, *Angew. Chem.* **1958**, *70*, 65.
[8] H. Awad, F. Mongin, F. Trecourt, G. Queguiner, F. Marsais, F. Balanco, B. Abarca, R. Ballesteros, *Tetrahedron Lett.* **2004**, *45*, 6697.
[9] O. Bayh, H. Awad, F. Mongin, C. Hoarau, F. Trecourt, G. Queguiner, F. Marsais, F. Blanco, B. Abarca, R. Ballesteros, *Tetrahedron* **2005**, *61*, 4779.
[10] H. Awad, F. Mongin, F. Trecourt, G. Queguiner, F. Marsais, *Tetrahedron Lett.* **2004**, *45*, 7873.
[11] F. Mongin, A. Bucher, J. P. Bazureau, O. Bayh, H. Awad, F. Trecourt, *Tetrahedron Lett.* **2005**, *46*, 7989.
[12] L. Lochmann, J. Petranek, *Tetrahedron Lett.* **1991**, 32.
[13] L. Lochmann, J. Popisil, D. Lim, *Tetrahedron Lett.* **1966**, 257.
[14] M. Schlosser, *J. Organomet. Chem.* **1967**, *8*, 9.
[15] L. Lochmann, *Eur. J. Inorg. Chem.* **2000**, 1115.
[16] M. Schlosser, *Mod. Synth. Methods* **1992**, *6*, 227.
[17] M. Schlosser, S. Strunk, *Tetrahedron Lett.* **1984**, *25*, 741.
[18] M. Schlosser, *Pure Appl. Chem.* **1988**, *60*, 1627.
[19] M. Schlosser, *Angew. Chem. Int. Ed.* **2005**, *44*, 376.
[20] G. Katsoulos, S. Takagishi, M. Schlosser, *Synlett* **1991**, 731.
[21] M. Schlosser, J. H. Choi, S. Takagishi, *Tetrahedron* **1990**, *46*, 5633.
[22] P. Caubére, *Chem. Rev.* **1993**, *93*, 2317.
[23] P. Gros, Y. Fort, *Eur. J. Org. Chem.* **2002**, 3375.
[24] A. Krasovskiy, P. Knochel, *Angew. Chem. Int. Ed.* **2004**, *43*, 3333.
[25] H. Ren, A. Krasovskiy, P. Knochel, *Chem. Commun.* **2005**, 543.
[26] H. Ren, A. Krasovskiy, P. Knochel, *Org. Lett.* **2004**, *6*, 4215.
[27] A. Krasovskiy, V. Krasovskaya, P. Knochel, *Angew. Chem. Int. Ed.* **2006**, *45*, 2958.
[28] P. Garcia-Álvarez, D. V. Graham, E. Hevia, A. R. Kennedy, J. Klett, R. E. Mulvey, C. T. O'Hara, S. Weatherstone, *Angew. Chem. Int. Ed.* **2008**, *47*, 8079.
[29] Y. Kondo, M. Fujinami, M. Uchiyama, T. Sakamoto, *J. Chem. Soc., Perkin Trans.* **1997**, *1*, 799.
[30] Y. Kondo, N. Takazawa, C. Yamazaki, T. Sakamoto, *J. Org. Chem.* **1994**, *59*, 4717.
[31] M. Uchiyama, M. Kameda, O. Mishima, N. Yokoyama, M. Koike, Y. Kondo, T. Sakamoto, *J. Am. Chem. Soc.* **1998**, *120*, 4934.
[32] Y. Kondo, T. Komine, M. Fujinami, M. Uchiyama, T. Sakamoto, *J. Comb. Chem.* **1999**, *1*, 123.
[33] Y. Kondo, M. Shilai, M. Uchiyama, T. Sakamoto, *J. Am. Chem. Soc.* **1999**, *121*, 3539.

[34] A. R. Kennedy, R. E. Mulvey, R. B. Rowlings, *J. Am. Chem. Soc.* **1998**, *120*, 7816.
[35] A. R. Kennedy, R. E. Mulvey, R. B. Rowlings, *Angew. Chem. Int. Ed.* **1998**, *37*, 3180.
[36] A. R. Kennedy, R. E. Mulvey, C. L. Raston, B. A. Robertson, R. B. Rowlings, *Chem. Commun.* **1999**, 353.
[37] G. C. Forbes, A. R. Kennedy, R. E. Mulvey, R. B. Rowlings, W. Clegg, S. T. Liddle, C. C. Wilson, *Chem. Commun.* **2000**, 1759.
[38] A. R. Kennedy, J. G. Mac Lellan, R. E. Mulvey, *Acta Cryst.* **2003**, *C59*, m302.
[39] K. J. Drewette, K. W. Henderson, A. R. Kennedy, R. E. Mulvey, C. T. O'Hara, R. B. Rowlings, *Chem. Commun.* **2002**, 1176.
[40] J. D. Gallagher, K. W. Henderson, A. R. Kennedy, C. T. O'Hara, R. E. Mulvey, R. B. Rowlings, *Chem. Commun.* **2002**, 376.
[41] P. C. Andrikopoulos, D. R. Armstrong, A. R. Kennedy, C. T. O'Hara, R. B. Rowlings, R. E. Mulvey, *Chem. Commun.* **2002**, 3354.
[42] D. R. Armstrong, A. R. Kennedy, R. E. Mulvey, R. B. Rowlings, *Angew. Chem. Int. Ed.* **1999**, *38*, 131.
[43] P. C. Andrikopoulos, D. R. Armstrong, D. V. Graham, E. Hevia, A. R. Kennedy, R. E. Mulvey, C. T. O'Hara, C. Talmard, *Angew. Chem. Int. Ed.* **2005**, *44*, 3459.
[44] C. D. Broaddus, *J. Org. Chem.* **1970**, *35*, 10.
[45] C. D. Broaddus, *J. Am. Chem. Soc.* **1966**, *88*, 4174.
[46] E. Hevia, J. D. Gallagher, A. R. Kennedy, R. E. Mulvey, C. T. O'Hara, C. Talmard, *Chem. Commun.* **2004**, 2422.
[47] F. Rebiere, O. Samuel, H. B. Kagen, *Tetrahedron Lett.* **1990**, *31*, 3121.
[48] I. R. Butler, W. R. Cullen, J. Ni, S. J. Rettig, *Organometallics* **1985**, *3*, 2196.
[49] W. Clegg, K. W. Henderson, A. R. Kennedy, R. E. Mulvey, C. T. O'Hara, R. B. Rowlings, D. M. Tooke, *Angew. Chem. Int. Ed.* **2001**, *40*, 3902.
[50] P. C. Andrikopoulos, D. R. Armstrong, W. Clegg, C. J. Gilfillan, E. Hevia, A. R. Kennedy, R. E. Mulvey, C. T. O'Hara, D. M. Tooke, J. A. Parkinson, *J. Am. Chem. Soc.* **2004**, *126*, 11612.
[51] P. C. Andrikopoulos, D. R. Armstrong, H. R. L. Barley, W. Clegg, E. Hevia, G. W. Honeyman, A. R. Kennedy, R. E. Mulvey, *J. Am. Chem. Soc.* **2005**, *127*, 6184.
[52] H. Gilman, R. L. Bebb, *J. Am. Chem. Soc.* **1939**, *61*, 109.
[53] E. Baston, R. Maggi, F. Friedrich, M. Schlosser, *Eur. J. Org. Chem.* **2001**, 3985.
[54] J. Garcia-Alvarez, D. V. Graham, A. R. Kennedy, R. E. Mulvey, S. Weatherstone, *Chem. Commun.* **2006**, *30*, 3208.
[55] J. Garcia-Alvarez, A. R. Kennedy, J. Klett, R. E. Mulvey, *Angew. Chem. Int. Ed.* **2007**, *46*, 1105.
[56] L. M. Carrella, W. Clegg, D. V. Graham, L. M. Hogg, A. R. Kennedy, J. Klett, R. E. Mulvey, E. Rentschler, L. Russo, *Angew. Chem. Int. Ed.* **2007**, *46*, 4662.
[57] G. Wittig, G. Fuhrmann, *Chem. Ber.* **1940**, 1197.
[58] G. C. Hartung, V. Snieckus, (Ed.: D. Astruc), Wiley-VCH, New York, **2002**, p. 330.
[59] E. Anctil, V. Snieckus, in *Metal Catalysed Cross-Coupling Reactions*, 2 ed., Wiley-VCH, Weinheim, **2004**, p. 761.
[60] *Ullman's Encyclopedia of Industrial Chemistry, Vol. 20*, 6th ed., Wiley-VCH, Weinheim, Germany, **2003**.

[61] For selected examples see a) L. Main, B. K. Nicholson, *Adv. Met-Org. Chem.* **1994**, *3*, 1. b) T. C. Flood in *Comprehensive Organometallic Chemistry*, *Vol. 6*, Permagon, Oxford, **1995**, pp.21-82.
[62] R. A. Layfield, *Chem. Soc. Rev.* **2008**, *37*, 1098.
[63] H. Gilman, J. C. Bailie, *J. Org. Chem.* **1937**, *2*, 84.
[64] H. Gilman, R. J. Kirby, *J. Am. Chem. Soc.* **1941**, *63*, 2046.
[65] G. Wilkinson, F. A. Cotton, *Chem. Ind. (London)* **1954**, *11*, 307.
[66] G. Wilkinson, F. A. Cotton, J. M. Birmingham, *J. Inorg. Nucl. Chem.* **1956**, *2*, 95.
[67] N. Long, *Metallocenes: an Introduction to Sandwich Complexes*, Blackwell Science Ltd., London, **1998**.
[68] H. Sitzmann, *Coord. Chem. Rev.* **2001**, *214*, 287.
[69] G. Balazs, F. G. N. Cloke, A. Harrison, P. B. Hitchcock, J. Green, O. T. Summerscales, *Chem. Commun.* **2007**, 873.
[70] C. S. Aluarez, A. Bashall, A. D. Bond, D. Cave, E. A. Harron, R. A. Layfield, M. McPartlin, J. M. Rawson, P. T. Wood, D. S. Wright, *Dalton Trans.* **2003**, 3002.
[71] C. S. Aluarez, A. D. Bond, E. A. Harron, R. A. Layfield, J. A. McAllister, C. M. Pask, J. M. Rawson, D. S. Wright, *Organometallics* **2001**, *20*, 4135.
[72] G. Cahiez, C. Duplais, J. Buendia, *Chem. Rev.* **2009**, *109*, 1434.
[73] J. F. Normant, G. Cahiez, in *Modern Synthetic Methods, Vol. 3* (Ed.: R. Scheffold), Verlag, Frankfurt-am-Main, **1983**, pp. 173.
[74] G. Cahiez, S. Marquais, *Synlett* **1993**, 45.
[75] G. Cahiez, S. Marquais, *Pure Appl. Chem.* **1996**, *68*, 53.
[76] G. Cahiez, S. Marquais, *Tetrahedron Lett.* **1996**, *37*, 1773.
[77] G. Cahiez, J. F. Normant, *Tetrahedron Lett.* **1977**, *38*, 3383.
[78] G. Cahiez, G. Friour, A. Alexakis, J. F. Normant, *Bull. Chem. Soc. Chim. Fr.* **1979**, 515.
[79] M. Taniguchi, H. Fujii, K. Oshima, K. Utimoto, *Tetrahedron Lett.* **1992**, *33*, 4353.
[80] M. Taniguchi, H. Fujii, K. Oshima, K. Utimoto, *Bull. Chem. Soc. Jpn.* **1994**, *67*, 2514.
[81] M. Tamura, J. Kochi, *J. Organomet. Chem* **1971**, *29*, 111.
[82] N. H. Buttrus, C. Eaborn, P. B. Hitchcock, J. D. Smith, A. C. Sullivan, *J. Chem. Soc., Chem. Commun.* **1985**, 1380.
[83] R. A. Andersen, E. Carmona-Guzman, J. F. Gibson, G. Wilkinson, *J. Chem. Soc., Dalton Trans.* **1976**, 2204.
[84] S. Gambarotta, C. Floriani, A. Chiesi-Villa, C. Guastini, *Chem. Commun.* **1983**, 1128.
[85] C. G. Howard, G. Wilkinson, M. Thornton-Pett, M. B. Hursthouse, *J. Chem. Soc., Dalton Trans.* **1983**, 2025.
[86] C. G. Howard, G. S. Girolami, G. Wilkinson, M. Thornton-Pett, M. B. Hursthouse, *J. Chem. Soc., Dalton Trans.* **1983**, 2631.
[87] G. S. Girolami, C. G. Howard, G. Wilkinson, H. M. Dawes, M. Thornton-Pett, M. Motevalli, M. B. Hursthouse, *J. Chem. Soc., Dalton Trans.* **1985**, 921.
[88] K. Maruyama, T. Ito, A. Yamamoto, *Bull. Chem. Soc. Jpn.* **1979**, *52*, 849.
[89] G. S. Girolami, G. Wilkinson, A. M. R. Galas, M. Thornton-Pett, M. B. Hursthouse, *J. Chem. Soc., Dalton Trans.* **1985**, 1339.
[90] B. L. Small, M. Brookhart, A. A. Bennet, *J. Am. Chem. Soc.* **1998**, *120*, 4049.
[91] B. L. Small, M. Brookhart, *J. Am. Chem. Soc.* **1998**, *120*, 7143.
[92] V. C. Gibson, S. K. Spitzmesser, *Chem. Rev.* **2003**, *103*, 283.

[93] J. Campora, C. M. Perez, A. Rodriguez-Delgado, A. M. Naz, P. Palma, E. Alvarez, *Organometallics* **2007**, *26*, 1104.
[94] V. Riollet, E. A. Quadrelli, C. Coperet, J. M. Basset, R. A. Andersen, K. Kohler, R. M. Bottcher, E. Herdtweck, *Chem. Eur. J.* **2005**, *11*, 7358.
[95] R. A. Bartlett, M. M. Olmstead, P. P. Power, S. C. Shoner, *Organometallics* **1988**, *7*, 1801.
[96] R. J. Morris, G. S. Girolami, *J. Am. Chem. Soc.* **1988**, *110*, 6245.
[97] R. J. Morris, G. S. Girolami, *Organometallics* **1989**, *8*, 1478.
[98] K. Oshima, *J. Organomet. Chem* **1999**, *575*, 1.
[99] M. Hojo, H. Harada, H. Ito, A. Hosomi, *Chem. Commun.* **1997**, *21*, 2077.
[100] R. A. Layfield, S. M. Humphrey, *Angew. Chem. Int. Ed.* **2004**, *43*, 3067.
[101] S. H. Wunderlich, M. Kienle, P. Knochel, *Angew. Chem. Int. Ed.* **2009**, *48*, 7256.
[102] G. Cahiez, A. Alexakis, J. F. Normant, *Synth. Commun.* **1979**, *9*, 639.
[103] B. D. Murray, P. P. Power, *Inorg. Chem.* **1984**, *23*, 4584.
[104] G. C. Forbes, A. R. Kennedy, R. E. Mulvey, P. J. A. Rodger, R. B. Rowlings, *J. Chem. Soc., Dalton Trans.* **2001**, 1477.
[105] R. A. Andersen, E. Carmona-Guzman, J. F. Gibson, G. Wilkinson, *Chem. Commun.* **1976**, 1369.
[106] W. Bunder, E. Weiss, *Z. Naturforsch., B: Chem. Sci.* **1978**, *33*, 1235.
[107] R. Fischer, H. Gorls, M. Friedrich, M. Westerhausen, *J. Org. Chem.* **2008**.
[108] It is mentioned in ref 83 that the structure of [$\{Mn(CH_2CMe_3)_2\}_4$] is tetrameric as found by x-ray diffraction study, though no details are given.
[109] P. R. Markies, G. Schat, O. S. Akkerman, F. Bickelhaupt, W. J. J. Smeets, A. J. M. Duisenberg, A. L. Spek, *J. Organomet. Chem.* **1989**, *375*, 11.
[110] R. E. Mulvey, Unpublished Results, **2009**.
[111] S. C. Bart, E. J. Hawrelak, A. K. Schmisseur, E. Lobkovsky, P. J. Chirik, *Organometallics* **2004**, *23*, 237.
[112] B. Tecle', A. F. M. M. Rahman, J. P. Oliver, *J. Organomet. Chem.* **1986**, *317*, 267.
[113] P. Sobota, J. Utko, S. Szafert, Z. Janas, T. Glowiak, *J. Chem. Soc., Dalton Trans.,* **1996**, 3469.
[114] T. Komuro, H. Kawaguchi, K. Tatsumi, *Inorg. Chem.* **2002**, *41*, 5083.
[115] A. Panda, M. Stender, M. M. Olmstead, P. Klavins, P. P. Power, *Polyhedron* **2003**, *22*, 67.
[116] S. C. Shoner, P. P. Power, *Inorg. Chem.* **1991**, *31*, 1001.
[117] J. C. Barnes, *Acta Crystallogr., Sect. E: Struct. Rep. Online* **2004**, *E60*, m971.
[118] M. J. Almond, M. P. Beer, M. G. B. Drew, D. A. Rice, *J. Organomet. Chem.* **1991**, *421*, 129.
[119] R. Taube, H. Windisch, S. Maiwald, H. Hemling, H. Schumann, *J. Organomet. Chem.* **1996**, *513*, 49.
[120] L. F. Sanchez-Barba, D. L. Hughes, S. M. Humphrey, M. Bochmann, *Organometallics* **2005**, *24*, 5329.
[121] S. Fokken, F. Reichwald, T. P. Spaniol, J. Okuda, *J. Organomet. Chem.* **2002**, *663*, 158.
[122] J. I. Davies, C. G. Howard, A. C. Skapski, G. Wilkinson, *Chem. Commun.* **1982**, 1077.
[123] P. Crewdson, S. Gambarotta, G. P. A. Yap, L. K. Thompson, *Inorg. Chem.* **2003**, *42*, 8579.
[124] H. Burger, U. Wannagat, *Monatsh. Chemie* **1964**, *95*, 1099.
[125] J. J. Ellison, P. P. Power, S. C. Schoner, *J. Am. Chem. Soc.* **1989**, *111*, 8044.

[126] P. G. Eller, D. C. Bradley, M. B. Hursthouse, D. W. Meek, *Coord. Chem. Rev.* **1977**, *24*, 1.
[127] D. C. Bradley, M. B. Hursthouse, K. M. A. Malik, R. Moseler, *Transition Met. Chem.* **1978**, *3*, 253.
[128] D. C. Bradley, M. B. Hursthouse, A. A. Ibrahim, K. M. A. Malik, M. Motevalli, R. Moseler, H. Powell, J. D. Runnacles, A. C. Sullivan, *Polyhedron* **1990**, *9*, 2959.
[129] E. Solari, F. Musso, E. Gallo, C. Floriani, *Organometallics* **1995**, *14*, 2265.
[130] M. C. Bohm, R. D. Ernst, R. Gleiter, D. R. Wilson, *Inorg. Chem.* **1982**, *22*, 3851.
[131] D. K. Kennepohl, S. Brooker, G. M. Sheldrick, H. W. Roesky, *Z. Naturforsch., B: Chem. Sci.* **1991**, *47b*, 9.
[132] M. P. Mingos, P. Knochel, in *Comprehensive Organometallic Chemistry III, Vol. 2*, Wiley-VCH, Weinheim, Germany, **2005**, p. 541.
[133] B. D. Murray, H. Hope, P. P. Power, *J. Am. Chem. Soc.* **1985**, *107*, 169.
[134] H. J. Gosink, H. W. Roesky, H. G. Schmidt, M. Noltemeyer, E. Irmer, R. Herbst-Irmer, *Organometallics* **1994**, *13*, 3420.
[135] E. Hevia, G. W. Honeyman, A. R. Kennedy, R. E. Mulvey, *J. Am. Chem. Soc.* **2005**, *127*, 13106.
[136] B. Jacques, M. Chavarot, F. Rose-Munch, E. Rose, *Angew, Chem. Int. Ed.* **2006**, *45*, 3481.
[137] M. A. O. Volland, S. Kudis, G. Helmchen, I. Hyla-Kryspin, F. Rominger, R. Gleiter, *Organometallics* **2001**, *20*, 227.
[138] B. Jacques, A. Chanaewa, M. Chavarot-Kerlidou, F. Rose-Munch, E. Rose, H. Gerard, *Organometallics* **2008**, *27*, 626.
[139] J. Zabicky, *The Chemistry of Metal Enolates*, Wiley, **2009**.
[140] E. Hevia, K. W. Henderson, A. R. Kennedy, R. E. Mulvey, *Organometallics* **2006**, *25*, 1778.
[141] L. Alig, J. Alsen, M. Andjelkovic, S. Bendels, A. Benardeau, K. Bleicher, A. Bourson, P. David-Pierson, W. Guba, S. Hildbrand, D. Kube, T. Lubbers, A. V. Mayweg, R. Narquizian, W. Neidhart, M. Nettekoven, J. Plancher, C. Rocha, M. Rogers-Evans, S. Rover, G. Schneider, S. Taylor, P. Waldmeier, *J. Med. Chem.* **2008**, *51*, 2115.
[142] Shagufta, A. K. Srivastava, R. Sharma, R. Mishra, A. K. Balapure, P. S. R. Murthy, G. Panda, *Bioinorganic and Medicinal Chemisrty* **2006**, *14*, 1497.
[143] A. S. Kalgutkar, K. R. Kozak, B. C. Crews, G. P. Hochgesang, L. J. Marnett, *J. Med. Chem.* **1998**, *41*, 4800.
[144] D. V. Graham, R. E. Mulvey, Unpublished results.
[145] G. Honeyman, R. E. Mulvey, Unpublished results.
[146] R. S. Laufer, G. I. Dmitrienko, *J. Am. Chem. Soc.* **2002**, *124*, 1854.
[147] N. Ackerley, A. G. Brewster, G. R. Brown, D. S. Clarke, A. J. Foubister, S. J. Griffin, J. A. Hudson, M. J. Smithers, P. R. O. Whittamore, *J. Med. Chem.* **1995**, *38*, 1608.
[148] P. Bowles, J. Clayden, M. Helliwell, C. McCarthy, M. Tomkinson, N. Westlund, *J. Chem. Soc., Perkin Trans.* **1997**, *1*, 2607.
[149] Related examples are also extremly rare in cyclomanganation(I) chemsirty, see W. Truly, L. Martin, B. K. Nicholson, *J. Organomet. Chem.***1995**, *503*, 75; M. Pfeffer, E. P. Urriolabeitia, J. Fischer, *Inorg. Chem*, **1995**, *34*, 643.
[150] C. K. Green, T. P. Hanusa, A. L. Rheingold, *Organometallics* **2007**, *26*, 1643.
[151] D. Noboto, M. Uchiyama, *J. Org. Chem.* **2008**, 1117.

[152] Y. Kondo, J. V. Morey, J. C. Morgan, H. Naka, D. Hiroshi, P. R. Raithby, M. Uchiyama, A. E. H. Wheatley, *J. Am. Chem. Soc.* **2007**, *129*, 12734.
[153] M. Uchiyama, Y. Matsumoto, D. Noboto, T. Furuyama, K. Morokuma, *J. Am. Chem. Soc.* **2006**, *128*, 8748.
[154] M. Uchiyama, Y. Matsumoto, S. Usui, Y. Hashimoto, K. Morokuma, *Angew. Chem., Int. Ed.* **2007**, *46*, 926.
[155] W. Clegg, B. Conway, P. Garcia-Alvarez, A. R. Kennedy, R. E. Mulvey, L. Russo, J. Sassmannshausen, T. Tuttle, *Chem. Eur. J.* **2009**, *15*, 10702.
[156] A. Keys, T. J. Barbarich, S. G. Bott, A. R. Barron, *J. Chem. Soc., Dalton Trans.* **2000**, 577.
[157] G. Cahiez, E. Riguet, M. Alami, *J. Organomet. Chem* **2001**, *624*, 376.
[158] G. Cahiez, F. Lepifre, P. Ramiandrasoa, *Synthesis* **1999**, 2138.
[159] J. Clayden, in *Organolithiums: Selectivity in Synthesis, Vol. 23*, Pergamon, Oxford, **2002**, pp. 80.
[160] D. R. Armstrong, W. Clegg, S. H. Dale, E. Hevia, A. R. Kennedy, R. E. Mulvey, C. T. O'Hara, C. Talmard, *Angew. Chem. Int. Ed.* **2005**, *44*, 3459.
[161] D. R. Armstrong, J. Garcia-Alvarez, D. V. Graham, G. W. Honeyman, E. Hevia, A. R. Kennedy, R. E. Mulvey, *Chem. Eur. J.* **2009**, *15*, 3800.
[162] A. A. Morton, E. L. Little, W. O. Strong, *J. Am. Chem. Soc.* **1943**, *65*, 1339.
[163] C. D. Boaddus, *J. Org. Chem.* **1970**, *35*, 10.
[164] W. Clegg, G. C. Forbes, A. R. Kennedy, R. E. Mulvey, S. T. Liddle, *Chem. Commun.* **2003**, 406.
[165] B. Yearwood, S. U. Ghazi, M. J. Heeg, N. Richardson, J. P. Oliver, *Organometallics* **2000**, *19*, 865.
[166] I. Wharf, M. G. Simard, *J. Organomet. Chem.* **1997**, *532*, 1.
[167] J. Ito, H. Nishiyama, *Eur. J. Inorg. Chem.* **2007**, 1114.
[168] T. Yagyu, J. Ohashi, M. Maeda, *Organometallics* **2007**, *26*, 2383.
[169] K. H. Chan, W. K. Leong, K. H. G. Mak, *Organometallics* **2006**, *25*, 250.
[170] F. Zhang, C. W. Kirby, D. W. Hairsine, M. C. Jennings, R. J. Puddephatt, *J. Am. Chem. Soc.* **2005**, *127*, 14196.
[171] A. A. Morton, J. B. Davidson, T. R. P. Gibb, E. L. Little, E. W. Clarke, A. G. Green, *J. Am. Chem. Soc.* **1942**, *64*, 2250.
[172] R. L. Thompson, S. Lee, A. L. Reingold, N. J. Cooper, *Organometallics* **1991**, *10*, 1657.
[173] J. A. Reingold, K. L. Virkaitis, G. B. Carpenter, S. Sun, D. A. Sweigart, P. T. Czech, K. R. Overly, *J. Am. Chem. Soc.* **2005**, *127*, 11146.
[174] W. Clegg, S. H. Dale, E. Hevia, L. M. Hogg, G. W. Honeyman, R. E. Mulvey, C. T. O'Hara, *Angew. Chem., Int. Ed.* **2006**, *45*, 6548.
[175] A. V. Protchenko, O. G. Almazova, L. N. Zakharov, G. K. Fukin, Y. T. Struchkov, M. N. Bochkarev, *J. Organomet. Chem.* **1997**, *536*, 457.
[176] C. Kielf, A. Mannschreck, *Synthesis* **1995**, 1033.
[177] J. Betz, F. Hampel, W. Bauer, *Org. Lett.* **2000**, *2*, 3805.
[178] J. Betz, W. Bauer, *J. Am. Chem. Soc.* **2001**, *124*, 8699.
[179] D. A. Shirley, C. F. Cheng, *J. Organomet. Chem.* **1969**, *20*, 251.
[180] G. S. Hair, S. L. Battle, A. Decken, A. H. Cowley, R. A. Jones, *Inorg. Chem.* **2000**, *39*, 27.
[181] H. Schumann, S. Dechert, M. Hummert, K. C. H. Lange, S. Schuttle, B. C. Wassermann, K. Kohler, J. Eichhorn, *Z. Anorg. Allg. Chem.* **2004**, *630*, 1196.

[182] H. Schumann, B. C. Wassermann, S. Schuttle, B. Heymer, S. Nickel, T. D. Seuss, S. Wemik, J. Demtschuk, F. Girgsdies, R. Weimann, *Z. Anorg. Allg. Chem.* **2000**, *626*, 2081.
[183] A. Mannschrek, C. Kiefl, *Synthesis* **1995**, 1033.
[184] E. Wehman, G. van Koten, M. Knotter, H. Spelten, D. Heijdenrijk, A. N. S. Mak, C. H. Stam, *J. Organomet. Chem.* **1987**, *325*, 293.
[185] J. T. B. H. Jastrzebski, G. van Koten, K. Goubitz, C. Arlen, M. Pfeffer, *J. Organomet. Chem.* **1983**, *246*, C75.
[186] M. H. P. Rietveld, I. C. M. Wehmann-Ooyevarr, G. M. Kapteijn, D. M. Grove, W. J. J. Smeets, H. Kooijman, A. L. Spek, G. van Koten, *Organometallics* **1994**, *13*, 3782.
[187] K. Sorger, P. v. R. Schleyer, R. Fleischer, D. Stalke, *J. Am. Chem. Soc.* **1996**, *118*, 6924.
[188] J. Betz, F. Hampel, W. Bauer, *J. Chem. Soc., Dalton Trans.* **2001**, 1876.
[189] J. Mc Murray, *Organic Chemistry*, Fifth ed., International Thomson Computer Press, **2000**.
[190] A. Maercker, *Angew. Chem. Int. Ed.* **1987**, *26*, 972.
[191] J. J. Eisch, W. Kaska, *Chem. and Ind. (London)* **1961**, 470.
[192] J. J. Eisch, *J. Org. Chem.* **1963**, *28*, 707.
[193] A. N. Cherkasov, K. K. Pivnitskii, *Zh. Org. Khim.* **1972**, *8*, 211.
[194] R. E. Mulvey, L. M. Hogg, Unpublished results.
[195] M. L. Hsueh, B. T. Ko, T. Athar, C. C. Lin, T. M. Wu, S. F. Hsu, *Organometallics* **2006**, *25*, 4144.
[196] V. L. Blair, L. M. Carrella, W. Clegg, B. Conway, R. W. Harrington, L. M. Hogg, J. Klett, R. E. Mulvey, E. Rentschler, L. Russo, *Angew. Chem., Int. Ed.* **2008**, *47*, 6208.
[197] A. R. Kennedy, J. Klett, R. E. Mulvey, S. Newton, D. S. Wright, *Chem. Commun.* **2008**, 308.
[198] P. C. Andrikopoulos, D. R. Armstrong, A. R. Kennedy, R. E. Mulvey, C. T. O'Hara, R. B. Rowlings, *Eur. J. Inorg. Chem.* **2003**, 3354.
[199] V. E. Antonov, K. Cornell, B. Dorner, V. K. Fedotov, G. Grosse, A. I. Kolesnikov, F. E. Wagner, H. Wipf, *Solid State Commun.* **2000**, *113*, 569.
[200] Manganese hydrides are non-stoichiometric compounds with wide composition ranges. Average distance taken from fcc-Mn-$H_{0.41}$ (1.888 Å) and hcp-Mn-$H_{0.86}$ (1.899 Å).
[201] F. A. Cotton, G. Wilkinson, C. A. Murillo, M. Bochmann, *Advanced Inorganic Chemistry*, 6th ed., Wiley-VCH, Weinheim, **1999**.
[202] J. F. Garcia Alonso, M. G. Sanz, V. Riera, M. A. Ruiz, A. Tiripicchio, M. T. Camellini, *Angew. Chem. Int. Ed.* **1988**, *27*, 1167.
[203] R. Carreno, V. Riera, M. A. Ruiz, C. Bois, Y. Jeannin, *Organometallics* **1992**, *11*, 2923.
[204] R. Carreno, V. Riera, M. A. Ruiz, A. Tiripicchio, M. Tiripicchio-Camellini, *Organometallics* **1994**, *13*, 993.
[205] A. Belforte, F. Calderazzo, U. Englert, J. Strahle, K. Wurst, *J. Chem. Soc., Dalton Trans.* **1991**, 2419.
[206] K. Sanchez, W. Scott, *Organometallics* **1988**, *29*, 139.
[207] For a review on metallocenophanes see: D. E. Herbert, U. F. Mayer, I. Manners, *Angew. Chem. Int. Ed.* **2007**, *46*, 5060.
[208] K. W. Henderson, A. R. Kennedy, R. E. Mulvey, C. T. O'Hara, R. B. Rowlings, *Chem. Commun.* **2001**, 1678.

[209] N. D. R. Barnett, W. Clegg, A. R. Kennedy, R. E. Mulvey, S. Weatherstone, *Chem. Commun.* **2005**, 375.
[210] X. He, B. C. Noll, A. Beatty, R. E. Mulvey, K. W. Henderson, *J. Am. Chem. Soc.* **2004**, *126*, 7444.
[211] B. D. Murray, P. P. Power, *J. Am. Chem. Soc.* **1984**, *106*, 7011.
[212] B. Conway, E. Hevia, A. R. Kennedy, R. E. Mulvey, C. T. O'Hara, S. Weatherstone, *Dalton Trans.* **2005**, *8*, 1532.
[213] D. R. Armstrong, W. Clegg, S. H. Dale, D. V. Graham, E. Hevia, L. M. Hogg, G. W. Honeyman, A. R. Kennedy, R. E. Mulvey, *Chem. Commun.* **2007**, 598.
[214] A. R. Kennedy, J. Klett, R. E. Mulvey, D. S. Wright, *Science* **2009**, *326*, 706.
[215] R. E. Mulvey, *Organometallics* **2006**, *25*, 1060.
[216] R. E. Mulvey, *Acc. Chem. Res.* **2009**, *42*, 743.
[217] M. R. Churchill, J. Wormald, *Chem. Commun.* **1968**, 1217.
[218] C. H. Campbell, M. L. H. Green, *Chem. Commun.* **1970**, 1009.
[219] F. A. L. Anet, O. J. Abrams, *Chem. Commun.* **1970**, 1611.
[220] W. P. Giering, *Chem. Commun.* **1971**, 4.
[221] U. Schollkopf, *Angew. Chem. Int. Ed.* **1970**, *9*, 763.
[222] H. Gilman, B. J. Gaj, *J. Org. Chem.* **1957**, *22*, 1165.
[223] R. B. Bates, L. M. Kroposki, D. E. Potter, *J. Org. Chem.* **1972**, *37*, 560.
[224] J. Clayden, S. A. Yasin, *New J. Chem.* **2002**, *26*, 191.
[225] I. Fleming, S. R. Mack, B. P. Clark, *Chem. Commun.* **1998**, 713.
[226] W. Schlenk, E. Bergmann, *Liebigs Annalen* **1928**, *463*, 77.
[227] L. I. Smith, H. H. Hoehn, *J. Am. Chem. Soc.* **1941**, *63*, 1184.
[228] M. C. Chung, X. Gu, B. A. Etzenhouser, A. M. Spuches, P. T. Rye, S. K. Seetharaman, D. J. Rose, J. Zubieta, M. B. Sponsler, *Organometallics* **2003**, *22*, 3485.
[229] M. Mathew, G. J. Palenik, A. J. Carty, H. N. Paik, *Chem. Commun.* **1974**, 25.
[230] G. Higashihara, M. Terada, A. Inagaki, M. Akita, *Organometallics* **2007**, *26*, 439.
[231] D. M. Norton, D. F. Shriver, *Inorg. Chem.* **2000**, *39*, 5118.
[232] R. J. Restivo, G. Ferguson, *J. Chem. Soc., Dalton Trans.* **1979**, 893.
[233] R. E. Davis, *Chem. Commun.* **1968**, 1218.
[234] M. R. Churchill, J. Wormald, *Inorg. Chem.* **1969**, *8*, 1936.
[235] C. J. Adams, M. I. Bruce, P. A. Humphrey, B. W. Skelton, A. H. White, *Aust. J. Chem.* **2001**, *54*, 325.
[236] M. I. Bruce, B. G. Ellis, B. W. Skelton, A. H. White, *Organometallics* **2005**, *690*, 792.
[237] H. P. Xia, R. C. Y. Yeung, G. Jia, *Organometallics* **1998**, *17*, 4762.
[238] C. W. Shiu, Y. Chi, C. Chung, S. M. Peng, G. H. Lee, *Organometallics* **1998**, *17*, 2970.
[239] R. Diercks, L. Stamp, J. Kopf, H. Dieck, *Angew. Chem. Int. Ed.* **1984**, *23*, 893.
[240] C. J. Lawrie, K. P. Gable, B. K. Carpenter, *Organometallics* **1989**, *8*, 2274.
[241] D. J. Mindiola, R. Waterman, D. M. Jenkins, G. L. Hillhouse, *Inorg. Chim. Acta* **2003**, *345*, 299.
[242] C. J. Lawrie, H. E. Dankosh, B. K. Carpenter, *J. Organomet. Chem* **1991**, *411*, C7.
[243] L. E. Smart, J. Browning, M. Green, A. Laguna, J. L. Spencer, F. G. A. Stone, *J. Chem. Soc., Dalton Trans.* **1977**, 1777.
[244] F. Maassarani, M. Pfeffer, G. Le Borgne, E. Wehman, G. van Koten, *J. Am. Chem. Soc.* **1984**, *106*, 8002.

[245] K. Mochida, M. Akazawa, M. Goto, A. Sekine, Y. Ohashi, Y. Nakadaira, *Organometallics* **1998**, *17*, 1782.
[246] W. Uhl, F. Breher, *J. Organomet. Chem.* **2000**, *608*, 54.
[247] F. Pauer, P. P. Power, *J. Organomet. Chem* **1994**, *474*, 27.
[248] A. J. I. Ashe, J. W. Kampf, P. M. savla, *Organometallics* **1993**, *12*, 3350.
[249] L. Liu, W. X. Zhang, Q. Luo, H. Li, Z. Xi, *Organometallics* **2009**.
[250] R. A. Adams, M. P. Pompeo, W. Wu, J. H. Yamamoto, *J. Am. Chem. Soc.* **1993**, *115*, 8207.
[251] G. N. Glavee, L. M. Daniels, R. J. Angelici, *Organometallics* **1989**, *8*, 1856.
[252] C. Strohmann, T. Seibel, K. Strochfeldt, *Angew. Chem. Int. Ed.* **2003**, *42*, 4531.
[253] C. Strohmann, K. Strochfeldt, D. Schildbach, *J. Am. Chem. Soc.* **2003**, *125*, 13672.
[254] J. C. Kizirian, *Chem. Rev.* **2008**, *108*, 140.
[255] P. O'Brien, *J. Chem. Soc., Perkin Trans. 1* **1998**, 1439.
[256] D. Hoppe, T. Hense, *Angew. Chem. Int. Ed.* **1997**, *36*, 2282.
[257] A. R. Kennedy, C. T. O'Hara, *Dalton Trans.* **2008**, 4975.
[258] B. H. Lipshutz, *Chem. Rev.* **1986**, *86*, 795.
[259] E. Lukevits, O. A. Pudova, *Chem. Heterocycl. Compd.* **1995**, *31*, 377.
[260] E. Lukevits, O. A. Pudova, *Chem. Heterocycl. Compd.* **1995**, *31*, 412.
[261] D. V. Graham, E. Hevia, A. R. Kennedy, R. E. Mulvey, C. T. O'Hara, C. Talmard, *Chem. Commun.* **2006**, 417.
[262] V. Ramanathan, R. Levine, *J. Org. Chem.* **1962**, *27*, 1216.
[263] F. Eymery, P. Burattin, F. Mathey, P. Savignac, *Eur. J. Org. Chem.* **2000**, 2425.
[264] G. Zein, D. Alves, A. L. Braga, H. A. Stefani, C. W. Nogueira, *Tetrahedron Lett.* **2004**, *45*, 4823.
[265] G. Mezei, C. M. Zaleski, V. L. Pecoraro, *Chem. Rev.* **2007**, *107*, 4933.
[266] M. Veith, C. Ruloff, V. Huch, F. Tollner, *Angew. Chem. Int. Ed. Engl.* **1988**, *27*, 1381.
[267] W. Y. Wong, F. L. Ting, W. L. Lam, *J. Chem. Soc., Dalton Trans.* **2001**, 2981.
[268] W. Y. Wong, F. L. Ting, W. L. Lam, *Eur. J. Inorg. Chem.* **2002**, 2103.
[269] D. Himmelreich, G. Muller, *Journal of Organometallic Chemistry* **1985**, *297*, 341.
[270] S. N. Ringelberg, A. Meetsma, S. I. Troyanov, B. Hessen, J. H. Teuben, *Organometallics* **2002**, *21*, 1759.
[271] H. W. Gschwend, H. R. Rodriguez, *Org. React.* **1979**, *26*, 1.
[272] K. L. Jantzi, C. L. Puckett, I. A. Guzei, H. J. Reich, *J. Org. Chem.* **2005**, *70*, 7520.
[273] H. Gilman, D. A. Shirley, *J. Am. Chem. Soc.* **1949**, *71*, 1870.
[274] D. R. Powell, W. L. Whippie, H. J. Reich, *Acta Crystallogr., Sect. C: Cryst. Struct. Commun.* **1996**, *52*, 1346.
[275] C. Selinka, D. Stalke, *Z. Naturforsch., B: Chem. Sci.* **2003**, *58*, 291.
[276] A. L. Speck, N. Veldman, Private Communication, **1999**.
[277] A. L. Speck, Private Communication, **1999**.
[278] A. L. Speck, W. J. J. Smeets, Private Communication, **1999**.
[279] A. L. Speck, M. T. Lakin, R. den Besten, Private Communication, **1999**.
[280] M. Vestergren, B. Gustafsson, O. Davidsson, M. Hakansson, *Angew. Chem. Int. Ed.* **2000**, *39*, 3435.
[281] T. T. Nguyen, F. Chevallier, V. Jouikov, F. Mongin, *Tetrahedron Lett.* **2009**, *50*, 6787.

[282] H. Yasuda, M. Yamauchi, Y. Ohnuma, A. Nakamura, *Bull. Chem. Soc. Jpn.* **1981**, *54*, 1481.
[283] G. J. Heiszwolf, H. Kloosterziel, *Recl. Trav. Chim. Pays-Bas* **1967**, *86*, 807.
[284] H. Kloosterziel, J. A. A. vanDrunen, *Recl. Trav. Chim. Pays-Bas* **1969**, *88*, 1377.
[285] H. Kloosterziel, J. A. A. vanDrunen, *Recl. Trav. Chim. Pays-Bas* **1970**, *89*, 270.
[286] H. Kloosterziel, J. A. A. vanDrunen, *Recl. Trav. Chim. Pays-Bas* **1970**, *89*, 368.
[287] R. D. Ernst, *Acc. Chem. Res.* **1985**, *18*, 56.
[288] J. R. Bleeke, M. K. Hays, R. J. Wittenbrink, *Organometallics* **1988**, *7*, 1417.
[289] C. Kruger, *Angew. Chem.* **1969**, *81*, 708.
[290] A. F. Orchard, *Magnetochemistry*, Oxford University Press, Oxford, **2003**.
[291] C. Krebs, E. Bill, F. Birkelbach, V. Staemmler, unpublished results.
[292] E. Bill, Max-Planck Institute for Bioinorganic Chemistry, Mulheim, http://ewww.mpi-muelheim.mpg.de/bac/logins/bill/julX en.php
[293] D. F. Evans, G. V. Fazakerley, R. F. Phillips, *J. Chem. Soc. A* **1971**, 1931.
[294] D. F. Evans, *J. Chem. Soc.* **1959**, 2003.
[295] E. Velez, A. Alberola, V. Polo, *J. Phys. Chem. A* **2009**, *113*, 14008.
[296] M. D. Fryzuk, D. B. Leznoff, S. J. Rettig, R. C. Thompson, *Inorg. Chem.* **2004**, *33*, 5528.
[297] W. L. F. Armarego, D. D. Perrin, *Purification of Laboratory Chemicals, Vol. 4*, Oxford, **1996**.
[298] B. E. Love, E. G. Jones, *J. Org. Chem.* **1999**, *64*, 3755.
[299] C. Schade, W. Bauer, P. v. R. Schleyer, *J. Organomet. Chem* **1985**, C25.

Appendix I

Compound	1	2
Chemical formula (total)	$C_8H_{22}MnSi_2$	$C_{14}H_{38}MnN_2Si_2$
Formula weight	229.38	345.58
Crystal system, space group	triclinic, P1	monoclinic, C2/c
a [Å]	5.7011(5)	18.3438(10)
b [Å]	10.5246(12)	9.8222(5)
c [Å]	11.0936(13)	12.5923(7)
α [°]	106.652(12)	90
β [°]	100.101(11)	107.800(3)
γ [°]	92.256(12)	90
Cell volume [$Å^3$]	625.00(12)	2160.2(2)
Z	2	4
D_c, g cm^{-3}	1.219	1.063
μ, mm^{-1}	1.199	0.715
T, K	150	123
θ_{max}	25	30
Reflections collected	7633	16907
Independent reflections	2187	3146
R_{int}	0.0231	0.044
No. refined parameters	106	100
Final R indices [$F^2>2\sigma$]	R1 = 0.0221, wR2 = 0.0531	R1 = 0.0330, wR2 = 0.0701
R indices (all data)	R1 = 0.0275, wR2 = 0.0553	R1 = 0.0587, wR2 = 0.0784
Goodness-of-fit on F^2	1.055	1.053
Max and min residual ρ, e $Å^{-3}$	+0.28, –0.44	+0.33, -0.34

Compound	3	4
Chemical formula (total)	$C_{18}H_{32}MnN_2Si_2$	$C_{20}H_{52}Mn_2O_2Si_4$
Formula weight	387.58	546.86
Crystal system, space group	triclinic, P1	triclinic, P1
a [Å]	12.3232(6)	8.2341(10)
b [Å]	12.5823(6)	10.6831(18)
c [Å]	16.7053(6)	20.141(3)
α [°]	101.911(4)	82.895(16)
β [°]	110.874(4)	88.064(15)
γ [°]	103.379(4)	67.505(12)
Cell volume [$Å^3$]	2232.51(7)	1625.9(4)
Z	4	2
D_c, g cm^{-3}	1.153	1.117
μ, mm^{-1}	0.700	0.936
T, K	123	150
θ_{max}	29.9	25
Reflections collected	43395	18694
Independent reflections	11882	5626
R_{int}	0.0334	0.0418
No. refined parameters	459	293
Final R indices [$F^2>2\sigma$]	R1 = 0.0221, wR2 = 0.0531	R1 = 0.0327, wR2 = 0.0616
R indices (all data)	R1 = 0.0275, wR2 = 0.0553	R1 = 0.0590, wR2 = 0.0695
Goodness-of-fit on F^2	1.094	1.029
Max and min residual ρ, e $Å^{-3}$	+1.49, -0.59	+0.26, -0.23

Compound	5	6
Chemical formula (total)	$C_{12}H_{30}MnO_2Si_2$	$C_{52}H_{74}Mn_2P_2Si_4$
Formula weight	317.48	983.29
Crystal system, space group	monoclinic, C2/c	triclinic, P1
a [Å]	18.118(4)	10.5608(2)
b [Å]	9.849(2)	11.5070(2)
c [Å]	10.870(2)	13.1463(3)
α [°]	90	65.5790(10)
β [°]	99.58(3)	87.4160(10)
γ [°]	90	69.1810(10)
Cell volume [$Å^3$]	1912.7(7)	1349.90(5)
Z	4	1
D_c, g cm^{-3}	1.103	1.210
μ, mm^{-1}	0.81	0.648
T, K	150	123
θ_{max}	27.5	27.49
Reflections collected	10466	12026
Independent reflections	2185	6175
R_{int}	0.0315	0.0255
No. refined parameters	82	293
Final R indices [$F^2>2\sigma$]	R1 = 0.0221, wR2 = 0.0531	R1 = 0.0305, wR2 = 0.0629
R indices (all data)	R1 = 0.0275, wR2 = 0.0553	R1 = 0.0447, wR2 = 0.0680
Goodness-of-fit on F^2	1.098	1.015
Max and min residual ρ, e $Å^{-3}$	+0.36, -0.31	+0.358, -0.268

Compound	11	13
Chemical formula (total)	$C_{72}H_{108}Mn_3N_6$	$C_{79}H_{106}Mn_3O_4Si_6$
Formula weight	1222.46	1416.97
Crystal system, space group	monoclinic, C2/c	monoclinic, $P2_1/n$
a [Å]	21.945(4)	13.9501(2)
b [Å]	14.087(3)	36.4314(6)
c [Å]	24.134(5)	15.4835(2)
α [°]	90	90
β [°]	111.57(3)	90.236(1)
γ [°]	90	90
Cell volume [$Å^3$]	6939(2)	7868(2)
Z	4	4
D_c, g cm^{-3}	1.170	1.196
μ, mm^{-1}	0.581	0.609
T, K	150	123
θ_{max}	27.5	27.49
Reflections collected	20354	161118
Independent reflections	6043	18004
R_{int}	0.0254	0.097
No. refined parameters	411	839
Final R indices [$F^2>2\sigma$]	R1 = 0.0356, wR2 = 0.0814	R1 = 0.0449, wR2 = 0.0840
R indices (all data)	R1 = 0.0555, wR2 = 0.0915	R1 = 0.0881, wR2 = 0.0981
Goodness-of-fit on F^2	1.053	1.011
Max and min residual ρ, e $Å^{-3}$	+0.34, -0.31	+0.640, -0.345

Compound	16	17
Chemical formula (total)	$C_{28}H_{63}MnN_4NaSi$	$C_{31}H_{59}MnN_4NaO$
Formula weight	561.84	581.75
Crystal system, space group	orthorhombic, $Pna2_1$	triclinic, P1
a [Å]	14.8720(4)	10.059(3)
b [Å]	19.3190(6)	11.212(4)
c [Å]	12.0740(3)	15.952(5)
α [°]	90	75.986(5)
β [°]	90	47.632(5)
γ [°]	90	87.910(5)
Cell volume [$Å^3$]	3469.01(17)	1682.3(9)
Z	4	2
D_c, g cm^{-3}	1.076	1.148
μ, mm^{-1}	0.448	0.433
T, K	123	150
θ_{max}	27.48	25
Reflections collected	29475	11833
Independent reflections	7617	5782
R_{int}	0.058	0.0223
No. refined parameters	339	356
Final R indices [$F^2>2\sigma$]	R1 = 0.0482, wR2 = 0.0906	R1 = 0.0393, wR2 = 0.0959
R indices (all data)	R1 = 0.0765, wR2 = 0.1014	R1 = 0.0427, wR2 = 0.0986
Goodness-of-fit on F^2	1.069	1.038
Max and min residual ρ, e $Å^{-3}$	+0.265, -0.212	+0.84, -0.40

Compound	18	20
Chemical formula (total)	$C_{32}H_{63}MnN_4NaOSi$	$C_{34}H_{60}MnN_2O_2Si_2$
Formula weight	625.22	639.96
Crystal system, space group	orthorhombic, $Pca2_1$	triclinic, P1
a [Å]	21.854(4)	9.9826(3)
b [Å]	11.239(3)	10.9135(3)
c [Å]	31.590(8)	20.2736(6)
α [°]	90	100.345(2)
β [°]	90	95.144(2)
γ [°]	90	113.836(2)
Cell volume [$Å^3$]	7759(3)	1954.91(10)
Z	8	2
D_c, g cm^{-3}	1.072	1.087
μ, mm^{-1}	0.409	0.427
T, K	150	123
θ_{max}	22.5	27.09
Reflections collected	17286	39613
Independent reflections	8970	8595
R_{int}	0.0520	0.068
No. refined parameters	1085	405
Final R indices [$F^2>2\sigma$]	R1 = 0.054, wR2 = 0.1299	R1 = 0.0469, wR2 = 0.0859
R indices (all data)	R1 = 0.068, wR2 = 0.1396	R1 = 0.0861, wR2 = 0.1000
Goodness-of-fit on F^2	1.064	1.015
Max and min residual ρ, e $Å^{-3}$	+0.49, -0.29	+0.609, -0.398

Compound	21	22
Chemical formula (total)	$C_{32}H_{62}MnN_5Na$	$C_{36}H_{70}MnN_5Na$
Formula weight	679.62	650.90
Crystal system, space group	monoclinic, C2/c	monoclinic, $P2_1/c$
a [Å]	30.6029(9)	11.678(5)
b [Å]	17.3154(5)	18.378(5)
c [Å]	20.2156(6)	18.413(5)
α [°]	90	90
β [°]	127.677(1)	94.507(5)
γ [°]	90	90
Cell volume [$Å^3$]	8478.4(4)	3940(2)
Z	8	4
D_c, g cm^{-3}	1.065	1.097
μ, mm^{-1}	0.351	3.035
T, K	123	123
θ_{max}	27.48	72.17
Reflections collected	17799	19820
Independent reflections	9676	7358
R_{int}	0.0415	0.1246
No. refined parameters	532	404
Final R indices [$F^2>2\sigma$]	R1 = 0.0594, wR2 = 0.1423	R1 = 0.1198, wR2 = 0.03091
R indices (all data)	R1 = 0.1072, wR2 = 0.1677	R1 = 0.2706, wR2 = 0.3504
Goodness-of-fit on F^2	1.063	0.901
Max and min residual ρ, e $Å^{-3}$	+0.752, -0.394	+0.831, -0.527

Compound	23	24
Chemical formula (total)	$C_{32}H_{61}MnN_4Na$	$C_{34}H_{59}MnN_4Na$
Formula weight	579.78	601.8
Crystal system, space group	monoclinic, $P2_1/m$	orthorhombic, Pbca
a [Å]	9.8615(3)	11.432(4)
b [Å]	15.2591(4)	19.935(7)
c [Å]	11.3910(3)	30.932(10)
α [°]	90	90
β [°]	96.083(2)	90
γ [°]	90	90
Cell volume [$Å^3$]	1704.44	7049(4)
Z	2	8
D_c, g cm^{-3}	1.130	1.134
μ, mm^{-1}	0.425	0.413
T, K	123	150
θ_{max}	27.52	25
Reflections collected	7703	48024
Independent reflections	4056	6130
R_{int}	0.0294	0.055
No. refined parameters	217	452
Final R indices [$F^2>2\sigma$]	R1 = 0.0379, wR2 = 0.0830	R1 = 0.0786, wR2 = 0.1990
R indices (all data)	R1 = 0.0567, wR2 = 0.0900/	R1 = 0.1196, wR2 = 0.2380
Goodness-of-fit on F^2	1.046	1.03
Max and min residual ρ, e $Å^{-3}$	+0.547, -0.338	+0.86, -0.77

Compound	25	26
Chemical formula (total)	$C_{30}H_{54}MnN_3NaOSi$	$C_{35}H_{61}MnN_4NaO$
Formula weight	578.8	631.8
Crystal system, space group	triclinic, P1	monoclinic, C2/c
a [Å]	9.736(3)	32.418(7)
b [Å]	11.466(3)	11.58(3)
c [Å]	15.810(4)	19.770(4)
α [°]	78.302(4)	90
β [°]	79.619(4)	99.003(4)
γ [°]	84.163(4)	90
Cell volume [$Å^3$]	1696.0(7)	7335(3)
Z	2	8
D_c, g cm^{-3}	1.133	1.144
μ, mm^{-1}	0.462	0.402
T, K	150	150
θ_{max}	28.3	28.3
Reflections collected	12089	12721
Independent reflections	5866	6355
R_{int}	0.016	0.021
No. refined parameters	346	362
Final R indices [$F^2>2\sigma$]	R1 = 0.0418, wR2 = 0.1101	R1 = 0.0399, wR2 = 0.0973
R indices (all data)	R1 = 0.0500, wR2 = 0.1180	R1 = 0.0514, wR2 = 0.1045
Goodness-of-fit on F^2	1.03	1.04
Max and min residual ρ, e $Å^{-3}$	+0.70, -0.49	+0.59, -0.36

Compound	28	29
Chemical formula (total)	$C_{28}H_{63}MgN_4NaSi$	$C_{36}H_{64}MgN_5Na$
Formula weight	531.21	614.22
Crystal system, space group	orthorhombic, $Pna2_1$	orthorhombic, $Pna2_1$
a [Å]	14.8470(2)	22.837(4)
b [Å]	19.3770(3)	9.5472(11)
c [Å]	12.0280(4)	17.633(2)
α [°]	90	90
β [°]	90	90
γ [°]	90	90
Cell volume [$Å^3$]	3460.34(14)	3844.5(9)
Z	4	4
D_c, g cm^{-3}	1.020	1.061
μ, mm^{-1}	0.119	0.717
T, K	123	123
θ_{max}	27.50	60.00
Reflections collected	7665	16382
Independent reflections	6037	5450
R_{int}	0.0495	0.0587
No. refined parameters	387	402
Final R indices [$F^2>2\sigma$]	R1 = 0.0495, wR2 = 0.1089	R1 = 0.0671, wR2 = 0.1442
R indices (all data)	R1 = 0.0732, wR2 = 0.1210	R1 = 0.1304, wR2 = 0.1664
Goodness-of-fit on F^2	1.048	0.884
Max and min residual ρ, e $Å^{-3}$	+0.321, -0.167	+0.375, -0.276

Compound	30	31
Chemical formula (total)	$C_{32}H_{61}MgN_4NaO$	$C_{76}H_{148}Mn_4N_8Na_4$
Formula weight	565.15	1485.74
Crystal system, space group	monoclinic, $P2_1/c$	orthorhombic, Pnnm
a [Å]	10.687(2)	9.981(2)
b [Å]	28.579(6)	12.196(2)
c [Å]	11.680(2)	17.249(3)
α [°]	90	90
β [°]	104.11(3)	90
γ [°]	90	90
Cell volume [$Å^3$]	3459.7(12)	2099.7(7)
Z	4	1
D_c, g cm^{-3}	1.085	1.175
μ, mm^{-1}	0.092	0.651
T, K	150	150
θ_{max}	27.6	27.5
Reflections collected	33093	17872
Independent reflections	7945	2669
R_{int}	0.0439	0.0168
No. refined parameters	366	119
Final R indices [$F^2>2\sigma$]	R1 = 0.0483, wR2 = 0.1038	R1 = 0.0234, wR2 = 0.0618
R indices (all data)	R1 = 0.0855, wR2 = 0.1191	R1 = 0.0271, wR2 = 0.0651
Goodness-of-fit on F^2	1.027	1.111
Max and min residual ρ, e $Å^{-3}$	+0.26, -0.18	+0.30, -0.16

Compound	34	36
Chemical formula (total)	$C_{54}H_{82}Fe_3Mn_3N_4Na_2$	$C_{42}H_{86}Mn_2N_4Na_2O_4Si_2$
Formula weight	1165.6	923.19
Crystal system, space group	triclinic, P1	triclinic, P1
a [Å]	10.463(5)	10.949(2)
b [Å]	17.226(9)	11.582(3)
c [Å]	17.454(9)	12.071(3)
α [°]	114.905(6)	72.369(3)
β [°]	103.972(7)	67.101(3)
γ [°]	90.860(7)	84.003(3)
Cell volume [$Å^3$]	2744(2)	1343.8(5)
Z	2	1
D_c, g cm^{-3}	1.411	1.141
μ, mm^{-1}	1.495	0.568
T, K	123	150
θ_{max}	27.5	28.2
Reflections collected	19192	7472
Independent reflections	9412	4469
R_{int}	0.0568	0.0154
No. refined parameters	611	310
Final R indices [$F^2>2\sigma$]	R1 = 0.0659, wR2 = 0.1621	R1 = 0.0378, wR2 = 0.0962
R indices (all data)	R1 = 0.1119, wR2 = 0.1944	R1 = 0.0442, wR2 = 0.1036
Goodness-of-fit on F^2	0.996	1.060
Max and min residual ρ, e $Å^{-3}$	+1.87, -0.94	+0.55, -0.40

Compound	38	42
Chemical formula (total)	$C_{54}H_{108}Mn_2N_8Na_2$	$C_{52}H_{108}Mn_2N_8Na_2$
Formula weight	1025.34	1006.13
Crystal system, space group	monoclinic, $P2_1/n$	monoclinic, $P2_1/n$
a [Å]	8.333(3)	8.2875(3)
b [Å]	22.027(7)	21.6756(9)
c [Å]	16.320(5)	16.5068(7)
α [°]	90	90
β [°]	91.466(5)	90.465(4)
γ [°]	90	90
Cell volume [$Å^3$]	2994.3(17)	2965.2(2)
Z	2	2
D_c, g cm^{-3}	1.137	1.127
μ, mm^{-1}	0.475	0.479
T, K	150	123
θ_{max}	25.0	
Reflections collected	20471	35537
Independent reflections	5207	7821
R_{int}	0.0286	0.0389
No. refined parameters	310	323
Final R indices [$F^2>2\sigma$]	R1 = 0.0770, wR2 = 0.1575	R1 = 0.0549, wR2 = 0.1318
R indices (all data)	R1 = 0.0799, wR2 = 0.1584	R1 = 0.0882, wR2 = 0.1424
Goodness-of-fit on F^2	1.518	1.072
Max and min residual ρ, e $Å^{-3}$	+0.46, -0.76	+0.973, -0.450

Compound	43	44
Chemical formula (total)	$C_{52}H_{108}Mg_2N_8Na_2$	$C_{36}H_{72}Mn_2N_4Na_2O$
Formula weight	940.06	732.84
Crystal system, space group	monoclinic, $P2_1/n$	monoclinic, $P2_1/c$
a [Å]	8.2736(3)	11.982(2)
b [Å]	21.4955(8)	11.559(2)
c [Å]	16.5688(6)	16.445(6)
α [°]	90	90
β [°]	90.708(4)	116.75
γ [°]	90	90
Cell volume [$Å^3$]	2946.46(19)	2033.9(9)
Z	2	2
D_c, g cm^{-3}	1.060	1.197
μ, mm^{-1}	0.094	0.673
T, K	123	150
θ_{max}	29	25
Reflections collected	31164	15138
Independent reflections	7797	3543
R_{int}	0.0273	0.0228
No. refined parameters	323	213
Final R indices [$F^2>2\sigma$]	R1 = 0.0378, wR2 = 0.0985	R1 = 0.0232, wR2 = 0.0533
R indices (all data)	R1 = 0.0610, wR2 = 0.1036	R1 = 0.0338, wR2 = 0.0589
Goodness-of-fit on F^2	1.069	1.087
Max and min residual ρ, e $Å^{-3}$	+0.357, -0.174	+0.26, -0.17

Compound	47	48
Chemical formula (total)	$C_{28}H_{59}MgN_4NaS$	$C_{37}H_{73}MgN_4NaSi$
Formula weight	531.15	649.38
Crystal system, space group	triclinic, P-1	orthorhombic, $P2_12_12_1$
a [Å]	10.3631(7)	11.7239(4)
b [Å]	11.1764(8)	16.8855(8)
c [Å]	15.5624(10)	20.4974(7)
α [°]	102.133(6)	90
β [°]	107.474(6)	90
γ [°]	98.968(6)	90
Cell volume [$Å^3$]	1633.88(19)	4057.7(3)
Z	2	4
D_c, g cm^{-3}	1.080	1.063
μ, mm^{-1}	0.153	0.112
T, K	123	123
θ_{max}	28	28
Reflections collected	27005	16903
Independent reflections	7698	9484
R_{int}	0.0286	0.0520
No. refined parameters	370	409
Final R indices [$F^2>2\sigma$]	R1 = 0.0569, wR2 = 0.1619	R1 = 0.0463, wR2 = 0.0962
R indices (all data)	R1 = 0.0835, wR2 = 0.1712	R1 = 0.0749, wR2 = 0.0998
Goodness-of-fit on F^2	1.087	0.808
Max and min residual ρ, e $Å^{-3}$	+0.827, -0.433	+0.452, -0.299

Compound	49	50
Chemical formula (total)	$C_{37}H_{69}MgN_4NaS$	$C_{108}H_{160}Mg_6N_{12}Na_{12}O_{16}Si_2$
Formula weight	649.32	2360.40
Crystal system, space group	orthorhombic, $P1_12_12_1$	triclinic, P-1
a [Å]	17.0398(3)	15.5127(6)
b [Å]	20.1459(3)	16.7993(7)
c [Å]	22.0003(4)	17.7608(8)
α [°]	90	61.930(5)
β [°]	90	73.749(4)
γ [°]	90	63.757(4)
Cell volume [$Å^3$]	7552.3(2)	3648.0(3)
Z	8	1
D_c, g cm^{-3}	1.142	1.074
μ, mm^{-1}	0.144	0.140
T, K	123	123
θ_{max}	26	25
Reflections collected	41732	21042
Independent reflections	14747	12205
R_{int}	0.0599	0.0234
No. refined parameters	803	705
Final R indices [$F^2>2\sigma$]	R1 = 0.0528, wR2 = 0.0917	R1 = 0.0557, wR2 = 0.1495
R indices (all data)	R1 = 0.1000, wR2 = 0.1024	R1 = 0.0937, wR2 = 0.1624
Goodness-of-fit on F^2	0.875	0.958
Max and min residual ρ, e $Å^{-3}$	+0.298, -0.296	+0.748, -0420

Compound	51	54
Chemical formula (total)	$C_{24}H_{41}MgN_4NaS_3$	$C_{74}H_{146}Mg_4N_8Na_8O_4$
Formula weight	529.09	1493.15
Crystal system, space group	monoclinic, $P2_1/c$	monoclinic, $C1_2/c1$
a [Å]	10.1527(8)	27.331(3)
b [Å]	27.855(2)	26.8976(12)
c [Å]	11.1678(8)	16.0390(11)
α [°]	90	90
β [°]	113.372(9)	118.922(7)
γ [°]	90	90
Cell volume [$Å^3$]	2899.2(4)	10320.3
Z	4	4
D_c, g cm^{-3}	1.212	0.961
μ, mm^{-1}	0.311	0.109
T, K	123	150
θ_{max}	27.49	22.5
Reflections collected	19264	25224
Independent reflections	6494	6588
R_{int}	0.0757	0.0751
No. refined parameters	327	481
Final R indices [$F^2>2\sigma$]	R1 = 0.0451, wR2 = 0.0699	R1 = 0.0634, wR2 = 0.1690
R indices (all data)	R1 = 0.1234, wR2 = 0.0809	R1 = 0.1316, wR2 = 0.1896
Goodness-of-fit on F^2	0.794	0.958
Max and min residual ρ, e $Å^{-3}$	+0.262, -0.315	+0.57, -0.23

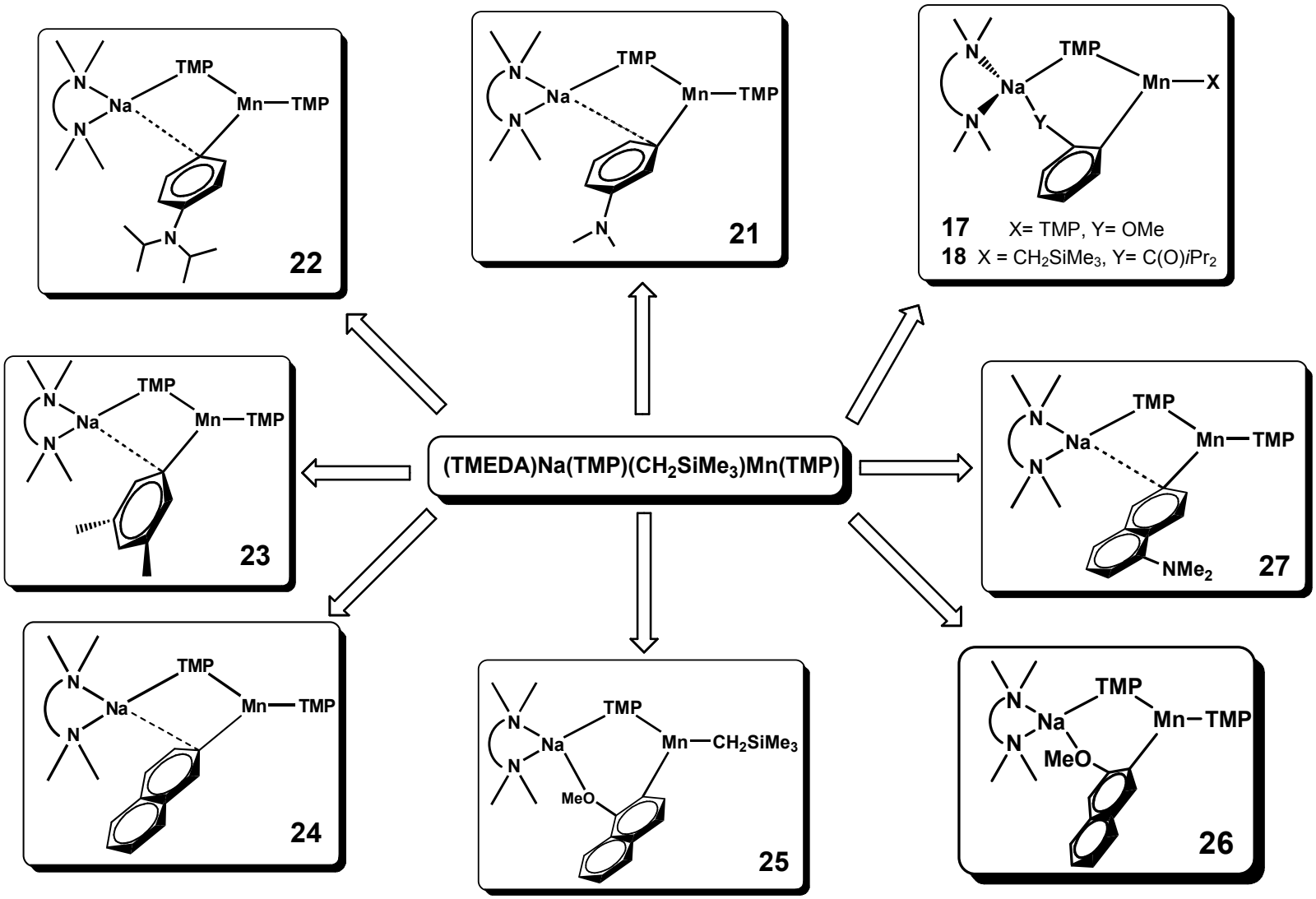

Figure 59: Summary of examples of AMM*Mn* with the synergic base.